Neuroimaging markers of Alzheimer's disease, Mild Cognitive Impairment and Normal Healthy Ageing

Khan, Wasim Nawaz

Awarding institution:
King's College London

Neuroimaging Markers of Alzheimer's Disease, Mild Cognitive Impairment, and Normal Healthy Ageing

Thesis submitted for the degree of Doctor of Philosophy

Wasim Khan

Department of Neuroimaging

Institute of Psychiatry, Psychology, and Neuroscience

(IoPPN), King's College London

2017

ABSTRACT

Alzheimer's disease (AD) is a progressive neurodegenerative disorder clinically characterised by memory loss and cognitive decline that severely affect activities of daily living. Neuropathologically, the disease is characterised by two major proteinopathies, extracellular amyloid-beta (Aβ) plaques and intraneuronal neurofibrillary tangle pathology. The development of neuroimaging biomarkers for AD have transformed the assessment of brain changes associated with these pathological processes for the earlier detection of AD. However, additional work is needed to validate more robust neuroimaging techniques for early diagnosis in the predementia stages of AD pathophysiology. The aim of this PhD is to investigate the utility of advanced Magnetic Resonance Imaging (MRI) techniques for the earlier detection of AD across different biomarker endophenotypes of pathogenesis. These PhD investigations consist of: 1) A comparison of an automated hippocampal subfield technique over standard hippocampal volumetry for AD classification and Mild Cognitive Impairment (MCI) to AD conversion prediction, 2) A neuroimaging-proteomic study for testing the prognostic ability of novel cerebrospinal fluid (CSF) proteins in combination with structural MRI measurements for AD classification and MCI to AD conversion prediction, 3) An extensive multi-cohort study testing the neuroanatomic relationship between Apolipoprotein E (APOE), hippocampal volume, and Aβ deposition across the AD spectrum, 4) A study of the neurodevelopmental effect of APOE polymorphisms on brain structure in adolescence and 5) A neuroimaging study testing the utility of resting-state functional MRI (rsfMRI) for characterising the functional systems-level pathology of intrinsic networks anchored in the highly metabolically active posteromedial cortex. In conclusion, in this thesis I provide evidence to show the diagnostic efficacy of structural MRI techniques across different biomarker interactions for disease classification and prediction in AD, and explain the neuroanatomic role of APOE on the hippocampus across the AD spectrum, as well as demonstrating the utility of rsfMRI methods as an emerging biomarker of AD.

ACKNOWLEDGEMENTS

I am enormously grateful to my supervisor Dr Andrew Simmons for introducing me to the world of research and giving me the opportunity to further my ability and develop my skills as a researcher. I would also like to thank my supervisor and good friend Dr Eric Westman at the Department of Neurobiology and Care Sciences, Karolinska Institutet, for always helping me and being there to provide fantastic supervision and guidance, and sharing his unabating love for Peach Bellini's. I would also like to express my gratitude and thanks to my supervisor Dr Vincent Giampietro for being immensely supportive and allowing me to develop and hone my research interests.

I am also very grateful for the support and guidance provided by Professor Steve Williams, who has always been there to help and given me the freedom to work independently. I would like to thank my friends and colleagues, Dr Owen O'Daly and Jonathon O'Muircheartaigh, for introducing me to the world of fMRI and for their stimulating pub discussions. I would very much like to thank my collaborators, Professor Colin Masters, at the University of Melbourne, Australia and Dr Ali Amad, at Centre Hospitalier Régional Universitaire de Lille, Lille, France, without whom some of this work may not have come to fruition.

I would like to express my appreciation to Heather Hipwell, for allowing me to (occasionally) raid the biscuit cupboard in search of chocolate hob-nobs during the late hours of thesis writing. I would also like to thank my chum and PhD colleague Peter Hawkins for sharing my self-perpetuating misery and for all the fantastic discussions totally unrelated to science, and to Fernando Zelaya and Jed Wingrove for the cathartic Friday boxing classes. I am also very thankful to all the administrative/accounting staff, especially Amin Kausar at the Department of Neuroimaging.

Finally, I am eternally grateful for the support of my family, in particular my dearest mother who would always tolerate my dramatized pensive melancholy and put my wellbeing first. I would especially like to thank my girlfriend Phoebe, who has been incredibly supportive and always being there to help and comfort me when I needed it the most.

AUTHOR DECLARATION AND CONTRIBUTIONS

The work presented in this thesis was funded by the NIHR Biomedical Research Centre for Mental Health and Dementia at the South London and Maudsley NHS Foundation Trust, and the Institute of Psychiatry, Psychology, and Neuroscience (IoPPN), King's College London. Prior to commencing my PhD, a part of the neuroimaging data from the Alzheimer's Disease Neuroimaging Initiative (ADNI) and AddNeuroMed studies had already been preprocessed by Dr Andrew Simmons (IoPPN, King's College London), Dr Eric Westman (Karolinska Institutet), and Sebastian Muehlboeck (IoPPN, King's College London, Karolinska Institutet). Dr Andrew Simmons performed the quality control criteria on the preprocessed FreeSurfer images from the ADNI and AddNeuroMed cohorts. Dr Eric Westman and Dr Carlos Aguilar (Karolinska Institutet) provided assistance and support on multivariate analysis techniques, and machine learning algorithms for AD classification and MCI to AD conversion prediction.

Data was used from the AddNeuroMed study was supported by InnoMed, (Innovative Medicines in Europe) an Integrated Project funded by the European Union of the Sixth Framework program priority FP6-2004-LIFESCIHEALTH-5, Life Sciences, Genomics and Biotechnology for Health. Data collection and sharing for this project was funded by the ADNI (National Institutes of Health Grant U01 AG024904). Publicly accessible data for the ADNI study used in this thesis was funded by the Alzheimer's Disease Neuroimaging Initiative (ADNI) (National Institutes of Health Grant U01 AG024904) and DOD ADNI (Department of Defence award number W81XWH-12-2-0012). ADNI is funded by the National Institute on Aging, the National Institute of Biomedical Imaging and Bioengineering, and through generous contributions from the following: Alzheimer's Association; Alzheimer's Drug Discovery Foundation; BioClinica, Inc.; Biogen Idec Inc.; Bristol- Myers Squibb Company; Eisai Inc.; Elan Pharmaceuticals, Inc.; Eli Lilly and Company; F. Hoffmann-La Roche Ltd and its affiliated company Genentech, Inc.; GE Healthcare; Innogenetics, N.V.; IXICO Ltd.; Janssen Alzheimer Immunotherapy Research & Development, LLC.; Johnson & Johnson Pharmaceutical Research & Development LLC.; Medpace, Inc.; Merck & Co., Inc.; Meso Scale Diagnostics, LLC.; NeuroRx Research; Novartis Pharmaceuticals Corporation; Pfizer Inc.; Piramal Imaging; Servier; Synarc Inc.; and Takeda Pharmaceutical Company. The Canadian Institutes of Health Research is providing funds to support ADNI clinical sites in Canada. Private sector contributions are facilitated by the Foundation for the National Institutes of Health (www.fnih.org). The grantee organization is the Northern California Institute for Research and Education, and the study is coordinated by the Alzheimer's Disease Cooperative Study at the University of California, San Diego. ADNI data are disseminated by the Laboratory for Neuro Imaging at the University of California, Los Angeles.

Also, thanks to the Foundation Gamla Tjanarinnor, the Swedish Alzheimer's Association and Swedish Brain Power, Health Research Council of Academy of Finland and Stockholm Medical Image Laboratory and Education (SMILE).

In all other respects, to the best of my knowledge, the work presented in this thesis is my original work, except where acknowledged in the text.

LIST OF PUBLICATIONS FROM THESIS

1) Khan W, Westman E, Jones N, Wahlund L-O, Mecocci P, Vellas B, Tsolaki M, Kłoszewska I, Soininen H, Spenger C, Lovestone S, Muehlboeck J-S, Simmons A (2014) Automated Hippocampal Subfield Measures as Predictors of Conversion from Mild Cognitive Impairment to Alzheimer's Disease in Two Independent Cohorts. *Brain Topogr*.

2) Khan W, Giampietro V, Ginestet C, Dell'Acqua F, Bouls D, Newhouse S, Dobson R, Banaschewski T, Barker GJ, Bokde ALW, Büchel C, Conrod P, Flor H, Frouin V, Garavan H, Gowland P, Heinz A, Ittermann B, Lemaître H, Nees F, Paus T, Pausova Z, Rietschel M, Smolka MN, Ströhle A, Gallinat J, Westman E, Schumann G, Lovestone S, Simmons A (2014) No differences in hippocampal volume between carriers and non-carriers of the ApoE e4 and e2 alleles in young healthy adolescents. *J Alzheimers Dis* 40, 37–43.

3) Dell'Acqua F, Khan W, Gottlieb N, Giampietro V, Ginestet C, Bouls D, Newhouse S, Dobson R, Banaschewski T, Barker GJ, Bokde ALW, Büchel C, Conrod P, Flor H, Frouin V, Garavan H, Gowland P, Heinz A, Lemaítre H, Nees F, Paus T, Pausova Z, Rietschel M, Smolka MN, Ströhle A, Gallinat J, Westman E, Schumann G, Lovestone S, Simmons A (2015) Tract Based Spatial Statistic Reveals No Differences in White Matter Microstructural Organization between Carriers and Non-Carriers of the APOE ε4 and ε2 Alleles in Young Healthy Adolescents. *J Alzheimers Dis* 47, 977–984.

4) Khan W, Aguilar C, Kiddle SJ, Doyle O, Thambisetty M, Muehlboeck S, Sattlecker M, Newhouse S, Lovestone S, Dobson R, Giampietro V, Westman E, Simmons A (2015) A subset of cerebrospinal fluid proteins from a multi-analyte panel associated with brain atrophy, disease classification and prediction in Alzheimer's disease. *PLoS One* 10, 1–16.

5) Khan W, Giampietro V, Banaschewski T, Barker GJ, Bokde ALW, Büchel C, Conrod P, Flor H, Frouin V, Garavan H, Gowland P, Heinz A, Ittermann B, Lemaître H, Nees F, Paus T, Pausova Z, Rietschel R, Smolka MN,′ Ströhle A, Gallinat J, Vellas B, Soininen H, Kloszewska I, Tsolaki M, Mecocci M, Spenger C, Villemagne VL, Masters CL, Muehlboeck SJ, Bäckman L, Fratiglioni L, Kalpouzos G, Wahlund LO, Schumann G, Lovestone S, Williams SCR, Westman E, Simmons A (*In Press*). A multi-cohort study of APOE ε4 and β-Amyloid effects on the Hippocampus in Alzheimer's disease. *J Alzheimer Dis*.

TABLE OF CONTENTS

INDEX OF TABLES

CHAPTER 2: AUTOMATED HIPPOCAMPAL SUBFIELD MEASURES AS PREDICTORS OF CONVERSION FROM MILD COGNITIVE IMPAIRMENT TO ALZHEIMER'S DISEASE

CHAPTER 3: A SUBSET OF CEREBROSPINAL FLUID PROTEINS FROM A MULTI-ANALYTE PANEL ASSOCIATED WITH BRAIN ATROPHY, DISEASE CLASSIFICATION, AND PREDICTION IN ALZHEIMER'S DISEASE

***CHAPTER 4*: A MULTI-COHORT STUDY OF APOE ε4 AND β-AMYLOID EFFECTS ON THE HIPPOCAMPUS IN ALZHEIMER'S DISEASE**

***CHAPTER 5*: NO DIFFERENCES IN HIPPOCAMPAL VOLUME BETWEEN CARRIERS AND NON-CARRIERS OF THE APOE ε4 AND ε2 ALLELES IN YOUNG HEALTHY ADOLESCENTS**

***CHAPTER 6*: TRACT-BASED SPATIAL STATISTIC REVEALS NO DIFFERENCES IN WHITE MATTER MICROSTRUCTURAL ORGANIZATION BETWEEN CARRIERS AND NON-CARRIERS OF THE APOE ε4 AND ε2 ALLELES IN YOUNG HEALTHY ADOLESCENTS**

***CHAPTER 7*: DISTINCT FUNCTIONAL PROPERTIES OF THE POSTEROMEDIAL CORTEX REVEAL ABERRANT FUNCTIONAL CONNECTIVITY PATTERNS IN ALZHEIMER'S DISEASE:MORE THAN JUST THE DEFAULT-MODE**

INDEX OF FIGURES

***CHAPTER 1*: INTRODUCTION**

***CHAPTER 2*: AUTOMATED HIPPOCAMPAL SUBFIELD MEASURES AS PREDICTORS OF CONVERSION FROM MILD COGNITIVE IMPAIRMENT TO ALZHEIMER'S DISEASE**

***CHAPTER 3*: A SUBSET OF CEREBROSPINAL FLUID PROTEINS FROM A MULTI-ANALYTE PANEL ASSOCIATED WITH BRAIN ATROPHY, DISEASE CLASSIFICATION, AND PREDICTION IN ALZHEIMER'S DISEASE**

***CHAPTER 4*: A MULTI-COHORT STUDY OF APOE ε4 AND β-AMYLOID EFFECTS ON THE HIPPOCAMPUS IN ALZHEIMER'S DISEASE**

***CHAPTER 7*: DISTINCT FUNCTIONAL PROPERTIES OF THE POSTEROMEDIAL CORTEX REVEAL ABERRANT FUNCTIONAL CONNECTIVITY PATTERNS IN ALZHEIMER'S DISEASE:MORE THAN JUST THE DEFAULT-MODE**

CHAPTER 1: INTRODUCTION

THE UTILITY OF NEUROIMAGING MARKERS IN ALZHEIMER'S DISEASE

INTRODUCTION

Alzheimer's disease (AD) was first described by Alois Alzheimer in 1907 [1]. It is a neurodegenerative disorder characterised by the progressive loss of cognitive functions such as episodic memory, to the devastating loss of independence and total disability in full-blown dementia. Dementia currently affects over 650,000 individuals in the UK alone and 27 million persons worldwide with predicted rates set to affect 86 million people by the year 2050 [2]. The current number of people affected by dementia in the UK population represents one person in every 88 (1.1%) with one in six individuals over 80 having a form of dementia. The total number of people with dementia in the UK is forecast to increase to over 940,000 by 2021 and 1,751,087 by 2051, an increase of 38% over the next 15 years, and 154% over the next 45 years [3]. At the current prevalence rate alone, the UK dementia report estimates that 416,967 people with dementia have AD [4]. With an ever increasing ageing population, AD poses a serious public health problem and an increasing worldwide economic burden.

Due to the complex neuropathology of AD, a definitive diagnosis is only achieved through post-mortem confirmation. However, accumulating evidence suggest that lesions begin to accrue decades prior to the clinical manifestation of AD. As a result, successful disease modifying therapies would benefit from an accurate earlier diagnosis of the disease, particularly at a stage prior to when pathological neurodegeneration has taken hold. Despite the discouraging statistics, advances in basic science, as well as the advent of modern technology, are providing a detailed view of the pathophysiology of AD, and are bound to foster better tools and methods for detecting the disease earlier than currently available.

This chapter focuses on how advances in neuroimaging techniques have been made in the quest for robust biomarker discovery, improved diagnosis and future treatment outcomes.

NEUROPATHOLOGY OF AD

The clinical features of AD are an observable phenotype of the cumulative burden from multiple pathological insults to the brain. These pathologies are defined by the combined presence of two predominant classes of abnormal hallmarks, extracellular senile plaques, and intraneuronal neurofibrillary tangles (NFTs), both of which comprise highly insoluble, densely packed filaments. Since their first description in 1907 [1], these pathological insults are considered the hallmark histopathological features of the disease. The soluble building blocks for these abnormal structures are amyloid-beta (Aβ) peptides for plaques and tau proteins for tangles.

Recent studies have suggested that it may be the lack of Aβ clearance rather than excess accumulation that is involved in the pathogenesis of AD [5,6]. Aβ peptides are proteolytic fragments of the transmembrane enriched amyloid precursor protein (APP), which when cleaved by secretases through a series of amyloidogenic pathways produces a 42-amino acid peptide ($A\beta_{(1-42)}$). This particular peptide has a high propensity for aggregation under certain conditions (e.g. acidosis). Analysis of cerebrospinal fluid (CSF) $A\beta_{(1-42)}$ shows a significant reduction in AD patients compared to healthy controls [7,8] and it has been suggested that reduced levels of $A\beta_{(1-42)}$ are caused by reduced clearance of Aβ oligomers in the brain [9]. Ultimately, it is these Aβ oligomers that become large Aβ fibrils, that further aggregate to form insoluble deposits in extracellular space, including diffuse plaques and dense-core plaques.

On the other hand, NFTs result from hyperphosphorylated microtubule-associated tau proteins. This process occurs when hyperphosphorylated tau undergoes a conformational change preventing normal binding to microtubules. This results in the impairment of axonal transport, axonal degeneration and ultimately apoptotic cell death. Insoluble filamentous structures resulting from self-propagating hyperphosphorylated tau assemble to form paired helical filaments – a key component of NFTs seen in post-mortem brains of AD patients [10]. The underlying cause of the toxic post-translational modifications of tau has long been debated in the tau hypothesis but still remain unknown. The likely cause may be due to the disruption of kinases and phosphatases that regulate the tau phosphorylation process [11].

The temporal relationship and direct link between these two proteinopathies are also not well understood. Studies have suggested that Aβ pathogenesis is upstream to tau pathology, with Aβ fibrils beginning to accrue during a long protracted pre-clinical stage of the disease (~10-15 years) [12,13] (**Figure 1.1**). A conceptual framework describing these conspicuous changes in histology suggests that abnormal Aβ initiates the pathological cascade resulting in the formation of NFTs that mediate synaptic dysfunction and neuronal death [14]. However, some accumulating evidence has conversely suggested that tau pathology is not merely an epiphenomenon of Aβ pathology. Instead, tau is actually required for Aβ toxicity in-vivo [15]. Regardless of the disparities in evidence, these studies demonstrate that Aβ and tau are two important proteinopathies involved in AD pathogenesis.

As these patterns of pathology spread through the brain they initiate an apoptotic cascade leading to widespread neuronal loss and eventually to the clinical symptoms associated with AD. These several specific stages of neurodegeneration have been thoroughly described by Braak and Colleagues [16,17].

CLINICAL SYMPTOMS AND DIAGNOSIS

In most patients with AD, the initial symptoms manifest from a progressive amnestic core that appears as an impairment of episodic memory. This is followed by a general decline in communication, reasoning and other behavioural domains [18]. Eventually patients lose their ability to function in daily life and require increasingly more day-to-day support and personal care. In a majority of cases (>95%) the onset of AD is sporadic, and is usually classified by its age of onset (>65 years). On the other hand, 1-5% of cases exhibit an earlier onset, typically in the late 40s or early 50s (so-called early-onset AD). These predominate two forms of AD are clinically indistinguishable; however, early-onset AD is generally more severe and is associated with a rapid rate of progression.

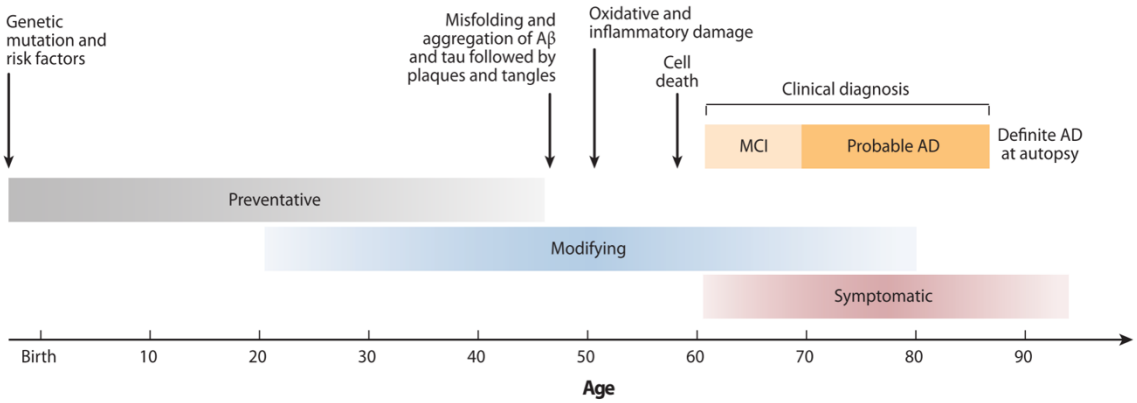

Figure 0: Hypothetical timeline for the pathological progression of AD
This figure shows a theoretical timeline for the progression of AD-related neuropathology and clinical changes, with changes in amyloid and tau pathology occurring years before the onset of AD. The grey, blue, and red shaded bars reflect time points at which different types of potential interventions may be beneficial (grey, preventative; blue, disease modifying; red, symptomatic). Figure from Shaw et al [29].

In clinical practice the diagnosis of AD is based on validated criteria from the National Institute on Aging-Alzheimer's Association (NIA-AA) [19] and National Institute of Neurological Disorders and Stroke-Alzheimer Disease and Related Disorders (NINCDS-ADRDA) [18]. The diagnosis of AD is made based on the clinical features of the disease, with a presence of a memory disorder and an impairment in at least one other cognitive domain, both of which interfere with social function or activities of daily living.

In an attempt to further elucidate the clinical phenotype of the AD syndrome, a clinical syndrome was developed and termed Mild Cognitive Impairment (MCI), now widely considered the prodromal at-risk stage of AD [20,21]. MCI is variably defined and includes the presence of memory impairment, cognitive symptoms, or both with generally unaffected daily living activities and was used to define individuals who did not currently meet the AD diagnostic criteria. Recently, revised core clinical criteria for the diagnosis of AD due to MCI were published for application in clinical and research settings [22]. These revised criteria now include (i) cognitive impairment in one or more cognitive domains (memory, executive function, attention, visuospatial, and language skills) greater than the expected for age and education level, (ii) preservation of independence in daily life activities, and (iii) changes should be mild so that they do not interfere with social or occupational functioning.

Much of these improved diagnostic criteria, as well as the impetus to diagnose AD earlier, have been supported by the emergence of biomarker discovery for testing sensitive and specific markers of disease. For instance, the current AD diagnosis is anchored on the support of biomarkers (e.g. neuroimaging and/or CSF protein levels) to corroborate the presence of AD pathology and rule out the presence of other dementias. Some important refinements to these criteria [23] were proposed in a recent lexicon that drew a distinction between the clinical AD syndrome and AD pathology. In turn, this distinction broadened the spectrum of disease in the NIA-AA diagnostic criteria published in 2011 [24]. This includes 1) asymptomatic pre-clinical AD [6], referring to individuals with biomarkers of AD pathology but without the presence of clinical symptoms, 2) pre-dementia (MCI due to AD) [22] and 3) dementia (due to AD) [25].

BIOMARKER DISCOVERY IN AD

Biomarkers or a "biological marker" represent a category of objective and quantifiable medical signs which define a medical state from outside a patient. These medical signs are unlike medical symptoms which are indictors of health or illness described and perceived by patients themselves. According to the definition provided by the National Institutes of Health Biomarkers Definition Working Group in 1998, a biomarker is evidence of any normal biological processes, pathological processes, or pharmacological responses to therapeutic intervention that can be reproduced and measured accurately [26,27]. In order to identify a good biomarker with diagnostic utility it must be sensitive, specific, and easy to administer to patient populations. Such an ideal biomarker would distinguish AD from other forms of dementia, mixed forms of dementia, such as vascular or Lewy-body disease and MCI stages of AD development.

Currently available evidence strongly supports the position that the pathophysiological process of AD begins many years prior to the manifestation of clinical symptoms. However, in order to further elucidate the link between the pathological cascade of AD and the emergence of symptoms there is a need for robust biomarkers where disease-modifying therapies can have the most impact. Future disease-modifying therapies and clinical trials for drug discovery will be maximally effective in the prodromal stages of disease where at-risk individuals are yet to

develop clinical symptoms. The sensitivity, specificity, and accessibility are important factors to consider that ultimately define the diagnostic and prognostic ability of putative markers of AD pathology. Biomarkers are also important for clinical trials of novel pharmaceutical interventions to enrich samples with individuals most likely to progress to an AD diagnosis and monitor the outcome of therapeutic interventions. As a result, multi-centre consortium studies have been designed to longitudinally evaluate the role of neuroimaging, CSF, and blood biomarkers, neuropsychological, clinical, and genetic risk factors, in detecting AD pathophysiological changes, especially during the prodromal stages of development, to track disease progression and predict future decline. The US-based Alzheimer's Disease Neuroimaging Initiative (ADNI), established in 2004, is primarily intended to help inform the future design and performance of multi-centre clinical trials of putative AD-modifying treatments using a suite of biomarkers. Since its inception, the ADNI study has inspired similar multi-centre initiatives in Europe, with the AddNeuroMed study, and the Australian, Imaging, Biomarkers and Lifestyles (AIBL) study. Well-established and validated biochemical biomarkers from CSF (e.g. $A\beta_{(1-42)}$), total-tau, phospho-tau-181) are commonly used for AD research [28–30]. Neuroimaging techniques also provide an excellent set of tools for measuring in-vivo AD pathophysiology and cortical atrophy associated with AD, as well as for predicting disease progression in individuals with relatively minor cognitive impairments [31–33].

NEUROIMAGING BIOMARKERS

he two types of most commonly used neuroimaging techniques as AD biomarkers are Magnetic Resonance Imaging (MRI) and Positron Emission Tomography (PET). Structural imaging is most widely applied to measure in-vivo cortical atrophy changes reflective of neuronal loss, whereas PET imaging measures the fibrillar aggregation of Aβ plaques. Recent evidence suggests that Aβ biomarker abnormalities precede neurodegenerative biomarker abnormalities in the pathogenesis of AD [12,13] (Figure 1.2).

In this section, we will review the best established MRI measurements for the detection and tracking of AD, followed by a description of other important imaging measurements, some of which have been less extensively applied, or more recently developed for biomarker discovery.

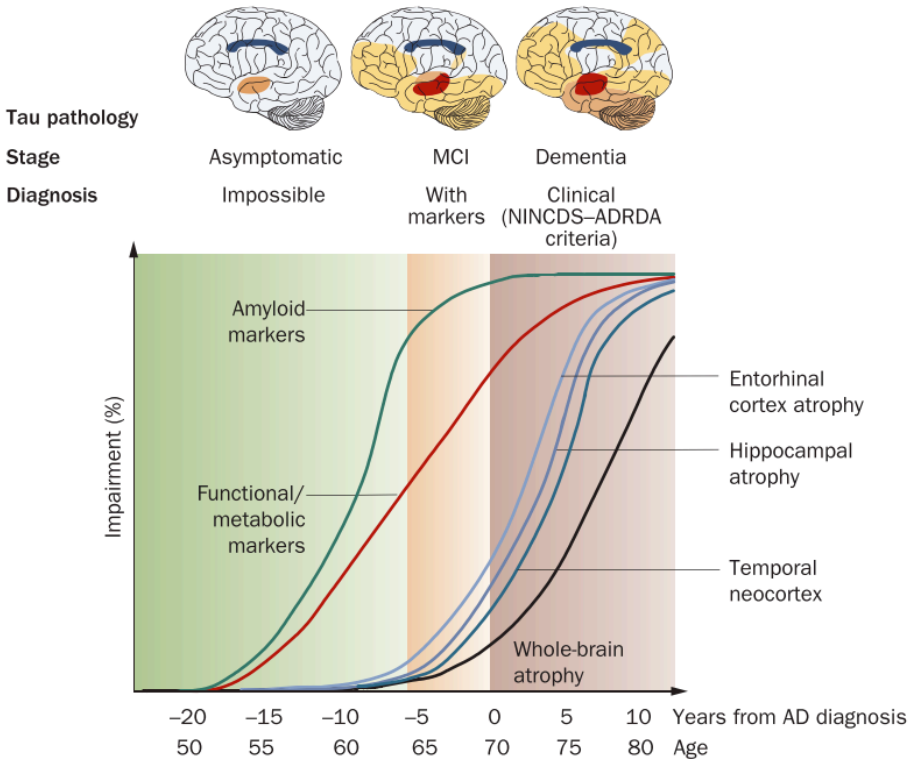

Figure 1 Dynamic biomarker trajectories of AD pathophysiology

A theoretical representation of the biomarker trajectories during different stages of AD pathogenesis. This illustration demonstrates that some markers may be more useful for detecting the pathological changes in AD during different stages of development. For instance, some markers may be useful for early diagnosis, whereas others may have more prognostic potential in tracking disease progression. Amyloid markers (CSF $A\beta_{(1-42)}$ and Aβ PET) represent the earliest detectable changes in AD, but begin to plateau at the MCI stage. Functional and metabolic markers (FDG-PET measurements of hypometabolism and functional MRI methods) become abnormal at the MCI stage and progressively change well into the dementia stage. Changes on structural MRI become abnormal during the MCI stage, often following a temporal pattern of changes that correspond to tau pathology in the brain. Most extensively used measurements included hippocampal and entorhinal volume, as well as measurements of whole-brain atrophy. Abbreviations: AD, Alzheimer's Disease; MCI, Mild Cognitive Impairment; NINCDS-ADRDA, National Institute of Neurological and Communicative Disorders and Stroke-Alzheimer's Disease and Related Disorders Association. Figure from Frisoni et al [41].

The use of structural MRI in AD

Structural MRI as a measure of atrophy is regarded as a valid marker of disease state and progression. It is also a widely established method for quantifying regional and global brain volumes in-vivo. Previous studies have shown that the topography of tissue loss, detected both cross-sectionally and longitudinally, correlates well with neuropathological disease progression [34,35] and the degree of cognitive impairment. Structural changes in the brain are a measure of tau-related neurodegeneration and accurately map upstream to the Braak stages of NFT development [36,37] and downstream to cognitive deficits [38,39]. The earliest sites of tau neurodegeneration typically include the medial temporal lobe (MTL), with the most common patterns of atrophy found in the transentorhinal and entorhinal cortex (Figure 1.2), followed by the hippocampal formation and other adjoining areas of the temporal neocortex. Later in the disease, atrophy in the temporal, parietal, and frontal neocortices is associated with overt stages of AD, as well as widespread language, visuospatial, and behavioural deficits [40,41].

Historically, manual delineation methods were implemented to extract volumetric and morphometric characteristics of atrophy, including manual tracings of region-of-interest that typically measure hippocampal and entorhinal volumes [42,43]. These manual volumetric methods have achieved promising accuracies for distinguishing patients with AD from normal healthy individuals [44], and predicting incipient AD in MCI patients that go on to receive a diagnosis at later follow-up [45]. An alternative to volumetric methods is a simple visual assessment rating scale of the MTL, originally used by neuroradiologists in clinical practice, is also promising for differentiating AD patients from older healthy individuals [46,47]. However, manual delineation methods, although consistent, are very time-consuming and expensive as high-throughput or front-line screening tools. Moreover, manual segmentation is not usually feasible for large datasets and often requires at least two experienced neuroanatomist tracers to avoid biases. Consequently, sophisticated computational algorithms that enable the automated segmentation of complex structures such as the hippocampus are highly desirable for quickly and efficiently performing segmentation. However, automated morphometric methods, such as voxel-based morphometry (VBM) have been previously criticised for being susceptible to inaccurate normalisation procedures and changes to processing pipelines. Since,

manual and automatic segmentation methods have been compared for validation purposes mostly using the hippocampus. These studies have largely shown that manual and automated volumetric estimates of the hippocampus are highly correlated and exhibit greater volume overlap. More recent work has compared two popular and more widely used automated software tools such as FreeSurfer and FSL FIRST to assess the accuracy of their segmentation algorithms [48,49]. Morey and colleagues [50] compared manual tracings to automated segmentations of the hippocampus from FreeSurfer and FSL and concluded that FreeSurfer was superior to FSL FIRST for all aspects of the objective measured used. Recent work has since corroborated this evidence by demonstrating FreeSurfer as the superior technique for hippocampal volumetry [51]. FreeSurfer is an automated technique which provides segmentation by assigning a neuroanatomical label to each voxel in the MR image volume. A probabilistic atlas is used to produce segmentations with a Bayesian inference algorithm from a manually labelled training set [52]. This probabilistic algorithm can also be used to define curvature information of the cerebral cortex into gyri-based neuroanatomical regions that represent standard measures of cortical thickness and surface area.

In AD pathology the spatial pattern of atrophic changes in the brain are complex and evolve over time as the disease progresses. Capturing these dynamic spatio-temporal patterns of cortical change often require high-dimensional image warping and sophisticated computational tools to quantify the regional distribution of brain tissue. In order to achieve this, studies have used advanced pattern classification methods and machine learning algorithms to detect patterns of cortical change for disease classification and prediction [53]. In particular, methods such as support vector machine (SVM) enable the automatic classification of patients with AD and MCI patients at-risk of developing AD [54]. Similar pattern classification schemes have also been used to determine a quantitative value of 'abnormality' for classification on an individual basis. For example, a previous study constructed a classifier, known as the SPARE-AD index (Spatial Pattern of Abnormality for Recognition of Early Alzheimer's Disease), that generates a quantitative control-like phenotype (negative values) and AD-like phenotype (positive values) of spatial atrophy patterns to detect incipient stages of AD in normal older adults [55]. Sophisticated multimodal pattern classifiers combining different modalities of biomarkers have also shown promise for distinguishing between MCI

patients that will convert to AD, from those that are not on the same pathophysiological spectrum [56].

Molecular Neuroimaging in AD

New insights into the molecular mechanisms of AD pathogenesis have opened avenues for the successful development of Positron Emission Tomography (PET) neuroimaging techniques. PET is a sensitive neuroimaging technique that measures the quantification of radiological compounds in-vivo, allowing the non-invasive assessment of molecular processes at different sites of action. Several radiological-contrast compounds, known as PET ligands have been developed to evaluate different metabolic and neurochemical processes in the brain. In AD research, two types of PET ligands are primarily utilised: 1) [^{18}F] fluorodeoxyglucose (FDG), which measures the functional neuronal metabolism of the brain [57,58] and 2) ligands for the in-vivo assessment of Aβ pathology, including [^{11}C] Pittsburgh compound B (PiB), [^{18}F] Flutemetamol, and [^{18}F] Florbetapir, which bind to fibrillar amyloid plaques in the brain [59–61]. Recently, efforts worldwide have also focused on the design of selected tau PET tracers for measuring the different stages and severity of tau aggregation and deposition [62].

Prior to the development of PET ligands for measuring fibrillar Aβ plaques in the brain, FDG-PET was the most widely utilised for measuring the functional effects of neuronal activity at the tissue level. More specifically, FDG-PET has been used to measure cerebral metabolic rates of glucose (CMRglc), a proxy for neuronal activity in AD patients and those at-risk of developing the disease. A growing body of evidence has highlighted the importance of FDG-PET as a tool for aiding in the differential diagnosis of AD from the presence of other comorbid conditions, such as frontotemporal dementia, vascular dementia, dementia with Lewy bodies (DLB), and depression [63,64]. In more than 85% of histopathologically confirmed cases of AD, patients show a consistent in-vivo pattern of glucose deficits with temporoparietal and posterior cingulate hypometabolism [63,65]. Due to the high sensitivity of FDG-PET (~90%) in detecting this characteristic pattern of hypometabolism, it has an improved diagnostic and prognostic accuracy for detecting individuals with probable AD [66]. Altogether, these findings support the utility of FDG-PET in the differential diagnosis of major neurodegenerative dementia disorders.

In the last decade, the use of PET for measuring Aβ pathology has allowed the anatomical localisation of Aβ plaques in-vivo, and has provided tools for regional and global measurements of Aβ burden in the brain. Since the seminal study first published by Klunk and colleagues [59], several Aβ PET studies have been performed, extending our insight into its topography, rates of accumulation and the earliest sites of Aβ aggregation. The most commonly used PET ligand in AD studies to date is [^{11}C] PiB, which has been shown to bind to both neuritic and diffuse plaques, as well as cerebral Aβ within the vasculature [67]. The prevalence and anatomical distribution of Aβ plaques were found to be highly correlated with the level of Aβ post-mortem [68]. Longitudinal PiB studies have since shown that small, albeit significant changes in the accumulation of Aβ plaques can be quantified and represent changes across the different AD stages, from asymptomatic individuals to those with full-blown AD dementia [13,69]. Aβ deposition has been estimated to take approximately 11 years for an individual with a PIB-negative scan to reach the threshold of a PiB positive scan (1.5 SUVR), and approximately 15–20 years to go from this threshold to levels typically observed in mild AD [70,71]. These findings have since been corroborated by a wave of second generation PET ligands, namely [^{18}F] Flutemetamol, and [^{18}F] Florbetapir, which were designed to circumvent the radioactive decay half-life limitations of PiB, and ensure that Aβ PET imaging was more widely available for routine clinical use [72].

The success of Aβ PET imaging has spurred efforts worldwide to develop selective tau PET radiological tracers to enable the in-vivo assessment of regional tau burden. The hyperphosphorylated state of tau is complex, particularly since there are six different isoforms of tau in the human tissue. Consequently, the development of a selective tau PET tracer should provide the ability to evaluate the severity of tau pathology during different stages of AD pathogenesis. Currently, at least 7 different tau PET tracers have been developed and used in clinical studies [62], yet not all these agents provide the desired binding affinity to tau aggregates in the brain. For example, the development of ^{18}F-FDDNP [73] demonstrated a high binding and retention in AD patients, but did so by non-selectively binding to both extracellular Aβ plaques and intracellular NFTs in the brain. However, recent development of ^{18}F-AV-1451, a quinolone derivative, has demonstrated high selective binding and affinity to tau protein aggregates and has shown little binding affinity with Aβ plaques [74]. Further validation studies

of this new investigational PET tracer will determine its efficacy as a potential surrogate marker of tau burden.

Diffusion tensor imaging (DTI) in AD

More advanced structural imaging techniques that measure the accompanying microstructural loss (axonal and dendritic) in the presence atrophy have also been used to evaluate changes in patients with AD, and those with prodromal stages of the disease. Diffusion weighted imaging (DWI) and diffusion tensor imaging (DTI) are methods that enable the in-vivo quantification of differences in molecular diffusion at the cellular level [75]. These methods provide an opportunity to evaluate the integrity of white-matter (WM) tracts using two primary measures: 1) fractional anisotropy (FA), considered to be a general measure of axonal integrity, reflects the diffusion direction of water in the fibre tracts and 2) mean diffusivity (MD), which measures the overall diffusivity in WM tracts [76]. The two major methods for analysing diffusion imaging data are region-of-interest approaches, and whole-brain voxelwise analysis, of which the most widely used is tract-based spatial statistics (TBSS) [77]. Other MRI techniques, such as magnetic resonance spectroscopy (MRS) and magnetization transfer imaging methods can also provide further complimentary information to atrophy measures [78,79].

Resting-state Functional MRI in AD

Resting functional MRI (rsfMRI), a technique used to measure intrinsic functional brain connectivity, has recently emerged as a promising biomarker for AD research as disruptions in brain function are believed to manifest upstream to atrophy. rsfMRI offers several advantages, for one, its most salient feature is the relative ease of acquisition in patients with dementia, specifically the ability to measure functional connectivity without the presence of an explicit task paradigm. Furthermore, rsfMRI is a relatively non-invasive method that does not require the injection of a contrast agent, and thus can be repeated several times in studies of a longitudinal design, as well as, clinical trials for future drug development [80]. More importantly, for our understanding of declining memory in patients with AD, rsfMRI provides

useful information about the functional integrity of intrinsic networks supporting memory and attention across several different cognitive domains.

Blood oxygen level dependent (BOLD) fMRI represents an indirect measure of neuronal activity, thought to reflect the integrated synaptic activity of neurons through changes in the magnetic resonance signal due to changes in blood flow, blood volume, and blood oxyhaemoglobin/deoxyhaemoglobin ratio, inferred from measuring the BOLD fMRI signal [81,82]. In particular, rsfMRI techniques at their most rudimentary level, represent the measure of correlated signal between two or more spatially distinct regions across time. Since the discovery of low-frequency fluctuations (0.1 to 0.01 Hz) in the BOLD signal, and its specificity to grey matter [83], studies have revealed a number of brain networks that demonstrate coherence in the spontaneous activity of distributed nodes [84]. These large-scale brain networks exist whether or not they are functionally active at any given moment, and recent studies have shown that such major networks at 'rest' show close correspondence with similar networks derived from task-based fMRI data [85,86].

In AD research, the methodologies adopted by the majority of rsfMRI studies can primarily be isolated into two major techniques, known as seed-based correlation studies, and more data-driven methods such as independent component analysis (ICA). Seed-based methods are used when there is a priori-assumption that a particular node or region of an intrinsic network is known. In such cases, the fluctuations in the BOLD signal are extracted from this seed region, and may consist of individual voxels (typically known peak voxels from previous studies), a collection of voxels from a defined spherical seed region, or large functionally derived regions-of-interest (typically from previous atlases, such as Brodmann areas). The fluctuations in the BOLD signal from the seed region are then subsequently correlated with every other voxel in the brain in a whole-brain voxelwise analysis to measure seed-to-whole-brain connectivity, or with another pre-defined seed region to measure seed-to-seed connectivity. On the other hand, ICA is a multivariate analysis technique that can be used to extract a variety of distinct structured signals that are statistically independent. ICA methods do not necessitate the priori definition of regions from which BOLD fluctuations are to be extracted, but rather extracts networks corresponding to functionally different activations in the time-courses within the rsfMRI dataset.

BIOCHEMICAL BIOMARKERS

The most extensively studied peripheral biomarkers are derived from CSF, which represent the molecular extracellular and interstitial environments of the brain. As a result, CSF is considered the optimal source for obtaining sensitive and specific biomarkers that can reflect the underlying biochemical perturbations in the AD brain. Three major protein constituents of AD pathology, namely $A\beta_{(1-42)}$, total-tau, and phospho-tau-18 derived by enzyme-linked immunosorbent assays (ELISA's), have emerged as the leading diagnostic and prognostic fluid markers of the disease. These core biomarkers have been developed to reflect Aβ and NFT pathology, and axonal degeneration. However, alternative CSF markers reflecting biochemical changes in inflammation, microglial activity, and synaptic function are also being sought to characterise an accurate peripheral signature for improving the prognostic ability of existing CSF biomarkers. The main problem with CSF biomarkers is that they are hampered by the invasive lumbar puncture procedure required for CSF collection. Therefore, efforts are being

made to seek promising biomarkers in peripheral blood which can be used for routine diagnosis of AD. The different modalities of biochemical biomarkers in AD are described below.

Core Biomarkers in Cerebrospinal fluid (CSF)

Analysis of Aβ ($_{1\text{-}42}$) has been shown to be significantly reduced in AD patients compared normal healthy controls. The most widely accepted explanation for this reduction in Aβ ($_{1\text{-}42}$) levels in AD, is the reduced clearance of Aβ in the brain, as well as the enhanced aggregation of Aβ into senile plaques, hence the retention of the peptide in the brain parenchyma. This massive accumulation of Aβ into pathological deposits is believed to reflect a ~40% reduction in CSF Aβ ($_{1\text{-}42}$) levels in AD compared to healthy controls. Since the development of notable Aβ PET ligands, such as PiB, studies have reported a relationship between ^{11}C-PIB retention and CSF Aβ ($_{1\text{–}42}$), with high ^{11}C-PiB binding correlating with low CSF Aβ($_{1\text{–}42}$) levels [87,88].

CSF biomarkers reflecting tau neurodegeneration include CSF levels of total-tau (*t*-tau), which reflects the intensity of axonal and neuronal degeneration in the brain, and phospho-tau-181 (*p*-tau$_{181}$) which seems to reflect both the phosphorylated state of tau, and the formation of NFT pathology in the brain. Tau-neurodegeneration is concomitant with normal healthy ageing, hence t-tau levels are found to increase gradually with age [89]. Yet, levels in AD patients are still significantly increased when compared to age-matched healthy controls. In contrast, p-tau$_{181}$ is also significantly enhanced in AD patients compared to healthy controls, - and can also be used to distinguish AD from other forms of dementia.

Several validation studies have now shown that the combination of these three core CSF biomarkers significantly increases the diagnostic accuracy of detecting AD, yielding a sensitivity of >95% and specificity of >85% [7,90,91]. Recent work has also shown that CSF and structural MRI measures, which reflect different aspects of AD pathology, can provide complimentary predictive information for the earlier detection of AD [92,93].

Alternative biomarkers in CSF

Clinico-pathological studies have widely shown that insidious changes in the neuropathology of AD manifest several years prior to the development of symptoms. This is also reflected in the dynamic range of current CSF biomarker values, which show significant overlap between the preclinical and prodromal stages of AD, thus highlighting the need for improved specificity [90]. Ongoing advances in protein-handling technology have allowed for the development of unbiased techniques, such as multiplex immunoassay platforms for the simultaneous quantification of hundreds of proteins to discover novel empirically tested candidates in the CSF. Consequently, novel candidates without a known relevance to AD may provide insights about the pathophysiology that are not yet known or currently underappreciated. Some recent studies have discovered a small ensemble of novel biomarkers in CSF to improve the diagnostic accuracy of Aβ ($_{1–42}$) and tau [94,95], but more validation studies are required to evaluate their prognostic potential.

Novel blood-based biomarkers

Several promising novel blood-based biomarkers for AD have been documented. The earliest seminal study by Ray and colleagues [96] identified a panel of 18 plasma signalling proteins for accurately identifying AD patients from healthy controls. Since several other blood candidates have been proposed [97–99] but changes in these markers have been difficult to verify in well-characterised independent samples. As a result, efforts to identify reliable biomarkers in blood have met with little success. The future development of harmonized protocols for the collection, storage, and subsequent analytical procedures of blood biomarkers would help minimise variation in laboratory procedures, and thus allow for more accurate direct comparisons, both between laboratories and publications.

GENETIC RISK FACTORS – THE APOLIPOPROTEIN E GENE

The Apolipoprotein E (APOE) gene is known to modulate the risk for late-onset AD. An isoform of APOE, APOE ε4, has been shown to confer a substantially increased risk for late-onset AD [100,101]. The human APOE gene, encoded on chromosome 19, exists as three polymorphic alleles, ε2, ε3, and ε4 – which have a worldwide proportion of 8.4%, 77.9%, and 13.7% respectively [102]. The 3 different isoforms differ primarily by single amino-acid substitutions at residues 112 and 158 - ε2 possesses two cysteines, ε3 has a single cysteine and arginine, and ε4 possesses two arginines [103]. Amino-acid differences at these two positions affect the structure of each APOE isoform, and hence influence their activity in lipid homeostasis and trafficking.

The APOE ε4 isoform is dramatically increased in patients with AD, with approximate prevalence reaching over 40%. The APOE gene plays a critical role in Aβ homeostasis, by facilitating the proteolytic clearance of insoluble Aβ peptides in the brain. Immunohistological studies of Aβ, demonstrate that APOE is co-deposited in senile plaques in patients with AD. Moreover, Aβ pathology and accumulation is more prevalent in APOE ε4 carriers compared to non-carriers. This evidence is corroborated by PET studies of fibrillar Aβ burden, particularly a study by Barthel and colleagues [104], who reported that PET scans classified as Aβ positive were more common in APOE ε4 carriers compared to non-carriers (65% vs. 22%). Moreover, converging evidence demonstrates that abnormal fibrillar Aβ measured by [^{11}C] PiB PET, can be detected in normal APOE ε4 carriers at approximately 56 years compared to 76 years in non-carriers [105]. This difference likely suggests that APOE ε4 increases the risk of AD by a combination of accelerated Aβ accumulation and impaired clearance of insoluble Aβ fibrils, leading to increased deposition. Patients with AD and MCI possessing APOE ε4 also exhibit greater MTL atrophy, particularly in the hippocampus, as well as disrupted rsfMRI connectivity in the Default-Mode Network (DMN) [106,107]. Accumulating evidence also suggests that APOE ε4 carriers exhibit lower cerebral glucose metabolism than non-carriers, both at rest and during cognitively-demanding tasks [57]. These studies illustrate that APOE ε4 is associated with altered brain function, structure, metabolism, and increased Aβ deposition.

Understanding the neuroanatomic foothold of the APOE gene will help explain how APOE ε4 contributes to cognitive decline and AD pathogenesis.

The APOE ε2 allele is believed to exert a protective effect against AD, and carriers typically have a lower risk and delayed age of onset compared to ε3 and ε4 carriers [108]. Some in-vitro studies suggest that APOE ε2 more efficiently promotes the degradation and clearance of Aβ, thus restricting Aβ-mediated neurotoxicity in the brain [109]. Although the risk for AD in APOE ε2 carriers is lower compared to ε4 carriers, findings into the proposed protective role of APOE ε2 in staving off AD neuropathology are less consistent [108,110]. These studies are often limited by their sample size due to the inherent low allelic frequency of APOE ε2, and as a result, possess insufficient statistical power to test its function and biological mechanisms.

Although APOE ε4 is the most significant genetic variant associated with AD, it does not account for all AD heritability. In early-onset form of AD, rare autosomal dominant mutations in amyloid precursor protein (APP), a constituent of Aβ peptides, and the presenilins genes (PSEN1 and PSEN2) are commonly implicated in its development. Alternative to candidate-gene approaches, genome-wide association (GWA) studies have identified rare homozygous loss-of-function mutations in TREM2, a gene that encodes triggering receptor expressed on myeloid cells 2 protein [111,112]. This rare variant of TREM2, which results in a missense mutation, is found to contribute to the pathogenesis of AD through microglial dysfunction. Recent studies testing the impact of TREM2 deficiency on AD pathophysiology have found that TREM2 promotes microglial senescence through an inefficiency on the microglial response to Aβ deposition [113,114]. Since, several other genomic loci as low-risk factors for late-onset AD have been identified (implicating *CLU, PICALM, CR1, BIN1, MS4A, CD2AP, CD33, EPHA1, and ABCA7* [115–118]). Future genetic studies, and GWA studies using neuroimaging biomarkers as endophenotypes of AD, would further help identify new genetic markers to explain the biological mechanisms associated with AD pathogenesis.

NEUROIMAGING BIOMARKER SIGNATURE OF PATHOLOGY IN AD

Extraordinary progress in the last decade in the development of advanced imaging techniques and its application to AD, have led to the best established and most widely applied neuroimaging measurements for the sensitive detection of AD. These measurements include structural MRI markers of regional and global brain atrophy, FDG-PET measurements of decline in regional glucose metabolism, and PET measurements for fibrillar Aβ burden.

Structural MRI remains the most extensively applied MRI technique in AD research for estimating brain atrophy as a concomitant of progressive tau neurodegeneration. AD patients typically exhibit reduced hippocampal and entorhinal cortex volumes (Figure 1.3), reduced grey matter and cortical thickness, widening of sulci and increased ventricular volumes, cortical thinning in regions such as the precuneus and posterior cingulate, and accelerated decline in these regions, or widespread decline across the entire neocortex over time [31,55,119,120] (Figure 1.4a). Reductions in hippocampal volume, measured using high resolution T1-weighted MRI remains the best validated and most well established MRI marker of atrophy. For instance, a recent meta- analysis found that mean annualised hippocampal atrophy rates for AD patients were approximately 4.6% compared to only 1.4% for healthy controls [121]. Hippocampal and entorhinal neuroimaging studies have also linked the accelerated rates of atrophy with the possession of APOE ε4 in a dose-dependent fashion [122], as well as the rates of cognitive decline [33].

Since the spatio-temporal patterns of atrophy in AD is complex, and often associated with concurrent neurodegeneration in normal ageing, advanced pattern analysis techniques have been developed for better characterising AD-related atrophy [123–125]. Several studies have utilised multivariate analysis techniques, such as support vector machines (SVM), principal component analysis (PCA), and partial least squares to latent structures (PLS), to analyse MRI data for the purposes of discriminating AD patients from healthy controls, with almost 100% rates of accuracy [126,127,54,128].

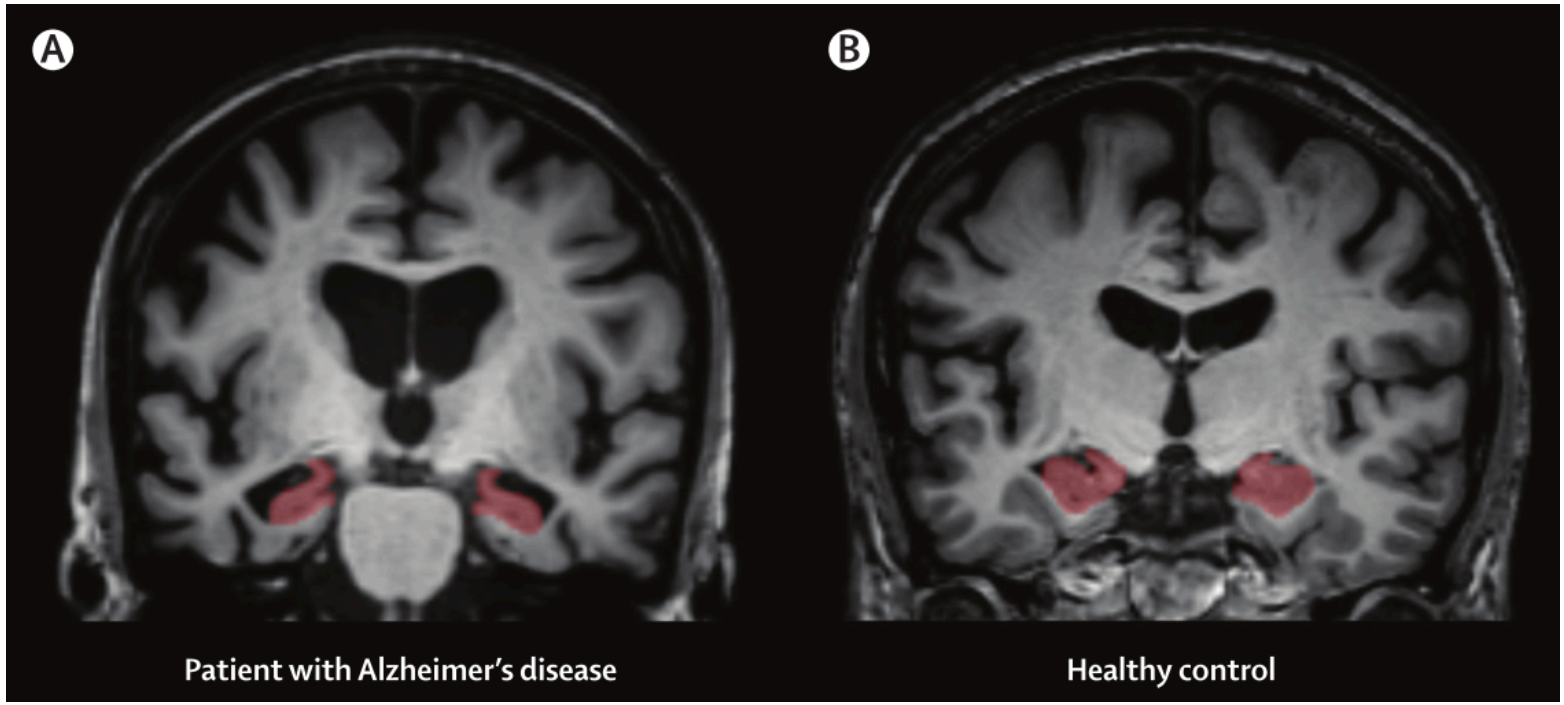

Figure 2: Hippocampal atrophy in AD

Coronal sections shown from high-resolution structural MRI scans depicting the head of the hippocampus (labelled in red) in a patient with Alzheimer's disease (A) and a healthy age-matched control (B). Severe atrophy of the hippocampus in the patient with Alzheimer's disease is evident by visual comparison with the healthy control. Figure from Teipel et al [224].

Structural MRI markers, particularly hippocampal measurements remain in extensive use for defining the different neurodegenerative stages of AD pathophysiology, but more advanced techniques, especially diffusion imaging is providing the tools for more sensitive measures to map the structural microstructure of the brain. Studies have also demonstrated the importance of core biomarkers from CSF in complementing structural MRI measures for the early accurate detection of AD [93,129].

FDG-PET is currently the most extensively characterised functional brain imaging method for AD. Numerous studies have reported reduced cerebral glucose metabolism in AD patients relative to healthy controls, especially in the temporoparietal cortex, posterior cingulate cortex, parietal lobe, and MTL, including the hippocampus (Figure 1.4b). Furthermore, these pattern of differences appear to progress to the frontal cortex and rest of the brain as the disease becomes progressively more severe. In particular, a study by Buckner and colleagues [130] showed that regions with poor cerebral glucose metabolism corresponded with areas commonly affected with abnormal levels of fibrillar Aβ deposition. In a clinical setting FDG-PET is occasionally used to aid in differential diagnosis between AD and other dementias, such as frontotemporal lobar degeneration. Currently it is most commonly used to complement other neuroimaging techniques and fluid marker measurements for accurately detecting AD [39,131].

PET measurements for detecting fibrillar Aβ plaques in the brain now developed almost a decade ago, are having a profound impact on the study of AD pathogenesis, and evaluation of Aβ-modifying therapies. Several validated Aβ PET radioligands, have consistently shown an increased uptake and binding of amyloid tracers, most commonly with PiB, to brain regions known to reflect abnormal Aβ levels in the AD brain, including frontal, parietal, posterior cingulate, and precuneal regions [59,61] (Figure 1.4c). Recent work has shown that across over 15 clinical studies of ^{11}[C] PiB-PET, almost 96% of AD patients were categorised as "Aβ-positive"[132]. However, longitudinal PiB-PET studies report that AD patients exhibit minimal increases in Aβ accumulation over 1-2 years [133]. This has led researchers to conclude that Aβ pathogenesis manifests during a long pre-symptomatic phase of AD, followed by an attenuation of Aβ accumulation when cognitive decline and clinical symptoms manifest during the latter stages of the disease. Recent ^{18}[F] labelled radioligands such as Florbetapir, originally

developed for clinical settings through the advantage of their longer radioactive half-life, have since validated findings from earlier PiB studies [134].

Other advanced neuroimaging techniques that have been less widely validated in AD research than structural MRI measurements include diffusion imaging for assessing brain microstructure, and rsfMRI for measuring functional connectivity at rest. New initiatives such as the Human Connectome Project (HCP) [135] have begun to construct a detailed map of the complete structural and functional neural connections in-vivo, both within and across individuals. This opportunity to develop sophisticated imaging tools for mapping the human connectome will provide an impetus for future AD studies to characterise both structural and functional differences in the disease using optimised high-field imaging technologies.

At present, DTI is used to study both the structural integrity and connectivity of white matter in patients with AD, and those at-risk of developing the disease. Differences in white-matter microstructure and integrity, generally quantified as decreases in fractional anisotropy, and increases in mean diffusivity, is now widely reported across many WM structures in AD patients when compared to healthy controls. The findings from FA studies in AD are conflicting, with differences reported in several regions, as well as some studies reporting a lack of differences between patients and healthy controls [136]. Despite the disparity in findings, region-of-interest studies have reported decreased FA in medial temporal lobe regions, including hippocampal, and parahippocampal WM [137], and regions such as the posterior cingulum [138] in AD patients when compared to healthy controls. Furthermore, unbiased whole-brain analysis methods such as TBSS also do not provide a definitive understanding into the WM changes involved in AD. These studies have generally reported widespread tensor abnormalities in parietal, temporal and frontal WM, and inter-hemispheric connections through the corpus callosum [139,140]. Overall, studies have highlighted the importance of the key limbic tracts, such as the fornix, and regions including the cingulum bundle and the corpus callosum as being vulnerable to AD pathogenesis. This suggests that tensor abnormalities in AD are concentrated to posterior regions that support memory function. This further lends support to the theory of retrogenesis that posits the high vulnerability of later-myelinating regions to degeneration and the relative sparing of early-myelinating regions [141]. Advances in optimising the acquisition protocol, tensor reconstruction routines and

image reconstruction to name a few, would help ensure reliable observations are made to corroborate or refute previous evidence from diffusion imaging studies in AD.

Functional methods in AD other than FDG-PET, include rsfMRI techniques that measure the BOLD signal to assess functional connectivity differences between AD patients and healthy controls at rest. The majority of earlier fMRI studies in AD had focused primarily on the pattern of activation in the hippocampus and surrounding MTL regions using explicit tasks of episodic and working memory. These studies have since reported a consistent deactivation of the hippocampal formation during the encoding of new information in patients with AD, suggesting these networks functionally succumb to a breakdown in memory processing. However, anatomical lesion studies and subsequent fMRI studies have shown that memory function is subserved by a heteromodal network of brain regions that includes the hippocampal memory system, and a set of other cortical regions such as the precuneus, posterior cingulate cortex, lateral parietal, lateral temporal, and medial prefrontal regions. Collectively termed the DMN, a region originally identified by Raichle and colleagues [142], this network is typically attenuated in the context of task performance [143]. Motivated by the potential link between DMN function and episodic memory impairment in AD, several studies have investigated the functional connectivity of the DMN in AD patients and those at risk of developing the disease[144–146]. The most consistent finding across previous studies is a decrease in DMN functional connectivity in AD patients compared to healthy controls [147,148]. Other intrinsic networks, such as the salience and executive control networks which are known to modulate DMN activity, have since also been implicated in AD pathogenesis [149,150]. Studies have also reported a pattern of frontal hyperconnectivity in AD patients, suggesting that this may reflect a compensatory mechanism to support brain function when other intrinsic networks supporting memory are in dysregulation [151]. The posterior cingulate cortex (PCC), considered a critical hub for integrating and processing information across key intrinsic networks [152,153], is the most studied region in AD rsfMRI studies. Previous studies have indicated that in the posterior DMN – a sub-component of the DMN [154], functional alterations in the PCC precede the manifestation of cortical atrophy [155], and disruptions in this network occur early in the disease process [156].

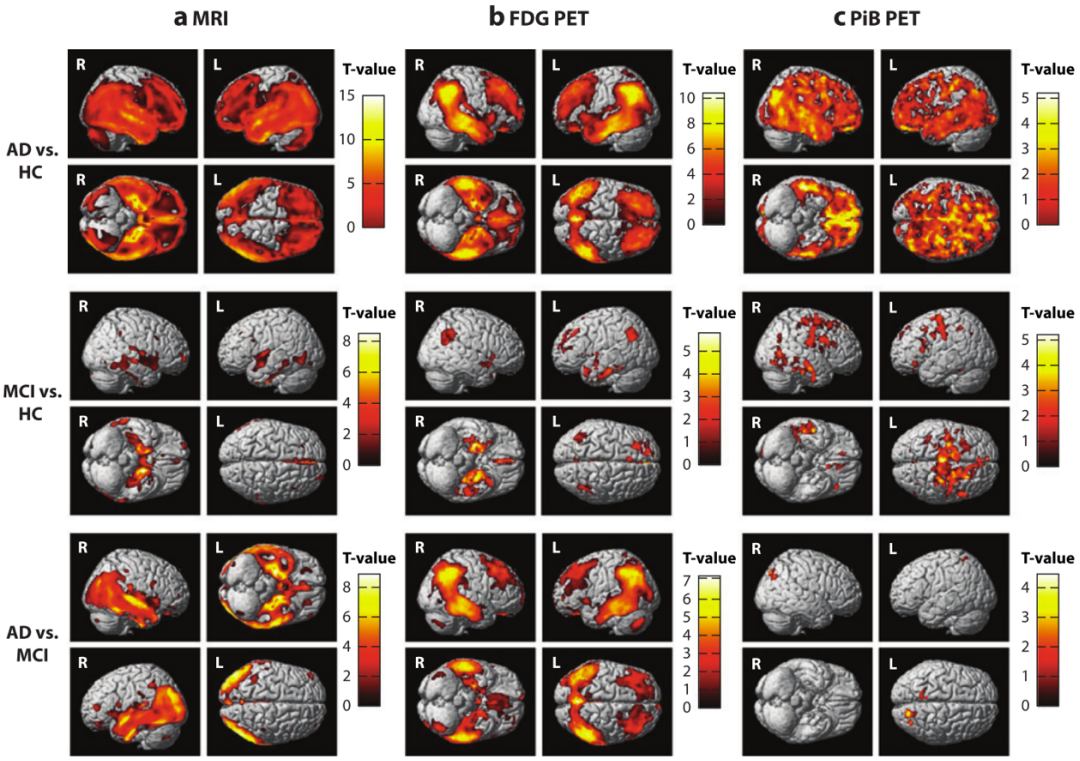

Figure 3: Differences in brain atrophy, metabolism, and Aβ deposition in the AD pathophysiological spectrum

The pattern of differences between AD patients, MCI subjects and Healthy Controls (HC) subjects is demonstrated in (a) brain atrophy, measured using structural MRI, (b) glucose metabolism, measured using FDG-PET, and (c) Aβ accumulation measuring using [^{11}C] PiB-PET. Relative to HC, patients with AD show significantly reduced brain grey matter (GM) density throughout cortical and subcortical regions (a; AD versus HC), reduced glucose metabolism in regions of the medial and lateral parietal lobe, medial and lateral temporal lobes, and medial and lateral frontal lobes (b; AD versus HC), as well as increased Aβ accumulation throughout the cerebral cortex (c; AD versus HC).MCI patients also show similar, although more focal, changes relative to HC, including reduced GM density in the medial and lateral temporal lobes (a; MCI versus HC), reduced glucose metabolism in the medial and lateral temporal lobes, medial and lateral parietal lobes, and frontal lobe (b; MCI versus HC), and greater Aβ deposition in the frontal, parietal, and temporal cortices (c; MCI versus HC). Specifically, patients with AD show significantly more GM atrophy in regions of the medial and lateral temporal lobes and parietal lobes (a; AD versus MCI) and reduced glucose metabolism in the medial and lateral temporal lobes, medial and lateral parietal lobes, and frontal lobe (b; AD versus MCI) relative to MCI patients. However, only minor differences in Aβ accumulation between AD and MCI patients are observed (c; AD versus MCI), suggesting the majority of Aβ accumulation occurs before a participant has reached the MCI stage.Figure from Risacher et al. [225]

NEUROIMAGING BIOMARKER SIGNATURE OF PATHOLOGY IN MCI

MCI is a clinical condition that is widely considered the intermediate stage from normal healthy and the eventual development of AD dementia. As a result, current biomarkers discovered in AD are being applied to the MCI stage in order to define a biomarker signature of pathology that might prospectively identify individuals at greatest risk of developing the disease in the future.

Structural MRI measurements have largely supported the notion of amnestic MCI representing a transitional stage of AD pathogenesis, with an intermediate severity of cortical atrophy between AD patients and healthy controls [157]. Although the presence of atrophy in AD is widespread throughout the neocortex, amnestic MCI is associated with a more focal pattern of structural vulnerability. Specifically, MCI patients exhibit significant atrophy in the MTL, particularly the hippocampus and entorhinal cortex, with focal reductions in temporal, parietal, and frontal regions [36,158] (Figure 1.4a). Studies have also used morphometric and 3-dimensional shape analysis methods to monitor the proliferation of atrophy in MCI patients as they progress over a short-term period of between 1-3 years. These patients showed an initial pattern of atrophy manifesting in MTL regions followed by an expansion to encompass more extensive cortical regions [31]. In particular, longitudinal studies have shown accelerated rates of atrophy in MCI patients [121,159,160], and greater rates of atrophy and ventricular enlargement when compared to healthy controls, especially amongst APOE ε4 carriers [33]. Moreover, pattern classification techniques using global and regional measures of atrophy have been able to distinguish MCI patients from normal healthy controls, with accuracies of ~85-89% [161]. Structural MRI measurements have also shown a prognostic potential in predicting MCI to AD conversion by retrospectively examining patients that convert to a probable AD diagnosis at future follow-up [45,128,162]. In some cases, these MCI-converter (those that progress to probable AD) patients exhibit similar patterns of widespread cortical atrophy when compared to AD patients up to two years prior to clinical conversion, relative to MCI patients that remain clinically stable over this period (MCI non-converters) [163]. The rates of cortical atrophy in MCI patients that convert to AD, particularly hippocampal and whole-brain measures, show an accelerated rate of decline [164]. Prediction studies have shown that

baseline MRI predictors, such as measures of hippocampal and entorhinal volume, demonstrate a prognostic ability in distinguishing MCI converters from MCI non-converters subjects with accuracies of ~75% [56,127,165]. Overall, structural MRI measurements can be used as antecedent markers of clinical progression of MCI to AD, as well as monitor disease progression in the MCI state.

In FDG-PET, MCI is associated with a lower cerebral glucose metabolism in similar regions affected in AD. Although the topography of these changes is not quite as extensive as observed in AD patients, MCI patients do show a pattern of hypometabolism in the posterior cingulate and hippocampus [166] (**Figure 1.4b**). In other studies, hypometabolism in some of these areas is also found to predict subsequent clinical conversion to probable AD [167,168], though distinguishing MCI converters from non-converters has been less successful than structural MRI measurements [56]. In particular, hypometabolism in the posterior cingulate and temporoparietal regions has been shown to predict future MCI to AD conversion, especially in combination with the APOE ε4 allele [169].

The use of Aβ PET methods, particularly studies using ^{11}[C] PiB, have shown that MCI patients have significantly higher ^{11}[C] PiB uptake compared to healthy controls in several areas, especially the frontal cortex, posterior cingulate, parietal and lateral temporal cortices, putamen, and caudate [170,171] (**Figure 1.4c**). Furthermore, clinical follow-up studies have also suggested that this pattern of high tracer uptake in MCI patients is predictive of future clinical conversion to probable AD [172]. However, longitudinal PET studies in AD patients have previously shown that there is relatively little tracer uptake during the progression of the disease, with the suggestion that most Aβ accumulation precedes cognitive impairment [13]. This evidence has been corroborated in MCI-converters to AD, who show relatively little annual increases in Aβ deposition when initially classified as Aβ-positive [71]. However, MCI patients that do not exhibit this pattern of Aβ accumulation, i.e. they are not classified as Aβ positive at baseline, may show some additional Aβ accumulation over time as they are considered to represent an atypical trajectory of AD development. Consequently, these methods have an important role as a biomarker for identifying MCI patients who are on the typical trajectory of future AD development.

In other advanced imaging techniques such as DTI, studies have further investigated the posterior circuitry (hippocampus, parahippocampal WM, posterior cingulate, and cingulum bundle) that is preferentially affected in AD. In general, MCI patients show an intermediate reduction of FA relative to healthy controls and AD patients in the cingulum bundle, temporal WM, hippocampus, and posterior cingulate regions [173]. In particular, the microstructural abnormalities present in the cingulum bundle have been linked to cognitive performance on delayed verbal recall tests of episodic memory function [138]. WM regions that connect the posterior cingulum to limbic structures have also been shown to be affected in MCI patients, with FA reductions reported in parietal and temporal WM. Parahippocampal WM, in particular, fibres that project from the hippocampus and entorhinal cortex, have also been reported as being affected in MCI patients [173]. Although distinctive similarities in tensor abnormalities between AD and MCI patients can be observed, it must be noted that there are many conflicting findings on the regional integrity of DTI measures. Some studies report no significant differences between MCI patients and healthy controls, while others have failed to reproduce earlier findings with consistency [174]. The most consistent findings have shown that more pronounced changes in WM microstructure are present in posterior regions in both AD and MCI patients. Since these regions are strongly implicated in memory function, they may help provide a more detailed representation of the WM pathways affected during the different stages of AD. Studies with further well-characterised MCI cases representative of its heterogeneity in the general population, as well as advances in DTI pulse sequences, will help improve our ability to observe more consistent findings in WM microstructure differences between AD and MCI patients.

On the other hand, rsfMRI studies in MCI patients have predominantly focused on the functional connectivity of the DMN, as this network is primarily active during episodic and autobiographical memory retrieval, but shows a decrease in activity during the performance on cognitive tasks that require attention. A recent study by Binnewijzend and colleagues [175], investigated the regional functional connectivity of the DMN, and found that MCI patients exhibited intermediate values of functional connectivity between AD patients and healthy controls, and these changes were subsequently found to be correlated with measures of cognitive dysfunction.

This is somewhat consistent with previous studies that have found DMN changes in AD patients [176,177], but recent meta-analyses of rsfMRI studies have highlighted the importance of posteromedial regions – areas particularly vulnerable to amyloid pathology, as being associated with the early stages of the disease process [178,179]. These posterior midline structures are also particularly vulnerable to hypometabolism, and previous work has shown that disruption of the PCC can lead to synaptic dysfunction in the hippocampus and eventual cognitive decline [146]. Evidence has suggested that the deterioration of the DMN is characterised by a breakdown in the posterior portions (primarily the PCC and precuneal regions), and by decreased connectivity between anterior and posterior sub-networks of the DMN [145,154]. This anterior-posterior disconnection is associated with an hypoconnectivity in the posterior DMN and hyperconnectivity of the anterior DMN. These reciprocal changes in the connectivity of the DMN have been suggested to signal the early signs of brain dysfunction in the pathophysiology of AD. However, the findings have been inconsistent, with some studies reporting reduced connectivity in the posterior DMN [180], and others reporting a notable increase in functional connectivity of this region [181] in MCI patients.

Some argue that hyperconnectivity in the posterior DMN precedes hypoconnectivity, as Bai and colleagues found that amnestic MCI patients exhibited this increased functional connectivity pattern, but later at follow-up, when the disease had progressed, connectivity in these areas was decreased, followed by an increased connectivity in the frontal lobes. These results suggest there is a complex interplay in the functional architecture of the DMN, primarily the posteromedial cortex hub, which has distinct functional connectivity cascades during different stages of the disease. It is important to note that despite the inconsistent findings, connectivity changes do follow the Braak stages of neuropathology, affecting the MTL regions first, followed by extensive tauopathy in the posterolateral regions of the brain, and eventually the frontal cortex. Consequently, the evidence highlights the potential of rsfMRI as a biomarker for incipient AD, but further work is needed in order to evaluate the variability and stability of these large-scale networks in the general population.

In summary, amnestic MCI patients display significant AD-related neuropathology, most notably brain atrophy in MTL structures, glucose hypometabolism detected by FDG-PET, amyloid accumulation, and alterations in brain function at rest. These biomarkers, in particular

structural MRI, often indicate that MCI patients with a greater AD-like neuroimaging phenotype of pathology are most likely to progress to the disease in the future. The enhancement of other biomarkers, such as DTI and rsfMRI in the future, may allow us to detect these individuals prior to development of brain atrophy. Biomarkers for characterising MCI subtypes are now being defined for their use in clinical settings for detecting the prodromal stages of disease.

NEUROIMAGING BIOMARKER SIGNATURE OF PATHOLOGY IN PRECLINICAL AD

With the emergence of investigational Aβ-modifying treatments in proposed prevention trials, the impetus to diagnose AD in its pre-clinical stages – before significant brain atrophy has ensued, has intensified. Many investigators believe the ideal preventive treatment would be prior to the emergence of the MCI clinical syndrome [6]. Recent advances in neuroimaging techniques now provide the ability to detect evidence of AD pathophysiological changes prior to the emergence of clinical symptoms. Emerging data from studies of clinically normal individuals suggest that biomarker evidence of Aβ accumulation is associated with structural and functional abnormalities in the brain, consistent with the pattern of changes observed in AD and MCI patients [182].

As a result, here, primarily three different avenues for identifying preclinical patients will be discussed: 1) cognitively normal individuals reflecting abnormal levels of Aβ accumulation using PET Aβ methods and CSF levels of abnormal Aβ ($_{1-42}$), 2) Individuals identified through a genetic risk for the disease, and 3) Older adults with cognitive complaints of a subjective nature, with no overt deficits in cognitive functioning.

Initial Aβ studies have been able to show that that 25% to 30% of healthy adults with normal cognition are Aβ positive [132,183]. Subsequent longitudinal studies have further corroborated this evidence and shown that Aβ accumulation is accompanied with subtle declines in cognition [184], as well as a greater risk of progression to memory impairment and an eventual AD diagnosis [185]. As a result, these subjects may represent a pre-clinical biomarker phenotype for characterising the earliest pathophysiological changes associated with the disease. Moreover, recent work has shown that emerging Aβ pathology is associated with cortical atrophy. For instance, some studies report structural changes in stereotypical areas associated with AD, such as the temporal cortex and hippocampal structures [186], whereas others report more subtle patterns of atrophy in regions less commonly associated with AD, such as the frontal lobes [187]. The disparity of findings from imaging studies of preclinical patients suggests that the temporal evolution of biomarker evidence is heterogeneous and varies on an individual level. Since the formulation of the NIA-AA pre-

clinical staging criteria for AD [6], a two-feature biomarker classification system has been adopted based on Aβ pathology and tau neurodegeneration. This provides an avenue for characterising the temporal overlap of biomarker trajectories between normal healthy ageing and preclinical AD, as well as, representing the full pathophysiological spectrum of typical and atypical AD risk.

Amongst Aβ positive cognitively normal individuals, rsfMRI studies have also demonstrated similar AD-like aberrant functional connectivity patterns in networks such as the DMN [152]. In particular, these individuals showed a decrease in DMN activity and distinctive correlation patterns between ^{11}[C] PiB retention and functional connectivity of the DMN [156]. Since, Lim and colleagues [188] have demonstrated more widespread functional connectivity cascades in pre-clinical AD patients, particularly in other stable networks such as the salience and central executive networks, which are known to share a reciprocal relationship in modulating the DMN. Functional abnormalities in preclinical patients has been further supported by FDG-PET, revealing poor glucose metabolism in areas of typically high metabolic activity, such as the posterior cingulate [189]. Although Aβ pathology is considered to increase the risk of future cognitive decline in older adults, some individuals are known to exhibit normal cognitive abilities despite high levels of Aβ burden in the brain. According to the cognitive reserve hypothesis, individuals with higher cognitive reserve can sustain normal cognitive function in the presence of AD-related pathology, as well as potentially stave off the sequelae associated with neurodegeneration [190]. In particular, a study using FDG-PET showed that individuals with greater cognitive reserve and high levels of Aβ burden had lower levels of glucose metabolism in the posterior cingulate, thus suggesting cognitive reserve has a compensatory function to sustain cognitive ability in the presence of AD pathology [191]. In contrast, others argue that the presence of such latent pathology may simply reflect non-pathological age-related decline as part of a normal healthy ageing process [192]. Altogether, these findings suggest that cognitive reserve plays an important role in understanding cognitive ability in the presence of typical AD neuropathology.

Other than the presence of Aβ pathology, healthy APOE ε4 carriers also show accelerated rates of cognitive decline [193], suggesting that the genetic risk of APOE ε4 is associated with cognitive decline years before memory impairment is clinically apparent. Structural

neuroimaging APOE studies have also found that APOE ε4 carriers generally exhibit higher rates of atrophy, particularly in regions commonly affected in AD, such as the MTL and temporoparietal regions, compared to non-carriers. Although studies do report brain differences associated with APOE ε4, many argue that in some this only represents non-pathological changes that are age-dependent, as not all APOE ε4 carriers go on to develop AD. [194]. However, these mixed findings may be attributed to differences in the aetiological representation of future AD-risk, particularly in some that could have an atypical trajectory of development.

Further insights into better characterising the pre-clinical stages of AD have come through understanding the relationship between APOE ε4 and Aβ metabolism. APOE ε4 has been well understood to influence Aβ accumulation and metabolism – studies show that APOE ε4 strongly affects Aβ deposition to form senile plaques and cause cerebral Aβ angiopathy [105,195]. Further evidence suggests that APOE ε4 combines synergistically with Aβ accumulation to promote cognitive decline in healthy older individuals, and that these individuals also possess subtle patterns of brain atrophy in similar regions associated with early AD and MCI [187,196].

Interestingly, APOE ε4 has differential effects on cognition and the brain depending on age. For instance, some studies in young adults and children have demonstrated evidence of better memory performance in APOE ε4 carriers compared to non-carriers, which could suggest antagonistic pleiotropy [197], whereas others report evidence of a detrimental effect of APOE ε4 on brain neurodevelopment in children and adolescents [198]. While studies have suggested that Aβ deposition in the brain begins many decades prior to AD development, recent neuroimaging studies have shown that structural and functional alterations may precede Aβ accumulation in APOE ε4 carriers [199]. This has since led to a further impetus to explore even earlier brain differences in young children and infants possessing the APOE ε4 variant.

An early study by Filippini et al [200], showed that APOE ε4 modulates brain function and activity decades prior to any clinical representation of neurodegeneration. This has led

researchers to postulate that APOE ε4 may possess neurodevelopmental changes that provides a foothold for a pathological cascade leading to subsequent AD [201]. Some multimodal imaging studies have since shown that APOE ε4 is associated with alterations in grey matter volume, white-matter, and brain function, both at rest and during a memory-encoding paradigm [201,202]. Despite this, it is difficult to imply that these early brain changes in infancy and childhood are solely associated with detrimental effects of APOE ε4. Neurodevelopment in infancy and later adolescence is a period in which several neurobiological processes may influence asynchronous brain maturation, thus making it difficult to isolate early brain changes to the effects of APOE ε4.

Finally, cognitively normal older individuals who have significant cognitive complaints, or report subjective memory impairment also represent a subset of individuals with a preclinical risk of developing AD [203]. Subjective memory impairment is defined as below-normal performance on memory tests, largely unimpaired functional activities of daily living, and the absence of dementia [204]. Studies have reported that, compared to those with no subjective memory complaints, individuals with subjective memory complaints show medial temporal lobe atrophy [205], cerebral glucose hypometabolism [39], an AD-like CSF biomarker phenotype [206], and more frequent AD neuropathology at autopsy. Epidemiological studies have shown that these individuals also have a higher likelihood of future cognitive decline and progression to MCI [207,208]. However, a lack of standardised definitions for subjective memory complaints has made it difficult to characterise this population and distinguish them from a normal healthy population. Further progress in developing standardised criteria will help provide an earlier detection of memory complaints in amnestic and non-amnestic cases and monitor AD risk.

REFERENCES

[1] Alzheimer A (1907) Uber eine eigenartige Erkrankung der Hirnrinde. Allg Z Psychiat Med 64, 146–8.

[2] Batsch N, Mittelman M (2012) World Alzheimer Report 2012: Overcoming the stigma of dementia, , London.

[3] Alzheimer's Disease International (ADI) (2015) World Alzheimer Report 2015, The Global Economic Impact of Dementia. Alzheimer's Dis. Int. (ADI) 1–52.

[4] Prince M, Wimo A, Guerchet M, Gemma-Claire A, Wu Y-T, Prina M (2015) World Alzheimer Report 2015: The Global Impact of Dementia - An analysis of prevalence, incidence, cost and trends. Alzheimer's Dis. Int. 84.

[5] Mawuenyega KG, Sigurdson W, Ovod V, Munsell L, Kasten T, Morris JC, Yarasheski KE, Bateman RJ (2010) Decreased Clearance of CNS b-Amyloid in Alzheimer's Disease. Science (80-.). 330, 1174–1174.

[6] Sperling RA, Aisen PS, Beckett LA, Bennett DA, Craft S, Fagan AM, Iwatsubo T, Jack CR, Kaye J, Montine TJ, Park DC, Reiman EM, Rowe CC, Siemers E, Stern Y, Yaffe K, Carrillo MC, Thies B, Morrison-Bogorad M, Wagster M V, Phelps CH (2011) Toward defining the preclinical stages of Alzheimer's disease: recommendations from the National Institute on Aging-Alzheimer's Association workgroups on diagnostic guidelines for Alzheimer's disease. Alzheimer's Dement 7, 280–92.

[7] Blennow K (2004) Cerebrospinal Fluid Protein Biomarkers for Alzheimer's Disease. NeuroRx J. Am. Soc. Exp. Neurother. 1, 213–225.

[8] Andreasen N, Sjögren M, Blennow K (2003) CSF markers for Alzheimer's disease: total tau, phospho-tau and Abeta42. world J. Biol. psychiatry Off. J. World Fed. Soc. Biol. Psychiatry 4, 147–155.

[9] Wildsmith KR, Holley M, Savage JC, Skerrett R, Landreth GE (2013) Evidence for impaired amyloid β clearance in Alzheimer's disease. Alzheimers Res Ther 5, 33.

[10] Iqbal K, Grundke-Iqbal I (2008) Alzheimer neurofibrillary degeneration: Significance, etiopathogenesis, therapeutics and prevention: Alzheimer Review Series. J Cell Mol Med 12, 38–55.

[11] Hampel H, Blennow K, Shaw LM, Hoessler YC, Zetterberg H, Trojanowski JQ (2010) Total

and Phosphorylated tau protein as biological markers of Alzheimer's disease. Exp Gerontol 45, 30.

[12] Jack CR, Knopman DS, Jagust WJ, Shaw LM, Aisen PS, Weiner MW, Petersen RC, Trojanowski JQ (2010) Hypothetical model of dynamic biomarkers of the Alzheimer's pathological cascade. Lancet Neurol. 9, 119–28.

[13] Villemagne VL, Burnham S, Bourgeat P, Brown B, Ellis K a, Salvado O, Szoeke C, Macaulay SL, Martins R, Maruff P, Ames D, Rowe CC, Masters CL (2013) Amyloid β deposition, neurodegeneration, and cognitive decline in sporadic Alzheimer's disease: a prospective cohort study. Lancet Neurol 12, 357–67.

[14] Jack CR, Knopman DS, Jagust WJ, Petersen RC, Weiner MW, Aisen PS, Shaw LM, Vemuri P, Wiste HJ, Weigand SD, Lesnick TG, Pankratz VS, Donohue MC, Trojanowski JQ (2013) Tracking pathophysiological processes in Alzheimer's disease: an updated hypothetical model of dynamic biomarkers. Lancet Neurol 12, 207–16.

[15] Erik D. Roberson, Kimberly Scearce-Levie, Jorge J. Palop FY, Irene H. Cheng, Tiffany Wu, Hilary Gerstein, Gui-Qiu Yu 1 Lennart Mucke (2007) Reducing Endogenous Tau Ameliorates Amyloid b–Induced Deficits in an Alzheimer's Disease Mouse Model. Science (80-.). 316, 750–754.

[16] Braak H, Braak E (1991) Neuropathological stageing of Alzheimer-related changes. Acta Neuropathol 82, 239–259.

[17] Braak H, Del Tredici K (2015) The pathological process underlying Alzheimer's disease in individuals under thirty. Brain 138, 171–181.

[18] McKhann GM, Knopman DS, Chertkow H, Hyman BT, Jack CR, Kawas CH, Klunk WE, Koroshetz WJ, Manly JJ, Mayeux R, Mohs RC, Morris JC, Rossor MN, Scheltens P, Carrillo MC, Thies B, Weintraub S, Phelps CH (2011) The diagnosis of dementia due to Alzheimer's disease: recommendations from the National Institute on Aging-Alzheimer's Association workgroups on diagnostic guidelines for Alzheimer's disease. Alzheimers Dement 7, 335–337.

[19] Dubois B, Feldman HH, Jacova C, Dekosky ST, Barberger-Gateau P, Cummings J, Delacourte A, Galasko D, Gauthier S, Jicha G, Meguro K, O'brien J, Pasquier F, Robert P, Rossor M, Salloway S, Stern Y, Visser PJ, Scheltens P (2007) Research criteria for the diagnosis of Alzheimer's disease: revising the NINCDS-ADRDA criteria. Lancet Neurol 6, 734–46.

[20] Petersen RC, Smith GE, Waring SC, Ivnik RJ, Tangalos EG, Kokmen E (1999) Mild Cognitive Impairment: Clinical Characterization and Outcome. Arch. Neurol. 56, 303–308.

[21] Petersen RC, Stevens JC, Ganguli M, Tangalos EG, Cummings JL, DeKosky ST (2001) Practice parameter: early detection of dementia: mild cognitive impairment (an evidence-based review). Report of the Quality Standards Subcommittee of the American Academy of Neurology. Neurology 56, 1133–1142.

[22] Albert MS, DeKosky ST, Dickson D, Dubois B, Feldman HH, Fox NC, Gamst A, Holtzman DM, Jagust WJ, Petersen RC, Snyder PJ, Carrillo MC, Thies B, Phelps CH (2011) The diagnosis of mild cognitive impairment due to Alzheimer's disease: Recommendations from the National Institute on Aging-Alzheimer's Association workgroups on diagnostic guidelines for Alzheimer's disease. Alzheimers Dement 7, 270–279.

[23] Dubois B, Feldman HH, Jacova C, Cummings JL, Dekosky ST, Barberger-Gateau P, Delacourte A, Frisoni G, Fox NC, Galasko D, Gauthier S, Hampel H, Jicha GA, Meguro K, O'Brien J, Pasquier F, Robert P, Rossor M, Salloway S, Sarazin M, De Souza LC, Stern Y, Visser PJ, Scheltens P (2010) Revising the definition of Alzheimer's disease: a new lexicon. Lancet Neurol 9, 1118–1127.

[24] Jack CR, Albert MS, Knopman DS, McKhann GM, Sperling RA, Carrillo MC, Thies B, Phelps CH (2011) Introduction to the recommendations from the National Institute on Aging-Alzheimer's Association workgroups on diagnostic guidelines for Alzheimer's disease. Alzheimers Dement 7, 257–262.

[25] Prestia A, Caroli A, Van Der Flier WM, Ossenkoppele R, Van Berckel B, Barkhof F, Teunissen CE, Wall AE, Carter SF, Schöll M, Choo IH, Nordberg A, Scheltens P, Frisoni GB (2013) Prediction of dementia in MCI patients based on core diagnostic markers for Alzheimer disease. Neurology 80, 1048–1056.

[26] Möller I, Gharbi M, Serrano HM, Barbero MH, Milano JV, Henrotin Y, Goldring S, Goldring M, Kraus V, Burnett B, Coindreau J, Cottrell S, Eyre D, Gendreau M, Gardiner J, Garnero P, Hardin J, Henrotin Y, Lotz M, Martel-Pelletier J, Christiansen C, Brandi M, Bruyere O, Chapurlat R, Collette J, Cooper C, Giacovelli G, Kanis J, Henrotin Y, Addison S, Kraus V, Deberg M, Birmingham J, Vilim V, Kraus V, Henrotin Y, Deberg M, Dubuc J, Quettier E, Christgau S, Reginster J, Deberg M, Labasse A, Christgau S, Cloos P, Henriksen DB, Chapelle J, Zegels B, Reginster J, Henrotin Y, Deberg M, Labasse A, Collette J, Seidel L, Reginster J, Henrotin Y, Dougados M, Clegg D, Reda D, Harris C, Klein M, O'Dell J, Hooper

M, Bradley J, Bingham C, Weisman M, Jackson C, Uebelhart D, Malaise M, Marcolongo R, DeVathaire F, Piperno M, Mailleux E, Fioravanti A, Matoso L, Vignon E, Uebelhart D, Thonar E, Delmas P, Chantraine A, Vignon E, Kahan A, Uebelhart D, Vathaire F, Delmas P, Reginster J, Verbruggen G, Goemaere S, Veys E, Verbruggen G, Goemaere S, Veys E, Wildi L, Raynauld J, Martel-Pelletier J, Beaulieu A, Bessette L, Morin F, Abram F, Dorais M, Pelletier J, Altman R, Asch E, Bloch D, Bole G, Borenstein D, Brandt K, Christy W, Cooke T, Greenwald R, Hochberg M, Kellgren J, Lawrence J, Wolfe F, Smythe H, Yunus M, Bennett R, Bombardier C, Goldenberg D, Tugwell P, Campbell S, Abeles M, Clark P, Wolfe F, Clauw D, Fitzcharles M, Goldenberg D, Hauser W, Katz R, Mease P, Russell A, Russell I, Winfield J, Pham T, Heijde D, Lassere M, Altman R, Anderson J, Bellamy N, Hochberg M, Simon L, Strand V, Woodworth T, Huskisson E, Lequesne M, Kraus V, Gabay C, Medinger-Sadowski C, Gascon D, Kolo F, Finckh A, Lequesne M, Wagner J, Williams S, Webster C, Conrozier T, Balblanc J, Richette P, Mulleman D, Maillet B, Henrotin Y, Rannou F, Piroth C, Hilliquin P, Mathieu P, Henrotin Y, Chevalier X, Deberg M, Balblanc J, Richette P, Mulleman D, Maillet B, Rannou F, Piroth C, Mathieu P (2001) Biomarkers and surrogate endpoints: Preferred definitions and conceptual framework. Clin. Pharmacol. Ther.

[27] Hampel H, Frank R, Broich K, Teipel SJ, Katz RG, Hardy J, Herholz K, Bokde ALW, Jessen F, Hoessler YC, Sanhai WR, Zetterberg H, Woodcock J, Blennow K (2010) Biomarkers for Alzheimer's disease: academic, industry and regulatory perspectives. Nat Rev Drug Discov 9, 560–574.

[28] Blennow K, Hampel H (2003) CSF markers for incipient Alzheimer's disease. Lancet 2, 605–613.

[29] Shaw LM, Korecka M, Clark CM, Lee VM-Y, Trojanowski JQ (2007) Biomarkers of neurodegeneration for diagnosis and monitoring therapeutics. Nat Rev Drug Discov 6, 295–303.

[30] Humpel C (2011) Identifying and validating biomarkers for Alzheimer's disease. Trends Biotechnol. 29, 26–32.

[31] Devanand DP, Pradhaban G, Liu X, Khandji A, De Santi S, Segal S, Rusinek H, Pelton GH, Honig LS, Mayeux R, Stern Y, Tabert MH, de Leon MJ (2007) Hippocampal and entorhinal atrophy in mild cognitive impairment: prediction of Alzheimer disease. Neurology 68, 828–36.

[32] Klöppel S, Stonnington CM, Chu C, Draganski B, Scahill RI, Rohrer JD, Fox NC, Jack CR, Ashburner J, Frackowiak RSJ (2008) Automatic classification of MR scans in Alzheimer's disease. Brain 131, 681–9.

[33] Schuff N, Woerner N, Boreta L, Kornfield T, Shaw LM, Trojanowski JQ, Thompson PM, Jack CR, Weiner MW (2009) MRI of hippocampal volume loss in early Alzheimer's disease in relation to ApoE genotype and biomarkers. Brain 132, 1067–77.

[34] Jack CR, Dickson DW, Parisi JE, Xu YC, Cha RH, O'Brien PC, Edland SD, Smith GE, Boeve BF, Tangalos EG, Kokmen E, Petersen RC (2002) Antemortem MRI findings correlate with hippocampal neuropathology in typical aging and dementia. Neurology 58, 750–7.

[35] Vemuri P, Gunter JL, Senjem ML, Whitwell JL, Kantarci K, Knopman DS, Boeve BF, Petersen RC, Jack CR (2008) Alzheimer's disease diagnosis in individual subjects using structural MR images: validation studies. Neuroimage 39, 1186–97.

[36] Whitwell JL, Josephs KA, Murray ME, Kantarci K, Przybelski SA, Weigand SD, Vemuri P, Senjem ML, Parisi JE, Knopman DS, Boeve BF, Petersen RC, Dickson DW, Jack CR (2008) MRI correlates of neurofibrillary tangle pathology at autopsy: A voxel-based morphometry study. Neurology 71, 743–749.

[37] Whitwell JL, Dickson DW, Murray ME, Weigand SD, Tosakulwong N, Senjem ML, Knopman DS, Boeve BF, Parisi JE, Petersen RC, Jack CR, Josephs KA (2012) Neuroimaging correlates of pathologically defined subtypes of Alzheimer's disease: A case-control study. Lancet Neurol 11, 868–877.

[38] Thompson PM, Hayashi KM, De Zubicaray GI, Janke AL, Rose SE, Semple J, Hong MS, Herman DH, Gravano D, Doddrell DM, Toga AW (2004) Mapping hippocampal and ventricular change in Alzheimer disease. Neuroimage 22, 1754–1766.

[39] Scheef L, Spottke A, Daerr M, Joe A, Striepens N, Kölsch H, Popp J, Daamen M, Gorris D, Heneka MT, Boecker H, Biersack HJ, Maier W, Schild HH, Wagner M, Jessen F (2012) Glucose metabolism, gray matter structure, and memory decline in subjective memory impairment. Neurology 79, 1332–9.

[40] McDonald CR, McEvoy LK, Gharapetian L, Fennema-Notestine C, Hagler DJ, Holland D, Koyama A, Brewer JB, Dale AM (2009) Regional rates of neocortical atrophy from normal aging to early Alzheimer disease. Neurology 73, 457–465.

[41] Frisoni GB, Fox NC, Jack CR, Scheltens P, Thompson PM (2010) The clinical use of

structural MRI in Alzheimer disease. Nat Rev Neurol 6, 67–77.

[42] Jack CR, Petersen RC, O'Brien PC, Tangalos EG (1992) MR-based hippocampal volumetry in the diagnosis of Alzheimer's disease. Neurology 42, 183–188.

[43] Csernansky JG, Wang L, Swank J, Miller JP, Gado M, McKeel D, Miller MI, Morris JC (2005) Preclinical detection of Alzheimer's disease: hippocampal shape and volume predict dementia onset in the elderly. Neuroimage 25, 783–792.

[44] Kantarci K (2005) Magnetic resonance markers for early diagnosis and progression of Alzheimer's disease. Expert Rev Neurother 5, 663–670.

[45] Devanand DP, Liu X, Tabert MH, Pradhaban G, Cuasay K, Bell K, de Leon MJ, Doty RL, Stern Y, Pelton GH (2008) Combining early markers strongly predicts conversion from mild cognitive impairment to Alzheimer's disease. Biol. Psychiatry 64, 871–9.

[46] Scheltens P, Launer LJ, Barkhof F, Weinstein HC, van Gool WA (1995) Visual assessment of medial temporal lobe atrophy on magnetic resonance imaging: interobserver reliability. J.Neurol. 242, 557–560.

[47] Wahlund LO, Julin P, Johansson SE, Scheltens P (2000) Visual rating and volumetry of the medial temporal lobe on magnetic resonance imaging in dementia: a comparative study. [Comment In: J Neurol Neurosurg Psychiatry. 2000 Nov;69(5):572 UI: 20487598]. J Neurol Neurosurg Psychiatry 69, 630–635.

[48] Doring TM, Kubo TTA, Cruz LCH, Juruena MF, Fainberg J, Domingues RC, Gasparetto EL (2011) Evaluation of hippocampal volume based on MR imaging in patients with bipolar affective disorder applying manual and automatic segmentation techniques. J Magn Reson Imaging 33, 565–572.

[49] Wenger E, Mårtensson J, Noack H, Bodammer NC, Kühn S, Schaefer S, Heinze HJ, Düzel E, Bäckman L, Lindenberger U, Lövdén M (2014) Comparing manual and automatic segmentation of hippocampal volumes: Reliability and validity issues in younger and older brains. Hum Brain Mapp 35, 4236–4248.

[50] Morey R a., Petty CM, Xu Y, Pannu Hayes J, Wagner HR, Lewis D V., LaBar KS, Styner M, McCarthy G (2009) A comparison of automated segmentation and manual tracing for quantifying hippocampal and amygdala volumes. Neuroimage 45, 855–866.

[51] Pardoe HR, Pell GS, Abbott DF, Jackson GD (2009) Hippocampal volume assessment in temporal lobe epilepsy: How good is automated segmentation? Epilepsia 50, 2586–92.

[52] Fischl B, H Salat D, Busa E, Albert M, Dieterich M, Haselgrove C, Van Der Kouwe A, Killiany

R, Kennedy D, Klaveness S, Montillo A, Makris N, Rosen B, Dale AM (2002) Whole brain segmentation: automated labeling of neuroanatomical structures in the human brain. Neuron 33, 341–355.

[53] Klöppel S, Stonnington CM, Barnes J, Chen F, Chu C, Good CD, Mader I, Mitchell LA, Patel AC, Roberts CC, Fox NC, Jack CR, Ashburner J, Frackowiak RSJ (2008) Accuracy of dementia diagnosis: a direct comparison between radiologists and a computerized method. Brain 131, 2969–74.

[54] Cui Y, Liu B, Luo S, Zhen X, Fan M, Liu T, Zhu W, Park M, Jiang T, Jin JS (2011) Identification of Conversion from Mild Cognitive Impairment to Alzheimer's Disease Using Multivariate Predictors. PLoS One 6, e21896.

[55] Davatzikos C, Xu F, An Y, Fan Y, Resnick SM (2009) Longitudinal progression of Alzheimer's-like patterns of atrophy in normal older adults: the SPARE-AD index. Brain 132, 2026–35.

[56] Zhang D, Wang Y, Zhou L, Yuan H, Shen D (2011) Multimodal classification of Alzheimer's disease and mild cognitive impairment. Neuroimage 55, 856–867.

[57] Langbaum JBS, Chen K, Lee W, Reschke C, Bandy D, Fleisher AS, Alexander GE, Foster NL, Weiner MW, Koeppe RA, Jagust WJ, Reiman EM (2009) Categorical and correlational analyses of baseline fluorodeoxyglucose positron emission tomography images from the Alzheimer's Disease Neuroimaging Initiative (ADNI). Neuroimage 45, 1107–1116.

[58] Jagust WJ, Bandy D, Chen K, Foster NL, Landau SM, Mathis C a, Price JC, Reiman EM, Skovronsky D, Koeppe R a (2010) The Alzheimer's Disease Neuroimaging Initiative positron emission tomography core. Alzheimer's Dement 6, 221–9.

[59] Klunk WE, Engler H, Nordberg A, Wang Y, Blomqvist G, Holt DP, Bergström M, Savitcheva I, Huang G, Estrada S, Ausén B, Debnath ML, Barletta J, Price JC, Sandell J, Lopresti BJ, Wall A, Koivisto P, Antoni G, Mathis CA, Långström B (2004) Imaging brain amyloid in Alzheimer's disease with Pittsburgh Compound-B. Ann. Neurol. 55, 306–319.

[60] Vandenberghe R, Van Laere K, Ivanoiu A, Salmon E, Bastin C, Triau E, Hasselbalch S, Law I, Andersen A, Korner A, Minthon L, Garraux G, Nelissen N, Bormans G, Buckley C, Owenius R, Thurfjell L, Farrar G, Brooks DJ (2010) 18F-flutemetamol amyloid imaging in Alzheimer disease and mild cognitive impairment a phase 2 trial. Ann Neurol 68, 319–329.

[61] Clark CM, Schneider JA, Bedell BJ, Beach TG, Bilker WB, Mintun M a, Pontecorvo MJ,

Hefti F, Carpenter AP, Flitter ML, Krautkramer MJ, Kung HF, Coleman RE, Doraiswamy PM, Fleisher AS, Sabbagh MN, Sadowsky CH, Reiman EP, Reiman PEM, Zehntner SP, Skovronsky DM (2011) Use of florbetapir-PET for imaging beta-amyloid pathology. JAMA 305, 275–83.

[62] Villemagne VL, Fodero-tavoletti MT, Masters CL, Rowe CC (2015) Tau imaging : early progress and future directions. Lancet Neurol 14, 114–124.

[63] Salmon E, Sadzot B, Maquet P, Degueldre C, Lemaire C, Rigo P, Comar D, Franck G (1994) Differential diagnosis of Alzheimer's disease with PET. J Nucl Med 35, 391–398.

[64] Mosconi L, Berti V, Glodzik L, Pupi A, De Santi S, De Leon MJ (2010) Pre-clinical detection of Alzheimer's disease using FDG-PET, with or without amyloid imaging. J Alzheimers Dis 20, 843–854.

[65] Coleman RE (2005) Positron emission tomography diagnosis of Alzheimer's disease. Neuroimaging Clin N Am 15, 837–846.

[66] Silverman DH, Small GW, Chang CY, Lu CS, Kung De Aburto MA, Chen W, Czernin J, Rapoport SI, Pietrini P, Alexander GE, Schapiro MB, Jagust WJ, Hoffman JM, Welsh-Bohmer KA, Alavi A, Clark CM, Salmon E, de Leon MJ, Mielke R, Cummings JL, Kowell AP, Gambhir SS, Hoh CK, Phelps ME (2001) Positron emission tomography in evaluation of dementia: Regional brain metabolism and long-term outcome. JAMA 286, 2120–2127.

[67] Johnson KA, Gregas M, Becker JA, Kinnecom C, Salat DH, Moran EK, Smith EE, Rosand J, Rentz DM, Klunk WE, Mathis CA, Price JC, DeKosky ST, Fischman AJ, Greenberg SM (2007) Imaging of amyloid burden and distribution in cerebral amyloid angiopathy. Ann Neurol 62, 229–234.

[68] Ossenkoppele R, Jansen WJ, Rabinovici GD, Knol DL, van der Flier WM, van Berckel BNM, Scheltens P, Visser PJ, Verfaillie SCJ, Zwan MD, Adriaanse SM, Lammertsma AA, Barkhof F, Jagust WJ, Miller BL, Rosen HJ, Landau SM, Villemagne VL, Rowe CC, Lee DY, Na DL, Seo SW, Sarazin M, Roe CM, Sabri O, Barthel H, Koglin N, Hodges J, Leyton CE, Vandenberghe R, van Laere K, Drzezga A, Forster S, Grimmer T, Sánchez-Juan P, Carril JM, Mok V, Camus V, Klunk WE, Cohen AD, Meyer PT, Hellwig S, Newberg A, Frederiksen KS, Fleisher AS, Mintun MA, Wolk DA, Nordberg A, Rinne JO, Chételat G, Lleo A, Blesa R, Fortea J, Madsen K, Rodrigue KM, Brooks DJ (2015) Prevalence of Amyloid PET Positivity in Dementia Syndromes. JAMA 313, 1939.

[69] Jack CR, Wiste HJ, Weigand SD, Knopman DS, Vemuri P, Mielke MM, Lowe V, Senjem

ML, Gunter JL, Machulda MM, Gregg BE, Pankratz VS, Rocca WA, Petersen RC (2015) Age, Sex, and APOE ε4 Effects on Memory, Brain Structure, and β-Amyloid Across the Adult Life Span. JAMA Neurol 55905, 1–9.

[70] Villain N, Chételat G, Grassiot B, Bourgeat P, Jones G, Ellis KA, Ames D, Martins RN, Eustache F, Salvado O, Masters CL, Rowe CC, Villemagne VL (2012) Regional dynamics of amyloid-?? deposition in healthy elderly, mild cognitive impairment and Alzheimer's disease: A voxelwise PiB-PET longitudinal study. Brain 135, 2126–2139.

[71] Jack CR, Wiste HJ, Lesnick TG, Weigand SD, Knopman DS, Vemuri P, Pankratz VS, Senjem ML, Gunter JL, Mielke MM, Lowe VJ, Boeve BF, Petersen RC (2013) Brain beta-amyloid load approaches a plateau. Neurology 80, 890–896.

[72] Villemagne VL (2016) Amyloid imaging: Past, present and future perspectives. Ageing Res Rev 30, 39–43.

[73] Smid LM, Kepe V, Vinters H V., Bresjanac M, Toyokuni T, Satyamurthy N, Wong KP, Huang SC, Silverman DHS, Miller K, Small GW, Barrio JR (2013) Postmortem 3-D brain hemisphere cortical tau and amyloid-?? pathology mapping and quantification as a validation method of neuropathology imaging. J Alzheimers Dis 36, 261–274.

[74] Chien DT, Bahri S, Szardenings AK, Walsh JC, Mu F, Su MY, Shankle WR, Elizarov A, Kolb HC (2013) Early Clinical PET Imaging Results with the Novel PHF-Tau Radioligand [F-18]-T807. J Alzheimers Dis 34, 457–468.

[75] Pierpaoli C, Jezzard P, Basser PJ, Barnett a, Di Chiro G (1996) Diffusion tensor MR imaging of the human brain. Radiology 201, 637–648.

[76] Basser PJ, Pierpaoli C (1996) Microstructural and physiological features of tissues elucidated by quantitative-diffusion-tensor MRI. J Magn Reson B 111, 209–19.

[77] Smith SM, Johansen-Berg H, Jenkinson M, Rueckert D, Nichols TE, Miller KL, Robson MD, Jones DK, Klein JC, Bartsch AJ, Behrens TEJ (2007) Acquisition and voxelwise analysis of multi-subject diffusion data with tract-based spatial statistics. Nat Protoc 2, 499–503.

[78] Westman E, Wahlund L, Foy C, Poppe M, Cooper A (2011) Magnetic Resonance Imaging and Magnetic Resonance Spectroscopy for Detection of Early Alzheimer ' s Disease. J Alzheimers Dis 26, 307–319.

[79] van der Flier WM, van den Heuvel DMJ, Weverling-Rijnsburger AWE, Bollen ELEM, Westendorp RGJ, van Buchem M a, Middelkoop H a M (2002) Magnetization transfer imaging in normal aging, mild cognitive impairment, and Alzheimer's disease. Ann

Neurol 52, 62–67.

[80] Sperling R (2011) The potential of functional MRI as a biomarker in early Alzheimer's disease. Neurobiol Aging 32, S37–S43.

[81] Ogawa S, Lee TM, Nayak a S, Glynn P (1990) Oxygenation-sensitive contrast in magnetic resonance image of rodent brain at high magnetic fields. Magn Reson Med 14, 68–78.

[82] Kwong KK, Belliveau JW, Chesler DA, Goldberg IE, Weisskoff RM, Poncelet BP, Kennedy DN, Hoppel BE, Cohen MS, Turner R (1992) Dynamic magnetic resonance imaging of human brain activity during primary sensory stimulation. Proc Natl Acad Sci U S A 89, 5675–5679.

[83] Biswal B, Zerrin Yetkin F, Haughton VM, Hyde JS (1995) Functional connectivity in the motor cortex of resting human brain using echo???planar mri. Magn Reson Med 34, 537–541.

[84] Vincent JL, Snyder AZ, Fox MD, Shannon BJ, Andrews JR, Raichle ME, Buckner RL, Justin L, Shannon J (2006) Coherent Spontaneous Activity Identifies a Hippocampal-Parietal Memory Network. J Neurophysiol 96, 3517–3531.

[85] Smith SM, Fox PT, Miller KL, Glahn DC, Fox PM, Mackay CE, Filippini N, Watkins KE, Toro R, Laird AR, Beckmann CF (2009) Correspondence of the brain's functional architecture during activation and rest. Proc Natl Acad Sci U S A 106, 13040–5.

[86] Tavor I, Parker Jones O, Mars RB, Smith SM, Behrens TE, Jbabdi S (2016) Task-free MRI predicts individual differences in brain activity during task performance. Science (80-.). 352, 216–20.

[87] Fagan AM, Mintun MA, Mach RH, Lee S-Y, Dence CS, Shah AR, LaRossa GN, Spinner ML, Klunk WE, Mathis CA, DeKosky ST, Morris JC, Holtzman DM (2006) Inverse relation between in vivo amyloid imaging load and cerebrospinal fluid Abeta42 in humans. Ann. Neurol. 59, 512–519.

[88] Forsberg A, Engler H, Almkvist O, Blomquist G, Hagman G, Wall A, Ringheim A, Långström B, Nordberg A (2008) PET imaging of amyloid deposition in patients with mild cognitive impairment. Neurobiol. Aging 29, 1456–65.

[89] Sjögren M, Vanderstichele H, Agren H, Zachrisson O, Edsbagge M, Wikkelsø C, Skoog I, Wallin A, Wahlund LO, Marcusson J, Nägga K, Andreasen N, Davidsson P, Vanmechelen E, Blennow K (2001) Tau and Abeta42 in cerebrospinal fluid from healthy adults 21-93 years of age: establishment of reference values. Clin Chem 47, 1776–1781.

[90] Mattsson N, Zetterberg H, Hansson O, Andreasen N, Parnetti L, Jonsson M, Herukka S-K, van der Flier WM, Blankenstein M a, Ewers M, Rich K, Kaiser E, Verbeek M, Tsolaki M, Mulugeta E, Rosén E, Aarsland D, Visser PJ, Schröder J, Marcusson J, de Leon M, Hampel H, Scheltens P, Pirttilä T, Wallin A, Jönhagen ME, Minthon L, Winblad B, Blennow K (2009) CSF biomarkers and incipient Alzheimer disease in patients with mild cognitive impairment. JAMA 302, 385–93.

[91] Blennow K, Hampel H, Weiner M, Zetterberg H (2010) Cerebrospinal fluid and plasma biomarkers in Alzheimer disease. Nat Rev Neurol 6, 131–144.

[92] Vemuri P, Wiste HJ, Weigand SD, Shaw LM, Trojanowski JQ, Weiner MW, Knopman DS, Petersen RC, Jack CR (2009) MRI and CSF biomarkers in normal, MCI, and AD subjects: predicting future clinical change. Neurology 73, 294–301.

[93] Westman E, Muehlboeck J-S, Simmons A (2012) Combining MRI and CSF measures for classification of Alzheimer's disease and prediction of mild cognitive impairment conversion. Neuroimage 62, 229–38.

[94] Perrin RJ, Craig-Schapiro R, Malone JP, Shah AR, Gilmore P, Davis AE, Roe CM, Peskind ER, Li G, Galasko DR, Clark CM, Quinn JF, Kaye J a, Morris JC, Holtzman DM, Townsend RR, Fagan AM (2011) Identification and validation of novel cerebrospinal fluid biomarkers for staging early Alzheimer's disease. PLoS One 6, e16032.

[95] Craig-Schapiro R, Kuhn M, Xiong C, Pickering EH, Liu J, Misko TP, Perrin RJ, Bales KR, Soares H, Fagan AM, Holtzman DM (2011) Multiplexed immunoassay panel identifies novel CSF biomarkers for Alzheimer's disease diagnosis and prognosis. PLoS One 6, e18850.

[96] Ray S, Britschgi M, Herbert C, Takeda-Uchimura Y, Boxer A, Blennow K, Friedman LF, Galasko DR, Jutel M, Karydas A, Kaye J a, Leszek J, Miller BL, Minthon L, Quinn JF, Rabinovici GD, Robinson WH, Sabbagh MN, So YT, Sparks DL, Tabaton M, Tinklenberg J, Yesavage J a, Tibshirani R, Wyss-Coray T (2007) Classification and prediction of clinical Alzheimer's diagnosis based on plasma signaling proteins. Nat. Med. 13, 1359–62.

[97] Thambisetty M, Simmons A, Velayudhan L, Hye A, Campbell J, Zhang Y, Wahlund L-O, Westman E, Kinsey A, Güntert A, Proitsi P, Powell J, Causevic M, Killick R, Lunnon K, Lynham S, Broadstock M, Choudhry F, Howlett DR, Williams RJ, Sharp SI, Mitchelmore C, Tunnard C, Leung R, Foy C, O'Brien D, Breen G, Furney SJ, Ward M, Kloszewska I, Mecocci P, Soininen H, Tsolaki M, Vellas B, Hodges A, Murphy DGM, Parkins S,

Richardson JC, Resnick SM, Ferrucci L, Wong DF, Zhou Y, Muehlboeck S, Evans A, Francis PT, Spenger C, Lovestone S (2010) Association of plasma clusterin concentration with severity, pathology, and progression in Alzheimer disease. Arch Gen Psychiatry 67, 739–48.

[98] Doecke JD, Laws SM, Faux NG, Wilson W, Burnham SC, Lam C-P, Mondal A, Bedo J, Bush AI, Brown B, De Ruyck K, Ellis K a, Fowler C, Gupta VB, Head R, Macaulay SL, Pertile K, Rowe CC, Rembach A, Rodrigues M, Rumble R, Szoeke C, Taddei K, Taddei T, Trounson B, Ames D, Masters CL, Martins RN (2012) Blood-Based Protein Biomarkers for Diagnosis of Alzheimer Disease. Arch Neurol 1–8.

[99] Burnham SC, Faux NG, Wilson W, Laws SM, Ames D, Bedo J, Bush a I, Doecke JD, Ellis K a, Head R, Jones G, Kiiveri H, Martins RN, Rembach A, Rowe CC, Salvado O, Macaulay SL, Masters CL, Villemagne VL (2013) A blood-based predictor for neocortical Aβ burden in Alzheimer's disease: results from the AIBL study. Mol Psychiatry 1–8.

[100] Schmechel DE, Saunders AM, Strittmatter WJ, Crain BJ, Hulette CM, Joo SH, Pericak-Vance MA, Goldgaber D, Roses AD (1993) Increased amyloid beta-peptide deposition in cerebral cortex as a consequence of apolipoprotein E genotype in late-onset Alzheimer disease. Proc. Natl. Acad. Sci. U. S. A. 90, 9649–9653.

[101] Poirier J, Davignon J, Bouthillier D, Kogan S, Bertrand P, Gauthier S (1993) Apolipoprotein E polymorphism and Alzheimer's disease. Lancet 342, 697–699.

[102] Farrer LA, Cupples LA, Haines JL, Hyman B, Kukull WA, Mayeux R, Myers RH, Pericak-Vance MA, Risch N, van Duijn CM (1997) Effects of Age, Sex, and Ethnicity on the Association Between Apolipoprotein E Genotype and Alzheimer Disease: A Meta-analysis. JAMA 278, 1349–1356.

[103] Weisgraber KH, Rall SC, Mahley RW (1981) Human E apoprotein heterogeneity. Cysteine-arginine interchanges in the amino acid sequence of the apo-E isoforms. J Biol Chem 256, 9077–9083.

[104] Barthel H, Gertz H-J, Dresel S, Peters O, Bartenstein P, Buerger K, Hiemeyer F, Wittemer-Rump SM, Seibyl J, Reininger C, Sabri O (2011) Cerebral amyloid-β PET with florbetaben (18F) in patients with Alzheimer's disease and healthy controls: a multicentre phase 2 diagnostic study. Lancet Neurol 10, 424–35.

[105] Fleisher AS, Chen K, Liu X, Ayutyanont N, Roontiva A, Thiyyagura P, Protas H, Joshi AD, Sabbagh M, Sadowsky CH, Sperling R a., Clark CM, Mintun M a., Pontecorvo MJ,

Coleman RE, Doraiswamy PM, Johnson K a., Carpenter AP, Skovronsky DM, Reiman EM (2013) Apolipoprotein E ε4 and age effects on florbetapir positron emission tomography in healthy aging and Alzheimer disease. Neurobiol Aging 34, 1–12.

[106] Jack CR, Petersen RC, Xu YC, O'Brien PC, Waring SC, Tangalos EG, Smith GE, Ivnik RJ, Thibodeau SN, Kokmen E (1998) Hippocampal atrophy and apolipoprotein E genotype are independently associated with Alzheimer's disease. Ann Neurol 43, 303–310.

[107] Sheline YI, Morris JC, Snyder AZ, Price JL, Yan Z, D'Angelo G, Liu C, Dixit S, Benzinger T, Fagan A, Goate A, Mintun M a (2010) APOE4 allele disrupts resting state fMRI connectivity in the absence of amyloid plaques or decreased CSF Aβ42. J Neurosci 30, 17035–40.

[108] Suri S, Heise V, Trachtenberg AJ, Mackay CE (2013) The forgotten APOE allele: A review of the evidence and suggested mechanisms for the protective effect of APOE e2. Neurosci Biobehav Rev 37, 2878–2886.

[109] Castellano JM, Kim J, Stewart FR, Jiang H, DeMattos RB, Patterson BW, Fagan AM, Morris JC, Mawuenyega KG, Cruchaga C, Goate AM, Bales KR, Paul SM, Bateman RJ, Holtzman DM (2011) Human apoE isoforms differentially regulate brain amyloid-β peptide clearance. Sci Transl Med 3, 89ra57.

[110] Liu Y, Paajanen T, Westman E, Zhang Y, Wahlund L-O, Simmons A, Tunnard C, Sobow T, Proitsi P, Powell J, Mecocci P, Tsolaki M, Vellas B, Muehlboeck S, Evans A, Spenger C, Lovestone S, Soininen H (2010) APOE ε2 allele is associated with larger regional cortical thicknesses and volumes. Dement Geriatr Cogn Disord 30, 229–37.

[111] Guerreiro R, Wojtas A, Bras J, Carrasquillo M, Rogaeva E, Majounie E, Cruchaga C, Sassi C, Kauwe JSK, Younkin S, Hazrati L, Collinge J, Pocock J, Lashley T, Williams J, Lambert J-C, Amouyel P, Goate A, Rademakers R, Morgan K, Powell J, St George-Hyslop P, Singleton A, Hardy J (2013) TREM2 variants in Alzheimer's disease. N Engl J Med 368, 117–27.

[112] Jonsson T, Stefansson H, Steinberg S, Jonsdottir I, Jonsson P V., Snaedal J, Bjornsson S, Huttenlocher J, Levey AI, Lah JJ, Rujescu D, Hampel H, Giegling I, Andreassen OA, Engedal K, Ulstein I, Djurovic S, Ibrahim-Verbaas C, Hofman A, Ikram MA, van Duijn CM, Thorsteinsdottir U, Kong A, Stefansson K (2013) Variant of TREM2 Associated with the Risk of Alzheimer's Disease. N Engl J Med 368, 107–116.

[113] Ulrich JD, Finn M, Wang Y, Shen A, Mahan TE, Jiang H, Stewart FR, Piccio L, Colonna M, Holtzman DM, Tanzi R, Corder E, Saunders A, Strittmatter W, Schmechel D, Gaskell P,

Small G, Roses A, Haines J, Pericak-Vance M, Guerreiro R, Wojtas A, Bras J, Carrasquillo M, Rogaeva E, Majounie E, Cruchaga C, Sassi C, Kauwe J, Younkin S, Hazrati L, Collinge J, Pocock J, Lashley T, Williams J, Lambert J, Amouyel P, Goate A, Rademakers R, Morgan K, Powell J, George-Hyslop PS, Singleton A, Hardy J, Jonsson T, Stefansson H, Steinberg S, Jonsdottir I, Jonsson P, Snaedal J, Bjornsson S, Huttenlocher J, Levey A, Lah J, Rujescu D, Hampel H, Giegling I, Andreassen O, Engedal K, Ulstein I, Djurovic S, Ibrahim-Verbaas C, Hofman A, Ikram M, Duijn C van, Thorsteinsdottir U, Kong A, Stefansson K, Bouchon A, Hernández-Munain C, Cella M, Colonna M, Paloneva J, Manninen T, Christman G, Hovanes K, Mandelin J, Adolfsson R, Bianchin M, Bird T, Miranda R, Salmaggi A, Tranebjaerg L, Konttinen Y, Peltonen L, Schmid C, Sautkulis L, Danielson P, Cooper J, Hasel K, Hilbush B, Sutcliffe J, Carson M, Takahashi K, Rochford C, Neumann H, Piccio L, Buonsanti C, Mariani M, Cella M, Gilfillan S, Cross A, Colonna M, Panina-Bordignon P, Sieber M, Jaenisch N, Brehm M, Guenther M, Linnartz-Gerlach B, Neumann H, Witte O, Frahm C, Melchior B, Garcia A, Hsiung B, Lo K, Doose J, Thrash J, Stalder A, Staufenbiel M, Neumann H, Carson M, Frank S, Burbach G, Bonin M, Walter M, Streit W, Bechmann I, Deller T, Meyer-Luehmann M, Spires-Jones T, Prada C, Garcia-Alloza M, Calignon A de, Rozkalne A, Koenigsknecht-Talboo J, Holtzman D, Bacskai B, Hyman B, Bolmont T, Haiss F, Eicke D, Radde R, Mathis C, Klunk W, Kohsaka S, Jucker M, Calhoun M, Aguzzi A, Barres B, Bennett M, Radde R, Bolmont T, Kaeser S, Coomaraswamy J, Lindau D, Stoltze L, Calhoun M, Jäggi F, Wolburg H, Gengler S, Haass C, Ghetti B, Czech C, Hölscher C, Mathews P, Jucker M, Jung S, Aliberti J, Graemmel P, Sunshine M, Kreutzberg G, Sher A, Littman D, Styren S, Hamilton R, Styren G, Klunk W, Gaikwad S, Heneka M, Mosher K, Wyss-Coray T, Bornemann K, Wiederhold K, Pauli C, Ermini F, Stalder M, Schnell L, Sommer B, Jucker M, Staufenbiel M, Forabosco P, Ramasamy A, Trabzuni D, Walker R, Smith C, Bras J, Levine A, Hardy J, Pocock J, Guerreiro R, Weale M, Ryten M, Koth L, Cambier C, Ellwanger A, Solon M, Hou L, Lanier L, Abram C, Hamerman J, Woodruff P, Bondolfi L, Calhoun M, Ermini F, Kuhn H, Wiederhold K-H, Walker L, Staufenbiel M, Jucker M, Otero K, Shinohara M, Zhao H, Cella M, Gilfillan S, Colucci A, Faccio R, Ross F, Teitelbaum S, Takayanagi H, Colonna M, Monica RE, Allison RN, Maya AK, Nabil ND, Elizabeth ES, Rachel AR, Kitazawa M, Matusow B, Nguyen H, Brian LW, Kim NG, Gómez-Nicola D, Fransen N, Suzzi S, Perry V, Wang Y, Szretter K, Vermi W, Gilfillan S, Rossini C, Cella M, Barrow A, Diamond M, Colonna M, Turnbull I, Gilfillan S, Cella M, Aoshi T, Miller

M, Piccio L, Hernandez M, Colonna M, Griciuc A, Serrano-Pozo A, Antonio RP, Andrea NL, Caroline NA, Mullin K, Hooli B, Se HC, Bradley TH, Rudolph ET, Bertram L, Lange C, Mullin K, Parkinson M, Hsiao M, Hogan M, Schjeide B, Hooli B, DiVito J, Ionita I, Jiang H, Laird N, Moscarillo T, Ohlsen K, Elliott K, Wang X, Hu-Lince D, Ryder M, Murphy A, Wagner S, Blacker D, Becker K, Tanzi R, Hollingworth P, Harold D, Sims R, Gerrish A, Lambert J, Carrasquillo M, Abraham R, Hamshere M, Pahwa J, Moskvina V, Dowzell K, Jones N, Stretton A, Thomas C, Richards A, Ivanov D, Widdowson C, Chapman J, Lovestone S, Powell J, Proitsi P, Lupton M, Brayne C, Rubinsztein D, Gill M, Lawlor B, Lynch A, Brown K, Passmore P, Craig D, Naj A, Jun G, Beecham G, Wang L, Vardarajan B, Buros J, Gallins P, Buxbaum J, Jarvik G, Crane P, Larson E, Bird T, Boeve B, Graff-Radford N, Jager P De, Evans D, Schneider J, Carrasquillo M, Ertekin-Taner N, Younkin S, Cruchaga C, Kauwe J, Nowotny P, Kramer P, Hardy J, Huentelman M, Myers A, Barmada M, Demirci F, Baldwin C, Bradshaw E, Chibnik L, Keenan B, Ottoboni L, Raj T, Tang A, Rosenkrantz L, Imboywa S, Lee M, Korff A Von, Neuroimaging IAD, Morris M, Evans D, Johnson K, Sperling R, Schneider J, Bennett D, Jager P De, Grathwohl S, Kalin R, Bolmont T, Prokop S, Winkelmann G, Kaeser S, Odenthal J, Radde R, Eldh T, Gandy S, Aguzzi A, Staufenbiel M, Mathews P, Wolburg H, Heppner F, Jucker M, Cady J, Koval E, Benitez B, Zaidman C, Jockel-Balsarotti J, Allred P, Baloh R, Ravits J, Simpson E, Appel S, Pestronk A, Goate A, Miller T, Cruchaga C, Harms M, Rayaprolu S, Mullen B, Baker M, Lynch T, Finger E, Seeley W, Hatanpaa K, Lomen-Hoerth C, Kertesz A, Bigio E, Lippa C, Josephs K, Knopman D, White C, Caselli R, Mackenzie I, Miller B, Boczarska-Jedynak M, Opala G, Krygowska-Wajs A, Barcikowska M, Younkin S, Petersen R, Ertekin-Taner N, Uitti R, Meschia J, Boylan K, Boeve B, Graff-Radford N, Wszolek Z (2014) Altered microglial response to Aβ plaques in APPPS1-21 mice heterozygous for TREM2. Mol. Neurodegener 9, 20.

[114] Wang Y, Cella M, Mallinson K, Ulrich JD, Young KL, Robinette ML, Gilfillan S, Krishnan GM, Sudhakar S, Zinselmeyer BH, Holtzman DM, Cirrito JR, Colonna M (2015) TREM2 lipid sensing sustains the microglial response in an Alzheimer's disease model. Cell 160, 1061–1071.

[115] Naj AC, Jun G, Beecham GW, Wang L-S, Vardarajan BN, Buros J, Gallins PJ, Buxbaum JD, Jarvik GP, Crane PK, Larson EB, Bird TD, Boeve BF, Graff-Radford NR, De Jager PL, Evans D, Schneider JA, Carrasquillo MM, Ertekin-Taner N, Younkin SG, Cruchaga C, Kauwe JSK, Nowotny P, Kramer P, Hardy J, Huentelman MJ, Myers AJ, Barmada MM, Demirci FY,

Baldwin CT, Green RC, Rogaeva E, St George-Hyslop P, Arnold SE, Barber R, Beach T, Bigio EH, Bowen JD, Boxer A, Burke JR, Cairns NJ, Carlson CS, Carney RM, Carroll SL, Chui HC, Clark DG, Corneveaux J, Cotman CW, Cummings JL, DeCarli C, DeKosky ST, Diaz-Arrastia R, Dick M, Dickson DW, Ellis WG, Faber KM, Fallon KB, Farlow MR, Ferris S, Frosch MP, Galasko DR, Ganguli M, Gearing M, Geschwind DH, Ghetti B, Gilbert JR, Gilman S, Giordani B, Glass JD, Growdon JH, Hamilton RL, Harrell LE, Head E, Honig LS, Hulette CM, Hyman BT, Jicha GA, Jin L-W, Johnson N, Karlawish J, Karydas A, Kaye JA, Kim R, Koo EH, Kowall NW, Lah JJ, Levey AI, Lieberman AP, Lopez OL, Mack WJ, Marson DC, Martiniuk F, Mash DC, Masliah E, McCormick WC, McCurry SM, McDavid AN, McKee AC, Mesulam M, Miller BL, Miller CA, Miller JW, Parisi JE, Perl DP, Peskind E, Petersen RC, Poon WW, Quinn JF, Rajbhandary RA, Raskind M, Reisberg B, Ringman JM, Roberson ED, Rosenberg RN, Sano M, Schneider LS, Seeley W, Shelanski ML, Slifer MA, Smith CD, Sonnen JA, Spina S, Stern RA, Tanzi RE, Trojanowski JQ, Troncoso JC, Van Deerlin VM, Vinters H V, Vonsattel JP, Weintraub S, Welsh-Bohmer KA, Williamson J, Woltjer RL, Cantwell LB, Dombroski BA, Beekly D, Lunetta KL, Martin ER, Kamboh MI, Saykin AJ, Reiman EM, Bennett DA, Morris JC, Montine TJ, Goate AM, Blacker D, Tsuang DW, Hakonarson H, Kukull WA, Foroud TM, Haines JL, Mayeux R, Pericak-Vance MA, Farrer LA, Schellenberg GD (2011) Common variants at MS4A4/MS4A6E, CD2AP, CD33 and EPHA1 are associated with late-onset Alzheimer's disease. Nat Genet 43, 436–41.

[116] Hollingworth P, Harold D, Sims R, Gerrish A, Lambert J-C, Carrasquillo MM, Abraham R, Hamshere ML, Pahwa JS, Moskvina V, Dowzell K, Jones N, Stretton A, Thomas C, Richards A, Ivanov D, Widdowson C, Chapman J, Lovestone S, Powell J, Proitsi P, Lupton MK, Brayne C, Rubinsztein DC, Gill M, Lawlor B, Lynch A, Brown KS, Passmore PA, Craig D, McGuinness B, Todd S, Holmes C, Mann D, Smith AD, Beaumont H, Warden D, Wilcock G, Love S, Kehoe PG, Hooper NM, Vardy ERLC, Hardy J, Mead S, Fox NC, Rossor M, Collinge J, Maier W, Jessen F, Rüther E, Schürmann B, Heun R, Kölsch H, van den Bussche H, Heuser I, Kornhuber J, Wiltfang J, Dichgans M, Frölich L, Hampel H, Gallacher J, Hüll M, Rujescu D, Giegling I, Goate AM, Kauwe JSK, Cruchaga C, Nowotny P, Morris JC, Mayo K, Sleegers K, Bettens K, Engelborghs S, De Deyn PP, Van Broeckhoven C, Livingston G, Bass NJ, Gurling H, McQuillin A, Gwilliam R, Deloukas P, Al-Chalabi A, Shaw CE, Tsolaki M, Singleton AB, Guerreiro R, Mühleisen TW, Nöthen MM, Moebus S, Jöckel K-H, Klopp N, Wichmann H-E, Pankratz VS, Sando SB, Aasly JO, Barcikowska M, Wszolek ZK, Dickson

DW, Graff-Radford NR, Petersen RC, van Duijn CM, Breteler MMB, Ikram MA, DeStefano AL, Fitzpatrick AL, Lopez O, Launer LJ, Seshadri S, Berr C, Campion D, Epelbaum J, Dartigues J-F, Tzourio C, Alpérovitch A, Lathrop M, Feulner TM, Friedrich P, Riehle C, Krawczak M, Schreiber S, Mayhaus M, Nicolhaus S, Wagenpfeil S, Steinberg S, Stefansson H, Stefansson K, Snaedal J, Björnsson S, Jonsson P V, Chouraki V, Genier-Boley B, Hiltunen M, Soininen H, Combarros O, Zelenika D, Delepine M, Bullido MJ, Pasquier F, Mateo I, Frank-Garcia A, Porcellini E, Hanon O, Coto E, Alvarez V, Bosco P, Siciliano G, Mancuso M, Panza F, Solfrizzi V, Nacmias B, Sorbi S, Bossù P, Piccardi P, Arosio B, Annoni G, Seripa D, Pilotto A, Scarpini E, Galimberti D, Brice A, Hannequin D, Licastro F, Jones L, Holmans PA, Jonsson T, Riemenschneider M, Morgan K, Younkin SG, Owen MJ, O'Donovan M, Amouyel P, Williams J (2011) Common variants at ABCA7, MS4A6A/MS4A4E, EPHA1, CD33 and CD2AP are associated with Alzheimer's disease. Nat Genet 43, 429–35.

[117] Lambert J-C, Heath S, Even G, Campion D, Sleegers K, Hiltunen M, Combarros O, Zelenika D, Bullido MJ, Tavernier B, Letenneur L, Bettens K, Berr C, Pasquier F, Fiévet N, Barberger-Gateau P, Engelborghs S, De Deyn P, Mateo I, Franck A, Helisalmi S, Porcellini E, Hanon O, de Pancorbo MM, Lendon C, Dufouil C, Jaillard C, Leveillard T, Alvarez V, Bosco P, Mancuso M, Panza F, Nacmias B, Bossù P, Piccardi P, Annoni G, Seripa D, Galimberti D, Hannequin D, Licastro F, Soininen H, Ritchie K, Blanché H, Dartigues J-F, Tzourio C, Gut I, Van Broeckhoven C, Alpérovitch A, Lathrop M, Amouyel P (2009) Genome-wide association study identifies variants at CLU and CR1 associated with Alzheimer's disease. Nat. Genet. 41, 1094–9.

[118] Harold D, Abraham R, Hollingworth P, Sims R, Gerrish A, Hamshere ML, Pahwa JS, Moskvina V, Dowzell K, Williams A, Jones N, Thomas C, Stretton A, Morgan AR, Lovestone S, Powell J, Proitsi P, Lupton MK, Brayne C, Rubinsztein DC, Gill M, Lawlor B, Lynch A, Morgan K, Brown KS, Passmore P a, Craig D, McGuinness B, Todd S, Holmes C, Mann D, Smith a D, Love S, Kehoe PG, Hardy J, Mead S, Fox N, Rossor M, Collinge J, Maier W, Jessen F, Schürmann B, van den Bussche H, Heuser I, Kornhuber J, Wiltfang J, Dichgans M, Frölich L, Hampel H, Hüll M, Rujescu D, Goate AM, Kauwe JSK, Cruchaga C, Nowotny P, Morris JC, Mayo K, Sleegers K, Bettens K, Engelborghs S, De Deyn PP, Van Broeckhoven C, Livingston G, Bass NJ, Gurling H, McQuillin A, Gwilliam R, Deloukas P, Al-Chalabi A, Shaw CE, Tsolaki M, Singleton AB, Guerreiro R, Mühleisen TW, Nöthen MM,

Moebus S, Jöckel K-H, Klopp N, Wichmann H-E, Carrasquillo MM, Pankratz VS, Younkin SG, Holmans P a, O'Donovan M, Owen MJ, Williams J (2009) Genome-wide association study identifies variants at CLU and PICALM associated with Alzheimer's disease. Nat Genet 41, 1088–93.

[119] Jack CR, Petersen RC, Xu YC, Waring SC, O'Brien PC, Tangalos EG, Smith GE, Ivnik RJ, Kokmen E (1997) Medial temporal atrophy on MRI in normal aging and very mild Alzheimer's disease. Neurology 49, 786–794.

[120] Dickerson BC, Bakkour A, Salat DH, Feczko E, Pacheco J, Greve DN, Grodstein F, Wright CI, Blacker D, Rosas HD, Sperling RA, Atri A, Growdon JH, Hyman BT, Morris JC, Fischl B, Buckner RL (2009) The cortical signature of Alzheimer's disease: regionally specific cortical thinning relates to symptom severity in very mild to mild AD dementia and is detectable in asymptomatic amyloid-positive individuals. Cereb. Cortex 19, 497–510.

[121] Barnes J, Bartlett JW, van de Pol L a, Loy CT, Scahill RI, Frost C, Thompson P, Fox NC (2009) A meta-analysis of hippocampal atrophy rates in Alzheimer's disease. Neurobiol Aging 30, 1711–23.

[122] Hostage C, Roy Choudhury K, Doraiswamy PM, Petrella JR (2013) Dissecting the gene dose-effects of the APOE ε4 and ε2 alleles on hippocampal volumes in aging and Alzheimer's disease. PLoS One 8, e54483.

[123] Fan Y, Batmanghelich N, Clark CM, Davatzikos C (2008) Spatial patterns of brain atrophy in MCI patients, identified via high-dimensional pattern classification, predict subsequent cognitive decline. Neuroimage 39, 1731–1743.

[124] Misra C, Fan Y, Davatzikos C (2009) Baseline and longitudinal patterns of brain atrophy in MCI patients, and their use in prediction of short-term conversion to AD: results from ADNI. Neuroimage 44, 1415–22.

[125] Westman E, Simmons A, Zhang Y, Muehlboeck J-S, Tunnard C, Liu Y, Collins L, Evans A, Mecocci P, Vellas B, Tsolaki M, Kłoszewska I, Soininen H, Lovestone S, Spenger C, Wahlund L-O (2011) Multivariate analysis of MRI data for Alzheimer's disease, mild cognitive impairment and healthy controls. Neuroimage 54, 1178–87.

[126] McEvoy LK, Fennema-Notestine C, Roddey JC, Hagler DJ, Holland D, Karow DS, Pung CJ, Brewer JB, Dale AM (2009) Alzheimer disease: quantitative structural neuroimaging for detection and prediction of clinical and structural changes in mild cognitive impairment. Radiology 251, 195–205.

[127] Ewers M, Walsh C, Trojanowski JQ, Shaw LM, Petersen RC, Jack CR, Feldman HH, Bokde ALW, Alexander GE, Scheltens P, Vellas B, Dubois B, Weiner M, Hampel H (2010) Prediction of conversion from mild cognitive impairment to Alzheimer's disease dementia based upon biomarkers and neuropsychological test performance. Neurobiol. Aging.

[128] Aguilar C, Westman E, Muehlboeck J-S, Mecocci P, Vellas B, Tsolaki M, Kloszewska I, Soininen H, Lovestone S, Spenger C, Simmons A, Wahlund L-O (2013) Different multivariate techniques for automated classification of MRI data in Alzheimer's disease and mild cognitive impairment. Psychiatry Res 212, 89–98.

[129] Davatzikos C, Bhatt P, Shaw LM, Batmanghelich KN, Trojanowski JQ (2010) Prediction of MCI to AD conversion, via MRI, CSF biomarkers, and pattern classification. Neurobiol Aging.

[130] Buckner RL (2005) Molecular, structural, and functional characterization of Alzheimer's disease: evidence for a relationship between default activity, amyloid, and memory. J. Neurosci 25, 7709–7717.

[131] Walhovd KB, Fjell a M, Brewer J, McEvoy LK, Fennema-Notestine C, Hagler DJ, Jennings RG, Karow D, Dale a M (2010) Combining MR imaging, positron-emission tomography, and CSF biomarkers in the diagnosis and prognosis of Alzheimer disease. AJNR. Am. J. Neuroradiol. 31, 347–54.

[132] Johnson KA, Fox NC, Sperling RA, Klunk WE (2012) Brain imaging in Alzheimer disease. Cold Spring Harb Perspect Med 2,.

[133] Klunk WE, Mathis C a, Price JC, Lopresti BJ, DeKosky ST, Engler H, Forsberg A, Almkvist O, Blomquist G, Larsson E, Savitcheva I, Wall A, Ringheim A, Långström B, Nordberg A (2006) Two-year follow-up of amyloid deposition in patients with Alzheimer's disease. Brain 129, 2856–66.

[134] Landau SM, Breault C, Joshi a. D, Pontecorvo M, Mathis C a., Jagust WJ, Mintun M a. (2013) Amyloid- Imaging with Pittsburgh Compound B and Florbetapir: Comparing Radiotracers and Quantification Methods. J Nucl Med 54, 70–77.

[135] Van Essen DC, Smith SM, Barch DM, Behrens TEJ, Yacoub E, Ugurbil K (2013) The WU-Minn Human Connectome Project: An overview. Neuroimage 80, 62–79.

[136] Stebbins GT, Murphy CM (2009) Diffusion tensor imaging in Alzheimer's disease and mild cognitive impairment. Behav Neurol 21, 39–49.

[137] Choo IH, Lee DY, Oh JS, Lee JS, Lee DS, Song IC, Youn JC, Kim SG, Kim KW, Jhoo JH, Woo JI (2010) Posterior cingulate cortex atrophy and regional cingulum disruption in mild cognitive impairment and Alzheimer's disease. Neurobiol Aging 31, 772–9.

[138] Fellgiebel A, Müller MJ, Wille P, Dellani PR, Scheurich A, Schmidt LG, Stoeter P (2005) Color-coded diffusion-tensor-imaging of posterior cingulate fiber tracts in mild cognitive impairment. Neurobiol Aging 26, 1193–1198.

[139] Acosta-Cabronero J, Williams GB, Pengas G, Nestor PJ (2010) Absolute diffusivities define the landscape of white matter degeneration in Alzheimer's disease. Brain 133, 529–39.

[140] Acosta-Cabronero J, Nestor PJ (2014) Diffusion tensor imaging in Alzheimer's disease: Insights into the limbic-diencephalic network and methodological considerations. Front Aging Neurosci 6, 1–21.

[141] Reisberg B, Franssen EH, Souren LEM, Auer SR, Akram I, Kenowsky S (2002) Evidence and mechanisms of retrogenesis in Alzheimer's and other dementias: management and treatment import. Am J Alzheimers Dis Other Demen 17, 202–212.

[142] Raichle ME, MacLeod AM, Snyder AZ, Powers WJ, Gusnard DA, Shulman GL (2001) A default mode of brain function. Proc Natl Acad Sci U S A 98, 676–82.

[143] Buckner RL, Andrews-Hanna JR, Schacter DL (2008) The brain's default network: Anatomy, function, and relevance to disease. Ann N Y Acad Sci 1124, 1–38.

[144] Wu X, Li R, Fleisher AS, Reiman EM, Guan X, Zhang Y, Chen K, Yao L (2011) Altered default mode network connectivity in alzheimer's disease-A resting functional MRI and bayesian network study. Hum. Brain Mapp. 32, 1868–1881.

[145] Damoiseaux JS, Prater KE, Miller BL, Greicius MD (2012) Functional connectivity tracks clinical deterioration in Alzheimer's disease. Neurobiol Aging 33,.

[146] Jones D, Machulda M, Vemuri P, McDade E, Zeng G, Senjem M, Gunter J, Przybelski S, Avula R, Knopman D, Boeve B, Petersen R, Jack C (2011) Age related changes in the default mode network are more advanced in Alzheimer's disease. Neurology 77, 1524–1531.

[147] Greicius MD, Srivastava G, Reiss AL, Menon V (2004) Default-mode network activity distinguishes Alzheimer's disease from healthy aging: evidence from functional MRI. Proc. Natl. Acad. Sci. U. S. A. 101, 4637–4642.

[148] Bai F, Watson DR, Yu H, Shi Y, Yuan Y, Zhang Z (2009) Abnormal resting-state functional

connectivity of posterior cingulate cortex in amnestic type mild cognitive impairment. Brain Res 1302, 167–174.

[149] Fransson P, Marrelec G (2008) The precuneus/posterior cingulate cortex plays a pivotal role in the default mode network: Evidence from a partial correlation network analysis. Neuroimage 42, 1178–1184.

[150] Chiong W, Wilson SM, D'Esposito M, Kayser AS, Grossman SN, Poorzand P, Seeley WW, Miller BL, Rankin KP (2013) The salience network causally influences default mode network activity during moral reasoning. Brain 136, 1929–1941.

[151] Mormino EC, Smiljic A, Hayenga AO, H. Onami S, Greicius MD, Rabinovici GD, Janabi M, Baker SL, V. Yen I, Madison CM, Miller BL, Jagust WJ (2011) Relationships between beta-amyloid and functional connectivity in different components of the default mode network in aging. Cereb Cortex 21, 2399–2407.

[152] Buckner RL, Sepulcre J, Talukdar T, Krienen FM, Liu H, Hedden T, Andrews-Hanna JR, Sperling R a, Johnson K a (2009) Cortical hubs revealed by intrinsic functional connectivity: mapping, assessment of stability, and relation to Alzheimer's disease. J Neurosci 29, 1860–73.

[153] Leech R, Braga R, Sharp DJ (2012) Echoes of the brain within the posterior cingulate cortex. J Neurosci 32, 215–222.

[154] Andrews-Hanna JR, Reidler JS, Sepulcre J, Poulin R, Buckner RL (2010) Functional-Anatomic Fractionation of the Brain's Default Network. Neuron 65, 550–562.

[155] Gili T, Cercignani M, Serra L, Perri R, Giove F, Maraviglia B, Caltagirone C, Bozzali M (2011) Regional brain atrophy and functional disconnection across Alzheimer's disease evolution. J Neurol Neurosurg Psychiatry 82, 58–66.

[156] Hedden T, Van Dijk KRA, Becker JA, Mehta A, Sperling RA, Johnson KA, Buckner RL (2009) Disruption of functional connectivity in clinically normal older adults harboring amyloid burden. J Neurosci 29, 12686–12694.

[157] Du A T, Schuff N, Amend D, Laakso M, Hsu Y, Jagust W, Yaffe K, Kramer J, Reed B, Norman D, Chui H, Weiner M (2001) Magnetic resonance imaging of the entorhinal cortex and hippocampus in mild cognitive impairment and Alzheimer's disease. J Neurol Neurosurg Psychiatry 71, 441–447.

[158] Chételat G, Desgranges B, De La Sayette V, Viader F, Eustache F, Baron J-C (2002) Mapping gray matter loss with voxel-based morphometry in mild cognitive impairment.

Neuroreport 13, 1939–1943.

[159] Apostolova LG, Dutton R a, Dinov ID, Hayashi KM, Toga AW, Cummings JL, Thompson PM (2006) Conversion of mild cognitive impairment to Alzheimer disease predicted by hippocampal atrophy maps. Arch Neurol 63, 693–9.

[160] Apostolova LG, Thompson PM, Green AE, Hwang KS, Zoumalan C, Jack CR, Harvey DJ, Petersen RC, Thal LJ, Aisen PS, Toga AW, Cummings JL, Decarli CS (2010) 3D comparison of low, intermediate, and advanced hippocampal atrophy in MCI. Hum Brain Mapp 31, 786–97.

[161] Cuingnet R, Gerardin E, Tessieras J, Auzias G, Lehéricy S, Habert M-O, Chupin M, Benali H, Colliot O (2011) Automatic classification of patients with Alzheimer's disease from structural MRI: a comparison of ten methods using the ADNI database. Neuroimage 56, 766–81.

[162] Desikan RS, Cabral HJ, Settecase F, Hess CP, Dillon WP, Glastonbury CM, Weiner MW, Schmansky NJ, Salat DH, Fischl B (2010) Automated MRI measures predict progression to Alzheimer's disease. Neurobiol. Aging 31, 1364–74.

[163] Risacher SL, Saykin AJ, West JD, Shen L, Firpi H a, McDonald BC (2009) Baseline MRI predictors of conversion from MCI to probable AD in the ADNI cohort. Curr. Alzheimer Res. 6, 347–61.

[164] Jack CR, Shiung MM, Gunter JL, O'Brien PC, Weigand SD, Knopman DS, Boeve BF, Ivnik RJ, Smith GE, Cha RH, Tangalos EG, Petersen RC (2004) Comparison of different MRI brain atrophy rate measures with clinical disease progression in AD. Neurology 62, 591–600.

[165] Doyle OM, Westman E, Marquand AF, Mecocci P, Vellas B, Tsolaki M, Kłoszewska I, Soininen H, Lovestone S, Williams SCR, Simmons A (2014) Predicting progression of Alzheimer's disease using ordinal regression. PLoS One 9, e105542.

[166] Mosconi L, Tsui WH, Herholz K, Pupi A, Drzezga A, Lucignani G, Reiman EM, Holthoff V, Kalbe E, Sorbi S, Diehl-Schmid J, Perneczky R, Clerici F, Caselli R, Beuthien-Baumann B, Kurz A, Minoshima S, de Leon MJ (2008) Multicenter standardized 18F-FDG PET diagnosis of mild cognitive impairment, Alzheimer's disease, and other dementias. J Nucl Med 49, 390–8.

[167] Drzezga A, Lautenschlager N, Siebner H, Riemenschneider M, Willoch F, Minoshima S, Schwaiger M, Kurz A (2003) Cerebral metabolic changes accompanying conversion of

mild cognitive impairment into alzheimer's disease: A PET follow-up study. Eur J Nucl Med Mol Imaging 30, 1104–1113.

[168] Drzezga A, Grimmer T, Riemenschneider M, Lautenschlager N, Siebner H, Alexopoulus P, Minoshima S, Schwaiger M, Kurz A (2005) Predicition of individual clinical outcome in MCI by means of genetic assessment and (18)F-FDG PET. J Nucl Med 2005, 1625–1632.

[169] Mosconi L, Perani D, Sorbi S, Herholz K, Nacmias B, Holthoff V, Salmon E, Baron J-C, De Cristofaro MTR, Padovani a, Borroni B, Franceschi M, Bracco L, Pupi a (2004) MCI conversion to dementia and the APOE genotype: A prediction study with FDG-PET. Neurology 63, 2332–2340.

[170] Kemppainen NM, Aalto S, Wilson IA, Någren K, Helin S, Brück A, Oikonen V, Kailajärvi M, Scheinin M, Viitanen M, Parkkola R, Rinne JO (2007) PET amyloid ligand [11C]PIB uptake is increased in mild cognitive impairment. Neurology 68, 1603–1606.

[171] Koivunen J, Scheinin N, Virta J. R, Aalto S, Vahlberg T, Nagren, Helin S, Parkkola R, Viitanen M, Rinne J. O, Någren K, Helin S, Parkkola R, Viitanen M, Rinne J. O (2011) Amyloid PET imaging in patients with mild cognitive impairment: a 2-year follow-up study. Neurology 76, 1085–90.

[172] Okello A, Koivunen J, Edison P, Archer HA, Turkheimer FE, Någren K, Bullock R, Walker Z, Kennedy A, Fox NC, Rossor MN, Rinne JO, Brooks DJ (2009) Conversion of amyloid positive and negative MCI to AD over 3 years: an 11C-PIB PET study. Neurology 73, 754–760.

[173] Zhang Y, Schuff N, Jahng G-H, Bayne W, Mori S, Schad L, Mueller S, Du A-T, Kramer JH, Yaffe K, Chui H, Jagust WJ, Miller BL, Weiner MW (2007) Diffusion tensor imaging of cingulum fibers in mild cognitive impairment and Alzheimer disease. Neurology 68, 13–19.

[174] Chua TC, Wen W, Slavin MJ, Sachdev PS (2008) Diffusion tensor imaging in mild cognitive impairment and Alzheimer ' s disease : a review. Curr Opin Neurol 21, 83–92.

[175] Binnewijzend MAA, Schoonheim MM, Sanz-Arigita E, Wink AM, van der Flier WM, Tolboom N, Adriaanse SM, Damoiseaux JS, Scheltens P, van Berckel BNM, Barkhof F (2012) Resting-state fMRI changes in Alzheimer's disease and mild cognitive impairment. Neurobiol Aging 33, 2018–2028.

[176] Zhang HY, Wang SJ, Xing J, Liu B, Ma ZL, Yang M, Zhang ZJ, Teng GJ (2009) Detection of PCC functional connectivity characteristics in resting-state fMRI in mild Alzheimer's

disease. Behav Brain Res 197, 103–108.

[177] Qi Z, Wu X, Wang Z, Zhang N, Dong H, Yao L, Li K (2010) Impairment and compensation coexist in amnestic MCI default mode network. Neuroimage 50, 48–55.

[178] Li H-J, Hou X-H, Liu H-H, Yue C-L, He Y, Zuo X-N (2015) Toward systems neuroscience in mild cognitive impairment and Alzheimer's disease: a meta-analysis of 75 fMRI studies. Hum. Brain Mapp 36, 1217–32.

[179] Lau WKW, Leung M-K, Lee TMC, Law ACK (2016) Resting-state abnormalities in amnestic mild cognitive impairment: a meta-analysis. Transl Psychiatry 6, e790.

[180] Jones DT, Knopman DS, Gunter JL, Graff-radford J, Vemuri P, Boeve BF, Petersen RC, Weiner MW, Jack CR (2015) Cascading network failure across the Alzheimer's disease spectrum. Brain 1–16.

[181] Gardini S, Venneri A, Sambataro F, Cuetos F, Fasano F, Marchi M, Crisi G, Caffarra P (2015) Increased Functional Connectivity in the Default Mode Network in Mild Cognitive Impairment: A Maladaptive Compensatory Mechanism Associated with Poor Semantic Memory Performance. J Alzheimers Dis 45, 457–470.

[182] Jack C, Wiste H, Weigand S (2013) Amyloid-first and neurodegeneration-first profiles characterize incident amyloid PET positivity. Neurology 81, 1732–1740.

[183] Villemagne VL, Pike KE, Chételat G, Ellis KA, Mulligan RS, Bourgeat P, Ackermann U, Jones G, Szoeke C, Salvado O, Martins R, O'Keefe G, Mathis CA, Klunk WE, Ames D, Masters CL, Rowe CC (2011) Longitudinal assessment of Aβ and cognition in aging and Alzheimer disease. Ann Neurol 69, 181–192.

[184] Mormino EC, Brandel MG, Madison CM, Rabinovici GD, Marks S, Baker SL, Jagust WJ (2012) Not quite PIB-positive, not quite PIB-negative: Slight PIB elevations in elderly normal control subjects are biologically relevant. Neuroimage 59, 1152–1160.

[185] Doraiswamy PM, Sperling R a, Johnson K, Reiman EM, Wong TZ, Sabbagh MN, Sadowsky CH, Fleisher a S, Carpenter A, Joshi a D, Lu M, Grundman M, Mintun M a, Skovronsky DM, Pontecorvo MJ (2014) Florbetapir F 18 amyloid PET and 36-month cognitive decline:a prospective multicenter study. Mol Psychiatry 1–8.

[186] Jack CR, Lowe VJ, Weigand SD, Wiste HJ, Senjem ML, Knopman DS, Shiung MM, Gunter JL, Boeve BF, Kemp BJ, Weiner M, Petersen RC (2009) Serial PIB and MRI in normal, mild cognitive impairment and Alzheimers disease: Implications for sequence of pathological events in Alzheimers disease. Brain 132, 1355–1365.

[187] Mattsson N, Insel PS, Nosheny R, Tosun D, Trojanowski JQ, Shaw LM, Jack CR, Donohue MC, Weiner MW (2014) Emerging β-amyloid pathology and accelerated cortical atrophy. JAMA Neurol 71, 725–34.

[188] Lim HK, Nebes R, Snitz B, Cohen A, Mathis C, Price J, Weissfeld L, Klunk W, Aizenstein HJ (2014) Regional amyloid burden and intrinsic connectivity networks in cognitively normal elderly subjects. Brain 137, 3327–38.

[189] Protas HD, Chen K, Langbaum JBS, Fleisher AS, Alexander GE, Lee W, Bandy D, Leon MJ De, Mosconi L, Buckley S, Truran-sacrey D, Schuff N, Weiner MW, Caselli RJ, Reiman EM (2013) Posterior Cingulate Glucose Metabolism, Hippocampal Glucose Metabolism, and Hippocampal Volume in Cognitively Normal, Late-Middle-Aged Persons at 3 Levels of Genetic Risk for Alzheimer Disease. JAMA Neurol 70, 320–325.

[190] Stern Y (2006) Cognitive reserve and Alzheimer disease. Alzheimer Dis. Assoc. Disord. 20, 112.

[191] Ewers M, Insel PS, Stern Y, Weiner MW (2013) Cognitive reserve associated with FDG-PET in preclinical Alzheimer disease. Neurology 80, 1194–1201.

[192] Fjell AM, Westlye LT, Grydeland H, Amlien I, Espeseth T, Reinvang I, Raz N, Dale AM, Walhovd KB (2014) Accelerating cortical thinning: Unique to dementia or universal in aging? Cereb Cortex 24, 919–934.

[193] Caselli R, Dueck A, Osborne D, Sabbagh M, Connor D, Ahern G, Baxter L, Rapcsak S, Shi J, Woodruff B, Locke D, Snyder C, Alexander G, Rademakers R, Reiman E (2009) Longitudinal modeling of age-related memory decline and the APOE ε4 effect. N Engl J Med 361, 255–263.

[194] Fjell AM, McEvoy L, Holland D, Dale AM, Walhovd KB (2014) What is normal in normal aging? Effects of aging, amyloid and Alzheimer's disease on the cerebral cortex and the hippocampus. Prog Neurobiol 117, 20–40.

[195] Jiang Q, Lee CYD, Mandrekar S, Wilkinson B, Cramer P, Zelcer N, Mann K, Lamb B, Willson TM, Collins JL, Richardson JC, Smith JD, Comery T a, Riddell D, Holtzman DM, Tontonoz P, Landreth GE (2008) ApoE promotes the proteolytic degradation of Abeta. Neuron 58, 681–93.

[196] Mormino EC, Betensky RA, Hedden T, Schultz AP, Ward A, Huijbers W, Rentz DM, Johnson KA, Sperling RA (2014) Amyloid and APOE e 4 interact to influence short-term decline in preclinical Alzheimer disease. Neurology 82, 1760–7.

[197] Tuminello ER, Han SD (2011) The Apolipoprotein E Antagonistic Pleiotropy Hypothesis: Review and Recommendations. Int J Alzheimers Dis 2011, 726197.

[198] Shaw LM, Korecka M, Clark CM, Lee VM-Y, Trojanowski JQ (2007) Biomarkers of neurodegeneration for diagnosis and monitoring therapeutics. Nat. Rev. Drug Discov. 6, 295–303.

[199] Knickmeyer RC, Wang J, Zhu H, Geng X, Woolson S, Hamer RM, Konneker T, Lin W, Styner M, Gilmore JH (2014) Common Variants in Psychiatric Risk Genes Predict Brain Structure at Birth. Cereb. Cortex 24, 1230–1246.

[200] Filippini N, MacIntosh BJ, Hough MG, Goodwin GM, Frisoni GB, Smith SM, Matthews PM, Beckmann CF, Mackay CE (2009) Distinct patterns of brain activity in young carriers of the APOE E4 allele. Proc Natl Acad Sci U S A 106, 7209–14.

[201] Dean DC, Jerskey B, Chen K, Protas H, Thiyyagura P, Roontiva A, O'Muircheartaigh J, Dirks H, Waskiewicz N, Lehman K, Siniard AL, Turk MN, Hua X, Madsen SK, Thompson PM, Fleisher AS, Huentelman MJ, Deoni SCL, Reiman EM (2014) Brain Differences in Infants at Differential Genetic Risk for Late-Onset Alzheimer Disease: A Cross-sectional Imaging Study. JAMA Neurol 71, 11–22.

[202] Chang L, Douet V, Bloss C, Lee K, Pritchett A, Jernigan TL, Akshoomoff N, Murray SS, Frazier J, Kennedy DN, Amaral DG, Gruen J, Kaufmann WE, Casey BJ, Sowell E, Ernst T, For the Pediatric Imaging, Neurocognition and G (PING) SC, Pediatric Imaging, Neurocognition and G (PING) SC, Jernigan TL, McCabe C, Chang L, Akshoomoff N, Newman E, Dale AM, Ernst T, Dale AM, Zijl P Van, Kuperman J, Murray S, Bloss C, Appelbaum M, Gamst A, Thompson W, Keating B, Amaral D, Kaufmann W, Zijl P Van, Mostofsky S, Casey BJ, Ruberry EJ, Powers A, Rosen B, Kenet T, Frazier J, Kennedy D, Gruen J (2016) Gray matter maturation and cognition in children with different APOE ε genotypes. Neurology 87, 585–94.

[203] Reisberg B, Shulman MB, Torossian C, Leng L, Zhu W (2010) Outcome over seven years of healthy adults with and without subjective cognitive impairment. Alzheimer's Dement 6, 11–24.

[204] Winblad B, Palmer K KM (2004) Mild cognitive impairment– beyond controversies, towards a consensus: report of the International Working Group on Mild Cognitive Impairment. J Intern Med 256, 240–246.

[205] Stewart R, Dufouil C, Godin O, Ritchie K, Maillard P, Delcroix N, Crivello F, Mazoyer B,

Tzourio C (2008) Neuroimaging correlates of subjective memory deficits in a community population. Neurology 70, 1601–1607.

[206] Visser PJ, Verhey F, Knol DL, Scheltens P, Wahlund LO, Freund-Levi Y, Tsolaki M, Minthon L, Wallin ÅK, Hampel H, Bürger K, Pirttila T, Soininen H, Rikkert MO, Verbeek MM, Spiru L, Blennow K (2009) Prevalence and prognostic value of CSF markers of Alzheimer's disease pathology in patients with subjective cognitive impairment or mild cognitive impairment in the DESCRIPA study: a prospective cohort study. Lancet Neurol 8, 619–627.

[207] Jonker C, Geerlings MI, Schmand B (2000) Are memory complaints predictive for dementia? A review of clinical and population-based studies. Int J Geriatr Psychiatry 15, 983–991.

[208] Jessen F, Wiese B, Bachmann C, Eifflaender-Gorfer S, Haller F, Kolsch H, Luck T, Mosch E, Van Den Bussche H, Wagner M, Wollny A, Zimmermann T, Pentzek M, Riedel-Heller SG, Romberg H-P, Weyerer S, Kaduszkiewicz H, Maier W, Bickel H (2010) Prediction of Dementia by Subjective Memory Impairment: Effects of Severity and Temporal association With Cognitive Impairment. Arch Gen Psychiatry 67, 414–422.

[209] Nyberg L, Lovden M, Riklund K, Lindenberger U, Backman L (2012) Memory aging and brain maintenance. Trends Cogn Sci 16, 292–305.

[210] Becker JA, Hedden T, Carmasin J, Maye J, Rentz DM, Putcha D, Fischl B, Greve DN, Marshall GA, Salloway S, Marks D, Buckner RL, Sperling RA, Johnson KA (2011) Amyloid-β associated cortical thinning in clinically normal elderly. Ann Neurol 69, 1032–42.

[211] Salthouse TA (2009) When does age-related cognitive decline begin? Neurobiol Aging 30, 507–514.

[212] Fjell AM, Walhovd KB, Fennema-Notestine C, McEvoy LK, Hagler DJ, Holland D, Brewer JB, Dale AM (2009) One-year brain atrophy evident in healthy aging. J Neurosci 29, 15223–31.

[213] Nelson PT, Alafuzoff I, Bigio EH, Bouras C, Braak H, Cairns NJ, Castellani RJ, Crain BJ, Davies P, Tredici K Del, Duyckaerts C, Frosch MP, Haroutunian V, Hof PR, Hulette CM, Hyman BT, Iwatsubo T, Jellinger KA, Jicha GA, Kukull WA, Leverenz JB, Love S, Mackenzie IR, Mann DM, Masliah E, Mckee AC, Montine TJ, Morris JC, Schneider JA, Sonnen JA, Thal DR, Trojanowski JQ, Troncoso JC, Wisniewski T, Woltjer RL, Beach TG (2012) Correlation of Alzheimer Disease Neuropathologic Changes With Cognitive Status : A Review of the

Literature. J Neuropathol Exp Neurol 71, 362–381.

[214] Nyberg L, Salami A, Andersson M, Eriksson J, Kalpouzos G, Kauppi K (2010) Longitudinal evidence for diminished frontal cortex function in aging. Proc Natl Acad Sci U S A 107, 22682–22686.

[215] Knopman DS, Jack CR, Wiste HJ, Weigand SD, Vemuri P, Lowe VJ, Kantarci K, Gunter JL, Senjem ML, Mielke MM, Roberts RO, Boeve BF, Petersen RC (2013) Brain injury biomarkers are not dependent on beta-amyloid in normal elderly. Ann Neurol 73, 472–480.

[216] Oh H, Mormino EC, Madison C, Hayenga A, Smiljic A, Jagust WJ (2011) β-Amyloid affects frontal and posterior brain networks in normal aging. Neuroimage 54, 1887–1895.

[217] Jack CR, Knopman DS, Chételat G, Dickson D, Fagan AM, Frisoni GB, Jagust WJ, Mormino EC, Petersen RC, Sperling RA, van der Flier WM, Villemagne VL, Visser PJ, Vos SJB (2016) Suspected non-Alzheimer disease pathophysiology - concept and controversy. Nat. Rev Neurol 12, 117–124.

[218] Crary JF, Trojanowski JQ, Schneider JA, Abisambra JF, Abner EL, Alafuzoff I, Arnold SE, Attems J, Beach TG, Bigio EH, Cairns NJ, Dickson DW, Gearing M, Grinberg LT, Hof PR, Hyman BT, Jellinger K, Jicha GA, Kovacs GG, Knopman DS, Kofler J, Kukull WA, Mackenzie IR, Masliah E, McKee A, Montine TJ, Murray ME, Neltner JH, Santa-Maria I, Seeley WW, Serrano-Pozo A, Shelanski ML, Stein T, Takao M, Thal DR, Toledo JB, Troncoso JC, Vonsattel JP, White CL, Wisniewski T, Woltjer RL, Yamada M, Nelson PT (2014) Primary age-related tauopathy (PART): a common pathology associated with human aging. Acta Neuropathol 128, 755–766.

[219] Fortea J, Sala-Llonch R, Bartrés-Faz D, Lladó A, Solé-Padullés C, Bosch B, Antonell A, Olives J, Sanchez-Valle R, Molinuevo JL, Rami L (2011) Cognitively preserved subjects with transitional cerebrospinal fluid β-amyloid 1-42 values have thicker cortex in Alzheimer's disease vulnerable areas. Biol Psychiatry 70, 183–190.

[220] Storandt M, Mintun MA, Head D, Morris JC (2009) Cognitive decline and brain volume loss as signatures of cerebral amyloid-beta peptide deposition identified with Pittsburgh compound B: cognitive decline associated with Abeta deposition. Arch Neurol 66, 1476–81.

[221] Arenaza-Urquijo EM, Molinuevo JL, Sala-Llonch R, Solé-Padullés C, Balasa M, Bosch B, Olives J, Antonell A, Lladó A, Sánchez-Valle R, Rami L, Bartres-Faz D (2013) Cognitive

reserve proxies relate to gray matter loss in cognitively healthy elderly with abnormal cerebrospinal fluid amyloid-β levels. J Alzheimers Dis 35, 715–726.

[222] Jack CR, Wiste HJ, Weigand SD, Rocca WA, Knopman DS, Mielke MM, Lowe VJ, Senjem ML, Gunter JL, Preboske GM, Pankratz VS, Vemuri P, Petersen RC (2014) Age-specific population frequencies of cerebral β-amyloidosis and neurodegeneration among people with normal cognitive function aged 50–89 years: a cross-sectional study. Lancet Neurol 13, 997–1005.

[223] Jack CR, Therneau TM, Wiste HJ, Weigand SD, Knopman DS, Lowe VJ, Mielke MM, Vemuri P, Roberts RO, Machulda MM, Senjem ML, Gunter JL, Rocca WA, Petersen RC (2016) Transition rates between amyloid and neurodegeneration biomarker states and to dementia: A population-based, longitudinal cohort study. Lancet Neurol 15, 56–64.

[224] Teipel S, Drzezga A, Grothe MJ, Barthel H, Ch??telat G, Schuff N, Skudlarski P, Cavedo E, Frisoni GB, Hoffmann W, Thyrian JR, Fox C, Minoshima S, Sabri O, Fellgiebel A (2015) Multimodal imaging in Alzheimer's disease: Validity and usefulness for early detection. Lancet Neurol 14, 1037–1053.

[225] Risacher SL, Saykin AJ (2013) Neuroimaging and other biomarkers for Alzheimer's disease: the changing landscape of early detection. Annu. Rev. Clin. Psychol. 9, 621–48.

AIMS AND OBJECTIVES

There is a great interest in the role that neuroimaging biomarkers could play in the evaluation of AD-modifying treatments and future drug development strategies. As a result, different hypotheses regarding the temporal evolution of neuroimaging biomarker changes have been postulated to best track the progression of AD. The dominant view of the neuropathological changes in AD is that Aβ initiates a pathological cascade of events that eventually leads to NFT formation, followed by synaptic and neuronal injury, and eventual cognitive decline.

Yet, several lines of evidence from neuroimaging studies has begun to debate this view. Firstly, the postulated sequence of events of 'Aβ-first' pathology has been questioned. The regional variation in atrophy, hypometabolism, and Aβ deposition, as well as the low interaction between Aβ pathology and neurodegeneration markers support the view that AD is a syndrome with a multitude of possible sequence of events. However, Aβ-centric models for biomarker discovery often consider neuroimaging markers of neuronal injury (hippocampal volume and FDG-PET hypometabolism measurements) downstream to Aβ pathogenies, and suggest that they only become abnormal a few years prior to the emergence of cognitive impairment. This inadvertently limits their utility to the latter stages of preclinical AD and different stages of cognitive impairment.

Alternative biomarker models now postulate that neuroimaging biomarkers of neuronal injury should be considered as carrying the same weight as neuroimaging biomarkers of Aβ deposition. The problem faced by current biomarker discovery is that a number of different less widely used brain imaging techniques have been applied to AD, but have not been as extensively validated as hippocampal volumetry. Therefore, I will briefly describe the challenges faced by current neuroimaging biomarkers for measuring different stages of AD pathophysiology, and shall propose how each chapter of the thesis will attempt to address some of these obstacles.

In biomarker models, it is also very important to determine how the APOE gene modulates the genetic risk of developing AD, and whether the temporal evolution of disease markers are

differentially affected in ε4 and ε2 allele carriers. I will describe the current gap in the literature, and the push to investigate the neurodevelopmental foothold of APOE ε4 from infancy, adolescence and early adulthood.

CHAPTER 2

Firstly, decline in hippocampal volume is the most extensively reported MRI finding in AD patients and MCI subjects progressing to the disease. However, hippocampal atrophy is not specific to the AD pathological process and is a feature observed in other psychiatric and neurological diseases. Furthermore, while the hippocampus is often mapped as a unitary structure, it is in fact anatomically heterogeneous and divided into several subfields with distinct histological characteristics. Previous studies have also reported that the different subfields of the hippocampus make unique contributions to memory processes, and thus appear to be differentially vulnerable to the neurodegenerative diseases such as AD. Although automated hippocampal volumetry can be a useful surrogate measure for detecting AD, recent studies have suggested that segmenting the subfields of the hippocampus may yield better results for detecting incipient AD at the MCI stage. Therefore, measuring volume loss in the hippocampal subfields may be more informative for the different stages of the AD pathological process than measuring global hippocampal volume loss. Consequently, Chapter 2 of this thesis will explore a relatively new automated technique for hippocampal subfield segmentation and test its utility over automated global hippocampal volume measurements.

In particular, the aim of *Chapter 2* will be to assess the pattern of hippocampal subfield volume loss in AD and MCI patients, and test its association with clinical risk factors such as age, gender, education and APOE ε4. I will also compare hippocampal subfield measurements against global hippocampal volume measurements for (1) distinguishing AD patients from older healthy controls and (2) predicting future MCI to AD conversion. The study sample will comprise two independent cohorts from two multi-centre studies of AD: The US-based Alzheimer's Disease Neuroimaging Initiative (ADNI), and the European AddNeuroMed study.

CHAPTER 3

From a disease classification and prediction perspective, several studies have proposed the advantages of combining structural MRI measurements with core CSF biomarkers for the improved detection of AD and prediction of MCI patients converting to the disease. Furthermore, studies using high-dimensional pattern classification techniques have also reported that structural MRI and CSF biomarkers provide mutually complimentary information for disease classification and prediction. Yet, despite these advantages, there remains a substantial overlap in CSF biomarker values between AD patients and MCI subjects and demonstrates a need for better prognostic ability. Neuropathologically, there is also a large overlap of proteinopathies observed in AD with other dementias, particularly vascular dementia and dementia with Lewy bodies. To improve specificity, recent proteomic studies have identified alternative CSF candidates associated with inflammation, microglial activity and synaptic dysfunction for increasing the diagnostic accuracy of existing CSF biomarkers in AD. However, these candidates have not yet been tested in relation with structural MRI measurements. Testing alternative CSF candidates with well-established neuroimaging endophenotypes of AD will facilitate a better understanding into their predictive ability and potential as biomarkers. In *Chapter 3* of this thesis, I will investigate prognostic ability of CSF proteins from a multiplex analyte panel together with regional MRI measurements for disease classification and prediction in the ADNI study.

CHAPTER 4

Converging evidence from several neuroimaging studies suggests that the APOE gene modifies the rate of hippocampal atrophy in AD pathophysiology. In particular, APOE ε4 carriers have been shown to exhibit an increased rate of hippocampal loss that is dose-dependent. Although the neuroanatomic effect of APOE ε4 in AD is extensively studied, the mechanisms that moderate APOE ε4's detrimental effect on the hippocampus are not well understood. Recent studies suggest that Aβ deposition may play an important role since APOE ε4 is known to enhance the aggregation of Aβ and/or decrease its clearance.

To further elucidate these mechanisms and capture the heterogeneity of varying AD risk, I used a large well-characterised and extensive multi-cohort of dataset. This included imaging and APOE data primarily from three multi-centre studies of AD: (1) The ADNI study; (2) the AddNeuroMed study, and (3) The Australian Imaging, Biomarkers and Lifestyle (AIBL) study. Imaging APOE data from a population-based sample of non-demented individuals the Swedish National Study on Ageing and Care in Kungsholmen (SNAC-K) and a dementia study from King's College London, UK (BRC-AD) were also included.

The aim of *Chapter 4* was to assess the neuroanatomic effect of different APOE gene polymorphisms on hippocampal volume in the different stages of AD, normal ageing, and a population-based sample of non-demented individuals. In a subset of individuals with PET measures of Aβ deposition from the ADNI and AIBL study cohorts, I aimed to further elucidate whether hippocampal atrophy is moderated by Aβ-dependent or Aβ-independent mechanisms in APOE ε4 carriers.

CHAPTERS 5 AND 6

A recent line of enquiry has led researchers to postulate what are the earliest structural brain changes associated with the genetic risk of sporadic AD. A study by Filippini et al [1] was the first to report functional alterations associated with APOE ε4 in young healthy carriers, decades before any abnormal proteinopathies such as Aβ are expected to take hold. This finding and others that have followed, are driving the impetus to discover early brain differences associated with a neurodevelopmental foothold of APOE ε4. For this particular avenue of APOE research current biomarker driven theoretical frameworks of AD rarely address the prospects of determining AD risk in young adulthood and adolescence. Consequently, *Chapter 5* will attempt to explore the relationship between APOE and brain structure by assessing the hippocampal volume of adolescents with a differential APOE risk to AD. The study sample will compromise a large cross-sectional cohort of healthy 14-yr old adolescents from a European multi-centre neuroimaging-genetics study known as IMAGEN.

As a follow-up, *Chapter 6* will assess the relationship between APOE and the WM microstructure of the brain in the subset sample of healthy adolescents with diffusion imaging. The rationale for this investigation was originally envisaged from the retrogenesis model of AD, which posits that later myelinating WM fibres would be more susceptible to the degenerative effects of AD later in life. As a result, the aim of the chapter will be to assess the WM microstructural properties of adolescents with a differential APOE risk of AD using an unbiased whole-analysis technique known as Tract-Based Spatial Statistics (TBSS).

CHAPTER 7

Finally, *Chapter 7* will shift focus to the application of rsfMRI techniques in AD. The most extensively studied and validated method for quantifying functional alterations in AD are measures of FDG-PET glucose hypometabolism. A disconnection in intrinsic functional connectivity of the DMN remains the most commonly observed in patients with AD, and also consists of regions that have a predilection of harbouring AD neuropathology. However, recent evidence suggests that the posteromedial cortex (PMC), consisting of the PCC, precuneus and retrosplenial cortices, also considered a central hub of the DMN, is not functionally homogeneous. In particular, the PMC has been shown to share a complex functional architecture with the rest of the brain associating with several intrinsically stable networks as well as the DMN. Recent work has begun to demonstrate that AD pathogenesis leads to a complex pattern of functional connectivity cascades of hyperconnectivity and hypoconnectivity, and cannot alone by explained by the DMN disruptions. Furthermore, the prospect of rsfMRI techniques detecting functional alterations prior to structural atrophy provides a promising step to monitoring the disease earlier than current structural MRI methods.

Using clinical phenotyping, metadata, and rsfMRI neuroimaging data, I will attempt to characterise the complex functional architecture of the PMC in AD. I hypothesise that brain activity of the PMC region should reveal a complex and dynamic pattern of intrinsic connectivity with the rest of the brain. Moreover, key regions of the PMC with discrete roles in supporting cognition, memory and attentional control will be affected in AD and MCI

patients converting to the disease. A disruption in the functional equilibrium of the PMC at rest will also have cascading effects on key nodes of the DMN, particularly the MTL and ventromedial prefrontal cortex (VMPFC) regions that are known to be disrupted in the disease.

SUMMARY

In summary, this thesis will investigate the utility of advanced neuroimaging techniques for detecting AD, across several complex biomarker phenotypes, including the MCI stage, APOE ε4 risk, abnormal Aβ accumulation, and cognitive decline. This thesis will address these investigations by establishing several key aims: **(1)** To compare an automated hippocampal subfield analysis technique over standard hippocampal volume measurements for disease classification and prediction (*Chapter 2*), **(2)** To evaluate the prognostic ability of alternative CSF proteins in combination with structural MRI measurements for disease classification and prediction (*Chapter 3*), **(3)** To assess the effect of different APOE gene polymorphisms on hippocampal volume and Aβ deposition in a large multi-cohort study (*Chapter 4*), **(4)** To explore the neurodevelopmental relationship between the APOE gene and brain structure in a large sample of healthy 14-yr old adolescents (*Chapters 5 and 6*), and **(5)** To test the application of rsfMRI techniques in AD by characterising the complex functional architecture of the PMC (*Chapter 7*).

REFERENCES

[1] Filippini N, MacIntosh BJ, Hough MG, Goodwin GM, Frisoni GB, Smith SM, Matthews PM, Beckmann CF, Mackay CE (2009) Distinct patterns of brain activity in young carriers of the APOE E4 allele. Proc Natl Acad Sci U S A 106, 7209–14.

CHAPTER 2: AUTOMATED HIPPOCAMPAL SUBFIELD MEASURES AS PREDICTORS OF CONVERSION FROM MILD COGNITIVE IMPAIRMENT TO ALZHEIMER'S DISEASE IN TWO INDEPENDENT COHORTS

This chapter is presented as a published paper and is the exact copy of the following journal publication:

Khan W*, Westman E*, Jones N, Wahlund L-O, Mecocci P, Vellas B, Tsolaki M, Kłoszewska I, Soininen H, Spenger C, Lovestone S, Muehlboeck J-S, Simmons A (2014). Automated Hippocampal Subfield Measures as Predictors of Conversion from Mild Cognitive Impairment to Alzheimer's Disease in Two Independent Cohorts. *Brain Topogr*.

*These authors contributed equally to this work

Author Contributions:

Study Concept and Design: Khan, Simmons, Westman

Acquisition, Analysis and Interpretation of data: Khan, Simmons, Westman, Jones

Drafting and Revision of Manuscript: All Authors

Statistical Analysis: Khan, Westman, Muehlboeck, Simmons

Brain Topogr
DOI 10.1007/s10548-014-0415-1

ORIGINAL PAPER

Automated Hippocampal Subfield Measures as Predictors of Conversion from Mild Cognitive Impairment to Alzheimer's Disease in Two Independent Cohorts

Wasim Khan · Eric Westman · Nigel Jones · Lars-Olof Wahlund · Patrizia Mecocci · Bruno Vellas · Magda Tsolaki · Iwona Kłoszewska · Hilkka Soininen · Christian Spenger · Simon Lovestone · J-Sebastian Muehlboeck · Andrew Simmons · for the AddNeuroMed consortium and for the Alzheimer's Disease Neuroimaging Initiative

Received: 25 June 2014 / Accepted: 24 October 2014

Abstract Previous studies have shown that hippocampal subfields may be differentially affected by Alzheimer's disease (AD). This study used an automated analysis technique and two large cohorts to (1) investigate patterns of subfield volume loss in mild cognitive impairment (MCI) and AD, (2) determine the pattern of subfield volume loss due to age, gender, education, *APOE* ε4 genotype, and neuropsychological test scores, (3) compare combined subfield volumes to hippocampal volume alone at discriminating between AD and healthy controls (HC), and predicting future MCI conversion to AD at 12 months. 1,069 subjects were selected from the AddNeuroMed and Alzheimer's disease neuroimaging initiative (ADNI) cohorts. Freesurfer was used for automated segmentation of the hippocampus and hippocampal subfields. Orthogonal partial least squares to latent structures (OPLS) was used to train models on AD and HC subjects using one cohort for training and the other for testing and the combined cohort was used to predict MCI conversion. MANCOVA and linear regression analyses showed multiple subfield volumes including Cornu Ammonis 1 (CA1), subiculum and presubiculum were atrophied in AD and MCI and were related to age, gender, education, *APOE* ε4 genotype, and neuropsychological test scores. For classifying AD from HC, combined subfield volumes achieved comparable classification accuracy (81.7 %) to total hippocampal (80.7 %), subiculum (81.2 %) and presubiculum (80.6 %) volume. For predicting MCI conversion to AD combined subfield volumes and presubiculum volume were more accurate (81.1 %) than total hippocampal volume. (76.7 %).

Data used in preparation of this article were obtained from the Alzheimer's disease Neuroimaging Initiative (ADNI) database (adni.loni.ucla.edu). As such, the investigators within the ADNI contributed to the design and implementation of ADNI and/or provided data but did not participate in analysis or writing of this report. A complete listing of ADNI investigators can be found at: http://adni.loni.ucla.edu/wp-content/uploads/how_to_apply/ADNI_Acknowledgement_List.pdf.

Wasim Khan and Eric Westman have contributed equally to the manuscript.

W. Khan · E. Westman · N. Jones · S. Lovestone · J.-S. Muehlboeck · A. Simmons (✉)
Department of Neuroimaging, Institute of Psychiatry, King's College London, De Crespigny Park, London SE5 8AF, UK
e-mail: andy.simmons@kcl.ac.uk

E. Westman · L.-O. Wahlund
Department of Neurobiology, Care Sciences and Society, Karolinska Institutet, Stockholm, Sweden

N. Jones · J.-S. Muehlboeck · A. Simmons
NIHR Biomedical Research Centre for Mental Health, London, UK

P. Mecocci
Institute of Gerontology and Geriatrics, University of Perugia, Perugia, Italy

B. Vellas
INSERM U 558, University of Toulouse, Toulouse, France

M. Tsolaki
Aristotle University of Thessaloniki, Thessaloniki, Greece

I. Kłoszewska
Medical University of Lodz, Lodz, Poland

H. Soininen
Department of Neurology, University of Eastern Finland and Kuopio University Hospital, Kuopio, Finland

C. Spenger
Department of Clinical Science, Intervention and Technology, Karolinska Institutet, Stockholm, Sweden

Published online: 05 November 2014

Keywords Alzheimer's disease · MCI conversion · MRI · Freesurfer · OPLS

Introduction

In recent years, research efforts in Alzheimer's disease (AD) have focused upon the discovery of clinically meaningful and non-invasive biomarkers that can reliably monitor disease progression and predict future conversion to the disease. Several groups including our own have proposed the use of magnetic resonance imaging (MRI) based tools to aid in the diagnosis of AD (Desikan et al. 2009; Liu et al. 2009) and predict future conversion from the prodromal stage of disease often referred to as mild cognitive impairment (MCI) (McEvoy et al. 2009; Westman et al. 2011a).

Hippocampal atrophy has been frequently observed in AD (Jack et al. 1992; Fox et al. 1996) and has been demonstrated in MCI subjects (Devanand et al. 2007), with increased risk of future conversion to AD in subjects with smaller hippocampal volumes (Apostolova et al. 2006; Csernansky et al. 2005). Hippocampal volumetry has been a useful marker of AD pathology but seems to be insufficiently sensitive for distinguishing between MCI subjects bearing a high risk of AD conversion from those who remain clinically stable (Mueller et al. 2010). Post-mortem studies have also demonstrated that hippocampal atrophy in AD is non-uniform, with Cornu Ammonis 1 (CA1) and subicular atrophy reported in early AD (Braak and Braak 1991; West et al. 2004).

So far, only a few studies have attempted to measure regional atrophic changes within the hippocampus using manual delineation and 3D surface mapping (Mueller and Weiner 2009; Apostolova et al. 2010; Costafreda et al. 2011). Manual delineation of the subfield boundaries is both a time consuming and labour intensive process which limits its widespread applicability in practice. However, recent developments in image acquisition have made it possible to segment the hippocampus into its subfields in a fully automated fashion and this method has now been validated using ultra high resolution MRI (Van Leemput et al. 2009). A recent small study applied this technique to 15 MCI subjects using conventional 3D T_1 weighted volume imaging and demonstrated that segmenting subfields increased sensitivity in diagnosing MCI (Hanseeuw et al. 2011). The current study uses an extensive dataset created by combining two large cohorts from the AddNeuroMed and the Alzheimer Disease Neuroimaging Initiative (ADNI) studies to build on and extend this earlier work.

In this study we aimed to (1) investigate the differences in hippocampal subfields between subject groups at baseline in a cohort of 1,069 subjects, (2) determine patterns of subfield volume loss in relation to age, gender, education, *APOE* ε4 genotype, and neuropsychological tests from mini mental state exam (MMSE) and Alzheimer disease Assessment Score-1 (ADAS-1) scores, and (3) compare combined subfield volumes using orthogonal partial least squares (OPLS) multivariate analysis to hippocampal volume alone for discriminating between AD and healthy control (HC) subjects and predicting future conversion from MCI to AD at 12 months.

Materials and Methods

Study Data and Inclusion and Diagnostic Criteria

The data used in this study were derived from two large multicentre cohorts, the AddNeuroMed and ADNI cohorts. The AddNeuroMed study is an integrated project funded by the European Union Sixth Framework Program and aims to establish and validate novel biomarkers of disease and treatment based upon in vitro and in vivo human and animal models of AD. Data was collected from six participating sites across Europe: University of Kuopio, Finland; University of Perugia, Italy; Aristotle University of Thessaloniki, Greece; King's College London, United Kingdom; University of Lodz, Poland; and University of Toulouse, France (Lovestone et al. 2009; Simmons et al. 2009, 2011).

Data from the ADNI study was downloaded from the ADNI at the LONI website (www.loni.ucla.edu/ADNI, PI Michael M. Weiner). The initiative was launched in 2003 by the National Institute on Ageing, the National Institute of Biomedical Imaging and Bioengineering, the Food and Drug Administration, private pharmaceutical companies and non-profit organisations, as a 5 years public–private partnership. The primary goal of ADNI has been to test whether MRI, positron emission tomography (PET), and other biological markers are useful in clinical trials of MCI and early AD. Subjects aged 55–90 from over 50 sites across the U.S and Canada participated in the research, and imaging, clinical, and biological samples were collected at multiple time points (Jack et al. 2008). A detailed description of the inclusion criteria for the study can be found on its webpage (http://www.adni-info.org/scientists/aboutADNI.aspx#).

A total of 1,069 subjects were included in this study (AD = 291, MCI = 447, HC = 331). The demographics of the cohorts are given in Table 1. Of the 447 MCI subjects in our whole cohort, 90 converted to an AD diagnosis (MCI converters) at 12 months.

For the AddNeuroMed cohort, subjects were patients who attended local memory clinics and received a diagnosis of MCI while HC subjects were recruited from non-

Table 1 Demographic, clinical and neuropsychological data in AD, MCI converters, stable MCI, and control subjects

	AD ($n = 291$)	MCI converters ($n = 90$)	Stable MCI ($n = 357$)	HC ($n = 331$)	p*
Gender (male/female)	131/160[a]	54/36	216/141[b]	166/165	0.001
Age	75.4 ± 7.0	74.1 ± 6.6	75.1 ± 7.0	75.0 ± 5.7	0.439
Years of education	12.1 ± 4.7[a,b,c]	14.0 ± 4.1	14.3 ± 4.4	14.3 ± 4.4	<0.001
MMSE	22.4 ± 3.4[a,b,c]	26.5 ± 1.8[b]	27.1 ± 1.7[b]	29.1 ± 1.1	<0.001
ADAS-1	6.3 ± 1.5[a,b,c]	5.3 ± 1.3[a,b]	4.6 ± 1.4[b,c]	3.1 ± 1.3	<0.001
CDR	0.9 ± 0.4[a,b,c]	0.5[b]	0.5[b]	0	<0.001
APOE ε4 genotype (+ive/-ive)	183/108	57/33	171/186	93/238	<0.001

Data are represented as mean ± and standard deviation. Chi square was used for gender and *APOE* ε4 genotype comparison. ANOVA with Bonferroni post hoc test was used for age, education, and neuropsychological scores

[a] Significant compared to stable MCI

[b] Significant compared to healthy controls (HC)

[c] Significant compared to MCI converters

* p values corrected for multiple comparisons using the Bonferroni method

related members of the patient's families, caregiver relatives, and social centres for the elderly or General Practitioner (GP) surgeries. Informed consent was obtained for all subjects and the study was approved by the ethical review boards of each participating country. The general inclusion and exclusion criteria were as follows.

AD

(1) diagnosis established by National Institute of Neurological and Communicative Disorders and Stroke and the Alzheimer's Disease and Related Disorders Association (NINCDS-ADRDA) and Diagnostic and Statistical Manual of Mental Disorders IV (DSM IV) criteria, (2) MMSE score ranged from 12 to 28. Subjects were excluded from the study if any psychiatric or neurological illness other than AD was present, and if subjects presented with a systemic illness or signs of organ failure.

MCI

(1) subjects had MMSE scores between 24 and 30, (2) subjective memory complaint with preserved activities of daily living, (3) Clinical Dementia Rating (CDR) score of 0.5, (4) Geriatric depression scale score less than or equal to 5, (5) absence of dementia in accordance with NINCDS-ARDA criteria. A 12 months follow up was used to determine whether MCI subjects converted to AD (MCI converters) or remained clinically stable (stable MCI).

HC

(1) MMSE scores between 24 and 30, (2) CDR score of 0, (3) no presence of neurological or psychiatric illness, and non-demented.

MMSE, CDR, and the Consortium to Establish a Registry for Alzheimer's Disease (CERAD) cognitive battery were assessed for each subject. The CERAD cognitive battery was replaced with the Alzheimer's disease assessment scale for AD subjects in AddNeuroMed. The CERAD battery employs the same 10 word recall task as the Alzheimer's assessment scale, only the scoring is inverted. Therefore, the mean number of words not recalled in the CERAD word list task was calculated in order to obtain comparable measures of memory for all diagnostic groups. This revised cognitive parameter was named ADAS-1 corresponding to the first subtest of the Alzheimer's disease assessment scale.

MRI Acquisition

Standardized MRI data acquisition techniques were in place for AddNeuroMed and ADNI to ensure homogeneity across data acquisition sites. A detailed description of the ADNI data acquisition protocol can be found at www.loni.ucla.edu/ADNI/research/Cores/index.shtml. The imaging protocol included a 1.5T high resolution T1 weighted sagittal 3D MP-RAGE volumes (voxel size $1.1 \times 1.1 \times 1.2$ mm^3), and axial proton density with T2 weighted fast spin echo images. A comprehensive quality control procedure was carried out on all MR images according to the AddNeuroMed quality control framework (Simmons et al. 2009, 2011).

Hippocampal Subfield Segmentation

Image analysis was carried out using the Freesurfer image analysis pipeline (version 5.1.0). These procedures have been described in detail in previous publications (Dale et al. 1999; Fischl et al. 2002; Ségonne et al. 2004; Fischl

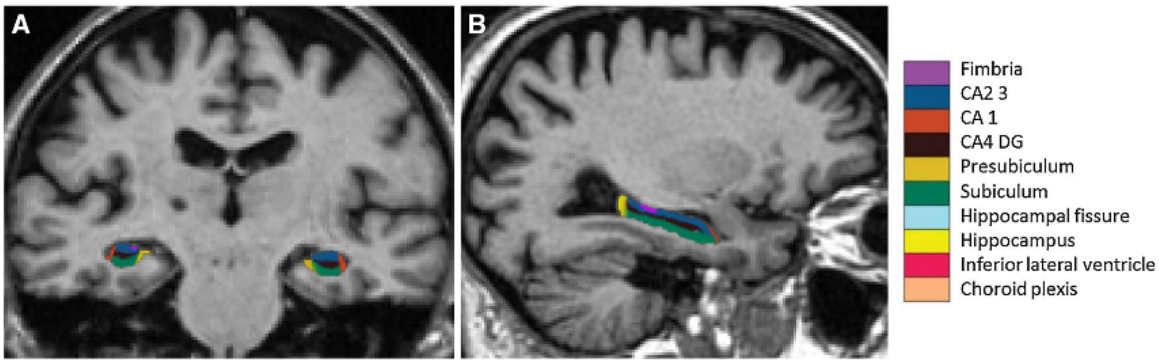

Fig. 1 **a** Coronal and **b** sagittal views of the hippocampus

et al. 2004). Initially volumetric segmentation involved the removal of non-brain tissue using a hybrid watershed/surface deformation procedure (Ségonne et al. 2004), automated Talairach transformation, segmentation of the subcortical white matter and deep grey matter volumetric structures (Fischl et al. 2004).

Automated segmentation of the hippocampus was performed to define anatomical subfield labels using a Bayesian modelling approach and a computational model of the areas surrounding the hippocampus. An atlas mesh had previously been built and validated from manual delineations in ultra-high resolution MRI scans of 10 individuals (Van Leemput et al. 2009). These delineations include the fimbria, presubiculum, subiculum, CA1, CA2/3, and CA4-DG subfields as well as the hippocampal fissure. Figure 1 illustrates the delineations made to define the different subfields of the hippocampus. For more details about this technique and the borders used to define the different subfields, see Van Leemput et al. (2009).

All subfield measures were normalised by the subject's intracranial volume derived from Freesurfer using the following formula: $\text{volume}_{\text{norm}} = \text{volume}_{\text{raw}} \times 1{,}000/\text{ICV}$ in cm^3 (Westman et al. 2013). This automated segmentation approach has been recently applied to a small group of MCI subjects (Hanseeuw et al. 2011).

Statistical Analysis

Statistical analysis was conducted using PASW Statistics (Version 17. 0; SPSS inc., USA). Categorical variables were inspected using the Chi square test while continuous variables were tested using ANOVA with Bonferroni post hoc comparisons. Hippocampal subfield volumes were first analysed using MANCOVA utilising Bonferroni correction by adopting a general linear model procedure, adjusting for age, gender, education, and *APOE* ε4 genotype as covariates. Bonferroni pairwise comparisons were performed to inspect subfield volume differences between the groups.

Multiple regression analyses were conducted in R version 2.15.2 using the lm function from the R stats package and Bonferroni correction for multiple comparisons. Patterns of subfield volume loss were tested in relation to the effects of age, gender, education, *APOE* ε4 genotype, and neuropsychological test scores from MMSE and ADAS-1. In this step, all subfield measures were tested as dependent variables by disease group (AD, MCI converters, stable MCI, and HC) as a whole. Age, gender, years of education, *APOE* ε4 genotype, and neuropsychological scores from MMSE and ADAS-1 tests was treated as independent variables for identifying subfield specific effects. 10 fold cross validation was performed by fitting linear regression models to the data, excluding 1/10th of the data in each fold and using the fitted model for prediction on data that was excluded from the fold.

Hippocampal subfields were subsequently analysed using Orthogonal Partial Least Squares (OPLS) (Wiklund et al. 2008; Trygg and Wold 2002), a supervised multivariate data analysis method included in the software package SIMCA (Umetrics AB, Umea, Sweden). All 14 variables (left and right subfields) were used for OPLS analysis. Classification models were created for distinguishing between AD and HC subjects at baseline. The AD versus HC models were subsequently treated as classifiers to investigate how well the hippocampal subfields could predict future MCI conversion to AD at 12 months follow up. Seven-fold cross validation was used for all models. Using this approach we created 4 OPLS models; 2 for the total hippocampus and 2 for the combination of subfield volumes. The first model for each region comprised the AddNeuroMed cohort and the second model comprised the ADNI cohort. To further validate the models created the AddNeuroMed cohort was used as the training set and the ADNI cohort as a test set (and vice versa) to see how well the models could predict new and unseen data. The combined ADNI and AddNeuroMed cohort from the AD versus HC comparison was used as a classifier to investigate the reliability of predicting MCI conversion to AD at

Table 2 Hippocampal subfield differences in AD, MCI converters, stable MCI, and healthy control subjects

	AD ($n = 291$)	MCI converters ($n- = 90$)	Stable MCI ($n = 357$)	HC ($n = 331$)	p
Left presubiculum	309.2 ± 63.5[a,b]	323.7 ± 64.6[a,b]	363.2 ± 70.9[b,c]	409.5 ± 62.963.1	<0.0001
Left subiculum	449.0 ± 86.7[a,b]	465.9 ± 84.1[a,b]	520.9 ± 91.0[b,c]	579.5 ± 76.2	<0.0001
Right presubiculum	307.9 ± 64.0[a,b]	318.7 ± 63.5[a,b]	359.2 ± 70.8[b,c]	399.0 ± 64.3	<0.0001
Right subiculum	449.9 ± 90.4[a,b]	467.1 ± 92.7[a,b]	523.5 ± 96.4[b,c]	575.5 ± 77.5	<0.0001
Left CA4-DG	399.2 ± 73.5[a,b]	416.2 ± 67.6[a,b]	453.1 ± 79.0[b,c]	494.2 ± 67.7	<0.0001
Left CA2-3	716.4 ± 134.2[a,b]	747.6 ± 127.1[a,b]	804.6 ± 139.8[b,c]	877.9 ± 121.0	<0.0001
Right CA4-DG	418.3 ± 78.0[a,b]	436.1 ± 80.6[a,b]	476.9 ± 83.2[b,c]	511.6 ± 69.8	<0.0001
Right CA2-3	765.4 ± 143.4[a,b]	793.5 ± 146.4[a,b]	858.8 ± 146.0[b,c]	920.7 ± 127.7	<0.0001
Left fimbria	29.9 ± 21.5[a,b]	33.6 ± 25.6[b]	37.9 ± 23.3[b]	49.1 ± 23.1	<0.0001
Left CA1	286.8 ± 55.5[a,b]	298.2 ± 49.1[b]	308.1 ± 50.1[b]	322.4 ± 45.0	<0.0001
Right CA1	293.8 ± 57.0[a,b]	301.5 ± 53.2[b]	315.7 ± 54.2[b,c]	328.5 ± 45.8	<0.0001
Right fimbria	26.9 ± 18.8[a,b]	31.8 ± 21.5[b]	32.3 ± 18.8[b]	41.5 ± 19.9	<0.0001
Right hippocampal fissure	44.8 ± 26.2	46.2 ± 23.8	45.1 ± 23.8	47.7 ± 24.1	2.144
Left hippocampal fissure	39.8 ± 22.7	37.6 ± 22.8	40.7 ± 21.6	41.4 ± 21.1	3.276

Absolute Hippocampal subfields are presented (mm^3). However, normalised hippocampal subfields (absolute hippocampal subfield/intracranial volume) were used in MANCOVA with Bonferroni pairwise comparisons. Age, gender, education, and *APOE* ε4 genotype were used as covariates. p values were corrected for multiple comparisons using the Bonferroni method

[a] Significant compared to stable MCI

[b] Significant compared to healthy controls (HC)

[c] Significant compared to MCI converters

12 months. This OPLS classification approach has been extensively validated (Bylesjo et al. 2006; Wiklund et al. 2008; Westman et al. 2011c) and applied to several biomarker discovery studies in AD (Mangialasche et al. 2010; Westman et al. 2011a, 2012; Spulber et al. 2013).

Sensitivity and specificity were calculated from the cross-validated prediction values of the OPLS models. The positive and negative likelihood ratios (LR+ = sensitivity/(100−specificity) and LR− = (100−sensitivity)/specificity)) were determined. A positive likelihood ratio between 5 and 10 or a negative likelihood ratio between 0.1 and 0.2 increases the diagnostic value in a moderate way, while a value above 10 or below 0.1 significantly increases the diagnostic value of the test.

Receiver operating characteristic (ROC) curves were calculated for the individual subfield volume models using the ROCR library (version 2.1) in R. ROC curves provide a graphical means to interpret the quality of separation and are created by plotting the true positive rate (sensitivity) versus the false positive rate (1−specificity) for various thresholds. The discriminant value of the corresponding ROC curve can be obtained by calculating the area under the curve (AUC). AUC values range from 0.5 (random discriminations no better than chance) to 1.0 (perfect discrimination). The pROC (Receiver Operating Characteristic) package (version 1.5.4) (Robin et al. 2011) in R was used to perform area under the curve (AUC) statistical comparisons between the combined subfield and total hippocampal volume models in the AD vs. HC and MCI converter vs MCI non-converter models.

Results

Demographics, Neuropsychological, and Global Clinical Measurements

1,069 subjects were included in the current study (AD = 291, MCI = 447, HC = 331) from the AddNeuroMed and ADNI cohorts. Results from global, clinical and cognitive assessments revealed that scores on MMSE, CDR, and ADAS-1 were poorest amongst AD and best amongst control subjects as expected (Table 1).

Hippocampal Subfields

Hippocampal subfield volumes from the left and the right hemisphere were used to determine the pattern of subfield atrophy in AD, MCI-converter, MCI stable and HC subjects. Comparisons of the bilateral CA1, CA2-3, CA4-DG, subiculum, and presubiculum were significant across all groups (<0.0001) after correction for multiple comparisons and demonstrated similar results in pairwise comparisons (Table 2 and Fig. 2). No significant volume differences were found for the left and right hippocampal fissure between these groups.

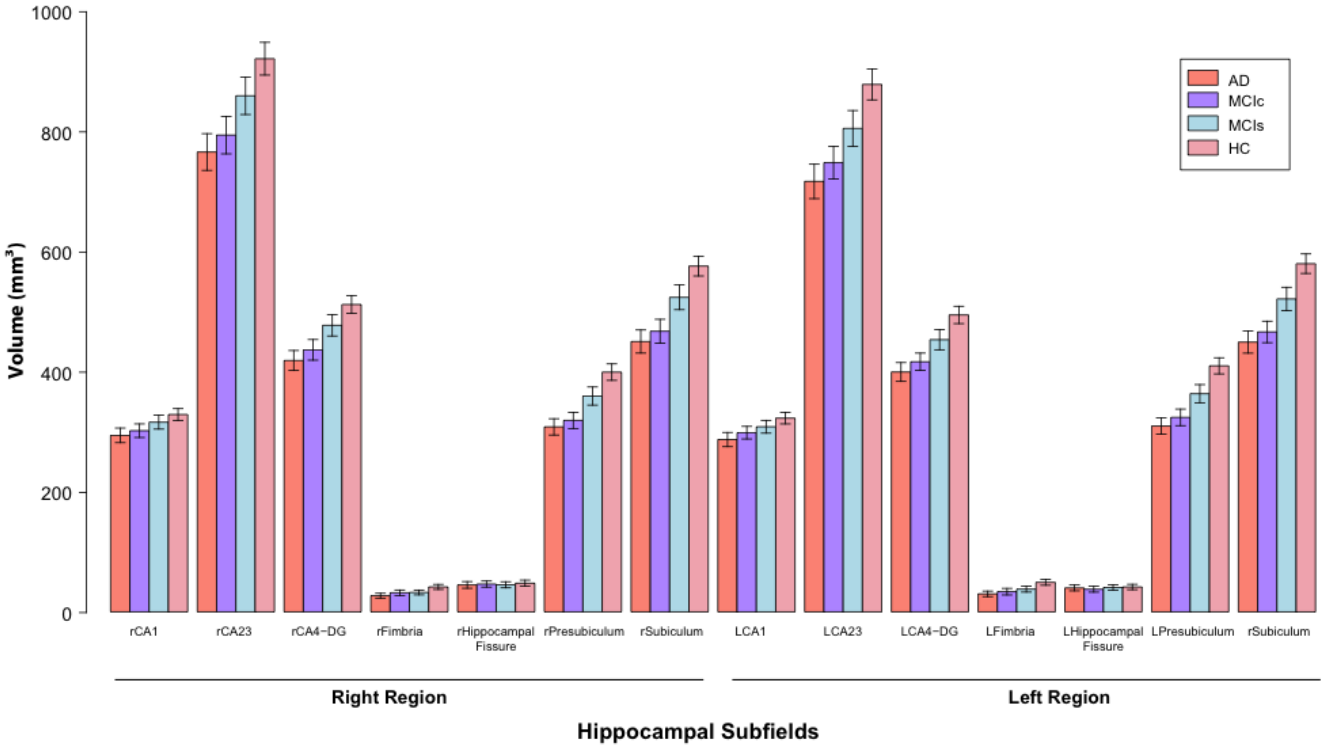

Fig. 2 *Bar* plot of subfield volumes of AD ($n = 291$), MCI converters ($n = 90$), MCI stable ($n = 357$), and healthy control (HC) subjects ($n = 331$). *Error bars* represent SEM = SD/$\sqrt{}$n. Subfield volumes are represented in mm3. R = subfield volumes from the *right hemisphere*, L = subfield volumes from the *left hemisphere*

In the left hippocampus, presubiculum ($F = 144.5$, $p < 0.0001$) and subiculum ($F = 144.3$, $p < 0.0001$) volumes were most significantly reduced in AD, MCI converter and MCI stable subjects compared to healthy controls. The same pattern of subfield atrophy was also observed in the right hippocampus for these groups for both presubiculum ($F = 122.1$, $p < 0.0001$) and subiculum ($F = 120.0$, $p < 0.0001$) relative to healthy controls. MCI-converters displayed significant subfield volume losses in the bilateral subiculum (right = $p < 0.0001$, left = $p < 0.0001$), subiculum (right = $p < 0.0001$, left = $p < 0.0001$), CA4-DG (right = $p < 0.0001$, left = $p < 0.0001$), and CA2-3 (right = $p < 0.0001$, left = $p < 0.0001$) relative to stable MCI subjects. However, no significant differences in any of the subfield volume measures were observed between AD and MCI-converter subjects.

Relationship Between Neuropsychological Test Scores and Hippocampal Subfields

A significant positive effect for MMSE was found in relation to all hippocampal subfield volumes except bilateral hippocampal fissure, indicating that subjects with lower MMSE scores had reduced subfield volumes (Table 3). On the other hand, a significant negative effect was observed for ADAS-1 scores across all subfield volumes except the bilateral hippocampal fissure, indicating that subjects with higher ADAS-1 scores (mean number of words not recalled) had lower subfield volumes (Table 3).

Relationship Between Age, Education, *APOE* ε4 Genotype, and Hippocampal Subfields

A significant negative effect of age was observed in relation to all subfield volumes indicating that older subjects had lower hippocampal subfield volumes. In particular, the strongest effects of age were found in the right presubiculum ($\beta = -0.32$, $p < 0.001$), and left presubiculum areas, the right fimbria ($\beta = -0.31$, $p < 0.001$), and the right subiculum and left subiculum areas ($\beta = -0.28$, $p < 0.001$).

Linear regression models were also created to test for the effect of gender on subfield volume differences in the male ($n = 567$) and female ($n = 502$) subjects. A significant positive effect of gender was found in the right fimbria and left fimbria areas, and in the right and left CA4-DG subfield volumes (Table 4).

A significant negative effect of education was only found in the right CA1 ($\beta = -0.95$, $p = 0.024$).

Table 3 MMSE and ADAS-1 effect on hippocampal subfield volumes in the combined cohort

	MMSE score			ADAS-1 score		
Hippocampus	β	*t*	*p**	β	*t*	*p**
Left CA1	0.24	8.41	<0.001	−0.19	−6.68	<0.001
Right CA1	0.23	8.15	<0.001	−0.16	−5.47	<0.001
Left CA2-3	0.34	12.29	<0.001	−0.34	−11.93	<0.001
Right CA2-3	0.35	12.40	<0.001	−0.28	−9.67	<0.001
Left CA4-DG	0.37	13.47	<0.001	−0.36	−12.51	<0.001
Right CA4-DG	0.37	13.31	<0.001	−0.31	−10.65	<0.001
Left Fimbria	0.23	8.08	<0.001	−0.23	−8.07	<0.001
Right Fimbria	0.19	6.51	<0.001	−0.18	−6.19	<0.001
Left Presubiculum	0.43	15.51	<0.001	−0.42	−15.19	<0.001
Right Presubiculum	0.40	14.11	<0.001	−0.39	−13.60	<0.001
Left Subiculum	0.43	15.57	<0.001	−0.42	−15.06	<0.001
Right Subiculum	0.40	14.49	<0.001	−0.36	−12.67	<0.001

Age, gender, education and *APOE* ε4 genotype were introduced as covariates in these models

* *p* values from the regression models were corrected for multiple comparisons using the Bonferroni method

The analysis was repeated for subjects that were carriers and non-carriers of the *APOE* ε4 allele. APOE E4 genotype was negatively related to all subfield volumes suggesting that subjects with an APOE E4 allele had smaller subfield volumes (Table 5).

AD and HC Classification for the Combined AddNeuroMed and ADNI Cohort

For the joint AddNeuroMed and ADNI AD versus HC model, combining the subfield volumes resulted in an accuracy of 81.7 % (sensitivity = 80.4 %, specificity = 82.8 %, AUC = 0.895) compared to 80.7 % for total hippocampal volume (sensitivity = 79.2 %, specificity = 82.8 %, AUC = 0.887) (Table 6). These result were statistically significantly different in terms of the observed AUC differences between the two models (AUC difference = 0.008, $p = 0.001$).

Combining subfield volumes resulted in similar classification accuracy to the subiculum (accuracy = 81.2 %, sensitivity = 83.5 %, specificity = 79.2 %, AUC = 0.887) and presubiculum alone (accuracy = 80.6 %, sensitivity = 83.2 %, specificity = 78.3 %, AUC = 0.882), but higher accuracies than the other individual subfield volume measures (Table 7). Figure 3 illustrates ROC curves for the corresponding individual subfield volumes for distinguishing AD and HC subjects.

Model Validation for AD and HC Classification

Seven fold cross validation was used to determine the robustness of all the models. In this study models were validated using an external test set. The ADNI model was used as a training set and predictions were made using the AddNeuroMed cohort as the external test set and vice versa. The results are similar to those obtained by cross validation (Table 6). For the combination of hippocampal subfields, using the AddNeuroMed cohort as the test set and the ADNI cohort as the training set resulted in a similar classification accuracy, 82.1 % (sensitivity = 77.1 %, specificity = 86.9 %, AUC = 0.90) compared to 81.1 % for total hippocampal volume (sensitivity = 75.2 %, specificity = 86.9 %, AUC = 0.897). Similar results for the combination of hippocampal subfields and total hippocampal volume were obtained when using the ADNI cohort as the test set and the AddNeuroMed cohort as the training set (Table 5). For further validation, we compared if subjects were classified differently between the different models for the combination of hippocampal subfields (for

Table 4 Age and Gender effect on hippocampal subfields in the combined cohort

Hippocampus	Age[a]				Gender[b]			
	β	*t*	PRESS	*p* value*	β	*t*	PRESS	*p* value*
Left CA1	−0.1	−3.31	42.8	0.012	0.04	1.16	0.239	2.964
Right CA1	−0.09	−3.01	42.7	0.036	0.04	1.3	0.239	2.304
Left CA2-3	−0.24	−7.75	41.0	<0.001	0.09	2.93	0.237	0.036
Right CA2-3	−0.23	−7.62	40.8	<0.001	0.1	3.2	0.237	0.012
Left CA4-DG	−0.24	−7.92	40.6	<0.001	0.1	3.19	0.237	0.012
Right CA4-DG	−0.25	−8.2	40.7	<0.001	0.12	3.74	0.236	<0.001
Left Fimbria	−0.25	−8.42	39.6	<0.001	0.12	3.74	0.236	<0.001
Right Fimbria	−0.29	−9.72	40.5	<0.001	0.13	4.24	0.235	<0.001
Left Presubiculum	−0.31	−10.28	40.0	<0.001	0.09	2.71	0.238	0.084
Right Presubiculum	−0.32	−10.91	40.1	<0.001	0.09	2.89	0.237	0.048
Left Subiculum	−0.28	−9.09	38.9	<0.001	0.12	3.85	0.236	0.012
Right Subiculum	−0.28	−9.25	39.3	<0.001	0.12	3.38	0.236	0.012

[a] Gender, years of education, and APOE E4 genotype were used as covariates

[b] Subject age, years of education, and APOE E4 genotype were used as covariates

* *p values* from each regression model were corrected for multiple comparisons using the Bonferroni method

Table 5 Years of education and APOE genotype effect on hippocampal subfields in the combined cohort

	Years of education[a]			APOE E4 genotype[b]		
	β	*t*	*p**	β	*t*	*p**
Left CA1	−0.59	−1.92	0.66	0.22	−7.29	0.012
Right CA1	−0.95	−3.11	0.024	0.17	−5.74	0.012
Left CA2-3	−0.004	−0.14	10.668	0.24	−7.89	<0.001
Right CA2-3	−0.01	−0.45	7.86	0.26	−8.46	<0.001
Left CA4-DG	−0.002	−0.06	11.46	0.253	−8.31	<0.001
Right CA4-DG	−0.009	−0.27	9.408	0.27	−8.8	<0.001
Left Fimbria	0.028	0.88	4.548	0.1	−3.05	0.024
Right Fimbria	0.08	2.39	0.204	0.07	−2.28	0.276
Left Presubiculum	0.03	0.81	5.004	0.24	−7.8	<0.001
Right Presubiculum	0.05	1.57	1.404	0.23	−7.28	<0.001
Left Subiculum	0.03	1.06	3.48	0.27	−8.84	<0.001
Right Subiculum	0.02	0.65	6.216	0.27	−8.66	<0.001

[a] Subject age, gender, and APOE E4 genotype were used as covariates

[b] † Subject age, gender and years of education were used as covariates

* *p values* from each regression model were corrected for multiple comparisons using the Bonferroni method

Table 6 Comparison of performance for the different cohort models in the AD vs. HC classification

	Total Hippocampus					Hippocampal subfields				
	ACC (%)	SENS (%)	SPE (%)	AUC	Q^2 (Y)	ACC (%)	SENS (%)	SPE (%)	AUC	Q^2 (Y)
AddNeuroMed (cv)	80.7 (74.8–85.4)	76.2 (67.2–83.3)	85.1 (77.1–90.6)	0.897	0.439	80.2 (74.3–85.0)	78.1 (69.3–84.9)	82.2 (73.9–88.3)	0.90	0.441
ADNI (cv)	81.5 (77.4–84.9)	81.2 (75.0–86.2)	81.7 (76.1–86.2)	0.884	0.404	82.0 (77.9–85.6)	81.2 (75.0–86.2)	82.6 (77.1–87.0)	0.892	0.433
Combined (cv)*	80.7 (77.4–83.6)	79.2 (74.1–83.5)	82.8 (78.3–86.5)	0.887	–	81.7 (78.4–84.5)	80.4 (75.5–84.6)	82.8 (78.3–86.5)	0.895	–
AddNeuroMed[a]	81.1 (75.3–85.8)	75.2 (66.2–82.5)	86.9 (79.2–92.0)	0.897	–	82.1 (76.4–86.7)	77.1 (68.2–84.1)	86.9 (79.2–92.0)	0.90	–
ADNI[b]	80.2 (76.1–83.8)	84.4 (78.5–88.9)	76.8 (70.8–81.8)	0.884	–	80.7 (76.6–84.3)	88.2 (82.7–92.1)	74.6 (68.5–79.8)	0.881	–

[a] AddNeuroMed dataset used as the test set and ADNI data as the training set

[b] ADNI data used as the test set and AddNeuroMed dataset as the training set

* AddNeuroMed and ADNI cohorts used as the combined cohort model, confidence intervals presented within parenthesis

CV cross validation, *AUC* area under the curve

example classified as AD in one model and HC in another model). We compared the single cohort cross validated models with the combined cohort model and the single cohort models using the train/test approach. The results demonstrate that classification agreement for the different comparisons were high, lying between 89.5–98.8 % (Table 8).

Predicting MCI Conversion

Models previously constructed using AD and HC subjects from the combined cohort were applied to our large external test set of MCI subjects ($n = 447$) to predict future conversion to AD. These classifiers subsequently identified MCI subjects with an AD like brain structure (percentage classified as AD-like) or a healthy control-like brain structure (percentage classified as HC-like). During the 12 month follow up interval, 90 MCI subjects from the AddNeuroMed and ADNI cohorts met the clinical criteria for AD, and 357 MCI subjects remained clinically stable.

The combined subfield volumes classifier correctly identified 81.1 % of MCI converters from baseline images, with the presubiculum also correctly identifying 81.1 % of MCI-c with an AD-like pattern of subfield atrophy. In comparison, total hippocampal volume identified 76.7 % of MCI-c correctly. The predictive accuracies from the classifiers ranged between 56.7–81.1 % for MCI-c predictions (Table 9).

However, a considerable number of MCI-s subjects were also predicted with an AD-like pattern of atrophy despite their clinically stable condition at 12 months follow up. For instance, the combined subfield volumes classifier, which was the most robust for MCI-c prediction, identified only 48.7 % of MCI-s with a HC-like subfield structure. A similar result was observed for the total hippocampal volume classifier which only identified 50.1 % of MCI-s correctly. Mean OPLS scores from the combined subfield volumes classifier and total hippocampal volume classifier were 0.50 ± 028 and 0.49 ± 0.27 (mean ± standard deviation) respectively (Fig. 4). As a result, differences in OPLS scores between the two classifiers were not statistically significant (Wilcoxon signed rank sum test, $Z = -0.725$, $p = 0.469$) despite the difference in AD-like MCI-c predictions. HC-like predictive accuracies in MCI-s

Table 7 Comparison of performance for OPLS AD vs. HC classification models

	ACC (%)	SEN (%)	SPE (%)	AUC	PPV (%)	NPV (%)	LR+	LR−
CA1	66.0 (62.2–69.6)	68.0 (62.5–73.1)	65.9 (60.6–70.8)	0.749	63.7	70.1	1.99 (1.68–2.36)	0.49 (0.40–0.58)
CA2-3	75.4 (71.9–78.6)	77.0 (71.8–81.4)	74.0 (69.0–78.5)	0.843	72.3	78.5	2.96 (2.44–3.59)	0.31 (0.25–0.39)
CA4-DG	76.9 (73.4–80.0)	79.7 (74.7–83.9)	74.3 (69.4–78.7)	0.853	73.2	80.7	3.11 (2.56–3.76)	0.27 (0.22–0.35)
Fimbria	68.2 (64.4–71.7)	69.8 (64.3–74.8)	66.8 (61.5–71.6)	0.745	64.9	71.5	2.10 (1.77–2.49)	0.45 (0.37–0.55)
Presubiculum	80.6 (74.9–83.4)	83.2 (78.4–87.0)	78.3 (73.5–82.4)	0.882	77.1	84.1	3.08 (3.10–4.72)	0.22 (0.17–0.28)
Subiculum	81.2 (77.9–84.1)	83.5 (78.8–87.3)	79.2 (74.5–83.2)	0.887	77.9	84.5	4.01 (3.23–4.97)	0.21 (0.16–0.27)

Confidence intervals are presented within parenthesis. *AUC* area under the curve, *PPV* positive predictive value, *NPV* negative predictive value, *LR+* positive likelihood ratio, *LR−* negative likelihood ratio

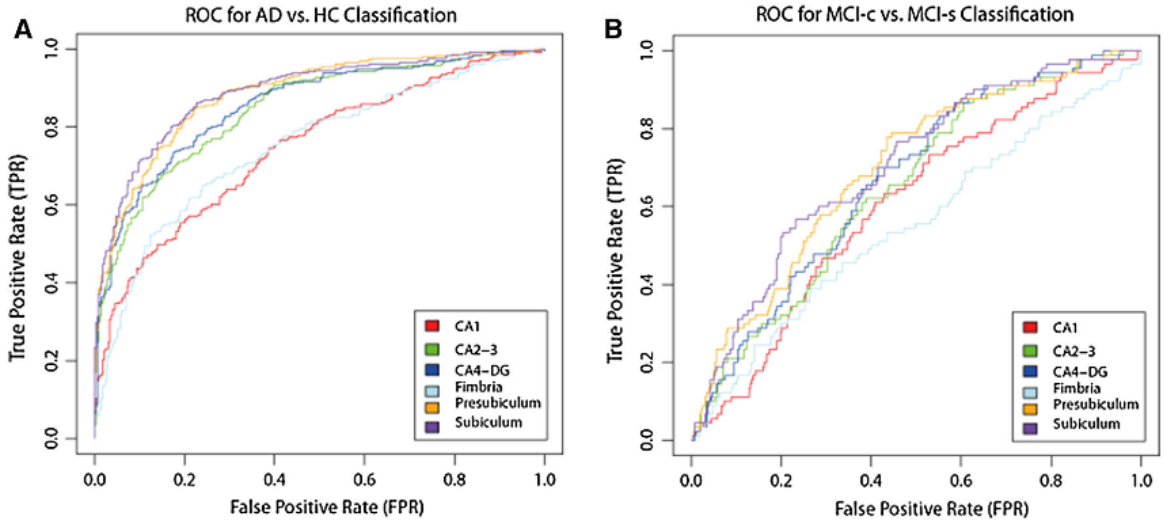

Fig. 3 **a** ROC curve for AD versus HC classification using individual subfield measures, **b** ROC curve for *MCI-c* and *MCI-s* classification using individual subfield measures. The curve is calculated with a 95 % probability assurance. *ROC* receiver operating characteristic, *AD* Alzheimer's disease, *HC* healthy control, *MCI-c* MCI-converter, *MCI-s* stable MCI

predictions only ranged between 46.8–51.8 % which is because many of these MCI-s subjects will convert to AD at a future stage and already demonstrate an Alzheimer like pattern of hippocampal subfield atrophy.

Discussion

Using an automated image analysis pipeline to explore the subfields of the hippocampus, we found that AD and MCI converters displayed a widespread pattern of subfield atrophy, including the bilateral subiculum, presubiculum and CA1 which have been reported in previous studies. Using the same image analysis approach, Hanseeuw et al. (2011) previously reported significant volume losses in the subiculum and CA2-3 region of the hippocampus in a small group of 15 amnestic MCI subjects and 15 healthy controls. We have extended this preliminary work to data from two large studies which together contain a more heterogeneous group of AD and MCI subjects that more accurately reflect the population of MCI and AD. The pattern of hippocampal volume loss that was found was wider than previous reports which have used either manual delineation techniques hippocampal subfield segmentation (Mueller and Weiner 2009; Mueller et al. 2010), 3D surface mapping (Apostolova et al. 2010) or shape analysis techniques (Csernansky et al. 2005; Costafreda et al. 2011) A similar pattern of subfield atrophy was observed for AD subjects and MCI converters suggesting that MCI converters may represent an imaging profile more similar to AD subjects than stable MCI. The pattern of hippocampal subfield loss, though wider than previously reported is in agreement with previous neuropathological studies reporting early neuronal loss in the subiculum, CA4-DG, and CA1 (West et al. 2004). Larger datasets are more likely to contain subjects with different types of atrophy which could explain the widespread pattern of subfield volume losses reported in the present study.

Table 8 Comparison of subject classification between cohort models

	ANM and ANM/ ADNI	ADNI and ANM/ ADNI	ANM and ANMon ADNI	ADNI on ADNI onANM
Total n	212	410	212	410
Same classification (n)	197	405	196	367
Same classification (%)	92.9	98.8	92.5	89.5
Different classification (n)	15	5	16	43
Different classification (%)	7.1	1.2	7.5	10.5

ANM AddNeuroMed cohort model, *ANM/ADNI* combined AddNeuroMed and ADNI cohort model, *ANMonADNI* AddNeuroMed cohort test set and ADNI training set, *ADNIonANM* ADNI cohort test set and AddNeuroMed cohort training set, *total n* AD and HC subjects, *Same classification* number of subjects predicted alike, *% same classification* percentage of subjects predicted alike, *Different classification* number of subjects predicted differently, *Different classification (%)* percentage of subjects predicted differently

Relationship Between Neuropsychological Test Scores and Hippocampal Subfields

A significant positive effect for both MMSE and ADAS-1 was found in relation to all hippocampal subfield volumes, indicating that subjects with lower MMSE scores and higher ADAS-1 scores had lower subfield volumes. This confirms the relationship between diffuse hippocampal volume loss and poorer neuropsychological test scores (Scheltens et al. 1992; Liu et al. 2009).

Relationship Between Age, Gender, Education, *APOE* ε4 Genotype, and Hippocampal Subfields

Previous studies investigating the influence of age on hippocampal subfields have found significant negative effects associated with CA1 and CA2-3 subfield volumes (Mueller and Weiner 2009). Consistent with this previous work, using a larger dataset we also found a significant negative effect of age but in relation to all subfield volumes. However, years of education was only significantly associated with the right CA1 and right fimbria. Gender specific differences in the pattern of subfield volume loss were found, with female subjects demonstrating lower bilateral CA2-3, CA4-DG, fimbria, presubiculum and subiculum volumes. Previous work with AD patients suggests that gender specific differences in the rate of hippocampal volume loss are not entirely clear. For example, a previous study has reported a higher prevalence and incidence of AD in females (Barnes et al. 2005), whereas sex hormone differences have been suggested as an explanation of any gender divergence (Gouras et al. 2000). On the other hand, our findings suggest that carriers of the ε4 allele had smaller subfield volumes. which is in agreement with previous studies that have demonstrated a strong neuroanatomic effect of *APOE* ε4 genotype on the entire hippocampal region. (Jack et al. 1998; Reiman et al. 1998).

Table 9 MCI predictions using the baseline OPLS AD versus HC classifiers

	MCI-c classification ($n = 90$)[b]		MCI-s classification ($n = 357$)	
	AD like (%)*	HC like (%) **	AD like (%)*	HC like (%) **
CA1	**65.6 (59)**	34.4 (31)	48.2 (172)	**51.8 (185)**
CA2-3	**75.6 (68)**	24.4 (22)	52.1 (186)	**47.9 (171)**
CA4-DG	**74.4 (67)**	25.6 (23)	51.8 (185)	**48.2 (172)**
Fimbria	**56.7 (51)**	43.3 (39)	53.2 (190)	**46.8 (167)**
Presubiculum	**81.1 (73)**	18.9 (17)	51.0 (182)	**49.0 (175)**
Subiculum	**77.8 (70)**	22.2 (20)	51.3 (183)	**48.7 (174)**
Combined[a]	**81.1 (73)**	18.9 (17)	51.3 (183)	**48.7 (174)**
Total Hippocampal volume	**76.7 (69)**	23.3 (21)	49.9 (178)	**50.1 (179)**

AD Alzheimer's disease, *MCI* mild cognitive impairment, *MCIc* MCI converter, *MCI-s* MCI stable, *HC* healthy control

* Sensitivity at each time point is the percentage of MCIc subjects correctly classified as AD in bold

** Specificity at each time point is the percentage of MCI-s subjects correctly classified as HC in bold

[a] The combined model used the combination of subfields for classification

[b] Only includes subjects that underwent conversion from MCI to AD at 12 months follow up

AD and HC Classification

In this study we used the multivariate OPLS technique to distinguish between AD and control subjects. This method has previously been used for distinguishing between AD and control subjects (Westman et al. 2011a, b, c, d), as well as predicting conversion from MCI to AD using MRI regional measures and a combination of MRI regional measures and magnetic resonance spectroscopy (MRS) measures (Westman et al. 2010, 2011a, b, c, d). Hippocampal subfields have not been studied using this approach but several other studies have used alternative multivariate techniques including support vector machines, principal components analysis, and partial least squares to latent structures and linear discriminant analysis to analyse multiple MRI regional measures (Fan et al. 2008; McEvoy et al. 2009; Klöppel et al. 2008; Vemuri et al. 2008; Plant et al. 2010).

Studies that have attempted to distinguish between AD and control subjects have often done so using medial temporal structures such as the hippocampus and entorhinal cortex and reported accuracies of 80–90 % (Fox et al. 1996; Jack et al. 1992). Although prior studies have reported accuracies of up to 100 % in discriminating between AD and control subjects(Fan et al. 2008; Lerch et al. 2008), some studies used smaller samples, included more severely impaired AD patients or failed to cross-validate their findings. Here, using two large multicentre studies we segmented the hippocampus into its different

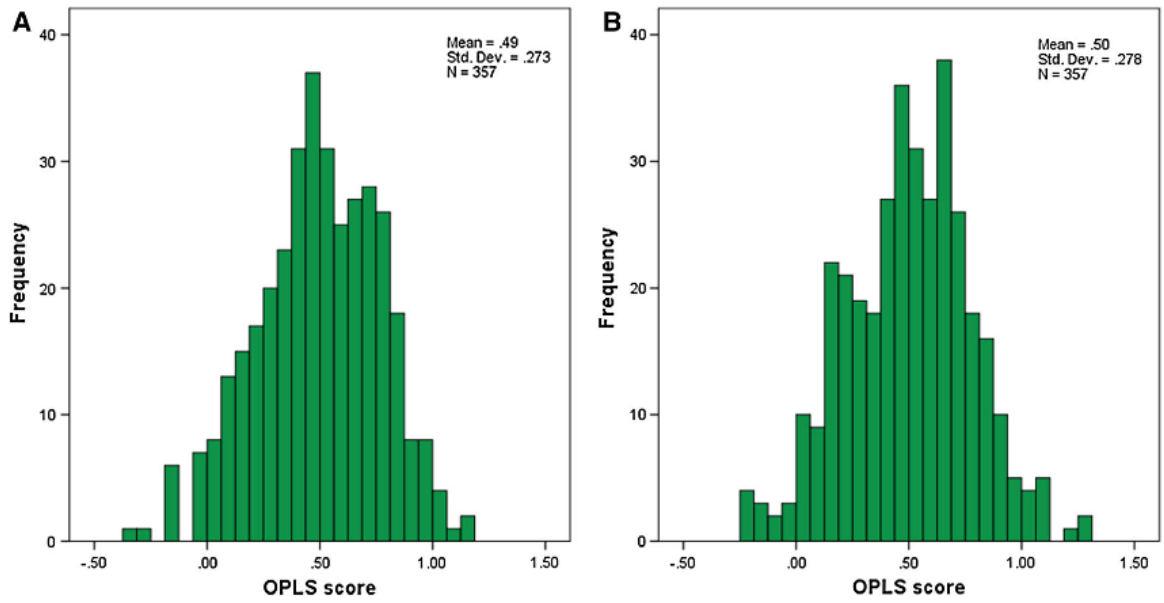

Fig. 4 **a** OPLS scores from the total hippocampal volume classifier for MCI-s predictions, **b** OPLS scores from the combined subfields volume classifier for MCI-s predictions

subfields to examine whether subfield volumes could improve the sensitivity of MRI in detecting AD. The results suggest that the OPLS technique with fully automated hippocampal subfield volumes performs as accurately as total hippocampal volume, presubiculum volume and subiculum volume in distinguishing between AD and control subjects. The OPLS method which combined hippocampal subfield measures produced a classification accuracy of 81.7 % (sensitivity = 80.4 %, specificity = 82.8 %, AUC = 0.895), while total automated hippocampal volume produced an accuracy of 80.7 % (sensitivity 79.2 %, specificity 82.8 %, AUC = 0.887). Although significantly different, the magnitude of the difference is small and does not offer a particular advantage over hippocampal volume. Recent work has also found that the visual rating assessment of the medial temporal lobe produces accuracies that are comparable to that of manual hippocampal volume in distinguishing between AD and controls (Westman et al. 2011d).

Although our study is the first to use multivariate analysis of automated hippocampal subfields, previous research has examined the combination of automated regional cortical thicknesses and regional volumes in distinguishing between AD and control subjects using support vector machines and linear discriminant analysis (Vemuri et al. 2008; McEvoy et al. 2009).

Predicting MCI Conversion

Building robust classification models on new and unseen data is of great importance for accurately predicting future MCI conversion to AD. MCI predictions were performed using AD vs. HC models in the combined ADNI and AddNeuroMed cohorts as classifiers and MCI subjects as our external validation test set. This approach has been applied previously and demonstrates how larger training sets can be used to assess MCI predictions that are more balanced in terms of sensitivity and specificity (Westman et al. 2011a). Previous studies in the neuroimaging literature utilising advanced methods of high dimensional pattern classification (Fan et al. 2008; Misra et al. 2009), and whole brain structural MRI (Karas et al. 2008; Davatzikos et al. 2010) have demonstrated the complexity of differential atrophy patterns observed in MCI-c and MCI-s subjects. Moreover, studies including our own have also shown heterogeneous patterns of brain atrophy exist in MCI subjects that convert to AD and those who remain clinically stable (Westman et al. 2011c; McEvoy et al. 2009). Consequently, hippocampal subfields were of interest following a small pilot study in MCI subjects (Hanseeuw et al. 2011).

Using a large external validation test set ($n = 447$) we sought to identify MCI subjects based on the similarity of their hippocampal subfield pattern to AD patients (% AD-like) or healthy control subjects (% HC-like). Unlike some previous studies, the large number of MCI subjects in our study served to more accurately represent the heterogeneity of MCI subjects and included both amnestic and non-amnestic subtypes.

The results demonstrated that the combination of subfield volumes and the presubiculum were the most robust classifiers, identifying 81.1 % of MCI-c correctly, and

were better than using total hippocampal volume alone. However, a considerable number of MCI-s subjects were also predicted with AD-like patterns of atrophy despite having a clinically stable MCI condition at 12 months follow up. Although beyond the scope of the current study we intend in future to study longitudinal change in hippocampal subfield measures over longer follow up times in the ADNI cohort. The utility of structural MRI plays a key role in this domain and represents one of the 3 main biomarkers for AD diagnosis (Dubois et al. 2007; Frisoni et al. 2010). However, more focus needs to be addressed towards the standardisation of acquisition and analysis methods in order to facilitate the integration of findings across studies. Recently there has been much interest in exploring the combination of different MRI imaging techniques (i.e. Tensor based morphometry, cortical thicknesses and volumes) with cerebrospinal fluid (CSF) biomarkers, 18F-fluorodeoxyglucose PET, and clinical examination for classifying AD and predicting MCI conversion to AD (Wolz et al. 2011; Vemuri et al. 2009; Zhang et al. 2011; Furney et al. 2011). In regards to our study, a longer follow up time would be helpful to refine our estimates of model specificity for MCI-s predictions. A more robust algorithm that could potentially predict future MCI time to AD conversion would be of future interest to validate our findings in this present study.

Conclusion

Hippocampal subfield volume loss in AD is widespread affecting regions such as the CA-1, subiculum, and presubiculum. Using an automated hippocampal subfield measurement technique we found prominent subfield volume losses in MCI converters and AD. Each of the subfield measures was related to both clinical predictors of AD (Age, gender, years of education, APOE E4 genotype) and cognitive scores (MMSE and ADAS-1 tests). Combined subfield volumes using the OPLS technique produced a similar classification accuracy to total hippocampal volume, presubiculum volume and subiculum volume in distinguishing between AD and HC subjects, but were more accurate than total hippocampal volume measurements at predicting MCI conversion to AD at 12 months.

Acknowledgments This study was supported by InnoMed, (Innovative Medicines in Europe) an Integrated Project funded by the European Union of the Sixth Framework program priority FP6-2004-LIFESCIHEALTH-5, Life Sciences, Genomics and Biotechnology for Health. Data collection and sharing for this project was funded by the ADNI (National Institutes of Health Grant U01 AG024904). Data collection and sharing for this project was funded by the Alzheimer's Disease Neuroimaging Initiative (ADNI) (National Institutes of Health Grant U01 AG024904) and DOD ADNI (Department of Defense award number W81XWH-12-2-0012). ADNI is funded by the National Institute on Aging, the National Institute of Biomedical Imaging and Bioengineering, and through generous contributions from the following: Alzheimer's Association; Alzheimer's Drug Discovery Foundation; BioClinica, Inc.; Biogen Idec Inc.; Bristol-Myers Squibb Company; Eisai Inc.; Elan Pharmaceuticals, Inc.; Eli Lilly and Company; F. Hoffmann-La Roche Ltd and its affiliated company Genentech, Inc.; GE Healthcare; Innogenetics, N.V.; IXICO Ltd.; Janssen Alzheimer Immunotherapy Research & Development, LLC.; Johnson & Johnson Pharmaceutical Research & Development LLC.; Medpace, Inc.; Merck & Co., Inc.; Meso Scale Diagnostics, LLC.; NeuroRx Research; Novartis Pharmaceuticals Corporation; Pfizer Inc.; Piramal Imaging; Servier; Synarc Inc.; and Takeda Pharmaceutical Company. The Canadian Institutes of Health Research is providing funds to support ADNI clinical sites in Canada. Private sector contributions are facilitated by the Foundation for the National Institutes of Health (www.fnih.org). The grantee organization is the Northern California Institute for Research and Education, and the study is coordinated by the Alzheimer's Disease Cooperative Study at the University of California, San Diego. ADNI data are disseminated by the Laboratory for Neuro Imaging at the University of California, Los Angeles. Also, thanks to the Foundation Gamla Tjänarinnor, the Swedish Alzheimer's Association and Swedish Brain Power, Health Research Council of Academy of Finland and Stockholm Medical Image Laboratory and Education (SMILE). AS, EW, J-SM and SL were supported by funds from NIHR Biomedical Research Centre for Mental Health at the South London and Maudsley NHS Foundation Trust and Institute of Psychiatry, King's College London.

References

Apostolova LG et al (2006) Conversion of mild cognitive impairment to Alzheimer disease predicted by hippocampal atrophy maps. Arch Neurol 63(5):693–699

Apostolova LG et al (2010) 3D comparison of low, intermediate, and advanced hippocampal atrophy in MCI. Hum Brain Mapp 31(5):786–797

Barnes LL et al (2005) Sex differences in the clinical manifestations of Alzheimer disease pathology. Arch Gen Psychiatry 62(6):685–691

Braak H, Braak E (1991) Neuropathological stageing of Alzheimer-related changes. Acta Neuropathol 82(4):239–259

Bylesjo M et al (2006) OPLS discriminant analysis : combining the strengths of PLS-DA and SIMCA classification y. J Chemom 20:341–351

Costafreda SG et al (2011) Automated hippocampal shape analysis predicts the onset of dementia in mild cognitive impairment. Neuroimage 56(1):212–219

Csernansky JG et al (2005) Preclinical detection of Alzheimer's disease: hippocampal shape and volume predict dementia onset in the elderly. Neuroimage 25(3):783–792

Dale AM, Fischl B, Sereno MI (1999) Cortical surface-based analysis. I. Segmentation and surface reconstruction. Neuroimage 9(2):179–194

Davatzikos C et al (2010) Prediction of MCI to AD conversion, via MRI, CSF biomarkers, and pattern classification. Neurobiol Aging 32(12):2322e19–2322e27

Desikan RS et al (2009) Automated MRI measures identify individuals with mild cognitive impairment and Alzheimer's disease. Brain 132(8):2048–2057

Devanand DP et al (2007) Hippocampal and entorhinal atrophy in mild cognitive impairment: prediction of Alzheimer disease. Neurology 68(11):828–836

Dubois B et al (2007) Research criteria for the diagnosis of Alzheimer's disease: revising the NINCDS-ADRDA criteria. Lancet Neurol 6(8):734–746

Fan Y et al (2008) Spatial patterns of brain atrophy in MCI patients, identified via high-dimensional pattern classification, predict subsequent cognitive decline. Neuroimage 39(4):1731–1743

Fischl B et al (2002) Whole brain segmentation: automated labeling of neuroanatomical structures in the human brain. Neuron 33(3):341–355

Fischl B et al (2004) Sequence-independent segmentation of magnetic resonance images. Neuroimage 23(Suppl 1):S69–S84

Fox NC et al (1996) Presymptomatic hippocampal atrophy in Alzheimer's disease. A longitudinal MRI study. Brain 119(Pt 6):2001–2007

Frisoni GB et al (2010) The clinical use of structural MRI in Alzheimer disease. Nat Rev Neurol 6(2):67–77

Furney, SJ et al (2011) Combinatorial markers of mild cognitive impairment conversion to Alzheimer's disease–cytokines and MRI measures together predict disease progression. J Alzheimers Dis 26(Suppl 3(3)):395–405

Gouras GK et al (2000) Testosterone reduces neuronal secretion of Alzheimer's β-amyloid peptides. Proc Natl Acad Sci USA 97(3):1202–1205

Hanseeuw BJ et al (2011) Mild cognitive impairment: differential atrophy in the hippocampal subfields. AJNR Am J Neuroradiol 32(9):1658–1661

Jack CR et al (1992) MR-based hippocampal volumetry in the diagnosis of Alzheimer's disease. Neurology 42(1):183–188

Jack CR et al (1998) Hippocampal atrophy and apolipoprotein E genotype are independently associated with Alzheimer's disease. Ann Neurol 43(3):303–310

Jack CR et al (2008) The Alzheimer's disease neuroimaging initiative (ADNI): MRI methods. J Magn Reson Imaging 27(4):685–691

Karas G et al (2008) Amnestic mild cognitive impairment: structural MR imaging findings predictive of conversion to Alzheimer disease. AJNR Am J Neuroradiol 29(5):944–949

Klöppel S et al (2008) Automatic classification of MR scans in Alzheimer's disease. Brain 131(Pt 3):681–689

Lerch JP et al (2008) Automated cortical thickness measurements from MRI can accurately separate Alzheimer's patients from normal elderly controls. Neurobiol Aging 29(1):23–30

Liu Y et al (2009) Combination analysis of neuropsychological tests and structural MRI measures in differentiating AD, MCI and control groups-The AddNeuroMed study. Neurobiol Aging 32(7):1198–1206

Lovestone S et al (2009) AddNeuroMed–the European collaboration for the discovery of novel biomarkers for Alzheimer's disease. Ann N Y Acad Sci 1180:36–46

Mangialasche F et al (2010) High plasma levels of vitamin E forms and reduced Alzheimer's disease risk in advanced age. J Alzheimers Dis 20(4):1029–1037

McEvoy LK et al (2009) Alzheimer disease: quantitative structural neuroimaging for detection and prediction of clinical and structural changes in mild cognitive impairment. Radiology 251(1):195–205

Misra C, Fan Y, Davatzikos C (2009) Baseline and longitudinal patterns of brain atrophy in MCI patients, and their use in prediction of short-term conversion to AD: results from ADNI. Neuroimage 44(4):1415–1422

Mueller SG, Weiner MW (2009) Selective effect of age, Apo e4, and Alzheimer's disease on hippocampal subfields. Hippocampus 19(6):558–564

Mueller SG et al (2010) Hippocampal atrophy patterns in mild cognitive impairment and Alzheimer's disease. Hum Brain Mapp 31(9):1339–1347

Plant C et al (2010) Automated detection of brain atrophy patterns based on MRI for the prediction of Alzheimer's disease. Neuroimage 50(1):162–174

Reiman EM et al (1998) Hippocampal volumes in cognitively normal persons at genetic risk for Alzheimer's disease. Ann Neurol 44(2):288–291

Robin X et al (2011) pROC: an open-source package for R and S + to analyze and compare ROC curves. Bioinformatics 12(1):77

Scheltens P et al (1992) Atrophy of medial temporal lobes on MRI in "probable" Alzheimer's disease and normal ageing: diagnostic value and neuropsychological correlates. J Neurol Neurosurg Psychiatry 55(10):967–972

Ségonne F et al (2004) A hybrid approach to the skull stripping problem in MRI. Neuroimage 22(3):1060–1075

Simmons A et al (2009) MRI measures of Alzheimer's disease and the AddNeuroMed study. Ann N Y Acad Sci 1180:47–55

Simmons A et al (2011) The AddNeuroMed framework for multi-centre MRI assessment of Alzheimer's disease: experience from the first 24 months. Int J Geriatr Psychiatry 26(1):75–82

Spulber G et al (2013) An MRI-based index to measure the severity of Alzheimer's disease-like structural pattern in subjects with mild cognitive impairment. J Intern Med 273(4):396–409

Trygg J, Wold S (2002) Orthogonal projections to latent structures (O-PLS). J Chemom 16(3):119–128

Van Leemput K et al (2009) Automated segmentation of hippocampal subfields from ultra-high resolution in vivo MRI. Hippocampus 19(6):549–557

Vemuri P et al (2008) Alzheimer's disease diagnosis in individual subjects using structural MR images: validation studies. Neuroimage 39(3):1186–1197

Vemuri P et al (2009) MRI and CSF biomarkers in normal, MCI, and AD subjects: predicting future clinical change. Neurology 73(4):294–301

West MJ et al (2004) Hippocampal neurons in pre-clinical Alzheimer's disease. Neurobiol Aging 25(9):1205–1212

Westman E, Wahlund LO, Foy C et al (2010) Combining MRI and MRS to distinguish between Alzheimer's disease and healthy controls. J Alzheimers Dis 22(1):171–181

Westman E, Simmons A, Muehlboeck J-S et al (2011a) AddNeuroMed and ADNI: similar patterns of Alzheimer's atrophy and automated MRI classification accuracy in Europe and North America. Neuroimage 58(3):818–828

Westman E, Wahlund L, Foy C et al (2011b) Magnetic Resonance Imaging and Magnetic Resonance Spectroscopy for Detection of Early Alzheimer' s Disease. J Alzheimers Dis 26:307–319

Westman E, Simmons A, Zhang Y et al (2011c) Multivariate analysis of MRI data for Alzheimer's disease, mild cognitive impairment and healthy controls. Neuroimage 54(2):1178–1187

Westman E, Cavallin L, Muehlboeck J-S et al (2011d) Sensitivity and Specificity of Medial Temporal Lobe Visual Ratings and Multivariate Regional MRI Classification in Alzheimer's Disease J. Laks, ed. PLoS One 6(7):9

Westman E, Muehlboeck J-S, Simmons A (2012) Combining MRI and CSF measures for classification of Alzheimer's disease and prediction of mild cognitive impairment conversion. Neuroimage 62(1):229–238

Westman E et al (2013) Regional magnetic resonance imaging measures for multivariate analysis in Alzheimer's disease and mild cognitive impairment. Brain Topogr 26(1):9–23

Wiklund S et al (2008) Visualization of GC/TOF-MS-based metabolomics data for identification of biochemically interesting compounds using OPLS class models. Anal Chem 80(1):115–122

Wolz R et al (2011) Multi-method analysis of MRI images in early diagnostics of Alzheimer's disease. PLoS One 6(10):e25446

Zhang D et al (2011) Multimodal classification of Alzheimer's disease and mild cognitive impairment. Neuroimage 55(3): 856–867

CHAPTER 3: A SUBSET OF CEREBROSPINAL FLUID PROTEINS FROM A MULTI-ANALYTE PANEL ASSOCIATED WITH BRAIN ATROPHY, DISEASE CLASSIFICATION AND PREDICTION IN ALZHEIMER'S DISEASE

This chapter is presented as a published paper and is the exact copy of the following journal publication:

Khan W, Aguilar C, Kiddle SJ, Doyle O, Thambisetty M, Muehlboeck S, Sattlecker M, Newhouse S, Lovestone S, Dobson R, Giampietro V, Westman E, Simmons A (2015) A subset of cerebrospinal fluid proteins from a multi-analyte panel associated with brain atrophy, disease classification and prediction in Alzheimer's disease. *PLoS One* 10, 1–16.

Author Contributions:

Study Concept and Design: Khan, Kiddle, Dobson, Westman, Simmons

Acquisition, Analysis and Interpretation of data: Khan, Kiddle, Muehlboeck, Westman, Simmons

Drafting and Revision of Manuscript: All Authors

Statistical Analysis: Khan, Kiddle, Westman, Muehlboeck, Simmons

PLOS | ONE

RESEARCH ARTICLE

A Subset of Cerebrospinal Fluid Proteins from a Multi-Analyte Panel Associated with Brain Atrophy, Disease Classification and Prediction in Alzheimer's Disease

Wasim Khan[1,2,3]*, Carlos Aguilar[4], Steven J. Kiddle[1,2], Orla Doyle[1], Madhav Thambisetty[5], Sebastian Muehlboeck[1,2,3], Martina Sattlecker[1,2], Stephen Newhouse[1,2], Simon Lovestone[6], Richard Dobson[1,2,3], Vincent Giampietro[1], Eric Westman[1,4], Andrew Simmons[1,2,3], Alzheimer's Disease Neuroimaging Initiative

1 King's College London, Institute of Psychiatry, Psychology & Neuroscience, London, United Kingdom, **2** NIHR Biomedical Research Centre for Mental Health, London, United Kingdom, **3** NIHR Biomedical Research Unit for Dementia, London, United Kingdom, **4** Department of Neurobiology, Care Sciences and Society, Karolinska Institutet, Stockholm, Sweden, **5** Laboratory of Behavioural Neuroscience, National Institute on Aging, National Institutes of Health, Baltimore, Maryland, United States of America, **6** Department of Psychiatry, University of Oxford, Oxford, United Kingdom

* wasim.khan@kcl.ac.uk

Citation: Khan W, Aguilar C, Kiddle SJ, Doyle O, Thambisetty M, Muehlboeck S, et al. (2015) A Subset of Cerebrospinal Fluid Proteins from a Multi-Analyte Panel Associated with Brain Atrophy, Disease Classification and Prediction in Alzheimer's Disease. PLoS ONE 10(8): e0134368. doi:10.1371/journal.pone.0134368

Editor: Stephen D Ginsberg, Nathan Kline Institute and New York University School of Medicine, UNITED STATES

Received: February 2, 2015

Accepted: July 8, 2015

Published: August 18, 2015

Data Availability Statement: Data is available from the ADNI online database repository (adni.loni.usc.edu).

Funding: Data collection and sharing for this project were funded by the ADNI (grant U01 393 AG024904 from the National Institutes of Health). This study was supported by funds from the NIHR Biomedical Research Centre for Mental Health and NIHR Biomedical Research Unit for Dementia at the South London and Maudsley NHS Foundation Trust and

Abstract

In this exploratory neuroimaging-proteomic study, we aimed to identify CSF proteins associated with AD and test their prognostic ability for disease classification and MCI to AD conversion prediction. Our study sample consisted of 295 subjects with CSF multi-analyte panel data and MRI at baseline downloaded from ADNI. Firstly, we tested the statistical effects of CSF proteins (n = 83) to measures of brain atrophy, CSF biomarkers, ApoE genotype and cognitive decline. We found that several proteins (primarily CgA and FABP) were related to either brain atrophy or CSF biomarkers. In relation to ApoE genotype, a unique biochemical profile characterised by low CSF levels of Apo E was evident in ε4 carriers compared to ε3 carriers. In an exploratory analysis, 3/83 proteins (SGOT, MCP-1, IL6r) were also found to be mildly associated with cognitive decline in MCI subjects over a 4-year period. Future studies are warranted to establish the validity of these proteins as prognostic factors for cognitive decline. For disease classification, a subset of proteins (n = 24) combined with MRI measurements and CSF biomarkers achieved an accuracy of 95.1% (Sensitivity 87.7%; Specificity 94.3%; AUC 0.95) and accurately detected 94.1% of MCI subjects progressing to AD at 12 months. The subset of proteins included FABP, CgA, MMP-2, and PPP as strong predictors in the model. Our findings suggest that the marker of panel of proteins identified here may be important candidates for improving the earlier detection of AD. Further targeted proteomic and longitudinal studies would be required to validate these findings with more generalisability.

Institute of Psychiatry, Kings College London, and Alzheimer's Research UK. This research was also supported by grants P30 AG010129 and K01 AG030514 from the National Institutes of Health and by the Dana Foundation.

Competing Interests: The authors have declared that no competing interests exist.

Introduction

Alzheimer's disease (AD) is a progressive neurodegenerative disorder pathologically characterised by lesions of misfolded proteins, the loss of synapses and an overall reduction in brain volume. There is accumulating evidence to suggest that the clinical symptoms of the disease are preceded by a long presymptomatic phase (~15–20 years) of abnormal β-amyloid (Aβ) aggregation in the form of extracellular senile plaques [1,2]. The neuropathology of the disease is associated with the development of neurofibrillary tangles prior to the onset of cognitive impairment and the subsequent emergence of full-blown dementia [3,4]. The failure of several clinical trials assessing therapeutic strategies to target amyloid deposition has led to the impetus to discover biomarkers earlier in the AD pathological cascade prior to the development of cognitive symptoms.

One method is to study structural neuroimaging biomarkers of AD which have been advocated for use in early diagnosis [5], as well as for predicting disease progression in a prodromal form of the disease known as Mild Cognitive Impairment (MCI) [6]. Another rich source of biomarkers can be found in analytes from cerebrospinal fluid (CSF), particularly, concentrations of Aβ142, p-tau181 and t-tau which reflect biochemical changes associated with Aβ deposition, neurofibrillary tangle formation, and neuronal cell death [7,8].

Several neuroimaging studies have since found that the combined use of MRI measures from regions affected in AD and CSF biomarkers can provide mutually complimentary information for disease classification and prediction [9,10]. Nevertheless, there still remains a substantial overlap in CSF biomarker concentrations between AD and cognitively normal (CN) individuals with an increased risk of developing the disease [11]. Moreover, additional biomarkers are still required to understand the exact temporospatial relationship between Aβ deposition and tau neurodegeneration during different stages of the disease pathophysiology. Early genetic and in-vivo experimental studies have suggested that markers of inflammation, microglial activity and synaptic function may be important for reflecting biochemical changes associated with the Aβ toxicity and tau neurodegeneration [12,13]. While some proteomic studies using multiplex platforms have identified a number of protein candidates detected in AD [14–16], few have been validated and tested in relation to well-established neuroimaging endophenotypes of AD pathology. Discovering proteins in relation to established measures of disease pathology may yield biologically important peripheral signatures associated with mechanisms early in the disease.

In this study we aimed to discover CSF proteins associated with AD pathophysiology by testing the multiplex panel with established neuroimaging measures, CSF biomarkers of AD, Apolipoprotein E (ApoE) genotype and cognitive decline. Most importantly, we aimed to identify a subset of proteins from the multiplex panel in order to test its diagnostic utility with existing AD biomarkers for disease classification and MCI to AD conversion prediction at follow up.

Materials and Methods

Participants

Data used in this study was obtained from the ADNI database (adni.loni.ucla.edu). ADNI was launched by the National Institute of Ageing (NIA) and is a multicenter project supported by private pharmaceutical companies, and non-profit organisations for the development of biomarkers in monitoring disease progression in MCI and AD [17]. ADNI subjects aged 55–90 from over 50 sites across the U.S and Canada participated in the research (for further information, see www.adni-info.org). Written informed consent was given from all participants in the

study and prior ethics committee approval was obtained from each participating site. A total of 295 subjects with baseline data that included structural imaging and multiplex CSF samples were available for analysis and consisted of 142 subjects with MCI, 65 patients with AD, and 88 healthy control subjects.

CSF protein measurements

CSF $A\beta_{1-42}$, T-tau and P-tau were measured at the ADNI Biomarker Core laboratory at the University of Pennsylvania Medical Center, using the multiplex xMAP Luminex platform (Luminex, Austin, TX, USA) with the INNOBIA AlzBio3 kit (Innogenetics, Ghent, Belgium) [18,19].

CSF multiplex proteomic samples were measured for levels of 159 analytes using the Human Discovery Multi-Analyte Profile (MAP) 1.0 panel and Luminex 100 platform developed by Rules Based Medicine, Inc. (RBM), (Austin, TX) [20]. This panel is based upon multiplex immunoassay technology to measure a range of inflammatory, metabolic, lipid, and other disease relevant proteins. The protocol used to quantify CSF analytes is described in detail elsewhere [21,22]. Of the 159 analytes, only those with <10% of missing values were quantifiable leaving 83 in total for analysis. The remaining 76 analytes were mostly below the assay detection limit, or had other assay limitations. Each analyte has an individual standard curve with between 6–8 reference standards. Each plate is run with 3 levels of QCs (low, medium and high) for each analyte. A total of 16 of the CSF samples were retested using a separate never before thawed replicate aliquot on the fifth of the five 96 well plates to provide blinded test/re-test quality control data. Assays are qualified based on least detectable dose, precision, cross-reactivity, dilutional linearity, spike recovery (assessment of accuracy), and test/re-test performance. Cross validation to alternative methods is reported for some assays where feasible. Further information on the process, aliquoting and storage of analytes is described in the ADNI Biomarker Core Laboratory Standard Operating Procedures (http://adni.loni.usc.edu/wp-content/uploads/2012/01/2011Dec28-Biomarkers-Consortium-Data-Primer-FINAL1.pdf). Further assay documentation and validation reports are available from Myriad RBM (www.myriadrbm.com). Distributions of data for individual CSF proteins were checked for normality using Box-Cox methods and, when appropriate, transformed to approximate a normal distribution. Information regarding the biological preparation of CSF samples and quality control criteria of the RBM Human Discovery MAP panel can be found on the ADNI websites [23,24]. A complete list of the analytes is given in S1 Table.

Magnetic Resonance Imaging Data Acquisition and Analysis

Structural MRI images (at 1.5T) were acquired at multiple ADNI sites across the US and Canada based on a standardized protocol [25]. The imaging protocol included a high resolution sagittal 3D T1-weighted MPRAGE volume (voxel size $1.1 \times 1.1 \times 1.2$ mm^3). The MPRAGE volume was acquired using a custom pulse sequence specifically designed for the ADNI study to ensure compatibility across scanners [26]. Full brain and skull coverage was required for all MR images according to previously published quality control criteria [27,28].

Image analysis was carried out using the Freesurfer image analysis pipeline (version 5.1.0) to produce 34 regional cortical thickness and 23 subcortical volumetric measures as previously described [29,30]. All volumetric measures from each subject were normalized by the subject's intracranial volume while cortical thickness measures were used in their raw form [31]. Measures of hippocampal and entorhinal cortex volume were selected as key *a priori* regions to reflect AD pathology. A previously validated MRI-based marker of AD and MCI known as SPARE-AD (Spatial Pattern of Abnormalities for Recognition of Early AD) was also used as a

neuroimaging marker of AD. Individualised scores of diagnostic and predictive value were used for analysis. A complete list of regional MRI measures is given in S2 Table. Details of this particular method have been widely published elsewhere [9,32,33].

Statistical Analysis

Firstly, the RBM panel of CSF proteins were tested in relation to regional MRI measurements (hippocampal and entorhinal volume), an MRI-based measure known as SPARE-AD score and CSF biomarkers (Aβ142, P-tau$_{181}$, T-tau) using a Spearman rank partial correlation test. This test was adjusted for covariates including age, gender, years of education and ApoE E4 genotype. Secondly, CSF proteins from the RBM panel were also tested in relation to different ApoE polymorphisms (ε2 carriers, ε3 carriers and ε4 carriers) using a generalized linear model adjusting for age, gender and years of education. Thirdly, to test the effect of CSF proteins on longitudinal MMSE score, we used a linear mixed model approach. Global MMSE score was used as the response variable and the time from baseline visit in months, CSF protein from the RBM panel, age, sex, years of education and ApoE ε4 genotype were included as fixed effects. Models contained a random intercept and slope. The applicability of our mixed models were assessed by examining models with and without the random effect of data collection site, the linearity of CSF proteins over time within subjects and the normality of model residuals using diagnostic plots. All models were tested in both AD patients (n = 59) and MCI subjects (n = 142) with serial MMSE measurements. As a large number of proteins from the RBM panel were tested we used a false discovery rate correction to account for multiple comparisons.

A multivariate support vector machine (SVM) algorithm was applied to the ADNI cohort, in an unbiased fashion, to distinguish AD patients from CN individuals. In particular, a linear SVM algorithm was constructed using the LIBSVM implementation [34]. In the algorithm, the parameter C (representing the error/trade off parameter used for adjusting separation error in the creation of separation space) was optimized using 5-fold cross validation on the training set. The grid search routine suggested by Hsu et al (2010) [35] was implemented to identify optimal parameter settings for differentiating AD from CN individuals. A multi-kernel learning approach for linear SVM [36] was implemented for treating variables of a different nature. A general framework for kernel methods used to integrate data from different modalities has been described previously in more extensive detail [36–38].

To identify a subset of CSF proteins associated with AD, we adopted a recursive feature elimination (RFE) wrapper. The final subset of CSF proteins (CSF RFE subset) were then combined with CSF biomarkers and regional MRI measurements to test their utility for disease classification. Classification accuracy in each of these models was evaluated using ten-fold cross validation. Measures of accuracy, sensitivity, specificity, and area under the curve (AUC) were used to compare AD vs. CN models.

MCI subjects were divided into subjects that progressed to an AD diagnosis (MCI-converters) and others that remained clinically stable over a 12 month follow up period (MCI non-converters). Subsequently, models from the AD vs. CN comparisons were used as training classifiers to prospectively predict MCI to AD conversion in MCI converters (MCI-c), as well as predicting MCI non-converters (MCI-nc) that remained stable at 12 months. Discriminant scores from the model were then used to classify MCI subjects as either having an AD-like or CN-like phenotype. The combined model (CSF RFE subset + CSF biomarkers + regional MRI measures) was also used to predict MCI to AD conversion in moderately late MCI-c (subjects that progressed to AD between 18–24 months follow up) and late MCI-c (subjects that progressed to AD at 36 months). MCI-nc predictions were also made using the combined model

for subjects that remained clinically stable between 0–12 months, 18–24 months and 36 months follow up.

The R statistical software environment (v. 3.1.0; The R Foundation for Statistical Computing), was used to perform all statistical analyses.

Results

Demographic Characteristics

Baseline sample characteristics of the ADNI cohort for demographic, cognitive, MRI and CSF biomarkers are presented by diagnostic group in Table 1. Significant differences between groups were found in hippocampal and entorhinal volume, as well as, SPARE-AD score, CSF biomarkers of AD, MMSE score and ApoE ε4 genotype. Subject age, gender and years of education were not found to differ significantly between groups.

CSF proteins from the multiplex RBM panel associated with neuroimaging markers of brain atrophy and CSF biomarkers of AD

Due to the exploratory nature of this study we first tested the association of the entire multiplex panel of CSF proteins (n = 83) with neuroimaging and CSF biomarkers to identify candidates related AD pathogenesis. Associations were tested using a partial spearman rank correlation test that co-varied for the effects of age, gender, years of education and ApoE ε4 genotype. For several proteins (n = 50) we found an association with either neuroimaging markers of brain atrophy or CSF biomarkers of AD (Fig 1). Many proteins in this subset (n = 37) were also found to be significantly associated with both P-tau181 and T-tau CSF levels. Reduced levels of CgA were found to be significantly associated across all comparisons with neuroimaging and CSF biomarkers, but only remained significant in association with hippocampal ($p = <0.001$) and entorhinal volume ($p = 0.008$) after multiple comparison correction. Increased levels of Fatty Acid Binding Protein (FABP) emerged as the most significantly associated with CSF levels of P-tau181 and T-tau as well as SPARE-AD score. Results from our partial spearman rank correlation test are displayed in S3 Table. Bear in mind most associations were mild and reflected by p-values that were uncorrected for multiple comparisons.

CSF proteins associated with different ApoE gene polymorphisms

CSF proteins from the RBM panel were also tested in relation to the ApoE polymorphism rather than diagnostic status. Significant differences in CSF levels were examined by ApoE genotype (ε2 carriers, ε3 carriers and ε4 carriers). We found that 9 CSF proteins were associated with the overall effect of ApoE genotype (Apo E, FABP, FGF-4, IL-8, AGRP, MIF, IL-3, ANG-2, and Osteopontin). However, only CSF levels of Apo E, IL-3 and MIF were found to differ between ApoE groups. CSF levels of these proteins compared to each ApoE group are shown in Fig 2. In particular, the strongest overall effect was observed for CSF levels of Apo- E which passed multiple comparison correction ($p = .00046$; FDR corrected = .034). Pairwise comparisons revealed that Apo-E levels were significantly lower in ε4 carriers irrespective of diagnosis compared to ε2 carriers ($t = -3.63$; $p = < .0001$) and significantly lower in ε3 carriers compared to ε2 carriers ($t = -2.57$; $p = .027$).

CSF proteins related to the rate of cognitive decline on longitudinal MMSE score

We also tested the association of baseline CSF proteins with the rate of cognitive decline using at least three or four serial measurements of MMSE score. Firstly, we tested this in a sample of

Table 1. Demographic characteristics of the ADNI cohort.

	AD (*n* = 65)	MCI (*n* = 142)	CN (*n* = 88)	*p*-value
Age	74.6 ± 7.6	74.9 ± 7.3	75.8 ± 5.5	0.491
Gender (male/female)	29/36	47/95	44/46	0.061
Education (years)	15.9 ± 3.1	15.5 ± 3.1	15.5 ± 2.9	0.560
MMSE score	23.5 ± 1.9[a,b]	27.1 ± 1.7[b]	29.1 ± 1.0	<0.001
ApoE ε4 genotype (+ve/-ve)	46/19	76/66	22/66	<0.001
Hippocampal Volume (mL)	1.82 ± 0.4[b]	1.94 ± 0.3[b]	2.34 ± 0.3	<0.001
Entorhinal Volume (mL)	0.95 ± 0.2[a,b]	1.12 ± 0.2[b]	1.28 ± 0.2	<0.001
ICV (mL)	1314 ± 158	1328 ± 139	1290 ± 136	0.146
SPARE-AD score	1.21 ± 0.8[a,b]	0.81 ± 0.8[b]	-1.5 ± 0.9	<0.001
Aβ1–42	140.4 ± 35.3[a,b]	159.6 ± 51.7[b]	205.7 ± 57.2	<0.001
t-tau	125.9 ± 60.3[a,b]	104.8 ± 52.5[b]	69.2 ± 27.9	<0.001
p-tau181	42.2 ± 20.7[b]	36.5 ± 16.1[b]	24.9 ± 13.2	<0.001

Data are represented as mean ± and standard deviation. AD = Alzheimer's disease, MCI = Mild Cognitive Impairment, CN = cognitively normal individuals, MMSE = Mini Mental State Examination, ICV = Intracranial Volume, SPARE-AD score = Spatial Pattern of Abnormalities for Recognition of Early AD. Chi-square was used for gender and ApoE ε4 genotype comparison. One way ANOVA with Bonferroni post hoc test was used for continuous measures.

[a] indicates significant compared to the MCI group.

[b] indicates significant compared to the CN group.

doi:10.1371/journal.pone.0134368.t001

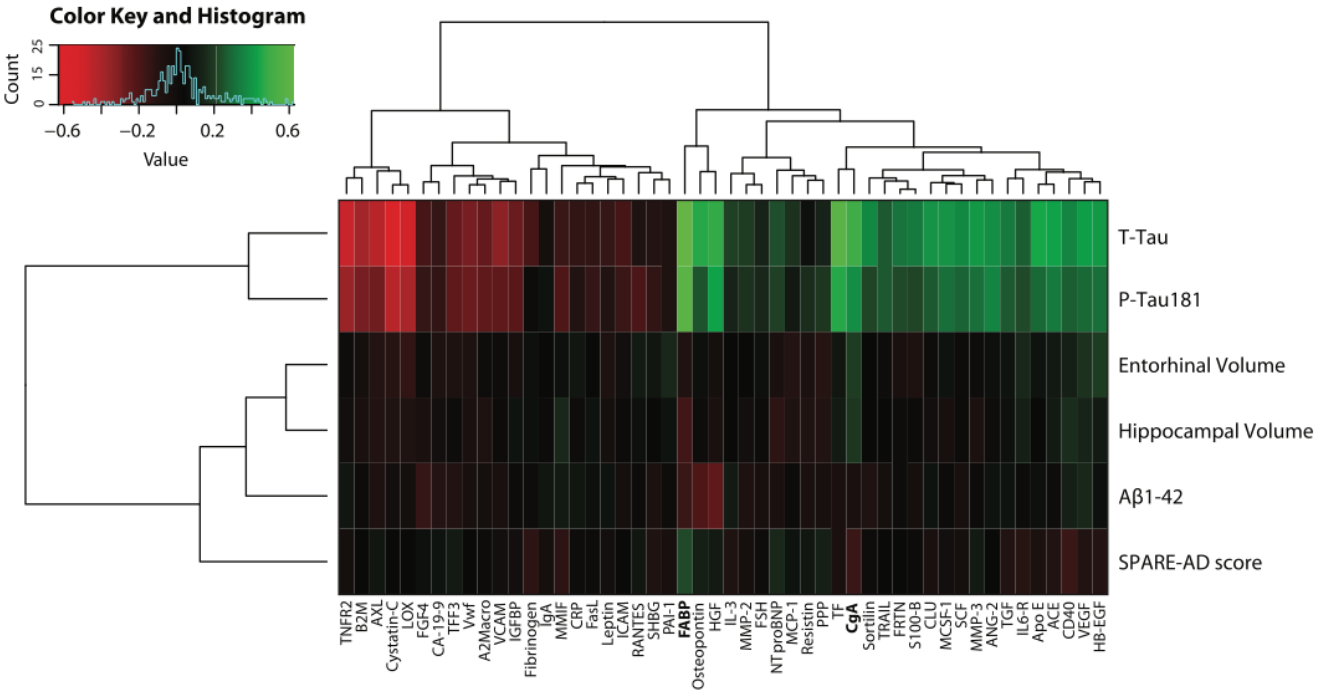

Fig 1. Heatmap of baseline CSF proteins that were significantly associated with regional MRI measures, SPARE-AD score or CSF biomarkers in AD patients and MCI subjects (n = 207).

doi:10.1371/journal.pone.0134368.g001

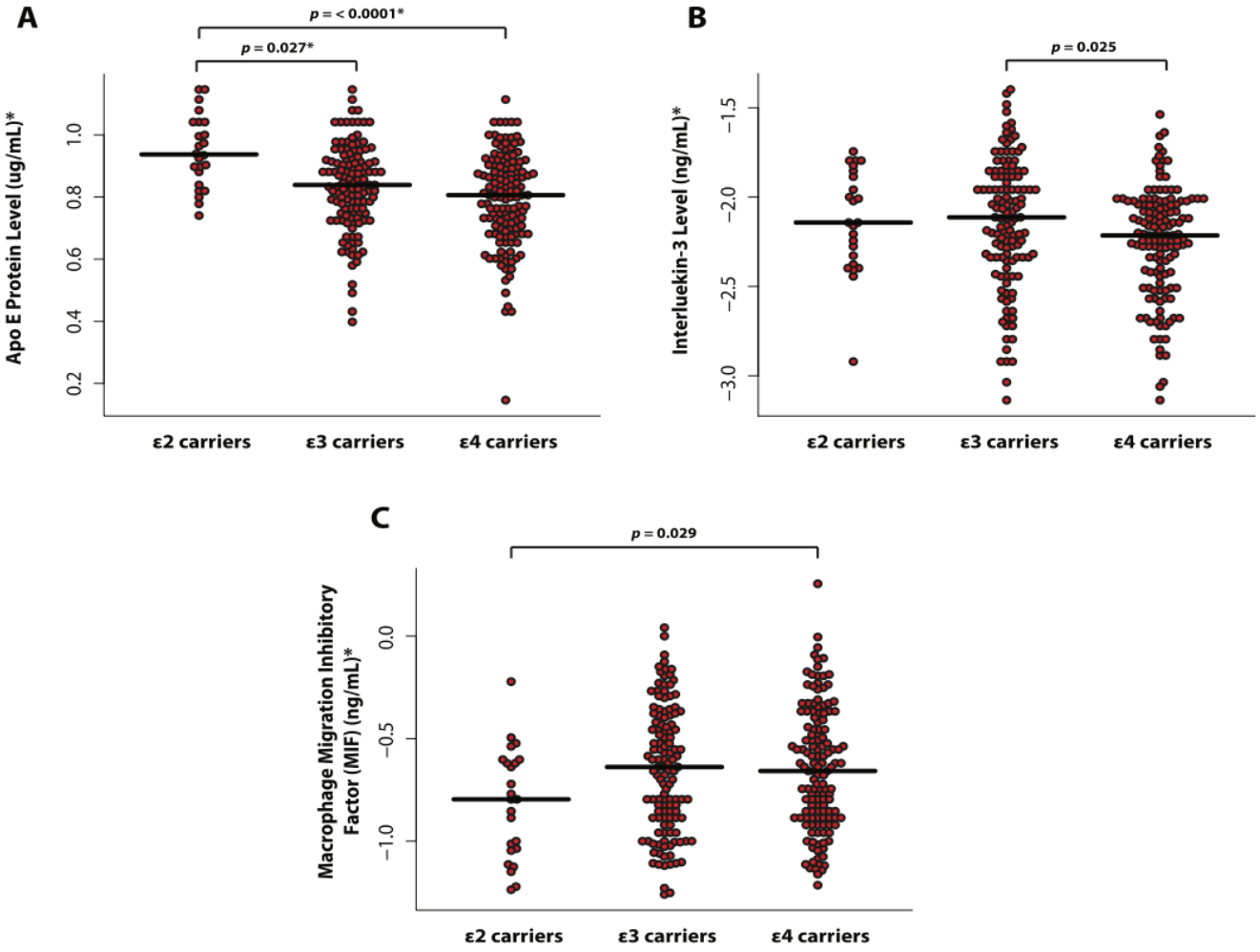

Fig 2. CSF proteins significantly associated with different ApoE gene polymorphisms (ε2 carriers, ε3 carriers, and ε4 carriers). (A) CSF levels of ApoE protein between ApoE groups; **(B)** CSF levels of Interleukin-3 (IL-3) between ApoE groups and **(C)** CSF levels of Macrophage migration inhibitory factor (MIF) between ApoE groups. *These units refer to data before transformation.

doi:10.1371/journal.pone.0134368.g002

AD patients (n = 59) and found no CSF proteins were able to significantly predict a longitudinal change in MMSE score. However, in a sample of MCI subjects (n = 142) we found three proteins (SGOT, MCP-1, and IL-6r) were able to significantly predict cognitive decline (Table 2). Again, it should be noted that these associations were mild and no protein remained significant after multiple comparison correction.

Disease Classification

The recursive feature elimination (RFE) wrapper method identified a subset of 24 CSF proteins which best distinguished AD patients from CN individuals (Table 3). Overall, we found that the inclusion of these CSF proteins from the RBM panel improved the accuracy and specificity of models. In particular, combining the CSF RFE subset with CSF biomarkers resulted in an accuracy of 84.3% and an AUC of 91% (Table 4). We found that combining the CSF RFE subset improved the sensitivity in a model generated using CSF biomarkers from 70.8% to 83.1%

Table 2. CSF proteins significantly predicting a longitudinal decline on MMSE score in a sample of MCI subjects (*n* = 142).

	Linear mixed effect models		
CSF protein	**β**	***S.E***	***P*-value**
Serum Glutamic Oxaloacetic Transaminase (SGOT)	0.34	0.13	0.0074
Monocyte Chemotactic Protein 1 (MCP-1)	-0.21	0.09	0.027
Interleukin-6 receptor (IL-6r)	0.20	0.08	0.022

Linear mixed effect model results are displayed as on b-coefficients (β), standard-error (*S.E*) and P-values for the interaction terms between proteins and time (years from baseline). Data were adjusted for age, gender, years of education and ApoE genotype as fixed effects and subject code and site-id as random effects.

doi:10.1371/journal.pone.0134368.t002

which was statistically significant (Venkatraman's Test: Z = 2.94; p = .0042). Moreover, the CSF RFE subset combined with CSF biomarkers and regional MRI measures, achieved an accuracy of 91.5% (SEN = 87.7%, SPE = 94.3%, AUC = 0.95) which was significantly better than using CSF biomarkers alone (Z = 2.91; p = .0036) (Fig 3). In the combined model (CSF RFE subset + CSF biomarkers + regional MRI measures) we found CgA, FABP, MMP-2, and PPP

Table 3. CSF proteins selected in the CSF RFE subset using a built-in importance measure (SVM-RFE wrapper) for differentiating AD patients from CN individuals.

Rank	CSF multi-analyte subset
1	Fatty acid binding protein (FABP)
2	Chromogranin-A (CgA)
3	Osteopontin
4	Pancreatic polypeptide (PPP)
5	Interleukin-3 (IL-3)
6	Resistin
7	Cancer Antigen 19–9 (CA-19-9)
8	Apolipoprotein E (Apo E)
9	Calcitonin
10	Hepatocyte Growth Factor (HGF)
11	Fibroblast Growth Factor 4 (FGF-4)
12	Matrix Metalloproteinase-3 (MMP-3)
13	C-Reactive Protein (CRP)
14	Adiponectin
15	AXL Receptor Tyrosine Kinase (AXL)
16	Endothelin-1 (ET-1)
17	Apolipoprotein(a) (Lp(a))
18	Pregnancy-Associated Plasma Protein A (PAPP-A)
19	CD 40 antigen (CD40)
20	Agouti-Related Protein (AGRP)
21	Myoglobin
22	Matrix Metalloproteinase-2 (MMP-2)
23	Thyroxine-Binding Globulin (TBG)
24	Plasminogen Activator Inhibitor 1 (PAI-1)

doi:10.1371/journal.pone.0134368.t003

Table 4. Accuracy, sensitivity, specificity and area under the curve of AD vs. CN models.

	ACC (%)	SEN (%)	SPE (%)	AUC
CSF RFE subset (n = 24)	72.6	70.8	73.9	0.80
CSF biomarkers	77.1	70.8	81.8	0.87
Regional MRI measures	87.6	81.5	92.1	0.93
CSF RFE subset + CSF biomarkers	83.0	83.1	83.0	0.90
CSF biomarkers + regional MRI measures	92.2	85.7	96.4	0.96
Combined	91.5	87.7	94.3	0.95

Data are percentages and confidence intervals are presented in parenthesis.

ACC = Accuracy, SENS = sensitivity, SPE = specificity, AUC = area under the curve.

The combined model includes regional MRI measures, CSF biomarkers of AD and the CSF RFE subset of proteins (n = 24).

doi:10.1371/journal.pone.0134368.t004

contributed most strongly toward the detection of AD. However, the regional MRI measures and CSF biomarkers model gave the best result with an accuracy of 92.2% (SEN = 85.7%, SPE = 96.4%, AUC = 0.96) but this was not found to be significantly better than the CSF RFE subset combined with CSF biomarkers and regional MRI measures ($Z = 0.38$; $p = 0.70$). All model results are shown in Table 4.

MCI to AD conversion prediction

Over a follow up period of 36 months, 72 MCI subjects (50.7%) from our sample converted to an AD diagnosis. Table 5 shows the number of MCI subjects that were predicted as either AD-like or CN-like at a 12 month follow-up interval using all AD vs. CN models.

Firstly, we tested all models in early MCI subjects who progressed to an AD diagnosis between 0–12 months ($n = 34$) [Early MCI-c]. We found that the inclusion of the CSF RFE subset with CSF biomarkers and regional MRI measures provided the best result, accurately predicting 94.1% of MCI-c progressing to AD whereas the regional MRI measures and CSF biomarker model was only able to achieve a prediction of 76.5%. Therefore, we further tested the combined model in moderately late MCI-c ($n = 26$) who were also correctly predicted with a 92.3% accuracy as progressing to AD, and late MCI-c ($n = 12$) who were predicted correctly with an 82.4% accuracy. Fig 4a displays the predicted probabilities from the combined model of MCI subjects that progressed to AD. For comparison, we also overlaid the predicted probabilities of AD patients and CN individuals. The majority of subjects that converted to AD at different follow up periods were found to already possess an AD-like phenotype at the prodromal MCI stage ($p > 0.05$; Kolmogorov-Smirnov test).

In contrast, MCI-nc predictions were less accurate with predictions ranging from 57.4% to 25.0%. Over a 36 month follow up period 70 MCI subjects (49.3%) remained clinically stable. The regional MRI measures model was found to yield the best prediction at a 12 month follow up. For the combined model, Fig 4b displays an almost bimodal distribution of MCI-nc predictive values, with some correctly predicted as CN-like and others predicted as having an AD-like phenotype. Despite these subjects remaining clinically stable at their respective period of follow up, some MCI subjects are expected to convert in the near future and as a result also display an AD-like phenotype at baseline. Further follow ups will determine whether these subjects remain clinically stable or convert to an AD diagnosis.

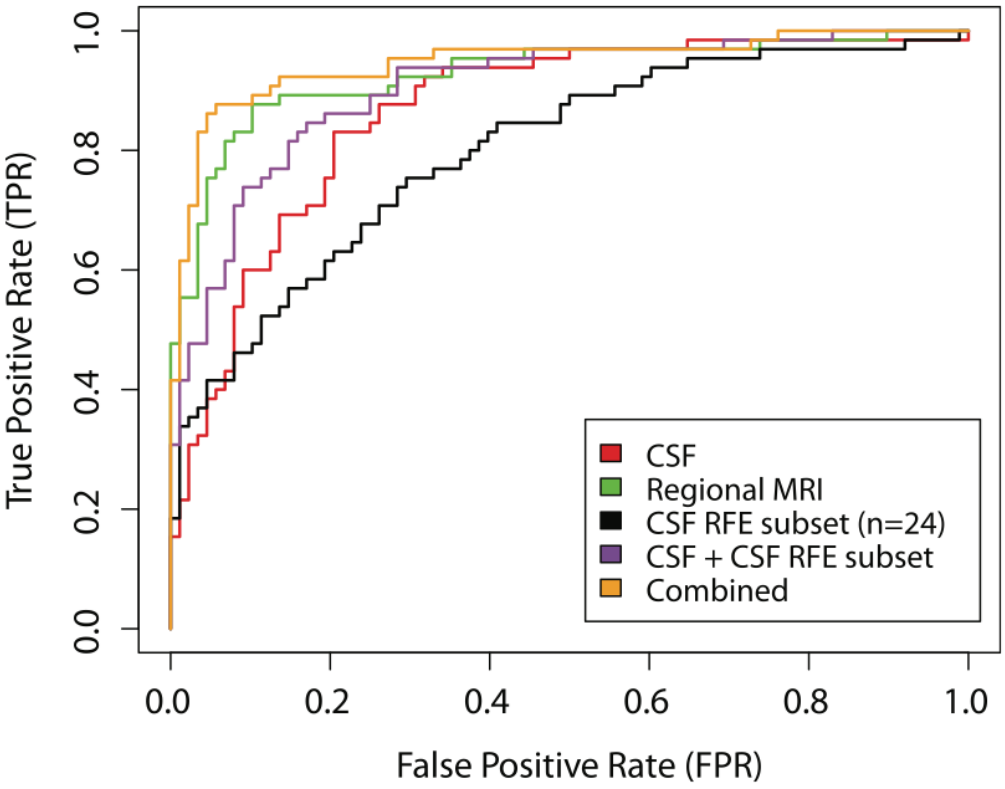

Fig 3. ROC curves from disease classification models for differentiating between AD and CN individuals.

doi:10.1371/journal.pone.0134368.g003

Table 5. MCI to AD conversion prediction at a one year follow up using the AD vs. CN multivariate models.

	MCI-c Classification (n = 34)		MCI-nc Classification (n = 108)	
	AD like (%)*	CN like (%) **	AD like (%)*	CN like (%) **
CSF RFE subset (n = 24)	**82.4 (28)**	17.6 (6)	71.3 (71)	**28.7 (31)**
CSF biomarkers	**73.5 (25)**	26.5 (9)	56.5 (61)	**43.5 (47)**
Regional MRI measures	**73.5 (25)**	26.5 (9)	42.6 (46)	**57.4 (64)**
CSF RFE subset + CSF biomarkers	**88.2 (30)**	11.8 (4)	67.6 (73)	**32.4 (35)**
CSF biomarkers + regional MRI measures	**76.5 (26)**	23.5(8)	38.9 (42)	**61.1 (66)**
Combined	**94.1 (32)**	5.9 (2)	75.0 (81)	**25.0 (27)**

AD = Alzheimer's disease, MCI = Mild Cognitive Impairment, MCI-c = MCI converter, MCI-nc = MCI non-converter, CN = Cognitively Normal.

*Sensitivity is the percentage of MCI-c subjects correctly classified as AD in bold.

**Specificity is the percentage of MCI-nc subjects correctly classified as CN in bold.

The combined model includes regional MRI measures, CSF biomarkers of AD and the CSF RFE subset of proteins (n = 24).

doi:10.1371/journal.pone.0134368.t005

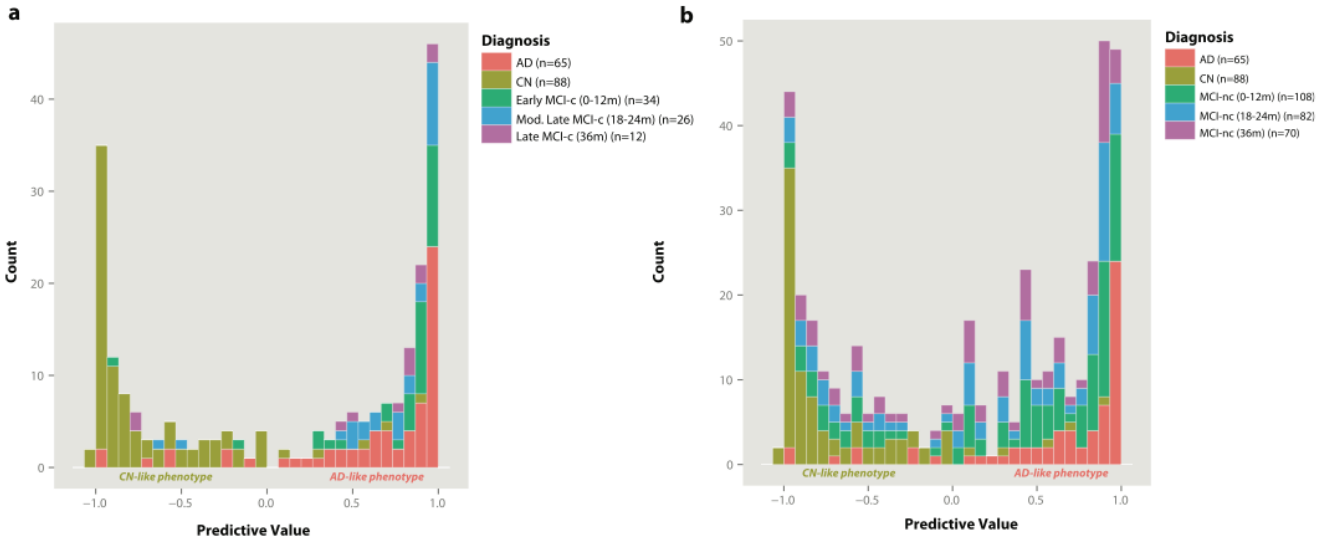

Fig 4. Predictive values from the combined CSF RFE subset CSF biomarker and regional MRI measures model for MCI to AD conversion prediction at several follow up timepoints. (A) Predictive values of MCI-c progressing to AD at different follow up timepoints overlaid with predictive values of AD and CN individuals and **(B)** predictive values of MCI-nc at different follow up timepoints overlaid with predictive values of AD and CN individuals.

doi:10.1371/journal.pone.0134368.g004

Discussion

In this neuroimaging-proteomic study there were a number of key findings. Firstly, we identified several CSF proteins (n = 50) related to neuroimaging phenotypes of brain atrophy and CSF biomarkers of AD, suggesting that these candidates may be related to AD pathophysiology. Second, a unique biochemical profile of CSF proteins was found to be associated with ApoE genotype characterised by reduced levels of Apo E protein in ε4 carriers. Third, some proteins (SGOT, MCP-1, and IL6-r) were found to be related to a longitudinal change in MMSE score over a 4 year period. Although the statistical effects associated with this finding were mild and no result passed multiple comparison correction, further studies will determine whether they may serve as important prognostic factors related to the rate of cognitive decline. More importantly, we showed that reducing the RBM panel to a subset of 24 CSF proteins complemented existing AD biomarkers for AD detection and MCI to AD conversion prediction.

Our findings were in agreement with some previous studies identifying a panel of candidate proteins associated with AD [15,21,39]. In particular, our first finding showed that several proteins were associated with brain atrophy and CSF biomarkers, however, levels of CgA and FABP emerged as the most consistently present across most our comparisons. Although the effects associated with these findings were mild, previous studies have linked these candidates to AD pathophysiology [40,41]. For instance, we found elevated levels of FABP protein to be significantly related to neuroimaging SPARE-AD score which is in agreement with previous findings reporting elevated levels of FABP protein in AD and prodromal MCI subjects [15,21,42]. Increased levels of CgA protein related to hippocampal and entorhinal volume has also been previously linked to early synaptic dysfunction in AD [40], reduced microglial regulation of synaptic function [43], and $A\beta_{1-42}$ metabolism in CN individuals [44].

We also found a unique biochemical profile of CSF proteins was associated with different ApoE gene polymorphisms. For instance, ApoE protein and IL-3 levels were reduced in ε4 carriers, whilst MIF protein levels were elevated. Previous studies have also reported a peripheral

CSF signature associated with ApoE genotype [44] and similar findings have also been observed in blood plasma [45]. Moreover, many of the CSF candidates previously described in the literature (e.g. FABP, FGF-4, IL-8, AGRP, ANG-2, and Osteopontin) also showed mild associations with ApoE genotype, suggesting that the biological variability of proteins identified in AD cases may also be in part driven by genotype status.

For differentiating between AD and CN individuals we found that a subset of proteins (n = 24) from the RBM multiplex panel improved the accuracy and performance of models but was unable to achieve a better accuracy when regional MRI measures and CSF biomarkers were combined. Despite this, the combination of regional MRI measures, CSF biomarkers ($A\beta_{1-42}$, T-tau and P-tau) and the CSF RFE subset achieved an accuracy of 91.5%. In this subset, four proteins namely CgA, FABP, MMP-2, and PPP were the strongest predictors for distinguishing AD from CN individuals.

This is in agreement with previous studies showing that CSF candidates identified using immunoassay panel technology can complement CSF biomarkers of AD for the earlier detection of AD [21,46]. Recent neuroimaging-proteomic studies have also shown several proteins to be associated with longitudinal rates of brain atrophy [39], as well as whole brain atrophy [47]. To our knowledge this is the first study to test whether CSF proteins from an immunoassay panel can complement CSF biomarkers and regional MRI measures for disease classification and prediction. Previous studies have suggested that the use of conventional imaging, such as MRI, combined with biomarkers from different modalities may be complimentary to the early and specific diagnosis of AD [48,49]. Several studies have reported that this combined approach improved AD disease classification [10,36] and future MCI to AD conversion prediction [9,50].

For MCI to AD conversion prediction, the CSF RFE subset, CSF biomarker and regional MRI measures model also gave the best results and outperformed all other models. The model was particularly sensitive for correctly predicting MCI-c with an AD-like phenotype (Fig 4a) suggesting that our panel of 24 proteins may also have the prognostic potential to detect prodromal AD. However, the model failed to correctly detect MCI-nc, with a large proportion of subjects being predicted as AD-like, suggesting that the model lacked specificity. Several previous studies on MCI to AD conversion prediction have also noted the heterogeneity of the MCI-nc group using similar high dimensional pattern classification algorithms [10,51]. It is anticipated that many MCI-nc will convert to AD in the near future. Although future studies with longer follow up times will refine our estimates of specificity, the ability to detect MCI-nc many years prior to clinical diagnosis could provide useful tools for an earlier diagnosis.

Despite some promising results, there exist a number of limitations to our findings. Firstly, although we identified a number of CSF proteins showing promise in AD detection and MCI to AD conversion prediction our results are somewhat limited by the inability to validate these candidates in an independent cohort. Therefore future studies are warranted to further explore the prognostic potential of the candidates identified here in other well-characterised prospective cohorts. Nonetheless, we do show that the panel of CSF proteins for detecting AD also have a good prognostic potential for detecting AD in the prodromal or amnestic MCI stage. Secondly, CSF proteins identified in this study were from a multiplex panel of proteins known to be associated with microglial activity and synaptic function. It may be likely that an alternative set of CSF proteins unrelated to these processes could also show strong effects in detecting AD and predicting MCI to AD conversion.

In summary, the relation of CSF proteins to key neuroimaging phenotypes and traditional CSF biomarkers provides some evidence of their importance in reflecting early neuropathological changes in AD pathogenesis. Combining a subset of proteins (n = 24) from the RBM multiplex panel with established biomarkers in AD provides further evidence to implicate the role of

peripheral CSF proteins for improving the accuracy and prognostic ability of biomarkers for disease classification and progression. Future studies are warranted to further validate our findings with more generalisability in other well-characterised independent cohorts.

Supporting Information

S1 Table. Complete list of analytes from the RBM multiplex panel used for analysis.
(DOCX)

S2 Table. Complete list of regional MRI measures from the Freesurfer image analysis pipeline used for analysis.
(DOCX)

S3 Table. Baseline CSF proteins that were significantly associated with regional MRI measures, SPARE-AD score or CSF biomarkers in AD patients and MCI subjects (n = 207).
(DOCX)

Acknowledgments

Data used in the preparation of this article were obtained from the ADNI database (adni.loni.ucla.edu). As such, the investigators within the ADNI study contributed to the design and implementation of ADNI or provided data but did not participate in the analysis or writing of the manuscript.

Data collection and sharing for this project were funded by the ADNI (grant U01 AG024904 from the National Institutes of Health). ADNI is funded by the National Institute on Aging and the National Institute of Biomedical Imaging and Bioengineering, as well as through generous contributions from the following: Abbott, Alzheimer's Association, Alzheimer's Drug Discovery Foundation, Amorfix Life Sciences Ltd, AstraZeneca, Bayer HealthCare, BioClinica Inc, Biogen Idec Inc, Bristol-Myers Squibb Company, Eisai Inc, Elan Pharmaceuticals Inc, Eli Lilly and Company, F. Hoffmann-La Roche Ltd and its affiliated company Genentech Inc, GE Healthcare, Innogenetics NV, Janssen Alzheimer Immunotherapy, Johnson & Johnson Pharmaceutical Research & Development LLC, Medpace Inc, Merck & Co, Meso Scale Diagnostics LLC, Novartis Pharmaceuticals Corporation, Pfizer Inc, Servier, Synarc, and Takeda Pharmaceutical Company. The Canadian Institutes of Health Research is providing funds to support ADNI clinical sites in Canada. Private sector contributions are facilitated by the Foundation for the National Institutes of Health (http://www.fnih.org). The grantee organization is the Northern California Institute for Research and Education, and the study is coordinated by the Alzheimer's Disease Cooperative Study at the University of California, San Diego. ADNI data are disseminated by the Laboratory of Neuro Imaging at the University of California, Los Angeles. This research was also supported by grants P30 AG010129 and K01 AG030514 from the National Institutes of Health and by the Dana Foundation.

This study was supported by funds from the NIHR Biomedical Research Centre for Mental Health and NIHR Biomedical Research Unit for Dementia at the South London and Maudsley NHS Foundation Trust and Institute of Psychiatry, Kings College London and Alzheimer's Research UK.

Author Contributions

Conceived and designed the experiments: WK CA SJK EW AS VG RD MS SL. Analyzed the data: WK CA MS. Contributed reagents/materials/analysis tools: WK OD MT SN SM MS. Wrote the paper: WK EW AS.

References

1. Jack CR, Knopman DS, Jagust WJ, Shaw LM, Aisen PS, Weiner MW, et al. Hypothetical model of dynamic biomarkers of the Alzheimer's pathological cascade. Lancet Neurol. 2010; 9: 119–28. PMID: 20083042
2. Villemagne VL, Burnham S, Bourgeat P, Brown B, Ellis K a, Salvado O, et al. Amyloid β deposition, neurodegeneration, and cognitive decline in sporadic Alzheimer's disease: a prospective cohort study. Lancet Neurol. 2013; 12: 357–67. PMID: 23477989
3. Braak H, Braak E. Neuropathological stageing of Alzheimer-related changes. Acta Neuropathol. Springer; 1991; 82: 239–259.
4. Jack CR, Wiste HJ, Weigand SD, Rocca WA, Knopman DS, Mielke MM, et al. Age-specific population frequencies of cerebral β-amyloidosis and neurodegeneration among people with normal cognitive function aged 50–89 years: a cross-sectional study. Lancet Neurol. 2014; 13: 997–1005. PMID: 25201514
5. Fox NC, Warrington EK, Freeborough PA, Hartikainen P, Kennedy AM, Stevens JM, et al. Presymptomatic hippocampal atrophy in Alzheimer's disease. A longitudinal MRI study. Brain. OXFORD UNIV PRESS; 1996; 119: 2001–2007.
6. Desikan RS, Cabral HJ, Hess CP, Dillon WP, Glastonbury CM, Weiner MW, et al. Automated MRI measures identify individuals with mild cognitive impairment and Alzheimer's disease. Brain. Oxford University Press; 2009; 132: 2048–2057.
7. Blennow K, Hampel H. CSF markers for incipient Alzheimer's disease. Lancet. 2003; 2: 605–613. PMID: 14505582
8. Shaw LM, Korecka M, Clark CM, Lee VM-Y, Trojanowski JQ. Biomarkers of neurodegeneration for diagnosis and monitoring therapeutics. Nat Rev Drug Discov. 2007; 6: 295–303. PMID: 17347655
9. Davatzikos C, Bhatt P, Shaw LM, Batmanghelich KN, Trojanowski JQ. Prediction of MCI to AD conversion, via MRI, CSF biomarkers, and pattern classification. Neurobiol Aging. Elsevier Inc.; 2010;
10. Westman E, Muehlboeck J-S, Simmons A. Combining MRI and CSF measures for classification of Alzheimer's disease and prediction of mild cognitive impairment conversion. Neuroimage. Elsevier B.V.; 2012; 62: 229–38.
11. Mattsson N, Zetterberg H, Hansson O, Andreasen N, Parnetti L, Jonsson M, et al. CSF biomarkers and incipient Alzheimer disease in patients with mild cognitive impairment. JAMA. 2009; 302: 385–93. doi: 10.1001/jama.2009.1064 PMID: 19622817
12. Fagan AM, Perrin RJ. Upcoming candidate cerebrospinal fluid biomarkers of Alzheimer's disease. Biomark Med. 2012; 6: 455–476. doi: 10.2217/bmm.12.42 PMID: 22917147
13. Guerreiro R, Wojtas A, Bras J, Carrasquillo M, Rogaeva E, Majounie E, et al. TREM2 variants in Alzheimer's disease. N Engl J Med. 2013; 368: 117–27. doi: 10.1056/NEJMoa1211851 PMID: 23150934
14. Zhang J, Goodlett DR, Peskind ER, Quinn JF, Zhou Y, Wang Q, et al. Quantitative proteomic analysis of age-related changes in human cerebrospinal fluid. Neurobiol Aging. 2005; 26: 207–27. PMID: 15582749
15. Hu WT, Chen-Plotkin A, Arnold SE, Grossman M, Clark CM, Shaw LM, et al. Novel CSF biomarkers for Alzheimer's disease and mild cognitive impairment. Acta Neuropathol. 2010; 119: 669–78. doi: 10.1007/s00401-010-0667-0 PMID: 20232070
16. Craig-Schapiro R, Perrin RJ, Roe CM, Xiong C, Carter D, Cairns NJ, et al. YKL-40: a novel prognostic fluid biomarker for preclinical Alzheimer's disease. Biol Psychiatry. Elsevier Inc.; 2010; 68: 903–12.
17. Weiner MW, Aisen PS, Jack CR, Jagust WJ, Trojanowski JQ, Shaw L, et al. The Alzheimer's disease neuroimaging initiative: progress report and future plans. Alzheimers Dement. Elsevier Ltd; 2010; 6: 202–11.
18. Shaw LM, Vanderstichele H, Knapik-Czajka M, Clark CM, Aisen PS, Petersen RC, et al. Cerebrospinal fluid biomarker signature in Alzheimer's disease neuroimaging initiative subjects. Ann Neurol. 2009; 65: 403–413. doi: 10.1002/ana.21610 PMID: 19296504
19. Shaw LM, Vanderstichele H, Knapik-Czajka M, Figurski M, Coart E, Blennow K, et al. Qualification of the analytical and clinical performance of CSF biomarker analyses in ADNI. Acta Neuropathol. 2011; 121: 597–609. doi: 10.1007/s00401-011-0808-0 PMID: 21311900
20. Trojanowski JQ, Vandeerstichele H, Korecka M, Clark CM, Aisen PS, Petersen RC, et al. Update on the biomarker core of the Alzheimer's Disease Neuroimaging Initiative subjects. Alzheimer's Dement. Elsevier Ltd; 2010; 6: 230–238.
21. Craig-Schapiro R, Kuhn M, Xiong C, Pickering EH, Liu J, Misko TP, et al. Multiplexed immunoassay panel identifies novel CSF biomarkers for Alzheimer's disease diagnosis and prognosis. PLoS One. 2011; 6: e18850. doi: 10.1371/journal.pone.0018850 PMID: 21526197

22. Hu WT, Holtzman DM, Fagan AM, Shaw LM, Perrin R, Arnold SE, et al. Plasma multianalyte profiling in mild cognitive impairment and Alzheimer disease. Neurology. 2012; 79: 897–905. PMID: 22855860
23. ADNI cerebrospinal fliud aliquot inventory description report [Internet]. Available: ADNI_CSF_Aliquot_Inventory_Description_v08_16_12.pdf
24. ADNI clinical procedures manual [Internet]. Dec. 10.1093/infdis/jis910
25. ADNI: Alzheimer's Disease Neuroimaging Initiative [Internet]. Available: http://www.adni-info.org/Scientists/ADNIStudyProcedures.aspx
26. Jack CR, Bernstein MA, Fox NC, Thompson P, Alexander G, Harvey D, et al. The Alzheimer's disease neuroimaging initiative (ADNI): MRI methods. J Magn Reson Imaging. Wiley Online Library; 2008; 27: 685–691.
27. Simmons A, Westman E, Muehlboeck S, Mecocci P, Vellas B, Tsolaki M, et al. MRI measures of Alzheimer's disease and the AddNeuroMed study. Ann N Y Acad Sci. 2009; 1180: 47–55.
28. Simmons A, Westman E, Muehlboeck S, Mecocci P, Vellas B, Tsolaki M, et al. The AddNeuroMed framework for multi-centre MRI assessment of Alzheimer's disease: experience from the first 24 months. Int J Geriatr Psychiatry. 2011; 26: 75–82. doi: 10.1002/gps.2491 PMID: 21157852
29. Westman E, Simmons A, Zhang Y, Muehlboeck J-S, Tunnard C, Liu Y, et al. Multivariate analysis of MRI data for Alzheimer's disease, mild cognitive impairment and healthy controls. Neuroimage. Elsevier Inc.; 2011; 54: 1178–87.
30. Westman E, Simmons A, Muehlboeck J-S, Mecocci P, Vellas B, Tsolaki M, et al. AddNeuroMed and ADNI: similar patterns of Alzheimer's atrophy and automated MRI classification accuracy in Europe and North America. Neuroimage. Elsevier Inc.; 2011; 58: 818–28.
31. Westman E, Aguilar C, Muehlboeck J-S, Simmons A. Regional magnetic resonance imaging measures for multivariate analysis in Alzheimer's disease and mild cognitive impairment. Brain Topogr. 2013; 26: 9–23. doi: 10.1007/s10548-012-0246-x PMID: 22890700
32. Fan Y, Batmanghelich N, Clark CM, Davatzikos C. Spatial patterns of brain atrophy in MCI patients, identified via high-dimensional pattern classification, predict subsequent cognitive decline. Neuroimage. 2008; 39: 1731–1743. PMID: 18053747
33. Davatzikos C, Xu F, An Y, Fan Y, Resnick SM. Longitudinal progression of Alzheimer's-like patterns of atrophy in normal older adults: the SPARE-AD index. Brain. 2009; 132: 2026–35. doi: 10.1093/brain/awp091 PMID: 19416949
34. Chang C, Lin C-J. LIBSVM: A Library for Support Vector Machines. ACM Trans Intell Syst Technol. 2011; 2: 1–27.
35. Hsu C, Chang C, Lin C. A Practical Guide to Support Vector Classification. Bioinformatics. Citeseer; 2010; 1: 1–16.
36. Zhang D, Wang Y, Zhou L, Yuan H, Shen D. Multimodal classification of Alzheimer's disease and mild cognitive impairment. Neuroimage. Elsevier Inc.; 2011; 55: 856–867.
37. Schölkopf B, Smola AJ. Learning with Kernels. Dietterich T, editor. Kybernetik. MIT Press; 2002.
38. Aguilar C, Westman E, Muehlboeck J-S, Mecocci P, Vellas B, Tsolaki M, et al. Different multivariate techniques for automated classification of MRI data in Alzheimer's disease and mild cognitive impairment. Psychiatry Res. Elsevier; 2013; 212: 89–98.
39. Mattsson N, Insel P, Nosheny R, Trojanowski JQ, Shaw LM, Jack CR, et al. Effects of cerebrospinal fluid proteins on brain atrophy rates in cognitively healthy older adults. Neurobiol Aging. Elsevier Ltd; 2014; 35: 614–22.
40. Blennow K, Davidsson P, Wallin A, Ekman R. Chromogranin A in cerebrospinal fluid: a biochemical marker for synaptic degeneration in Alzheimer's disease? Dementia. 1995; 6: 306–311. PMID: 8563783
41. Chiasserini D, Parnetti L, Andreasson U, Zetterberg H, Giannandrea D, Calabresi P, et al. CSF levels of heart fatty acid binding protein are altered during early phases of Alzheimer's disease. J Alzheimers Dis. 2010; 22: 1281–8. doi: 10.3233/JAD-2010-101293 PMID: 20930282
42. Olsson B, Hertze J, Ohlsson M, Nägga K, Höglund K, Basun H, et al. Cerebrospinal fluid levels of heart fatty acid binding protein are elevated prodromally in Alzheimer's disease and vascular dementia. J Alzheimers Dis. 2013; 34: 673–9. doi: 10.3233/JAD-121384 PMID: 23254629
43. Taylor DL, Diemel LT, Cuzner ML, Pocock JM. Activation of group II metabotropic glutamate receptors underlies microglial reactivity and neurotoxicity following stimulation with chromogranin A, a peptide up-regulated in Alzheimer's disease. J Neurochem. 2002; 82: 1179–1191. PMID: 12358765
44. Mattsson N, Insel P, Nosheny R, Zetterberg H, Trojanowski JQ, Shaw LM, et al. CSF protein biomarkers predicting longitudinal reduction of CSF β-amyloid42 in cognitively healthy elders. Transl Psychiatry. 2013; 3: e293. doi: 10.1038/tp.2013.69 PMID: 23962923

45. Soares HD, Potter WZ, Pickering E, Kuhn M, Immermann FW, Shera DM, et al. Plasma Biomarkers Associated With the Apolipoprotein E Genotype and Alzheimer Disease. Arch Neurol. 2012; 1–8.

46. Perrin RJ, Craig-Schapiro R, Malone JP, Shah AR, Gilmore P, Davis AE, et al. Identification and validation of novel cerebrospinal fluid biomarkers for staging early Alzheimer's disease. PLoS One. 2011; 6: e16032. doi: 10.1371/journal.pone.0016032 PMID: 21264269

47. Paterson RW, Bartlett JW, Blennow K, Fox NC, Shaw LM, Trojanowski JQ, et al. Cerebrospinal fluid markers including trefoil factor 3 are associated with neurodegeneration in amyloid-positive individuals. Transl Psychiatry. Nature Publishing Group; 2014; 4: 419.

48. Vemuri P, Wiste HJ, Weigand SD, Shaw LM, Trojanowski JQ, Weiner MW, et al. MRI and CSF biomarkers in normal, MCI, and AD subjects: predicting future clinical change. Neurology. 28 Jul 2009 73: 294–301. doi: 10.1212/WNL.0b013e3181af79fb PMID: 19636049

49. Apostolova LG, Hwang KS, Andrawis JP, Green AE, Babakchanian S, Morra JH, et al. 3D PIB and CSF biomarker associations with hippocampal atrophy in ADNI subjects. Neurobiol Aging. Elsevier Inc.; 2010; 31: 1284–1303.

50. Cui Y, Liu B, Luo S, Zhen X, Fan M, Liu T, et al. Identification of Conversion from Mild Cognitive Impairment to Alzheimer's Disease Using Multivariate Predictors. PLoS One. Public Library of Science; 2011; 6: e21896.

51. Misra C, Fan Y, Davatzikos C. Baseline and longitudinal patterns of brain atrophy in MCI patients, and their use in prediction of short-term conversion to AD: results from ADNI. Neuroimage. Elsevier Inc.; 2009; 44: 1415–22.

CHAPTER 4: A MULTI-COHORT STUDY OF APOE ε4 AND β-AMYLOID EFFECTS ON THE HIPPOCAMPUS IN ALZHEIMER'S DISEASE

This chapter is presented as a published paper and is the exact copy of the following journal publication:

Khan W, Giampietro V, Banaschewski T, Barker GJ, Bokde ALW, Büchel C, Conrod P, Flor H, Frouin V, Garavan H, Gowland P, Heinz A, Ittermann B, Lemaître H, Nees F, Paus T, Pausova Z, Rietschel R, Smolka MN,' Ströhle A, Gallinat J, Vellas B, Soininen H, Kloszewska I, Tsolaki M, Mecocci M, Spenger C, Villemagne VL, Masters CL, Muehlboeck SJ, Bäckman L, Fratiglioni L, Kalpouzos G, Wahlund LO, Schumann G, Lovestone S, Williams SCR, Westman E, Simmons A (*In Press*). A multi-cohort study of APOE ε4 and β-Amyloid effects on the Hippocampus in Alzheimer's disease. *J Alzheimer Dis*.

Author Contributions:

Study Concept and Design: Khan, Westman, Masters, Simmons

Acquisition, Analysis and Interpretation of data: Khan, Muehlboeck, Westman, Simmons

Drafting and Revision of Manuscript: All Authors

Statistical Analysis: Khan, Westman, Muehlboeck, Simmons

ABSTRACT

The Apolipoprotein E (APOE) gene has been consistently shown to modulate the risk of Alzheimer's disease (AD). Here, using an AD and normal ageing dataset primarily consisting of three AD multi-centre studies (n=1781), we compared the effect of APOE and amyloid-beta (Aβ) on baseline hippocampal volumes in AD patients, MCI subjects, and healthy controls. A large sample of healthy adolescents (n=1387) was also used to compared hippocampal volumes between APOE groups. Subjects had undergone a magnetic resonance imaging (MRI) scan and APOE genotyping. Hippocampal volumes were processed using FreeSurfer. In the AD and normal ageing dataset, hippocampal comparisons were performed in each APOE group and in ε4 carriers with Positron Emission Tomography (PET) Aβ who were dichotomized (Aβ+/Aβ-) using previous cut-offs. We found a linear reduction in hippocampal volumes with ε4 carriers possessing the smallest volumes, ε3 carriers possessing intermediate volumes, and ε2 carriers possessing the largest volumes. Moreover, AD and MCI ε4 carriers possessed the smallest hippocampal volumes and CN ε2 carriers possessed the largest hippocampal volumes. Subjects with both APOE ε4 and Aβ positivity had the lowest hippocampal volumes when compared to Aβ- ε4 carriers, suggesting a synergistic relationship between APOE ε4 and Aβ. However, we found no hippocampal volume differences between APOE groups in healthy 14-yr old adolescents. Our findings suggest that the strongest neuroanatomic effect of APOE ε4 on the hippocampus is observed in AD and groups most at risk of developing the disease, whereas hippocampi of old and young healthy individuals remain unaffected.

INTRODUCTION

The Apolipoprotein E (APOE) gene is a well-established genetic risk factor for the development of late-onset Alzheimer's disease (AD) and since its discovery, a large body of research has been conducted to explain its role in AD pathophysiology [1–3]. The APOE ε4 allele, a genetic risk factor known to substantially increase the risk of AD in a dose-dependent fashion, is associated with higher Aβ deposition [4,5]. By contrast, the APOE ε2 allele has been suggested to confer a protective effect against AD [6].

Hippocampal volumetry has been shown to be a sensitive, albeit non-specific marker of neurodegeneration in AD. Previously, it has been used to demonstrate accelerated rates of hippocampal atrophy in ε4 carriers with amnestic Mild Cognitive Impairment (MCI) [7,8]. Although the exact temporospatial relationship between Aβ and tau in the pathological cascade of AD is unclear, it has been suggested that both proteinopathies may have a synergistic effect on neuronal toxicity [9]. Emerging data also suggests that these pathological processes that influence cognitive decline in AD are moderated by APOE ε4 through both Aβ-dependent and Aβ-independent mechanisms [10]. However, evidence for the direct mechanistic actions of APOE ε4 is mixed.

Despite the numerous studies, our limited understanding of APOE ε4 risk in asymptomatic individuals and individuals with varying stages of AD pathophysiology warrants further study. Evidence has suggested that equivocal findings in neuroimaging studies of APOE ε4 may be attributed to the lack of specificity between changes that are due to normal ageing and those that manifest as a result of pathological neurodegeneration [11]. Furthermore, some APOE neuroimaging findings originate from studies with limitations in sample size and hence study power [12]. This is further exacerbated by the varying distribution of APOE ε4 carrier status across different samples. However, recent neuroimaging APOE studies with well-characterised samples (between 400-700 subjects) are beginning to address this methodological issue [13,14]. Also, recent neuroimaging evidence from young APOE ε4 carriers has also shown that structural and functional alterations in the brain may precede Aβ pathology [15,16]. This had

led researchers to postulate that that APOE ε4 may exert neurodevelopmental changes that provide a foothold for the pathological cascade of AD later in life.

In order to capture the heterogeneity of varying AD risk, we combined several well-characterised cohort studies to evaluate neuroanatomic the effect of APOE genotype on hippocampal volumes. The first dataset in our study, known as the AD and normal ageing dataset (n=1781) consisted of imaging data from three large multi-centre AD consortiums, (i) The Alzheimer's Disease Neuroimaging Initiative (ADNI), (ii) the AddNeuroMed study (ANM) and (iii) the Australian Imaging, Biomarkers and Lifestyles (AIBL) study, as well as a sample of non-demented individuals from the Swedish National Study on Ageing and Care in Kungsholmen (SNAC-K) and a dementia study from King's College London, UK (BRC-AD). The sample of non-demented individuals from the SNAC-K study were considered separate from healthy controls as the recruitment criteria for these subjects was epidemiological in nature and we could not exclude the possibility of memory impairment in some subjects. In our second dataset, we used a large sample of healthy 14-yr old adolescents (n=1387) in order to determine the neurodevelopmental effect of APOE ε4 genotype on hippocampal volume. This is particularly important because adolescence is a time of substantial dynamic neurobiological and behavioural changes. These changes are often beneficial and can optimise the brain for adult maturation, but can also confer neural vulnerabilities for certain types of psychiatric or neurological illness.

The aim of this study was to firstly evaluate the neuroanatomic effect of APOE genotype on the hippocampus in the AD and normal ageing dataset. Previous studies have demonstrated a linear effect of APOE genotype on disease risk, with ε2 carriers possessing a low risk of developing AD, and ε4 carriers possessing the greatest risk [17]. We aimed to test if this linear stepwise effect of APOE genotype also imparted a similar neuroanatomic effect on the hippocampus across the different stages of AD pathophysiology. We then tested the neuroanatomic effect of APOE genotype on hippocampal volumes of healthy 14-yr old adolescents to determine the role of APOE in adolescent brain development.

On the other hand, converging evidence suggests that APOE ε4 modifies Aβ accumulation and may have downstream effects on tau neurodegeneration [18]. To further elucidate the

mechanisms of this proposed synergistic relationship, we aimed to examine whether high levels of Aβ deposition would lead to greater hippocampal loss compared to low levels of Aβ deposition in APOE ε4 carriers.

MATERIALS AND METHOD

Datasets

Cohort specific inclusion criteria and details of the study design can be found in previous publications [19–23]. **Table 1** provides details of the number of subjects from each cohort included in the AD and normal ageing dataset.

AD and Normal Ageing Dataset (n=1781)

1) **Alzheimer's Disease Neuroimaging Initiative (n=779)**

   A detailed description of the study design can be found on the ADNI webpage (http://www.adni-info.org). Data was obtained for subjects from the ADNI online database (adni.loni.usc.edu). Subjects were between 55 and 90 years of age. ADNI was approved by the institutional review board and ethics committees of participating institutions, and written informed consent was obtained from all participants or their next of kin.

   i. **AD (n=177):** (General inclusion/exclusion criteria): 1) MMSE scores between 20 and 26. 2) CDR of 0.5 or 1.0. 3) Met NINCDS/ADRDA criteria for probable AD.

   ii. **MCI (n=383):** (General inclusion/exclusion criteria): 1) subjects had MMSE scores between 24 and 30 (inclusive). 2) Memory complaint had objective memory loss measured by education adjusted scores on Wechsler Memory Scale Logical Memory II. 3) CDR of 0.5. 4) Absence of significant levels of impairment in other cognitive domains, essentially preserved activities of daily living, and an absence of dementia.

iii. **CN (n=219):** (General inclusion/exclusion criteria): 1) MMSE scores between 24 and 30 (inclusive), 2) CDR of zero, 3) they were non- depressed, non MCI, and non-demented.

2) AddNeuroMed (ANM) study (n=303)

Information regarding the study design and enrolment criteria has been previously described elsewhere [21,24]. All AD and MCI subjects were recruited from the local memory clinics of one of the six participating sites while the control subjects were recruited from non-related members of the patient's families, caregiver's relatives and social centres for the elderly or GP surgeries. ANM was approved by the South London and Maudsley NHS Foundation Trust ethics committee and other ethical review boards of each participating country. Ethics committee approval was obtained at each of the participating centres in accordance with the Alzheimer's Associations published recommendations.

i. **AD (n=109):** (Inclusion criteria): 1) ADRDA/NINCDS and DSM-IV criteria for probable Alzheimer's disease. 2) Mini Mental State Examination score ranged from 12 to 28. 4) Age 65 years or above. Exclusion criteria: 1) Significant neurological or psychiatric illness other than Alzheimer's disease. 2) Significant unstable systematic illness or organ failure.

ii. **MCI (n=97)** and **CN (n=97)** (Inclusion criteria): 1) Mini Mental State Examination score range between 24 and 30. 2) Geriatric Depression Scale score less than or equal to 5. 3) Age 65 years or above. 4) Medication stable. 5) Good general health. Exclusion criteria: 1) Meet the DSM-IV criteria for Dementia. 2) Significant neurological or psychiatric illness other than Alzheimer's disease. 3) Significant unstable systematic illness or organ failure.

iii. The distinction between MCI and CN individuals was based on two criteria: 1) subject scores 0 on Clinical Dementia Rating Scale (CDR) = CN. 2) Subject scores 0.5 on CDR = MCI. For the MCI subjects it was preferable that the subject and informant reported occurrence of memory problems. All AD subjects had a CDR score of 0.5 or above.

3) The Australian, Imaging, Biomarkers, and Lifestyles (AIBL) study (n=228)

The AIBL study is a prospective longitudinal study of aging, integrating data from neuroimaging, biomarkers, lifestyle, clinical and neuropsychological analysis. Detailed information about the study design has been described in previous publications [20,25]. CN individuals were recruited by advertisement in the community while MCI and AD patients were recruited from tertiary memory disorders clinics or private geriatricians, psychiatrists and neurologists that subspecialise in dementia. All participants were at least 60 years of age, in good general health with no history of stroke or other neurological disease. The institutional ethics committees of Austin Health, St Vincent's Health, Hollywood Private Hospital and Edith Cowan University approved the AIBL study, and all volunteers gave written informed consent before participating.

i. AD (n=46): (Inclusion criteria): 1) all met NINCDS-ADRDA criteria for probable AD, and 2) had a CDR of 1 or more.

ii. MCI (n=42): (Inclusion Criteria): 1) Met criteria of subjective and objective cognitive difficulties in the absence of significant functional loss and 2) had a CDR of less than 1. 52 MCI participants fulfilled criteria for "amnestic" MCI, and 5 were non-amnestic cases (4 were non-amnestic multi-domain and 1 was non-amnestic single domain).

iii. CN (n=140): (Inclusion criteria): participants were separated in those who reported subjective memory complaints (n=95) and those who did not (n = 82), according to their response to the question: "Do you have any difficulty with your memory?"

4) Biomedical Research Centre for Mental Health and Dementia Cohort, King's College London (BRC-AD) (n=89)

BRC-AD is a neuroimaging study which was designed to establish imaging markers for the earlier detection and diagnosis of AD. Data was collected at the Institute of Psychiatry, Psychology, and Neuroscience (IoPPN), King's College London, UK. A total of 89 subjects (AD: 33, CN:56) were obtained with APOE data for this study. Diagnostic inclusion and exclusion criteria for this study were exactly the same as for the ANM study.

5) Swedish National study on Ageing and Care in Kungsholmen (SNAC-K) study (n=382)

Participants were recruited from a larger population-based epidemiological study, the Swedish National study on Ageing and Care in Kungsholmen (SNAC-K). In this study, participants were randomly selected to take part from the island of Kungsholmen in central Stockholm to examine ageing in late adulthood [26]. During the first data collection, a subsample of non-institutionalised and non-disabled participants were randomly selected to undergo MRI. Participants with dementia diagnoses, schizophrenia diagnosis, bipolar disorder diagnosis, self-reported stroke, stroke observed on MRI, self-reported Parkinson's disease, or epilepsy, were excluded. The study design has been described in detail elsewhere [22]. We used a sample of 459 individuals from SNAC-K, who underwent MRI imaging and APOE genotyping. 77 subjects with suboptimal MRI images and neurological and/or psychiatric conditions were excluded. The SNAC-K study was population-based, therefore subjects in this sample were considered a heterogeneous sample of elderly participants and treated separate from our sample CN individuals.

The SNAC-K study complies with the declaration of Helsinki, and has been approved by the ethical committee at Karolinska Institutet. All subjects gave informed consent, and in the case of severe cognitive impairment consent was collected from next-of-kin.

Neuroimaging-genetics IMAGEN study (n=1387)

This is the first European multi-centre study combining genetics with behavioural and neuropsychological measures, functional and structural neuroimaging and genome-wide association analyses in 2000 healthy 14-year-old adolescents. A description of the study design are provided in Schumann et al 2010 [23]. We selected 1387 healthy adolescents with available MRI data and ApoE status information.

Genome-wide genotyping was performed using Illumina Quad 610 and 660 arrays (San Diego, CA, USA). Quality control of the genome-wide data was performed and samples with the following criteria were excluded: genotype call rate <95%, and those with discordance between clinical and genotypic gender. Single Nucleotide Polymorphisms (SNP) quality control filters were used as described in the ENIGMA consortium imputation protocol

(http://enigma.ini.usc.edu/protocols/genetics-protocols/). Further details on the imputation of unobserved SNP's to determine APOE status are described in detail elsewhere [27].

Image Acquisition

High resolution 3D T1-weighted MRI were acquired for each subject and a comprehensive quality control procedure was applied to all MR images according to the AddNeuroMed study quality control framework [24,28].

ADNI: The protocol included a high resolution T1 weighted sagittal 3D MP-RAGE volume (voxel size 1.1 × 1.1 × 1.2 mm^3), and axial proton density with T2 weighted fast spin echo images. MRI scanner protocols from models of General Electric (GE) Healthcare, Philips Medical Systems, and Siemens Medical Solutions were supported.

ANM: Data acquisition took place using six different 1.5T MR systems (4 General Electric, 1 Siemens, and 1 Picker). At each site a quadrature birdcage coil was used for RF transmission and reception. Data acquisition was designed to be compatible with the ADNI. The imaging protocol included a high resolution sagittal 3D T1-weighted MPRAGE volume (voxel size 1.1 × 1.1 × 1.2 mm^3) and axial proton density / T2-weighted fast spin echo images. The BRC-AD study protocol was designed to be the same as the ANM protocol.

AIBL: T1-weighted MRI was obtained using the ADNI 3D Magnetization Prepared Rapid Gradient Echo (MPRAGE) sequence, with 1x1mm in-plane resolution and 1.2mm slice thickness, TR/TE/T1=2300/2.98/900, flip angle 9° and field of view 240x256 and 160 slices. T2 FSE and FLAIR sequences were also obtained. The AIBL protocol has been described in extensive detail previously [20].

SNAC-K: MRI scanning was undertaken on a 1.5T scanner (Philips Intera, Netherlands) on which 3D FFE (fast field echo) T1, Axial SE (spin echo) Proton Density/T2, DTI (Diffusion Tensor Imaging), and Axial FLAIR (fluid-attenuated inversion recovery) were acquired. In this study, the 3D FFE T1 images (TR = 15ms, TE = 7ms, Flip angle = 15◦, number of slices = 128, thickness

= 1.5mm, in-plane resolution = 0.94 x 0.94 mm, no gap, Field of view = 240, matrix = 256*256) were used.

IMAGEN: MRI images were acquired using 3T MRI systems from major manufacturers (Siemens, Philips, Bruker, and General Electric). The protocol included a high resolution 3D T1-weighted ultrafast gradient echo volume (voxel size 1.1×1.1×1.1mm^3) and axial proton density T2-weighted fast spin echo images based on the ADNI study protocol.

Aβ PET Methods

Data on Aβ imaging with positron emission tomography (PET) was accessed for a total of 95 ADNI and 57 AIBL ε4 carriers. Aβ imaging for these subjects was conducted using either ^{11}C-Pittsburgh Compound B (PiB), or ^{18}F-florbetapir. PET scans that were acquired as close as possible to the structural MRI scans in the ADNI and AIBL study were chosen. The PET imaging methodology of the ADNI and AIBL studies has been extensively described elsewhere [29,30]. For PiB PET, the measure of amyloid burden was calculated by averaging the ratio of cortical to cerebellar signal (SUVR) measurements from frontal, parietal, anterior cingulate and parietal regions of interest [29]. For ^{18}F-florbetapir, the SUVR was calculated for 6 pre-defined regions of interest (frontal, temporal, parietal, anterior cingulate, posterior cingulate, and precuneus). The whole cerebellum was used as a reference region for both PiB and ^{18}F-florbetapir PET.
Of the 95 subjects that underwent PET neuroimaging in the ADNI study, 66 were scanned using ^{18}F-florbetapir and 29 using PiB. For the AIBL study, all subjects underwent PET neuroimaging using PiB. The global measure of amyloid burden was used to define participants as Aβ positive (Aβ+) and Aβ negative (Aβ-). PiB participants were classified as Aβ+ when the measure of amyloid burden was ≥ 1.5 [30] and ^{18}F-florbetapir participants were classified as Aβ+ if the measure of amyloid burden was ≥ 1.11 [31].

Image Analysis

Volumetric segmentation of the hippocampus was performed using FreeSurfer (5.1.0). FreeSurfer utilises an affine rigid linear transformation and combines spatial information about voxel intensity relative to a probability distribution for tissue classes [32]. The FreeSurfer segmentation process includes motion correction of volumetric T1-weighted images, removal of non-brain tissue using a hybrid watershed/surface deformation procedure [33], automated Talairach transformation, segmentation of the subcortical white matter and deep grey matter volumetric structures (including hippocampus, amygdala, caudate, putamen, ventricles) [34], intensity normalization [33], tessellation of the grey matter white matter boundary, automated topology correction [35,36], and surface deformation following intensity gradients to optimally place the grey/white and grey/cerebrospinal fluid borders at the location where the greatest shift in intensity defines the transition to the other tissue class [37–39]. Further details of the segmentation approach have been described previously [34]. Quality control of hippocampal images were performed by visualising the subcortical segmentation borders of the hippocampus for every subject. Images reflecting a poor segmentation of the hippocampal structures were excluded from the study. Hippocampal volumes were normalised by subject intracranial volume ($volume_{normalised} = volume_{raw} \times 1{,}000/\text{intracranial volume}$) to correct for individual differences in head size.

Statistical Analysis

To compare demographic statistics, Fisher's exact tests and ANOVA with Tukey-Kramer HSD post-hoc tests were used. A linear mixed model regression was used to compare hippocampal volumes by APOE genotype (ε2/ε3/ε4). In accordance with previous work, 44 ε2/ε4 individuals were excluded from the analysis due to the opposing protective effect of the ε2 allele and detrimental effect of ε4 allele [40].The model treated subject age, gender, and baseline diagnosis as fixed terms in the final model. Interaction terms for APOE genotype and diagnosis were also included and image acquisition site was included as a random effect term.

Hippocampal comparisons were also performed in a sample of subjects from the ADNI and AIBL cohorts who were divided into Aβ+ and Aβ- participants. Pairwise multiple comparisons

were corrected using a stringent Bonferroni correction method. The R statistical software environment, version 3.1.1, was used to perform all statistical analyses in RStudio. The nlme v3.1-117 [41] package was used to create linear-mixed effects models and multcomp v1.3-6 [42] package for post-hoc comparisons.

RESULTS

Demographic Characteristics

In the AD group, a difference in age between APOE groups was significant (p = 0.016) with ε2 carriers being significantly older than ε3 carriers and ε4 carriers. For MCI subjects, ε2 and ε3 carriers had significantly higher MMSE scores than ε4 carriers (p=0.016). No other demographic characteristics differed between the groups (Table 2).

Comparing the effect of APOE Genotype on Hippocampal volume in the AD, and normal ageing dataset (n=1781) and the IMAGEN study of Healthy 14-yr Adolescents (n=1387)

In AD patients, ε4 carriers had significantly smaller hippocampal volumes than non-carriers. A significant linear stepwise reduction in hippocampal volume was observed with ε2 carriers possessing the largest volumes, ε3 carriers possessing intermediate volumes and ε4 carriers possessing the smallest volumes. This pattern was also observed in the MCI group (Table 3). The effect of the ε4 allele on hippocampal volume was found to be moderately dose-dependent in AD patients [left region: Cohen's d = 0.10, p = < .0001; right region: Cohen's d = 0.22, p = < .0001] and MCI subjects [left region: Cohen's d = 0.15, p = < .0001; right region: Cohen's d = 0.19, p = < .0001].

The effect of APOE genotype on hippocampal volumes in CN individuals was not significant (left region: p= 0.052; right region: p = 0.053) and the magnitude of this non-significant difference in both regions was small (Cohen's d = 0.16; effect size r = 0.08). This non-significant pattern was also observed in elderly individuals from the SNAC-K study, as well as in healthy adolescents from the IMAGEN study (Table 3). Figure 1 displays hippocampal volumes by APOE genotype in the AD and normal ageing dataset and IMAGEN study of adolescents.

Hippocampal volumes of AD ε4 carriers were found to be significantly smaller than MCI, CN, and non-demented ε4 carriers. This pattern was also observed in MCI ε4 carriers who had significantly smaller volumes than CN, and non-demented ε4 carriers (Table 4). In carriers of

the ε2 allele, the MCI and CN groups possessed significantly larger hippocampal volumes than ε2 carriers of the AD group (Table 5).

Comparison of Hippocampal volumes by APOE ε4 and Aβ Deposition

In this analysis, ε4 carriers from the ADNI and AIBL cohort studies were selected and divided into Aβ+ and Aβ- participants to assess if the effect of APOE ε4 on the hippocampus is modified by levels of Aβ deposition. Descriptive information for this sample is shown in Table 6. Among ε4+ CN individuals, hippocampal volumes between Aβ+ and Aβ- participants did not significantly differ (left region: p = 0.692; right region: p = 0.946). MCI Aβ+ participants were found to have significantly smaller hippocampal volumes than MCI Aβ- participants for the right hippocampus (left hippocampus: p = 0.295; right hippocampus: p = 0.054). Hippocampal volumes of MCI Aβ+ ε4+ participants did not differ when compared to AD Aβ+ ε4+ participants. AD Aβ+ ε4+ participants possessed significantly smaller hippocampal volumes than (i) the CN Aβ- ε4+ group (left region: Cohen's d = -1.05; p = <.001; right region: Cohen's d = -1.03; p = <.001) and the (ii) CN Aβ+ ε4+ group (left region: Cohen's d = -1.09; p = <.001; right region: Cohen's d = -1.02; p = <.001). The complete results for these comparisons are shown in Table 7. There was no interaction observed between gender and ε4 status in hippocampal volumes between groups. Hippocampal differences between the different Aβ+ and Aβ- participants are shown in Figure 2.

DISCUSSION

Prior neuroimaging studies of APOE ε4 have helped define our current observation of structural changes in the brain, but the mechanisms associated with the detrimental effect of APOE ε4, particularly across the different stages of AD, still remains poorly understood. With recent studies proposing a neurodevelopmental foothold of APOE ε4 on the brain [43,44], understanding whether atrophy in AD-susceptible areas, such as the hippocampus, are attributed to pre-clinical manifestations of the disease, or whether these constitute a part of non-specific normal ageing is of great importance for earlier diagnosis.

Here we present the largest cross-sectional multi-cohort study of APOE and hippocampal volume to date (*n*=3168) and discuss a number of key findings. Firstly, a linear neuroanatomic effect of the APOE genotype was observed for hippocampal volumes of AD and MCI subjects, whereby ε4 carriers presented with the lowest volumes, ε3 homozygotes possessed intermediate volumes, and ε2 carriers possessed the largest volumes. As expected, ε4 carriers in the AD and the MCI group had significantly lower hippocampal volumes when compared to CN individuals and a population-based sample of elderly non-demented individuals from the SNAC-K study. These findings are in agreement with previous studies demonstrating a distinct neuroanatomic effect of APOE genotype on brain structure, as well as studies reporting smaller hippocampal volumes in MCI subjects with prodromal stages of AD. Furthermore, our finding of larger hippocampal volumes in ε2 carriers in older healthy groups supports the ε2 allele's suggested effect of protection against neurodegeneration. Previous cellular models have advocated its role in a disease staving protective effect, in particular its ability to modify the neuropathological effects of Aβ accumulation [45].

The absence of APOE-dependent hippocampal volume loss in CN individuals and in a population-based sample of elderly individuals suggested that APOE ε4 may not be independently associated with hippocampal atrophy in normal ageing. Although the findings from previous APOE studies in non-demented individuals are mixed, our findings replicate a number of earlier neuroimaging studies showing no effect of APOE ε4 on regions such as the hippocampus in normal ageing [46–48]. One explanation for the discrepant APOE findings in

CN individuals may be related to differences in defining those that fulfil the criteria for pre-clinical AD from subjects showing typical normal ageing [11]. Recent studies have since shown that APOE ε4 is linked to Aβ deposition and may exert a synergistic effect to promote cognitive decline [49,50].

To test whether an Aβ-dependent effect of APOE ε4 would be associated with greater hippocampal volume loss, we examined the combined effect of APOE ε4 and Aβ on the hippocampus. We found no significant differences in hippocampal volume between CN Aβ+ ε4+ individuals and CN Aβ- ε4+ individuals, suggesting that in healthy individuals there is no effect of APOE ε4 and Aβ on the hippocampus. This is consistent with previous studies that have shown that the relationship between APOE ε4, Aβ and brain atrophy is mediated by CSF p-tau181 levels [51,52] and, in the absence of abnormal *p*-tau$_{181}$ levels, there is no synergistic relationship between APOE ε4 and Aβ deposition. Hippocampal volumes of MCI Aβ+ ε4+ individuals did not differ when compared to AD Aβ+ ε4+ participants, suggesting that a similar degree of hippocampal loss that is expected in AD has already manifested in MCI subjects. Our findings are supported by empirical evidence which has shown that APOE induces intracellular degradation of Aβ peptides facilitating synaptotoxicity, neuroinflammation, and tau hyper-phosphorylation [5,53]. It is therefore possible that Aβ and the ε4 in conjunction impart great levels of neuronal toxicity and injury in the presence of hippocampal neurodegeneration.

Recent studies have suggested an Aβ independent effect of the APOE ε4 on neuronal integrity as another explanation for the gene's effect on brain structure [47,54]. A study by Dean and colleagues [44] argued that an early neurodevelopmental foothold of APOE on the brain may render individuals more susceptible to the toxic and downstream neurodegenerative effects of Aβ later in life. However, findings from our large sample of 14-year old adolescents showed that there were no hippocampal volume differences present between the APOE groups, suggesting that ε4 carriers are unlikely to be at risk in adolescence, but may perhaps develop a greater risk later in life. Similar studies, such as that of O'Dwyer and colleagues [15] reported lower hippocampal volumes in ε4 carriers aged in their mid-twenties. Although differences may be attributed to the methodological approach adopted for the automated segmentation of the hippocampus, we cannot exclude the possibility of a low APOE penetrance in our young sample. Nevertheless, previous studies in younger ε4 carriers have shown that APOE plays a

fundamental role in modulating brain function in the absence of any differences in brain volume [47].

An important caveat when interpreting the results of this study is that the multi-cohort data was cross-sectional and a more complete understanding of how hippocampal trajectories vary with age would require longitudinal data. In particular, more neuroimaging studies need to be conducted into typical cognitive ageing across the lifespan [18] in order to differentiate between brain changes that are associated with typical normal ageing from those that arise from APOE ε4 dependent mechanisms and β-amyloidosis. Additionally, when combining data across cohort studies it is important to consider study design differences that may complicate the interpretation of our results. For instance, the use of different AD diagnostic criteria across the different cohort studies may contribute to a level of diagnostic variability between groups. Participants from the ADNI and AIBL study were also highly educated, had few comorbidities, and were of Caucasian background. As such, future prospective studies with more representative samples should be conducted to address how these comorbidities, namely the presence of vascular disease, could potentially influence the size of the hippocampus. We demonstrated that systematic bias was not present in our dataset when comparing hippocampal volumes between APOE groups within each cohort study separately (Supplementary Information).Additional factors such as the use of two different PET radioligands meant that SUVR values of tracer uptake could not be compared as a single continuous measure. However, ongoing working groups such as the Centiloid project will further enable a more standardised approach for the direct comparability of results across different labs when different tracers and methods of analysis are employed [55].

Despite these limitations, this is first multi-cohort neuroimaging study of APOE genotype that attempts to characterise the differential risk of APOE on hippocampal volumes of subjects with varying stages of AD. Using metadata and clinical phenotyping pooled across several cohort studies, we were systematically able to demonstrate differential effects of the different APOE gene polymorphisms on hippocampal volume. An independent sample of healthy 14yr old adolescents also provides an understanding into the role of APOE in adolescent brain neurodevelopment.

In conclusion, our findings in the largest APOE neuroimaging dataset show that hippocampal volume loss is present in patients with AD and in subjects with an increased risk of developing AD, particularly subjects with memory impairment. However, healthy older individuals did not show APOE ε4 dependent changes in the hippocampus, suggesting that the relationship between APOE ε4 and Aβ may be mediated by the presence of neurodegeneration. The same pattern was also observed in healthy young adolescents who possessed no hippocampal differences between different APOE groups. Our study thus shows hippocampal volume loss is moderated by APOE ε4 and Aβ in AD and the MCI stages of the AD pathological process. The influence of these 3 markers could be considered as prognostic tools in clinical trials and therapeutic interventions of AD.

ACKNOWLEDGMENTS

(1) Data used in preparation of this article were obtained from the Alzheimer's Disease Neuroimaging Initiative (ADNI) database (adni.loni.ucla.edu). As such, the investigators within the ADNI contributed to the design and implementation of ADNI and/or provided data but did not participate in analysis or writing of this report. A complete listing of ADNI investigators can be found on ADNI website (adni.loni.usc.edu/). (2) Data used in the preparation of this article were obtained from the Australian Imaging Biomarkers and Lifestyle Flagship Study of Ageing (AIBL) funded by the Commonwealth Scientific and Industrial Research Organisation (CSIRO), which was made available at the ADNI database (www.loni.ucla.edu/ADNI). The AIBL researchers contributed data but did not participate in analysis or writing of this report. AIBL researchers can be found on the AIBL website (aibl.csiro.au). (3) Data used in the preparation of this study was obtained from the AddNeuroMed study which was was supported by InnoMed, (Innovative Medicines in Europe) an Integrated Project funded by the European Union of the Sixth Framework program priority FP6-2004-LIFESCIHEALTH-5, Life Sciences, Genomics and Biotechnology for Health, Health Research Council of Academy of Finland (HS), The Gamla Tjanarinnor Foundation, The Swedish Alzheimer's Association and Swedish Brain Power. (4) Data used in the preparation of this study were obtained from the Swedish National Study of Ageing and Care in Kungsholmen (SNACK) which was supported by Stiftelsen för Gamla Tjänarinnor and Sigurd och Elsa Goljes Minne, the Swedish Research Council, the Swedish Council for Working Life and Social Research, Swedish Brain Power, an Alexander von Humboldt Research Award, and a donation from the af Jochnick Foundation. (5) Data used in the preparation of this study were obtained for the IMAGEN study which was supported by the IMAGEN project, which receives research funding from the European Community's Sixth Framework Program (LSHM-CT-2007-037286) and coordinated project ADAMS (242257), as well as the NIHR Biomedical Research Centre for Mental Health and NIHR Biomedical Research Unit for Dementia at South London and Maudsley NHS Foundation Trust and Institute of Psychiatry, Psychology, and Neuroscience (IoPPN), King's College London, Alzheimer Research UK and the IMI funded European Medical Information Framework.

REFERENCES

[1] Saunders AM, Strittmatter WJ, Schmechel D, St. George-Hyslop PH, Pericak-Vance M a., Joo SH, Rosi BL, Gusella JF, Crapper-MacLachlan DR, Alberts MJ, Hulette C, Crain B, Goldgaber D, Roses a. D (1993) Association of apolipoprotein E allele 4 with late-onset familial and sporadic Alzheimer's disease. Neurology 43, 1467–1472.

[2] Lehtovirta M, Soininen H, Laakso MP, Partanen K, Helisalmi S, Mannermaa A, Ryynänen M, Kuikka J, Hartikainen P, Riekkinen PJ (1996) SPECT and MRI analysis in Alzheimer's disease: relation to apolipoprotein E epsilon 4 allele. J Neurol Neurosurg Psychiatry 60, 644–649.

[3] Harold D, Abraham R, Hollingworth P, Sims R, Gerrish A, Hamshere ML, Pahwa JS, Moskvina V, Dowzell K, Williams A, Jones N, Thomas C, Stretton A, Morgan AR, Lovestone S, Powell J, Proitsi P, Lupton MK, Brayne C, Rubinsztein DC, Gill M, Lawlor B, Lynch A, Morgan K, Brown KS, Passmore PA, Craig D, McGuinness B, Todd S, Holmes C, Mann D, Smith AD, Love S, Kehoe PG, Hardy J, Mead S, Fox N, Rossor M, Collinge J, Maier W, Jessen F, Schürmann B, Van Den Bussche H, Heuser I, Kornhuber J, Wiltfang J, Dichgans M, Frölich L, Hampel H, Hüll M, Rujescu D, Goate AM, Kauwe JSK, Cruchaga C, Nowotny P, Morris JC, Mayo K, Sleegers K, Bettens K, Engelborghs S, De Deyn PP, Van Broeckhoven C, Livingston G, Bass NJ, Gurling H, McQuillin A, Gwilliam R, Deloukas P, Al-Chalabi A, Shaw CE, Tsolaki M, Singleton AB, Guerreiro R, Mühleisen TW, Nöthen MM, Moebus S, Jöckel K-H, Klopp N, Wichmann H-E, Carrasquillo MM, Pankratz VS, Younkin SG, Holmans PA, O'Donovan M, Owen MJ, Williams J (2009) Genome-wide association study identifies variants at CLU and PICALM associated with Alzheimer's disease. Nat. Genet. 41, 1088–1093.

[4] Jiang Q, Lee CYD, Mandrekar S, Wilkinson B, Cramer P, Zelcer N, Mann K, Lamb B, Willson TM, Collins JL, Richardson JC, Smith JD, Comery T a, Riddell D, Holtzman DM, Tontonoz P, Landreth GE (2008) ApoE promotes the proteolytic degradation of Abeta. Neuron 58, 681–93.

[5] Verghese PB, Castellano JM, Garai K, Wang Y, Jiang H, Shah A, Bu G, Frieden C, Holtzman DM (2013) ApoE influences amyloid-β (Aβ) clearance despite minimal apoE/Aβ association in physiological conditions. Proc Natl Acad Sci U S A 110, E1807-16.

[6] Kim J, Basak JM, Holtzman DM (2009) The Role of Apolipoprotein E in Alzheimer's Disease. Neuron 63, 287–303.

[7] Farlow MR, He Y, Tekin S, Xu J, Lane R, Charles HC (2004) Impact of APOE in mild cognitive impairment. Neurology 63, 1898–901.

[8] Fleisher A, Grundman M, Jack CR, Petersen RC, Taylor C, Kim HT, Schiller DHB, Bagwell V, Sencakova D, Weiner MF, DeCarli C, DeKosky ST, van Dyck CH, Thal LJ (2005) Sex, apolipoprotein E epsilon 4 status, and hippocampal volume in mild cognitive impairment. Arch. Neurol. 62, 953–7.

[9] Jack CR, Knopman DS, Jagust WJ, Petersen RC, Weiner MW, Aisen PS, Shaw LM, Vemuri P, Wiste HJ, Weigand SD, Lesnick TG, Pankratz VS, Donohue MC, Trojanowski JQ (2013) Tracking pathophysiological processes in Alzheimer's disease: an updated hypothetical model of dynamic biomarkers. Lancet Neurol 12, 207–16.

[10] Fouquet M, Besson FL, Gonneaud J, La Joie R, Chételat G (2014) Imaging brain effects of APOE4 in cognitively normal individuals across the lifespan. Neuropsychol Rev 24, 290–9.

[11] Fjell AM, McEvoy L, Holland D, Dale AM, Walhovd KB (2014) What is normal in normal aging? Effects of aging, amyloid and Alzheimer's disease on the cerebral cortex and the hippocampus. Prog Neurobiol 117, 20–40.

[12] Cherbuin N, Leach LS, Christensen H, Anstey KJ (2007) Neuroimaging and APOE genotype: a systematic qualitative review. Dement Geriatr Cogn Disord 24, 348–62.

[13] Morra JH, Tu Z, Apostolova LG, Green AE, Avedissian C, Madsen SK, Parikshak N, Toga AW, Jack CR, Schuff N, Weiner MW, Thompson PM (2009) Automated mapping of hippocampal atrophy in 1-year repeat MRI data from 490 subjects with Alzheimer's disease, mild cognitive impairment, and elderly controls. Neuroimage 45, S3-15.

[14] Shi J, Leporé N, Gutman B a, Thompson PM, Baxter LC, Caselli RL, Wang Y Genetic influence of apolipoprotein E4 genotype on hippocampal morphometry: An N = 725 surface-based Alzheimer's disease neuroimaging initiative study. Hum Brain Mapp; e-pub ahead of print 22 January 2014; doi:10.1002/.

[15] O'Dwyer L, Lamberton F, Matura S, Tanner C, Scheibe M, Miller J, Rujescu D, Prvulovic D, Hampel H (2012) Reduced hippocampal volume in healthy young ApoE4 carriers: an MRI study. PLoS One 7, e48895.

[16] Alexopoulos P, Richter-Schmidinger T, Horn M, Maus S, Reichel M, Sidiropoulos C, Rhein C, Lewczuk P, Doerfler A, Kornhuber J (2011) Hippocampal volume differences between healthy young apolipoprotein E ε2 and ε4 carriers. J Alzheimers Dis 26, 207–10.

[17] Liu C-C, Liu C-C, Kanekiyo T, Xu H, Bu G (2013) Apolipoprotein E and Alzheimer disease: risk, mechanisms and therapy. Nat Rev Neurol 9, 106–18.

[18] Jack CR, Wiste HJ, Weigand SD, Knopman DS, Vemuri P, Mielke MM, Lowe V, Senjem ML, Gunter JL, Machulda MM, Gregg BE, Pankratz VS, Rocca WA, Petersen RC (2015) Age, Sex, and APOE ε4 Effects on Memory, Brain Structure, and β-Amyloid Across the Adult Life Span. JAMA Neurol 55905, 1–9.

[19] Aisen PS, Petersen RC, Donohue MC, Gamst A, Raman R, Thomas RG, Walter S, Trojanowski JQ, Shaw LM, Beckett L a., Jack CR, Jagust W, Toga AW, Saykin AJ, Morris JC, Green RC, Weiner MW (2010) Clinical core of the Alzheimer's disease neuroimaging initiative: Progress and plans. Alzheimer's Dement 6, 239–246.

[20] Ellis K, Bush AI, Darby D, De Fazio D, Foster J, Hudson P, Lautenschlager NT, Lenzo N, Martins RN, Maruff P, Masters C, Milner A, Pike K, Rowe C, Savage G, Szoeke C, Taddei K, Villemagne V, Woodward M, Ames D (2009) The Australian Imaging, Biomarkers and Lifestyle (AIBL) study of aging: methodology and baseline characteristics of 1112 individuals recruited for a longitudinal study of Alzheimer's disease. Int. Psychogeriatr. 21, 672–87.

[21] Lovestone S, Francis P, Kloszewska I, Mecocci P, Simmons A, Soininen H, Spenger C, Tsolaki M, Vellas B, Wahlund L-O, Ward M (2009) AddNeuroMed--the European collaboration for the discovery of novel biomarkers for Alzheimer's disease. Ann N Y Acad Sci 1180, 36–46.

[22] Lagergren M, Fratiglioni L, Hallberg IR, Berglund J, Elmståhl S, Hagberg B, Holst G, Rennemark M, Sjölund B-M, Thorslund M, Wiberg I, Winblad B, Wimo A (2004) A longitudinal study integrating population, care and social services data. The Swedish National study on Aging and Care (SNAC). Aging Clin Exp Res 16, 158–168.

[23] Schumann G, Loth E, Banaschewski T, Barbot A, Barker G, Büchel C, Conrod PJ, Dalley JW, Flor H, Gallinat J, Garavan H, Heinz A, Itterman B, Lathrop M, Mallik C, Mann K, Martinot J-L, Paus T, Poline J-B, Robbins TW, Rietschel M, Reed L, Smolka M, Spanagel R, Speiser C, Stephens DN, Ströhle A, Struve M (2010) The IMAGEN study:

reinforcement-related behaviour in normal brain function and psychopathology. Mol Psychiatry 15, 1128–39.

[24] Simmons A, Westman E, Muehlboeck S, Mecocci P, Vellas B, Tsolaki M, Kłoszewska I, Wahlund L-O, Soininen H, Lovestone S, Evans A, Spenger C (2009) MRI measures of Alzheimer's disease and the AddNeuroMed study. Ann N Y Acad Sci 1180, 47–55.

[25] Ellis K, Rainey-Smith SR, Rembach A, Macaulay SL, Villemagne VL (2013) Enabling a multidisciplinary approach to the study of ageing and Alzheimer's disease: an update from the Australian Imaging Biomarkers and Lifestyle (AIBL) study. Int Rev Psychiatry 25, 699–710.

[26] Ferencz B, Laukka EJ, Lövdén M, Kalpouzos G, Keller L, Graff C, Wahlund L-O, Fratiglioni L, Bäckman L (2013) The influence of APOE and TOMM40 polymorphisms on hippocampal volume and episodic memory in old age. Front Hum Neurosci 7, 198.

[27] Radmanesh F, Devan WJ, Anderson CD, Rosand J, Falcone GJ (2014) Accuracy of imputation to infer unobserved APOE epsilon alleles in genome-wide genotyping data. Eur J Hum Genet 1–4.

[28] Simmons A, Westman E, Muehlboeck S, Mecocci P, Vellas B, Tsolaki M, Kłoszewska I, Wahlund L-O, Soininen H, Lovestone S, Evans A, Spenger C (2011) The AddNeuroMed framework for multi-centre MRI assessment of Alzheimer's disease: experience from the first 24 months. Int J Geriatr Psychiatry 26, 75–82.

[29] Jagust WJ, Bandy D, Chen K, Foster NL, Landau SM, Mathis C a, Price JC, Reiman EM, Skovronsky D, Koeppe R a (2010) The Alzheimer's Disease Neuroimaging Initiative positron emission tomography core. Alzheimer's Dement 6, 221–9.

[30] Rowe CC, Ellis KA, Rimajova M, Bourgeat P, Pike KE, Jones G, Fripp J, Tochon-Danguy H, Morandeau L, O'Keefe G, Price R, Raniga P, Robins P, Acosta O, Lenzo N, Szoeke C, Salvado O, Head R, Martins R, Masters CL, Ames D, Villemagne VL (2010) Amyloid imaging results from the Australian Imaging, Biomarkers and Lifestyle (AIBL) study of aging. Neurobiol Aging 31, 1275–83.

[31] Clark CM, Schneider JA, Bedell BJ, Beach TG, Bilker WB, Mintun M a, Pontecorvo MJ, Hefti F, Carpenter AP, Flitter ML, Krautkramer MJ, Kung HF, Coleman RE, Doraiswamy PM, Fleisher AS, Sabbagh MN, Sadowsky CH, Reiman EP, Reiman PEM, Zehntner SP, Skovronsky DM (2011) Use of florbetapir-PET for imaging beta-amyloid pathology. JAMA 305, 275–83.

[32] Ségonne F, Dale AM, Busa E, Glessner M, Salat D, Hahn HK, Fischl B (2004) A hybrid approach to the skull stripping problem in MRI. Neuroimage 22, 1060–1075.

[33] Sled JG, Zijdenbos AP, Evans AC (1998) A nonparametric method for automatic correction of intensity nonuniformity in MRI data. IEEE Trans. Med. Imaging 17, 87–97.

[34] Fischl B, H Salat D, Busa E, Albert M, Dieterich M, Haselgrove C, Van Der Kouwe A, Killiany R, Kennedy D, Klaveness S, Montillo A, Makris N, Rosen B, Dale AM (2002) Whole brain segmentation: automated labeling of neuroanatomical structures in the human brain. Neuron 33, 341–355.

[35] Fischl B, Liu A, Dale AM (2001) Automated manifold surgery: constructing geometrically accurate and topologically correct models of the human cerebral cortex. IEEE Trans. Med. Imaging 20, 70–80.

[36] Ségonne F, Pacheco J, Fischl B (2007) Geometrically accurate topology-correction of cortical surfaces using nonseparating loops. IEEE Trans. Med. Imaging 26, 518–529.

[37] Fischl B, Sereno MI, Tootell RB, Dale AM (1999) High-resolution intersubject averaging and a coordinate system for the cortical surface. Hum. Brain Mapp. 8, 272–284.

[38] Dale AM, Sereno MI (1993) Improved Localization of Cortical Activity by Combining EEG and MEG with MRI Cortical Surface Reconstruction: A Linear Approach. J Cogn Neurosci 5, 162–176.

[39] Fischl B, Dale a M (2000) Measuring the thickness of the human cerebral cortex from magnetic resonance images. Proc Natl Acad Sci U S A 97, 11050–5.

[40] Shaw P, Lerch JP, Pruessner JC, Taylor KN, Rose AB, Greenstein D, Clasen L, Evans A, Rapoport JL, Giedd JN (2007) Cortical morphology in children and adolescents with different apolipoprotein E gene polymorphisms: an observational study. Lancet Neurol 6, 494–500.

[41] Pinheiro J, Bates D, DebRoy S, Sarkar D, Team TRC (2009) nlme: Linear and Nonlinear Mixed Effects Models. October R package, 1–3.

[42] Hothorn T, Bretz F, Westfall P (2008) Simultaneous inference in general parametric models. Biom J 50, 346–63.

[43] Knickmeyer RC, Wang J, Zhu H, Geng X, Woolson S, Hamer RM, Konneker T, Lin W, Styner M, Gilmore JH (2014) Common Variants in Psychiatric Risk Genes Predict Brain Structure at Birth. Cereb. Cortex 24, 1230–1246.

[44] Dean DC, Jerskey B, Chen K, Protas H, Thiyyagura P, Roontiva A, O'Muircheartaigh J, Dirks H, Waskiewicz N, Lehman K, Siniard AL, Turk MN, Hua X, Madsen SK, Thompson PM, Fleisher AS, Huentelman MJ, Deoni SCL, Reiman EM (2014) Brain Differences in Infants at Differential Genetic Risk for Late-Onset Alzheimer Disease: A Cross-sectional Imaging Study. JAMA Neurol 71, 11–22.

[45] Tiraboschi P, Hansen LA, Masliah E, Alford M, Thal LJ, Corey-Bloom J (2004) Impact of APOE genotype on neuropathologic and neurochemical markers of Alzheimer disease. Neurology 62, 1977–1983.

[46] Schuff N, Woerner N, Boreta L, Kornfield T, Shaw LM, Trojanowski JQ, Thompson PM, Jack CR, Weiner MW (2009) MRI of hippocampal volume loss in early Alzheimer's disease in relation to ApoE genotype and biomarkers. Brain 132, 1067–77.

[47] Filippini N, MacIntosh BJ, Hough MG, Goodwin GM, Frisoni GB, Smith SM, Matthews PM, Beckmann CF, Mackay CE (2009) Distinct patterns of brain activity in young carriers of the APOE E4 allele. Proc Natl Acad Sci U S A 106, 7209–14.

[48] Hostage C, Roy Choudhury K, Doraiswamy PM, Petrella JR (2013) Dissecting the gene dose-effects of the APOE ε4 and ε2 alleles on hippocampal volumes in aging and Alzheimer's disease. PLoS One 8, e54483.

[49] Reiman EM, Chen K, Liu X, Bandy D, Yu M, Lee W, Ayutyanont N, Keppler J, Reeder SA, Langbaum JBS, Alexander GE, Klunk WE, Mathis CA, Price JC, Aizenstein HJ, DeKosky ST, Caselli RJ (2009) Fibrillar amyloid-beta burden in cognitively normal people at 3 levels of genetic risk for Alzheimer's disease. Proc Natl Acad Sci U S A 106, 6820–6825.

[50] Mormino EC, Betensky RA, Hedden T, Schultz AP, Ward A, Huijbers W, Rentz DM, Johnson KA, Sperling RA (2014) Amyloid and APOE e 4 interact to influence short-term decline in preclinical Alzheimer disease. Neurology 82, 1760–7.

[51] Desikan RS, McEvoy LK, Thompson WK, Holland D, Rddey JC, Blennow K, Aisen PS, Brewer JB, Hyman BT, Dale AM (2011) Amyloid-b associated volume loss occurs only in the presence of phospho-tau. Ann Neurol 70, 657–661.

[52] Fortea J, Vilaplana E, Alcolea D, Carmona-Iragui M, Sánchez-Saudinos M-B, Sala I, Antón-Aguirre S, González S, Medrano S, Pegueroles J, Morenas E, Clarimón J, Blesa R, Lleó A (2014) Cerebrospinal fluid β-amyloid and phospho-tau biomarker interactions affecting brain structure in preclinical Alzheimer disease. Ann Neurol 76, 223–30.

[53] Lee CYD, Tse W, Smith JD, Landreth GE (2012) Apolipoprotein E promotes ??-amyloid trafficking and degradation by modulating microglial cholesterol levels. J Biol Chem 287, 2032–2044.

[54] Suri S, Heise V, Trachtenberg AJ, Mackay CE (2013) The forgotten APOE allele: A review of the evidence and suggested mechanisms for the protective effect of APOE e2. Neurosci Biobehav Rev 37, 2878–2886.

[55] Klunk WE, Koeppe RA, Price JC, Benzinger TL, Devous MD, Jagust WJ, Johnson KA, Mathis CA, Minhas D, Pontecorvo MJ, Rowe CC, Skovronsky DM, Mintun MA (2015) The Centiloid Project: Standardizing quantitative amyloid plaque estimation by PET. Alzheimer's Dement 11, 1–15.e4.

Table 1: Number of subjects obtained from each cohort study in the AD and normal ageing dataset (n=1781).

Cohort Study	Clinical Diagnosis	Number of subjects (%)
ADNI (n=779)	Alzheimer's disease	177 (22.7%)
	Mild Cognitive Impairment	383 (49.2%)
	Healthy Controls	219 (28.1%)
AddNeuroMed (n=303)	Alzheimer's disease	109 (36.0%)
	Mild Cognitive Impairment	97 (32.0%)
	Healthy Controls	97 (32.0%)
AIBL (n=228)	Alzheimer's disease	46 (20.2%)
	Mild Cognitive Impairment	42 (18.4%)
	Healthy Controls	140 (61.4%)
BRC-AD (n=89)	Alzheimer's disease	33 (37.1%)
	Healthy Controls	56 (62.9%)
SN-ACK (n=382)	Healthy Controls	382 (100%)

Abbreviations: ADNI, Alzheimer's Disease Neuroimaging Initiative; AIBL, Australian Imaging, Biomarkers, and Lifestyles study; BRC-AD, Biomedical Research Centre for Dementia, King's College London; SN-ACK, Swedish National study on ageing and care in Kungsholmen.

Table 2: Demographic characteristics of 1) the AD and normal ageing dataset by subject group and 2) the IMAGEN study of healthy adolescents.

	ε2 carriers (*n*=344)	ε3 carriers (*n*=1754)	ε4 carriers (*n*=1070)	
	ε2/ε3 (n=326) ε2/ε2 (*n*=18)	ε3 Homozygotes	ε4/ε3 (*n*=893) ε4/ε4 (n=177)	*p*-value
1) AD and normal ageing dataset (n=1781)				
i) AD (n=375)				
Number of subjects (*n* (%)) †	17 (4.5)	125 (33.3)	223 (59.5)	--
Age (years)	**78.1 ± 6.6**	**76.9 ± 7.4**	**74.9 ± 6.7**	**0.016**
Male (*n* (%))	4 (23.5)	56 (44.8)	112 (50.2)	0.085
Education †	12.0 ± 3.6	11.8 ± 5.1	12.2 ± 4.5	0.847
MMSE	21.3 ± 5.8	22.1 ± 4.1	22.1 ± 3.7	0.734
ICV (mL)	1437 ± 165	1520 ± 166	1532 ± 188	0.110
ii) MCI (n=522)				
Number of subjects (*n* (%)) †	29 (5.6)	233 (44.6)	260 (49.8)	--
Age (years)	75.6 ± 7.1	75.3 ± 7.5	74.2 ± 6.9	0.186
Male (*n* (%))	15 (2.9)	144 (27.6)	152 (29.1)	0.508
MMSE	**27.6 ± 1.4**	**27.1 ±1.8**	**26.8 ± 1.8**	**0.016**
ICV (mL)	1491 ± 173	1558 ± 173	1559 ± 169	0.123
iii)CN individuals (n=512)				
Number of subjects (*n* (%))	66 (12.9)	275 (53.7)	171 (33.4)	--
Age (years)	75.8 ± 6.5	75.9 ± 6.3	75.6 ± 6.2	0.936
Male (*n* (%))	28 (5.5)	139 (27.1)	84 (16.4)	0.495
MMSE	28.9 ± 1.1	29.0 ± 1.1	29.1 ± 1.1	0.537
ICV (mL)	1506 ± 174	1521 ± 162	1518 ± 160	0.797
iv) SNACK (n=382)				
Number of subjects (*n* (%)) †	45 (11.8)	239 (62.6)	98 (25.7)	--
Age (years)	67.9 ± 7.8	70.1 ± 8.6	69.5 ± 8.6	0.269
Male (*n* (%))	15 (3.9)	102 (26.7)	37 (9.7)	0.420
MMSE	29.2 ± 0.9	29.2 ± 1.0	29.1 ± 1.1	0.365
ICV (mL)	1478 ± 265	1509 ± 248	1522 ± 275	0.649
2) IMAGEN (*n*=1387)				
Number of subjects (*n* (%)) †	187 (13.5)	882 (63.6)	318 (22.9)	--
Age (years)	14.4 ± 0.4	14.5 ± 0.4	14.5 ± 0.4	0.523
Male (*n* (%))	97 (7.0)	437 (31.5)	152 (11)	0.674
Body Mass Index (BMI)	20.6 ± 3.2	20.7 ± 3.6	20.8 ± 3.3	0.843
CANTAB SWM	31.3 ± 5.3	31.2 ± 5.5	31.0 ± 5.5	0.866
Verbal IQ	109.6 ± 15.7	111.6 ± 15.5	111.0 ± 14.9	0.258
Nonverbal IQ	106.5 ± 14.9	107.8 ± 14.4	107.7 ± 14.1	0.523
ICV (mL)	1472 ± 155	1487 ± 156	1490 ± 162	0.397

Abbreviations: MMSE, Mini Mental State Examination; ICV, Intracranial Volume; CANTAB SWM, Cambridge Neuropsychological Test Automated Battery [CANTAB] Spatial Working Memory; IQ, Intelligence Quotient.
Data are Mean ± SD. Percentages are displayed in parentheses.

Table 3: Hippocampal volume results by ApoE genotype in each subject group.

	ε2 carriers	ε3 Homozygotes	ε4 carriers	*p*-value	*t*-value (ε4 vs. ε2 carrier)	Pairwise Difference (ε2 > ε3 > ε4)
Alzheimer's disease (*n*=365)						
Left Hippocampus	2.00 (0.11; 1.77-2.22)	1.91 (0.04; 1.83-1.97)	1.80 (0.02; 1.75-1.84)	0.0001	-2.2	*ε4<ε3* = 0.0006; *ε4<ε2* = 0.07; *ε3<ε2* = 0.86
Right Hippocampus	2.04 (0.12; 1.80-2.29)	1.98 (0.04; 1.91-2.06)	1.81 (0.02; 1.77-1.86)	<0.0001	-2.3	*ε4<ε3* = <0.0001; *ε4<ε2* = 0.042; *ε3<ε2* = 0.99
Mild Cognitive Impairment (*n*=522)						
Left Hippocampus	2.22 (0.06; 2.09-2.35)	2.09 (0.03; 2.03-2.14)	1.97 (0.02; 1.93-2.02)	<0.0001	-3.4	*ε4<ε3* = 0.0004; *ε4<ε2* = 0.0015; *ε3<ε2* = 0.19
Right Hippocampus	2.27 (0.06; 2.14-2.39)	2.13 (0.03; 2.07-2.18)	2.01 (0.02; 1.97-2.05)	<0.0001	-3.3	*ε4<ε3* = <0.0001; *ε4<ε2* = 0.0019; *ε3<ε2* = 0.22
Healthy Controls (*n*=512)						
Left Hippocampus	2.40 (0.04; 2.32-2.47)	2.36 (0.02; 2.32-2.40)	2.30 (0.03; 2.25-2.36)	0.052	-1.9	*ε4<ε3* = 0.076; *ε4<ε2* = 0.367; *ε3<ε2* = 0.865
Right Hippocampus	2.43 (0.04; 2.35-2.51)	2.39 (0.02; 2.34-2.51)	2.33 (0.03; 2.27-2.39)	0.053	-2.0	*ε4<ε3* = 0.085; *ε4<ε2* = 0.115; *ε3<ε2* = 0.827
Population-based sample of non-demented elders: SNACK study (*n*=382)						
Left Hippocampus	2.72 (0.08; 2.56-2.87)	2.56 (0.03; 2.49-2.62)	2.56 (0.06; 2.45-2.67)	0.395	-1.9	*ε4<ε3* = 0.660; *ε4<ε2* = 0.367; *ε3<ε2* = 0.669
Right Hippocampus	2.66 (0.08; 2.50-2.82)	2.53 (0.03; 2.46-2.59)	2.53 (0.06; 2.42-2.64)	0.509	-2.0	*ε4<ε3* = 0.625; *ε4<ε2* = 0.530; *ε3<ε2* = 0.868
Healthy 14-year old adolescents: IMAGEN study (*n*=1387)						
Left Hippocampus	2.88 (0.02; 2.84-2.93)	2.86 (0.01; 2.84-2.88)	2.88 (0.02; 2.84-2.92)	0.972	-0.3	*ε4<ε3* = 0.714; *ε4<ε2* = 0.960; *ε3<ε2* = 0.611
Right Hippocampus	2.95 (0.02; 2.91-3.00)	2.91 (0.01; 2.89-2.93)	2.94 (0.02; 2.91-2.97)	0.751	-0.8	*ε4<ε3* = 0.399; *ε4<ε2* = 0.731; *ε3<ε2* = 0.136

Data are mean (SE; min-max). Mean values of normalised hippocampal volumes are reported.

Table 4: Hippocampal volume comparisons of ApoE ε4 carriers (ε4+) from different subject groups

	AD ε4+ group (*n*=223)	MCI ε4+ group (*n*=260)	healthy controls ε4+ group (*n*=171)	SNACK elderly ε4+ group (*n*=98)	*p*-value	Pairwise Difference (t-value; p-value)
	ε3/ε4 (*n*=159) ε4/ ε4 (*n*=64)	ε3/ε4 (*n*=203) ε4/ ε4 (*n*=57)	ε3/ε4 (*n*=151) ε4/ ε4 (*n*=20)	ε3/ε4 (*n*=84) ε4/ ε4 (*n*=14)		
Left Hippocampus	1.79 (0.02; 1.75-1.84)	1.97 (0.02; 1.93-2.02)	2.30 (0.03; 2.25-2.36)	2.56 (0.06; 2.45-2.67)	<.0001	AD vs. MCI= -5.7; <.001 AD vs. CTL= -14.0; <.001 AD vs. SNACK= -8.7; <.001 MCI vs. CTL= -9.0; <.001 MCI vs. SNACK = -6.3; <.001 SNACK vs. CTL= 1.9; .208
Right Hippocampus	1.81 (0.02; 1.77-1.86)	2.01 (0.02; 1.97-2.05)	2.33 (0.03; 2.27-2.39)	2.53 (0.06; 2.42-2.64)	<.0001	AD vs. MCI= -6.0; <.001 AD vs. CTL= -13.4; <.001 AD vs. SNACK= -7.9; <.001 MCI vs. CTL= -8.1; <.001 MCI vs. SNACK = -5.3; <.001 SNACK vs. CTL= 1.2; .579

Data are presented as the mean of normalised hippocampal volumes (Volume/ICV$^{\times 1000}$). SE with min-max is shown in parentheses.

Table 5: Hippocampal volume comparisons of ApoE ε2 carriers (ε2+) from different subject groups.

	AD ε2+ group (*n*=17)	MCI ε2+ group (*n*=29)	healthy controls ε2+ group (*n*=66)	SNACK elderly ε2+ group (*n*=45)	*p*-value	Pairwise Difference (t-value; p-value)
	ε3/ε2 (*n*=17) ε2/ε2 (*n*=0)	ε3/ε2 (*n*=29) ε2/ε2 (*n*=0)	ε3/ε2 (*n*=64) ε2/ε2 (*n*=2)	ε3/ε2 (*n*=42) ε2/ε2 (*n*=3)		
Left Hippocampus	2.00 (0.11; 1.77-2.22)	2.22 (0.06; 2.09-2.35)	2.40 (0.04; 2.32-2.47)	2.72 (0.08; 2.56-2.87)	.0003	AD vs. MCI= -2.1; .141 AD vs. CTL= -4.0; <.001 AD vs. SNACK= -3.6; .002 MCI vs. CTL= -1.9; .211 MCI vs. SNACK = -2.1; .137 SNACK vs. CTL= 1.0; .753
Right Hippocampus	2.04 (0.12; 1.80-2.29)	2.27 (0.06; 2.14-2.39)	2.43 (0.04; 2.35-2.51)	2.66 (0.08; 2.50-2.82)	.0035	AD vs. MCI= -2.1; .144 AD vs. CTL= -3.8; <.001 AD vs. SNACK= -2.1; .129 MCI vs. CTL= -1.5; .410 MCI vs. SNACK = -0.9; .796 SNACK vs. CTL= 0.2; .998

Table 6: Demographic characteristics of ε4 carriers from the ADNI and AIBL study divided into Aβ+ and Aβ- participants

	AD Aβ+	MCI Aβ+	MCI Aβ-	CN Aβ+	CN Aβ-	*p*-value
ADNI study (n=95)						
Number of subjects (*n* (%))	8 (8.4)	58 (61.1)	7 (7.4)	14 (14.7)	8 (8.4)	--
Age (years)	70.2 ± 7.3	72.5 ± 7.3	77.3 ± 4.9	77.1 ± 3.4	75.1 ± 4.0	0.041
Gender (Male/Female)	4/4	37/21	5/2	4/10	6/2	0.113
MMSE score	23 ± 1.7	27.2 ± 1.7	27.1 ± 1.9	29.4 ± 0.8	29.4 ± 0.9	<.001
ICV (mL)	1556 ± 210	1583 ± 198	1494 ± 176	1429 ± 98	1591 ± 209	0.08
AIBL study (n=57)						
Number of subjects (*n* (%))	7 (12.2)	1 (1.8)	3 (5.3)	20 (35.0)	26 (45.6)	--
Age (years)	77.7 ± 7.8	58 ± --	79.7 ± 12.o	78.1 ± 6.5	71.5 ± 5.8	0.001
Gender (Male/Female)	1/6	1/0	1/2	10/10	14/12	0.296
MMSE score	19.4 ± 3.8	27.0 ± .	27.7 ± 2.5	27.4 ± 3.1	27.2 ± 4.3	<.001
ICV (mL)	1466 ± 87	1515 ± --	1592 ± 301	1535 ± 159	1545 ± 165	0.781

Abbreviations: MMSE, Mini Mental State Examination, ICV, Intracranial Volume. Number of subjects (*n* (%)) corresponds to the number of participants in the respective group with percentage values in parentheses. Bolded values are significant at $p < 0.05$ or the $p < 0.001$ level. In the ADNI study, of the 95 subjects who underwent PET neuroimaging, 66 were scanned using ^{18}F-florbetapir and 29 using ^{11}C-Pittsburgh Compound B (PiB). In the AIBL study, all subjects underwent PET neuroimaging using ^{11}C-Pittsburgh Compound B (PiB).

Table 7: Hippocampal volume results in CN individuals, MCI subjects, and AD patient ε4 carriers by levels of Aβ deposition

	CN Aβ- (*n*=34)	CN Aβ+ (*n*=34)	MCI Aβ- (*n*=10) ¥	MCI Aβ+ (*n*=27) ¥	AD Aβ+ (*n*=15)	*p*-value	Pairwise Difference (*Cohen's d*; *p-value*) *(vs.CN Aβ- ε4+)*
Left Hippocampus	2.42 (.052)	2.39 (.053)	2.18 (.095)	1.97 (.04)	1.88 (.078)	<.0001	CN Aβ+ = -0.08; 0.692 MCI Aβ- = -0.42; <.0001 MCI Aβ+ = -1.26; <.0001 AD Aβ+ = -1.09; <.0001
Right Hippocampus	2.45 (.056)	2.44 (.058)	2.27 (.01)	1.94 (.043)	1.90 (.084)	<.0001	CN Aβ+ = -0.01; 0.946 MCI Aβ- = -0.29; 0.147 MCI Aβ+ = -1.26; <.0001 AD Aβ+ = -1.02; <.0001

Data are presented as the estimated marginal mean of normalised hippocampal volumes and SE in parentheses.
¥ MCI follow diagnosis was available for ADNI (0-36 months) and AIBL (0-54 months).

Figure 1

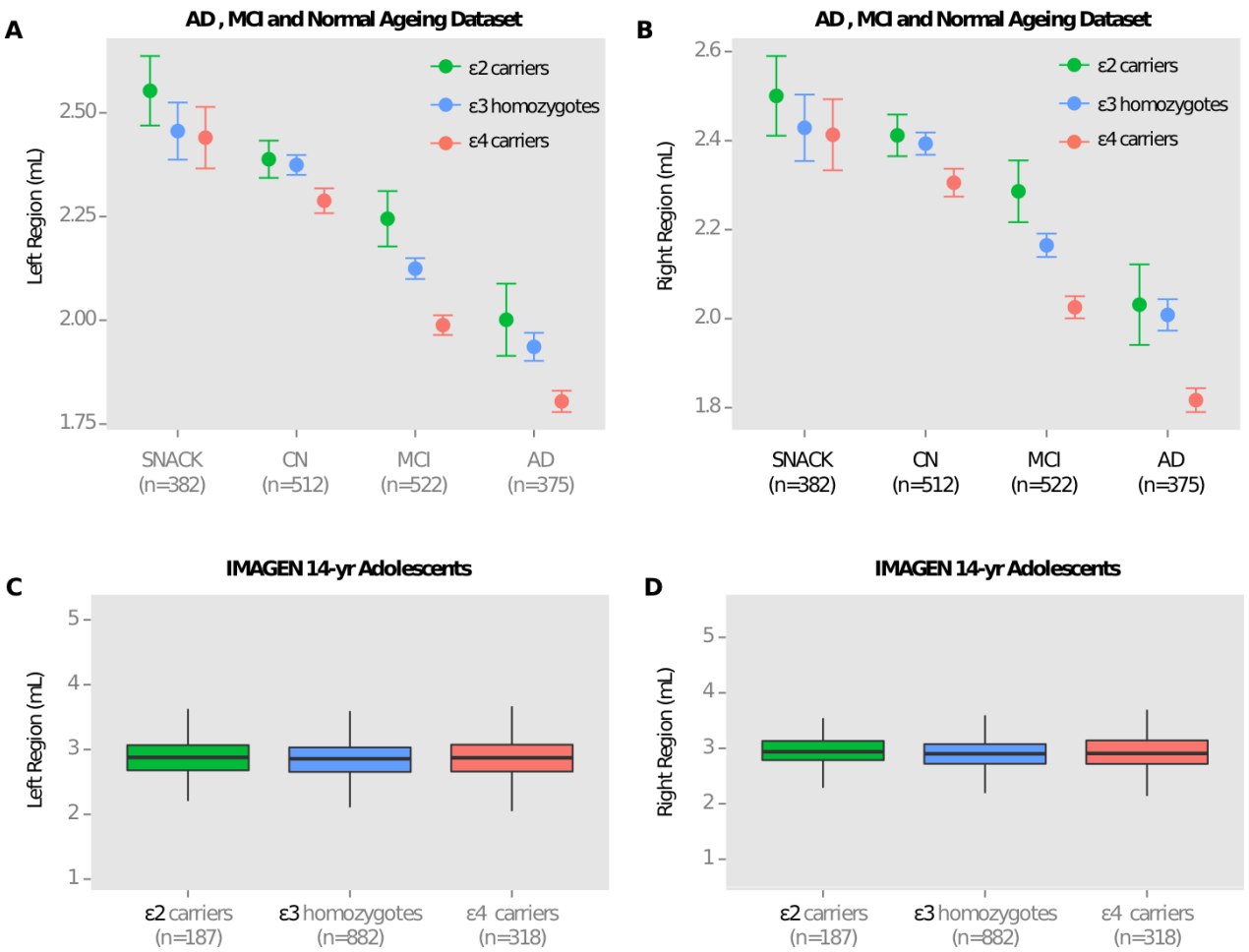

Figure 12 Hippocampal volumes and ApoE genotype in the AD and normal ageing dataset and IMAGEN study
Shown are hippocampal volumes from (a) the left and (b) the right region in the AD and normal ageing dataset by baseline diagnosis ApoE genotype (ε2 carriers, ε3 homozygotes, and ε4 carriers). Hippocampal volumes from (c) the left and (d) right region of healthy 14-year old adolescents in the IMAGEN study. SNACK indicates Swedish National study on Ageing and Care in Kungsholmen.

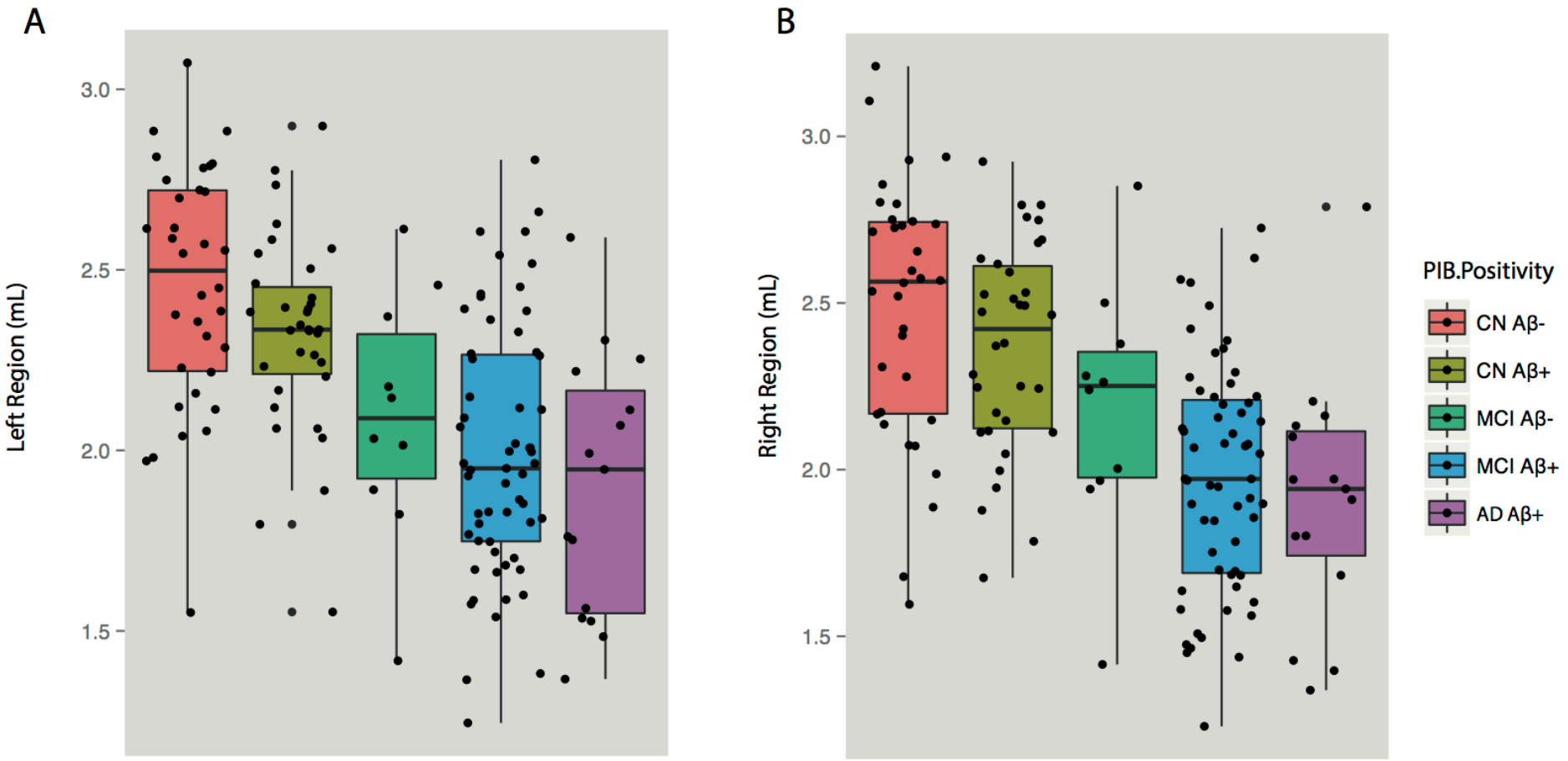

Figure 2: Hippocampal volumes of ε4 carriers by diagnosis and Aβ.

Data was used from the ADNI and AIBL cohorts for subjects that had available PET Aβ. MCI subjects were further divided by follow-up diagnosis in ADNI (0-36 months) and AIBL (0-54 months). Shown are baseline hippocampal volumes from **(a)** the left and **(b)** the right region. Note: There were no MCI-nc Aβ- ε4 carriers that converted to AD during the current follow-up period of the ADNI and AIBL studies. Aβ indicates β-amyloid; CN, cognitively normal; CN Aβ-, Aβ- negative CN group; CN Aβ+, Aβ positive CN group, MCI, Mild Cognitive Impairment; MCI Aβ-, Aβ negative MCI group, MCI-c, MCI non-converter; MCI-nc Aβ+, Aβ positive MCI-nc group, MCI-c, MCI-converter; MCI-c Aβ+, Aβ positive MCI-c group, AD, Alzheimer's disease; AD Aβ+, Aβ positive AD group.

CHAPTER 5: NO DIFFERENCES IN HIPPOCAMPAL VOLUME BETWEEN CARRIERS AND NON-CARRIERS OF THE APOE ε4 AND ε2 ALLELES IN YOUNG HEALTHY ADOLESCENTS

This chapter is presented as a published paper and is the exact copy of the following journal publication:

Khan W, Giampietro V, Ginestet C, Dell'Acqua F, Bouls D, Newhouse S, Dobson R, Banaschewski T, Barker GJ, Bokde ALW, Büchel C, Conrod P, Flor H, Frouin V, Garavan H, Gowland P, Heinz A, Ittermann B, Lemaître H, Nees F, Paus T, Pausova Z, Rietschel M, Smolka MN, Ströhle A, Gallinat J, Westman E, Schumann G, Lovestone S, Simmons A (2014) No differences in hippocampal volume between carriers and non-carriers of the ApoE e4 and e2 alleles in young healthy adolescents. *J Alzheimers Dis* 40, 37–43.

Author Contributions:

Study Concept and Design: Khan, Dobson, Westman, Simmons

Acquisition, Analysis and Interpretation of data: Khan, Muehlboeck, Westman, Simmons, Newhouse, Dobson, Barker

Drafting and Revision of Manuscript: All Authors

Statistical Analysis: Khan, Westman, Muehlboeck, Simmons

Journal of Alzheimer's Disease 40 (2014) 37–43
DOI 10.3233/JAD-131841
IOS Press

Short Communication

No Differences in Hippocampal Volume between Carriers and Non-Carriers of the ApoE ε4 and ε2 Alleles in Young Healthy Adolescents

Wasim Khan[a,b,c], Vincent Giampietro[a], Cedric Ginestet[a,b], Flavio Dell'Acqua[a,b,c], David Bouls[a,b,c], Steven Newhouse[a,b,c], Richard Dobson[a,b,c], Tobias Banaschewski[d,e], Gareth J. Barker[a], Arun L.W. Bokde[i], Christian Büchel[f], Patricia Conrod[a,h], Herta Flor[d,e], Vincent Frouin[o], Hugh Garavan[r,s], Penny Gowland[t], Anreas Heinz[h], Bernd Ittermann[j], Hervé Lemaître[k], Frauke Nees[d,e], Tomas Paus[l,m,n], Zdenka Pausova[q], Marcella Rietschel[d,e], Michael N. Smolka[p], Andreas Ströhle[h], Jean Gallinat[h], Eric Westman[u], Gunther Schumann[a,b], Simon Lovestone[a,b,c], Andrew Simmons[a,b,c,*] and the IMAGEN consortium (http://www.imagen-europe.com)

[a]*King's College London, Institute of Psychiatry, London, UK*
[b]*NIHR Biomedical Research Centre for Mental Health, King's College London, London, UK*
[c]*NIHR Biomedical Research Unit for Dementia, King's College London, London, UK*
[d]*Central Institute of Mental Health, Mannheim, Germany*
[e]*Medical Faculty Mannheim, University of Heidelberg, Heidelberg, Germany*
[f]*Universitaetsklinikum Hamburg Eppendorf, Hamburg, Germany*
[g]*Department of Psychiatry, Universite de Montreal, CHU Ste Justine Hospital, Montreal, Canada*
[h]*Department of Psychiatry and Psychotherapy, Campus Charité Mitte, Charité–Universitätsmedizin Berlin, Berlin, Germany*
[i]*Institute of Neuroscience and Discipline of Psychiatry, School of Medicine, Trinity College Dublin, Dublin, Ireland*
[j]*Physikalisch-Technische Bundesanstalt (PTB), Braunschweig und Berlin, Berlin, Germany*
[k]*Institut National de la Santé et de la Recherche Médicale, INSERM CEA Unit 1000 "Imaging & Psychiatry", University Paris Sud, Orsay, and AP-HP Department of Adolescent Psychopathology and Medicine, Maison de Solenn, University Paris Descartes, Paris, France*
[l]*Rotman Research Institute, University of Toronto, Toronto, Canada*
[m]*School of Psychology, University of Nottingham, Nottingham, UK*
[n]*Montreal Neurological Institute, McGill University, Montreal, Canada*
[o]*Neurospin, Commissariat à l'Energie Atomique et aux Energies Alternatives, Paris, France*
[p]*Neuroimaging Center, Department of Psychiatry and Psychotherapy, Technische Universität Dresden, Germany*
[q]*The Hospital for Sick Children, University of Toronto, Toronto, Canada*
[r]*Institute of Neuroscience, Trinity College Dublin, Dublin, Ireland*

*Correspondence to: Dr. Andrew Simmons, Department of Neuroimaging, Institute of Psychiatry, King's College London, De Crespigny Park, London SE5 8AF, UK. Tel.: +44 20 3228 3055; Fax: +44 20 3228 2116; E-mail: andy.simmons@kcl.ac.uk.

ISSN 1387-2877/14/$27.50

[s]*Departments of Psychiatry and Psychology, University of Vermont, Burlington, VT, USA*
[t]*School of Physics and Astronomy, University of Nottingham, Nottingham, UK*
[u]*Karolinska Institute, Stockholm, Sweden*

Accepted 28 October 2013

Abstract. Alleles of the apolipoprotein E (ApoE) gene are known to modulate the genetic risk for developing late-onset Alzheimer's disease (AD) and have been associated with hippocampal volume differences in AD. However, the effect of these alleles on hippocampal volume in younger subjects has yet to be clearly established. Using a large cohort of more than 1,400 adolescents, this study found no hippocampal volume or hippocampal asymmetry differences between carriers and non-carriers of the ApoE ε4 or ε2 alleles, nor dose-dependent effects of either allele, suggesting that regionally specific effects of these polymorphisms may only become apparent in later life.

Keywords: Apolipoprotein E, hippocampal volume, magnetic resonance imaging, young healthy adolescents

INTRODUCTION

The hippocampus has a key role in Alzheimer's disease (AD) and is among one of the first brain regions to show characteristic signs of neurofibrillary tangle pathology, which can be observed pre-symptomatically in adults as young as 20 years [1, 2]. Although hippocampal atrophy is commonly seen in AD, studies have also demonstrated lower hippocampal volumes in healthy older adults and amnestic mild cognitive impairment subjects (MCI) [3–6].

The presence of the apolipoprotein (ApoE) ε4 allele is a major genetic risk factor for the development of late onset AD [7–9], whereas possession of the ε2 allele has been suggested to confer a protective effect against the disease [10, 11]. Healthy adult carriers of the ApoE ε4 allele may be more vulnerable to degeneration of the hippocampus as they enter middle age [12, 13], and show altered patterns of brain activity in response to non-verbal stimuli [14]. A recent study has also demonstrated that homozygous ApoE ε4 carriers (ε4/ε4) may demonstrate wider patterns of cortical atrophy than heterozygous carriers (ε4/no ε4), thus suggesting a possible ε4 allele dose-dependent effect [15]. However, a small number of studies have failed to replicate these findings [12, 16], and others have conversely reported advantageous effects of the ApoE ε4 genotype in young individuals [17].

Less work has addressed the effect of ApoE polymorphisms in healthy children and adolescents, and the core aspects of neuronal development in these individuals are less clear. ApoE ε2 allele carriers stave off the effects of AD [18, 19], but whether properties of the ε2 allele could have a positive effect on neuronal development in adolescence remains largely unexplored. Using a cohort of 1,412 adolescents from the IMAGEN study, we examined the possibility that the ε4 and ε2 alleles may affect hippocampal volume in adolescents, and either render them at risk or protect them from future age-related neurodegeneration.

MATERIALS AND METHOD

Healthy adolescents were studied from the European multi-center neuroimaging-genetics IMAGEN project [20]. A total of 1,412 adolescents had ApoE genotype available.

MR images were acquired using 3T MRI systems from major MR manufacturers (Siemens, Philips, Bruker, and General Electric). A standardized imaging protocol was used to ensure homogeneity in data acquisition across different scanners. The protocol included a high resolution 3D T1-weighted ultrafast gradient echo volume (voxel size $1.1 \times 1.1 \times 1.1$ mm^3) and axial proton density T2-weighted fast spin echo images based on the ADNI study protocol (http://adni.loni.ucla.edu/). Full details have been previously reported [20]. Quality control was carried out using previously described criteria for scanner related phantom work and to ensure adequate quality control of the T1-weighted volume images such as avoidance of wraparound artefacts and minimal levels of subject motion [20–22]. The Freesurfer analysis pipeline (version 5.1.0) was used to produce left and right hippocampal volumes for each subject. Raw hippocampal volumes and hippocampal volumes normalized by their respective intracranial volumes were determined [23] as detailed in previous publications [24, 25].

Table 1
Demographic and cognitive characteristics of carriers and non-carriers of the APOE ε4 allele

	ApoE ε4 carriers ($n=343$)	ApoE ε4 non-carriers ($n=1069$)	t-value	p	ApoE ε2 carriers ($n=212$)	ApoE ε2 non-carriers ($n=1200$)	t-value	p
Age (years)	14.44 ± 0.40	14.45 ± 0.41	−0.104	0.917	14.41 ± 0.39	14.45 ± 0.41	−1.248	0.212
Gender (Male/Female)	169/174	534/535	–	0.852	114/98	589/611	–	0.233
BMI	20.86 ± 3.27	20.71 ± 3.56	0.673	0.501	20.72 ± 3.26	20.75 ± 3.53	−0.126	0.900
Verbal IQ	111.29 ± 14.84	111.29 ± 15.51	−0.003	0.997	110.26 ± 15.56	111.48 ± 15.31	−1.06	0.289
Performance IQ	107.84 ± 13.93	107.54 ± 14.47	0.336	0.737	106.89 ± 14.58	107.74 ± 14.30	−0.80	0.424
CANTAB SWM strategy	31.10 ± 5.41	31.22 ± 5.42	−0.336	0.737	31.36 ± 5.20	31.16 ± 5.46	0.490	0.367
Normalized R hippocampus*	4351.8 ± 436.9	4305.1 ± 474.4	–	0.289	4332.4 ± 504.9	4313.6 ± 458.8	–	0.103
Normalized L hippocampus*	4226.0 ± 504.1	4224.2 ± 475.3	–	0.406	4232.4 ± 518.2	4234.7 ± 476.3	–	0.357
Raw R hippocampus	4351.8 ± 436.9	4305.1 ± 474.4	–	0.074	4332.4 ± 504.9	4313.6 ± 458.8	–	0.893
Raw L hippocampus	4226.0 ± 504.1	4224.2 ± 475.3	–	0.111	4232.4 ± 518.2	4234.7 ± 476.3	–	0.564

Values represent Mean ± Standard Deviation. A p-value of 0.05 was considered significant for all tests. Continuous variables were inspected using parametric t-tests (t-value) and categorical variables were inspected using fisher exact tests. Hippocampal volume differences were examined using ANCOVA models which co-varied for age, gender, and site ID. *Normalized hippocampal volumes (Hippocampal volume/intracranial volume) were analyzed but raw hippocampal volumes are reported in mm^3. BMI, body mass index; Verbal IQ, verbal intelligence scale; Performance IQ, performance intelligence scale; CANTAB SWM strategy; spatial working memory task score.

Table 2
Dose-dependent effects of ApoE ε4 and ApoE ε2 allelic status on hippocampal volumes

	Right hippocampal volume (mm^3)	p	Left hippocampal volume (mm^3)	p
ApoE ε4 status				
ApoE ε4 allele = 0 ($n=1069$)	4305.0 ± 474.4	0.283	4224.2 ± 475.3	0.399
ApoE ε4 allele = 1 ($n=321$)	4351.2 ± 431.1	–	4226.4 ± 502.1	–
ApoE ε4 allele = 2 ($n=22$)	4360.9 ± 525.7	–	4260.2 ± 545.5	–
ApoE ε2 status				
ApoE ε2 allele = 0 ($n=1200$)	4313.6 ± 458.8	0.132	4234.7 ± 476.3	0.489
ApoE ε2 allele = 1 ($n=199$)	4343.1 ± 512.1	–	4247.0 ± 520.6	–
ApoE ε2 allele = 2 ($n=13$)	4168.4 ± 351.3	–	4008.2 ± 438.6	–

Values represent Mean ± standard deviation. Comparisons were made using ANCOVA, and models were adjusted for age, gender, and site ID.

Blood samples were collected for DNA analysis and extraction from each subject in the study. Samples were subsequently genotyped using the Illumina Quad 610 and 660 arrays (Illumina, San Diego, CA, USA) [20]. Two ApoE single nucleotide polymorphisms, rs429358 (T, C) and rs7412 (C, T), were used to identify 3 allelic variants of ApoE (ε2, ε3, and ε4) in order to define a subject's genotype.

The R statistical software environment, version 2.15.2, was used to perform all statistical analyses. To compare demographic statistics (age, gender, CANTAB SWM strategy scores, verbal and performance IQ), Fisher exact tests and two sample t-tests were conducted. A generalized linear model was used, adjusting for age and gender, to determine hippocampal volume differences between carriers and non-carriers of the ApoE ε4 and ε2 alleles and possible dose-dependent effects of each allele on hippocampal volume. Comparisons of the ApoE ε4 and ε2 alleles were also conducted using a previously described asymmetry index (AI) [26] for the hippocampus and were tested using one-way ANOVA.

RESULTS

Healthy adolescents possessing either the ApoE ε4 or ε2 alleles did not significantly differ in terms of demographics (Table 1). No hippocampal volume differences were observed between carriers and non-carriers of the ApoE ε4 allele (right hippocampus: $F=22.88$, $p=0.289$, left hippocampus: $F=18.9$, $p=0.406$) or the ε2 allele (right hippocampus: $F=23.42$, $p=0.103$, left hippocampus: $F=18.96$, $p=0.357$). These results were consistent when tests were repeated on raw hippocampal volumes (Table 1). No significant differences in the asymmetry index for the hippocampus were observed between ApoE ε4 carriers (AI = 2.23 ± 9.40) and non-carriers (AI = 1.90 ± 10.27) ($p=0.591$) and ApoE ε2 carriers (AI = 2.36 ± 11.01) and non-carriers (AI = 1.92 ± 9.89) ($p=0.547$). Furthermore, no evidence of a dose-dependent effect of ApoE ε4 or ε2 alleles on hippocampal volume and hippocampal asymmetry were established (Table 2). Direct comparisons of memory and IQ performance against both

ε2 and ε4 genotype did not produce any significant results.

DISCUSSION

In this study, a large cohort of young adolescents was used to compare the effects of different ApoE gene polymorphisms on hippocampal volume. Contrary to some recent studies [2, 13], no hippocampal volume differences were observed between carriers and non-carriers of the ApoE ε4 allele, a major genetic risk factor for the development of late-onset AD. Studies that have demonstrated an ApoE ε4 genotypic effect on structural brain phenotypes such as the hippocampus, entorhinal cortex, and other gray matter structures, have generally done so using older non-demented and healthy middle-aged individuals [27–32].

In healthy adults and elderly subjects, a normal asymmetry of the hippocampus exists with the right hippocampus larger than the left [33, 34]. Previous studies have suggested that alteration of asymmetry is associated with the ApoE ε4 genotype [26, 35] and is progressively reduced in AD patients possessing the ε4 allele [36]. In the current study, no differences in hippocampal asymmetry were found between carriers and non-carriers of the ApoE ε4 and ε2 alleles.

The possibility of a gene dose-dependent effect of ApoE ε4 was also investigated. Although the neuroanatomic effects of ApoE ε4 have been extensively studied [15, 37, 38], even less is known about the deleterious effects associated with the presence of two ε4 alleles in children and adolescents. However, direct comparisons of ε4 allele dosages in our cohort showed no differences in subject's hippocampal volumes, despite a previous study suggesting a linearly proportional rate of hippocampal atrophy to allele load [39].

One possible explanation for our findings are that ApoE ε4 genotype exerts a quiescent effect on the hippocampus, and as a result, neuroanatomic effects of the ε4 allele in this region may lie dormant in young adolescents and gradually become more salient in earlier adulthood. Evidence of this gradual effect can be seen in studies that observe early structural changes in volumes of gray matter [2, 40], as well as differences in white matter integrity [41, 42] among ε4 carriers aged 21 and above.

Prior studies comparing the effects of ApoE polymorphisms on brain imaging phenotypes have yielded equivocal findings; with some presenting no evidence of an ε4 genotypic effect on gray matter volumes [3, 43, 44], and others suggesting an antagonistic pleiotropic effect of the gene during neuronal development [45, 46]. Although a definitive conclusion has not been drawn, this could be due to differences in sample size, image pre-processing methods, and a lack of sample diversity or ethnic homogeneity.

Structural MRI studies have examined perinatal brain development in infants [47, 48] with ApoE ε4 found to predict reduced temporal cortex volumes. A confound of this study was that subjects were enriched for parents with psychiatric conditions, several of which are characterized by reduced hippocampal volume. Although such studies provide a better understanding of the perinatal effects associated with brain development, adolescence is also a period in which neurobiological changes may influence asynchronous brain maturation [49, 50].

Regional differences in hippocampal volume between ApoE ε2 carriers and non-carriers were not found. Hence no evidence of a ε2 protective effect was established. The putative protective effect of ApoE ε2 remains a matter of debate and has generated contradictory findings. Some volumetric MRI studies do not support a disease staving protective effect in healthy older subjects [51, 52], however, postmortem examinations have shown less AD-related neuropathological changes in ε2 carriers relative to ε3 homozygotes [53]. Only one study [19] was able to establish a protective effect of the ε2 variant.

Direct comparisons of memory and IQ performance against the ε4 genotype also did not produce any significant results. However, as only a single test of cognition from the CANTAB battery was assessed, we cannot definitively exclude the possibility of a ε4 genotypic effect on cognitive function. Nevertheless, the finding that ApoE ε4 allelic status does not relate to intelligence and cognitive function fits with previous studies reporting little or no effect of the ε4 allele on working memory and intellectual capacity [54, 55].

In summary, this study suggests that hippocampal volume differences associated with ApoE ε4 and ε2 are not evident in 14-year olds, and that neuroanatomic effects of these variants may only become apparent later in life.

ACKNOWLEDGMENTS

Support for this study was provided by the IMAGEN project, which receives research funding from the European Community's Sixth Framework Program (LSHM-CT-2007-037286) and coordinated project

ADAMS (242257), as well as the NIHR Biomedical Research Centre for Mental Health and NIHR Biomedical Research Unit for Dementia at South London and Maudsley NHS Foundation Trust and Institute of Psychiatry, King's College London, Alzheimer Research UK and the IMI funded European Medical Information Framework. GJB received honoraria for teaching during the course of this study and receives consultancy payments from IXICO.

Authors' disclosures available online (http://www.j-alz.com/disclosures/view.php?id=2007).

REFERENCES

[1] Ghebremedhin E, Schultz C, Braak E, Braak H (1998) High frequency of apolipoprotein E epsilon4 allele in young individuals with very mild Alzheimer's disease-related neurofibrillary changes. *Exp Neurol* **153**, 152-155.

[2] Alexopoulos P, Richter-Schmidinger T, Horn M, Maus S, Reichel M, Sidiropoulos C, Rhein C, Lewczuk P, Doerfler A, Kornhuber J (2011) Hippocampal volume differences between healthy young apolipoprotein E ε2 and ε4 carriers. *J Alzheimers Dis* **26**, 207-210.

[3] Jack CR, Petersen RC, Xu YC, O'Brien PC, Waring SC, Tangalos EG, Smith GE, Ivnik RJ, Thibodeau SN, Kokmen E (1998) Hippocampal atrophy and apolipoprotein E genotype are independently associated with Alzheimer's disease. *Ann Neurol* **43**, 303-310.

[4] Devanand DP, Pradhaban G, Liu X, Khandji A, De Santi S, Segal S, Rusinek H, Pelton GH, Honig LS, Mayeux R, Stern Y, Tabert MH, de Leon MJ (2007) Hippocampal and entorhinal atrophy in mild cognitive impairment: Prediction of Alzheimer disease. *Neurology* **68**, 828-836.

[5] Morra JH, Tu Z, Apostolova LG, Green AE, Avedissian C, Madsen SK, Parikshak N, Toga AW, Jack CR, Schuff N, Weiner MW, Thompson PM (2009) Automated mapping of hippocampal atrophy in 1-year repeat MRI data from 490 subjects with Alzheimer's disease, mild cognitive impairment, and elderly controls. *NeuroImage* **45**, S3-S15.

[6] Lehtovirta M, Soininen H, Laakso MP, Partanen K, Helisalmi S, Mannermaa A, Ryynänen M, Kuikka J, Hartikainen P, Riekkinen PJ (1996) SPECT and MRI analysis in Alzheimer's disease: Relation to apolipoprotein E epsilon 4 allele. *J Neurol Neurosurg Psychiatry* **60**, 644-649.

[7] Poirier J, Davignon J, Bouthillier D, Kogan S, Bertrand P, Gauthier S (1993) Apolipoprotein E polymorphism and Alzheimer's disease. *Lancet* **342**, 697-699.

[8] Saunders AM, Strittmatter WJ, Schmechel D, St. George-Hyslop PH, Pericak-Vance Ma, Joo SH, Rosi BL, Gusella JF, Crapper-MacLachlan DR, Alberts MJ, Hulette C, Crain B, Goldgaber D, Roses AD (1993) Association of apolipoprotein E allele 4 with late-onset familial and sporadic Alzheimer's disease. *Neurology* **43**, 1467-1472.

[9] Lehtovirta M, Laakso MP, Soininen H, Helisalmi S, Mannermaa A, Helkala EL, Partanen K, Ryynänen M, Vainio P, Hartikainen P (1995) Volumes of hippocampus, amygdala and frontal lobe in Alzheimer patients with different apolipoprotein E genotypes. *Neuroscience* **67**, 65-72.

[10] West HL, Rebeck GW, Hyman BT (1994) Frequency of the apolipoprotein E epsilon 2 allele is diminished in sporadic Alzheimer disease. *Neurosci Lett* **175**, 46-48.

[11] Qiu C, Kivipelto M, Aguero-Torres H, Winblad B, Fratiglioni L (2004) Risk and protective effects of the APOE gene towards Alzheimer's disease in the Kungsholmen project: Variation by age and sex. *J Neurol Neurosurg Psychiatry* **75**, 828-833.

[12] Reiman EM, Uecker A, Caselli RJ, Lewis S, Bandy D, De Leon MJ, De Santi S, Convit A, Osborne D, Weaver A, Thibodeau SN (1998) Hippocampal volumes in cognitively normal persons at genetic risk for Alzheimer's disease. *Ann Neurol* **44**, 288-291.

[13] O'Dwyer L, Lamberton F, Matura S, Tanner C, Scheibe M, Miller J, Rujescu D, Prvulovic D, Hampel H (2012) Reduced hippocampal volume in healthy young ApoE4 carriers: An MRI study. *PloS one* **7**, e48895.

[14] Bondi MW, Houston WS, Eyler LT, Brown GG (2005) fMRI evidence of compensatory mechanisms in older adults at genetic risk for Alzheimer disease. *Neurology* **64**, 501-508.

[15] Liu Y, Paajanen T, Westman E, Wahlund L-O, Simmons A, Tunnard C, Sobow T, Proitsi P, Powell J, Mecocci P, Tsolaki M, Vellas B, Muehlboeck S, Evans A, Spenger C, Lovestone S, Soininen H (2010) Effect of APOE ε4 allele on cortical thicknesses and volumes: The AddNeuroMed study. *J Alzheimers Dis* **21**, 947-966.

[16] Schmidt H, Schmidt R, Fazekas F, Semmler J, Kapeller P, Reinhart B, Kostner GM (1996) Apolipoprotein E e4 allele in the normal elderly: Neuropsychologic and brain MRI correlates. *Clin Genet* **50**, 293-299.

[17] Mondadori CRA, De Quervain DJ-F, Buchmann A, Mustovic H, Wollmer MA, Schmidt CF, Boesiger P, Hock C, Nitsch RM, Papassotiropoulos A, Henke K (2007) Better memory and neural efficiency in young apolipoprotein E epsilon4 carriers. *Cereb Cortex* **17**, 1934-1947.

[18] Liu Y, Paajanen T, Westman E, Zhang Y, Wahlund L-O, Simmons A, Tunnard C, Sobow T, Proitsi P, Powell J, Mecocci P, Tsolaki M, Vellas B, Muehlboeck S, Evans A, Spenger C, Lovestone S, Soininen H (2010) APOE ε2 allele is associated with larger regional cortical thicknesses and volumes. *Dement Geriatr Cogn Disord* **30**, 229-237.

[19] Shaw P, Lerch JP, Pruessner JC, Taylor KN, Rose a B, Greenstein D, Clasen L, Evans A, Rapoport JL, Giedd JN (2007) Cortical morphology in children and adolescents with different apolipoprotein E gene polymorphisms: An observational study. *Lancet Neurol* **6**, 494-500.

[20] Schumann G, Loth E, Banaschewski T, Barbot A, Barker G, Büchel C, Conrod PJ, Dalley JW, Flor H, Gallinat J, Garavan H, Heinz A, Itterman B, Lathrop M, Mallik C, Mann K, Martinot J-L, Paus T, Poline J-B, Robbins TW, Rietschel M, Reed L, Smolka M, Spanagel R, Speiser C, Stephens DN, Ströhle A, Struve M (2010) The IMAGEN study: Reinforcement-related behaviour in normal brain function and psychopathology. *Mol Psychiatry* **15**, 1128-1139.

[21] Simmons A, Westman E, Muehlboeck S, Mecocci P, Vellas B, Tsolaki M, Kłoszewska I, Wahlund L-O, Soininen H, Lovestone S, Evans A, Spenger C (2009) MRI measures of Alzheimer's disease and the AddNeuroMed study. *Ann N Y Acad Sci* **1180**, 47-55.

[22] Simmons A, Westman E, Muehlboeck S, Mecocci P, Vellas B, Tsolaki M, Kłoszewska I, Wahlund L-O, Soininen H, Lovestone S, Evans A, Spenger C (2011) The AddNeuroMed framework for multi-centre MRI assessment of Alzheimer's disease: Experience from the first 24 months. *Int J Geriatr Psychiatry* **26**, 75-82.

[23] Westman E, Aguilar C, Muehlboeck J-S, Simmons A (2013) Regional magnetic resonance imaging measures for

multivariate analysis in Alzheimer's disease and mild cognitive impairment. *Brain Topogr* **26**, 9-23.

[24] Westman E, Simmons A, Zhang Y, Muehlboeck J-S, Tunnard C, Liu Y, Collins L, Evans A, Mecocci P, Vellas B, Tsolaki M, Kłoszewska I, Soininen H, Lovestone S, Spenger C, Wahlund L-O (2011) Multivariate analysis of MRI data for Alzheimer's disease, mild cognitive impairment and healthy controls. *NeuroImage* **54**, 1178-1187.

[25] Westman E, Simmons A, Muehlboeck J-S, Mecocci P, Vellas B, Tsolaki M, Kłoszewska I, Soininen H, Weiner MW, Lovestone S, Spenger C, Wahlund L-O (2011) AddNeuroMed and ADNI: Similar patterns of Alzheimer's atrophy and automated MRI classification accuracy in Europe and North America. *NeuroImage* **58**, 818-828.

[26] Basso M, Gelernter J, Yang J, MacAvoy MG, Varma P, Bronen R a, van Dyck CH (2006) Apolipoprotein E epsilon4 is associated with atrophy of the amygdala in Alzheimer's disease. *Neurobiol Aging* **27**, 1416-1424.

[27] Braak H, Braak E (1991) Neuropathological stageing of Alzheimer-related changes. *Acta Neuropathol* **82**, 239-259.

[28] Barboriak DP, Doraiswamy PM, Krishnan KR, Vidyarthi S, Sylvester J, Charles HC (2000) Hippocampal sulcal cavities on MRI: Relationship to age and apolipoprotein E genotype. *Neurology* **54**, 2150-2153.

[29] Du a T (2001) Magnetic resonance imaging of the entorhinal cortex and hippocampus in mild cognitive impairment and Alzheimer's disease. *J Neurol Neurosurg Psychiatry* **71**, 441-447.

[30] Reiman E, Chen K, Alexander GE, Caselli RJ, Bandy D, Osborne D, Saunders AM, Hardy J (2004) Functional brain abnormalities in young adults at genetic risk for late-onset Alzheimer's dementia. *Proc Natl Acad Sci U S A* **101**, 284-289.

[31] Lind J, Larsson A, Persson J, Ingvar M, Nilsson L-G, Bäckman L, Adolfsson R, Cruts M, Sleegers K, Van Broeckhoven C, Nyberg L (2006) Reduced hippocampal volume in non-demented carriers of the apolipoprotein E epsilon4: Relation to chronological age and recognition memory. *Neurosci Lett* **396**, 23-27.

[32] Wishart HA, Saykin AJ, McAllister TW, Rabin LA, McDonald BC, Flashman LA, Roth RM, Mamourian AC, Tsongalis GJ, Rhodes CH (2006) Regional brain atrophy in cognitively intact adults with a single APOE epsilon4 allele. *Neurology* **67**, 1221-1224.

[33] Soininen H, Partanen K, Pitkanen A, Halliokainen M (1995) Decreased hippocampal volume asymmetry on MRIs in nondemented elderly subjects carrying the apolipoprotein E epsilon 4 allele. *Neurology* **45**, 391-392.

[34] Geroldi C, Laakso MP, Decarli C, Beltramello A, Bianchetti A, Soininen H, Trabucchi M, Frisoni GB (2000) Apolipoprotein E genotype and hippocampal asymmetry in Alzheimer's disease: A volumetric MRI study. *J Neurol Neurosurg Psychiatry* **68**, 93-96.

[35] Bigler ED, Tate DF, Miller MJ, Rice SA, Hessel CD, Earl HD, Tschanz JT, Plassman B, Welsh-Bohmer KA (2002) Dementia, asymmetry of temporal lobe structures, and apolipoprotein E genotype: Relationships to cerebral atrophy and neuropsychological impairment. *J Int Neuropsychol Soc* **8**, 925-933.

[36] Lu PH, Thompson PM, Leow A, Lee GJ, Lee A, Yanovsky I, Parikshak N, Khoo T, Wu S, Geschwind D, Bartzokis G (2011) Apolipoprotein E genotype is associated with temporal and hippocampal atrophy rates in healthy elderly adults: A tensor-based morphometry study. *J Alzheimers Dis* **23**, 433-442.

[37] Naiki H, Gejyo F, Nakakuki K (1997) Concentration-dependent inhibitory effects of apolipoprotein E on Alzheimer's beta-amyloid fibril formation *in vitro*. *Biochemistry* **36**, 6243-6250.

[38] Bales KR, Dodart JC, DeMattos RB, Holtzman DM, Paul SM (2002) Apolipoprotein E, amyloid, and Alzheimer disease. *Mol Interv 2* **339**, 363-375.

[39] Hostage CA, Roy Choudhury K, Doraiswamy PM, Petrella JR (2013) Dissecting the gene dose-effects of the APOE ε4 and ε2 alleles on hippocampal volumes in aging and Alzheimer's disease. *PloS one* **8**, e54483.

[40] Sidiropoulos C, Jafari-Khouzani K, Soltanian-Zadeh H, Mitsias P, Alexopoulos P, Richter-Schmidinger T, Reichel M, Lewczuk P, Doerfler A, Kornhuber J (2011) Influence of brain-derived neurotrophic factor and apolipoprotein E genetic variants on hemispheric and lateral ventricular volume of young healthy adults. *Acta Neuropsychiatr* **23**, 132-138.

[41] Madden DJ, Whiting WL, Huettel SA, White LE, MacFall JR, Provenzale JM (2004) Diffusion tensor imaging of adult age differences in cerebral white matter: Relation to response time. *NeuroImage* **21**, 1174-1181.

[42] Dowell NG, Ruest T, Evans SL, King SL, Tabet N, Tofts PS, Rusted JM (2013) MRI of carriers of the apolipoprotein E e4 allele-evidence for structural differences in normal-appearing brain tissue in e4+ relative to e4- young adults. *NMR Biomed* **26**, 674-682.

[43] Cherbuin N, Anstey KJ, Sachdev PS, Maller JJ, Meslin C, Mack HA, Wen W, Easteal S (2008) Total and regional gray matter volume is not related to APOE*E4 status in a community sample of middle-aged individuals. *J Gerontol A Biol Sci Med Sci* **63**, 501-504.

[44] Drzezga A, Grimmer T, Henriksen G, Mühlau M, Perneczky R, Miederer I, Praus C, Sorg C, Wohlschläger A, Riemenschneider M, Wester HJ, Foerstl H, Schwaiger M, Kurz A (2009) Effect of APOE genotype on amyloid plaque load and gray matter volume in Alzheimer disease. *Neurology* **72**, 1487-1494.

[45] Han SD, Bondi MW (2008) Revision of the apolipoprotein E compensatory mechanism recruitment hypothesis. *Alzheimers Dement* **4**, 251-254.

[46] Tuminello ER, Han SD (2011) The apolipoprotein E antagonistic pleiotropy hypothesis: Review and recommendations. *Int J Alzheimers Dis* **2011**, 726197.

[47] Huttenlocher PR, Dabholkar AS (1997) Regional differences in synaptogenesis in human cerebral cortex. *J Comp Neurol* **387**, 167-178.

[48] Knickmeyer RC, Gouttard S, Kang C, Evans D, Wilber K, Smith JK, Hamer RM, Lin W, Gerig G, Gilmore JH (2008) A structural MRI study of human brain development from birth to 2 years. *J Neurosci* **28**, 12176-12182.

[49] Paus T (2005) Mapping brain maturation and cognitive development during adolescence. *Trends Cogn Sci* **9**, 60-68.

[50] Paus T, Keshavan M, Giedd JN (2008) Why do many psychiatric disorders emerge during adolescence? *Nat Rev Neurosci* **9**, 947-957.

[51] Heijer T, Den, Oudkerk M, Launer L, van Duijn C, Hofman A, Breteler M (2002) Hippocampal, amygdalar, and global brain atrophy in different apolipoprotein E genotypes. *Neurology* **59**, 746-748.

[52] Serra-Grabulosa JM, Salgado-Pineda P, Junqué C, Solé-Padullés C, Moral P, López-Alomar A, López T, López-Guillén A, Bargalló N, Mercader JM, Clemente IC, Bartrés-Faz D (2003) Apolipoproteins E and C1 and brain morphology in memory impaired elders. *Neurogenetics* **4**, 141-146.

[53] Tiraboschi P, Hansen LA, Masliah E, Alford M, Thal LJ, Corey-Bloom J (2004) Impact of APOE genotype on

neuropathologic and neurochemical markers of Alzheimer disease. *Neurology* **62**, 1977-1983.

[54] Turic D, Fisher PJ, Plomin R, Owen MJ (2001) No association between apolipoprotein E polymorphisms and general cognitive ability in children. *Neurosci Lett* **299**, 97-100.

[55] Small BJ, Rosnick CB, Fratiglioni L, Bäckman L (2004) Apolipoprotein E and cognitive performance: A meta-analysis. *Psychol Aging* **19**, 592-600.

CHAPTER 6: TRACT BASED SPATIAL STATISTIC REVEALS NO DIFFERENCES IN WHITE MATTER MICROSTRUCTURAL ORGANIZATION BETWEEN CARRIERS AND NON-CARRIERS OF THE APOE Ɛ4 AND Ɛ2 ALLELES IN YOUNG HEALTHY ADOLESCENTS

This chapter is presented as a published paper and is the exact copy of the following journal publication:

Dell'Acqua F*, Khan W*, Gottlieb N, Giampietro V, Ginestet C, Bouls D, Newhouse S, Dobson R, Banaschewski T, Barker GJ, Bokde ALW, Büchel C, Conrod P, Flor H, Frouin V, Garavan H, Gowland P, Heinz A, Lemaítre H, Nees F, Paus T, Pausova Z, Rietschel M, Smolka MN, Ströhle A, Gallinat J, Westman E, Schumann G, Lovestone S, Simmons A (2015) Tract Based Spatial Statistic Reveals No Differences in White Matter Microstructural Organization between Carriers and Non-Carriers of the APOE ε4 and ε2 Alleles in Young Healthy Adolescents. *J Alzheimers Dis* 47, 977–984.

*These authors contributed equally to this work

Author Contributions:

Study Concept and Design: Khan, Westman, Simmons

Acquisition, Analysis and Interpretation of data: Khan, Muehlboeck, Westman, Simmons, Newhouse, Dobson, Barker

Drafting and Revision of Manuscript: All Authors

Statistical Analysis: Khan, Westman, Muehlboeck, Simmons

Journal of Alzheimer's Disease 47 (2015) 977–984
DOI 10.3233/JAD-140519
IOS Press

Tract Based Spatial Statistic Reveals No Differences in White Matter Microstructural Organization between Carriers and Non-Carriers of the APOE ε4 and ε2 Alleles in Young Healthy Adolescents

Flavio Dell'Acqua[a,b,c,1], Wasim Khan[a,b,c,1], Natalie Gottlieb[a,b,c], Vincent Giampietro[a], Cedric Ginestet[a,b], David Bouls[a,b,c], Steven Newhouse[a,b,c], Richard Dobson[a,b,c], Tobias Banaschewski[d,e], Gareth J. Barker[a], Arun L.W. Bokde[i], Christian Büchel[f], Patricia Conrod[a,g], Herta Flor[d,e], Vincent Frouin[n], Hugh Garavan[q,r], Penny Gowland[s], Anreas Heinz[h], Hervé Lemaítre[j], Frauke Nees[d,e], Tomas Paus[k,l,m], Zdenka Pausova[p], Marcella Rietschel[d,e], Michael N. Smolka[o,], Andreas Ströhle[h], Jean Gallinat[h], Eric Westman[t], Gunther Schumann[a,b], Simon Lovestone[a,b,c], Andrew Simmons[a,b,c,*] and the IMAGEN consortium (http://www.imagen-europe.com)

[a]*King's College London, Institute of Psychiatry, London, UK*
[b]*NIHR Biomedical Research Centre for Mental Health, King's College London, London, UK*
[c]*NIHR Biomedical Research Unit for Dementia, King's College London, London, UK*
[d]*Central Institute of Mental Health, Mannheim, Germany*
[e]*Medical Faculty Mannheim, University of Heidelberg, Germany*
[f]*Universitaetsklinikum Hamburg Eppendorf, Hamburg, Germany*
[g]*Department of Psychiatry, Universite de Montreal, CHU Ste Justine Hospital, Canada*
[h]*Department of Psychiatry and Psychotherapy, Campus Charité Mitte, Charité – Universitätsmedizin Berlin, Germany*
[i]*Institute of Neuroscience and Discipline of Psychiatry, School of Medicine, Trinity College Dublin, Dublin, Ireland*
[j]*Institut National de la Santé et de la Recherche Médicale, INSERM CEA Unit 1000 "Imaging & Psychiatry", University Paris Sud, Orsay, and AP-HP Department of Adolescent Psychopathology and Medicine, Maison de Solenn, University Paris Descartes, Paris, France*
[k]*Rotman Research Institute, University of Toronto, Toronto, Canada*
[l]*School of Psychology, University of Nottingham, Nottingham, UK*
[m]*Montreal Neurological Institute, McGill University, Montreal, Quebec, Canada*
[n]*Neurospin, Commissariat à l'Energie Atomique et aux Energies Alternatives, Paris, France*
[o]*Neuroimaging Center, Department of Psychiatry and Psychotherapy, Technische Universität Dresden, Germany*
[p]*The Hospital for Sick Children, University of Toronto, Toronto, Canada*
[q]*Institute of Neuroscience, Trinity College Dublin, Dublin, Ireland*
[r]*Departments of Psychiatry and Psychology, University of Vermont, Burlington, VT, USA*
[s]*School of Physics and Astronomy, University of Nottingham, Nottingham, UK*
[t]*Karolinska Institute, Stockholm, Sweden*

Handling Associate Editor: Maheen Adamson
Accepted 15 May 2015

[1]These authors contributed equally to this work.

*Correspondence to: Dr. Andrew Simmons, Department of Neuroimaging, Institute of Psychiatry, King's College London, De Crespigny Park, London SE5 8AF, UK. Tel.: +44 20 3228 3055; Fax: +44 20 3228 2116; E-mail: andy.simmons@kcl.ac.uk.

Abstract. The apolipoprotein E (APOE) $\varepsilon 4$ allele is the best established genetic risk factor for Alzheimer's disease (AD) and has been previously associated with alterations in structural gray matter and changes in functional brain activity in healthy middle-aged individuals and older non-demented subjects. In order to determine the neural mechanism by which APOE polymorphisms affect white matter (WM) structure, we investigated the diffusion characteristics of WM tracts in carriers and non-carriers of the APOE $\varepsilon 4$ and $\varepsilon 2$ alleles using an unbiased whole brain analysis technique (Tract Based Spatial Statistics) in a healthy young adolescent (14 years) cohort. A large sample of healthy young adolescents ($n = 575$) were selected from the European neuroimaging-genetics IMAGEN study with available APOE status and accompanying diffusion imaging data. MR Diffusion data was acquired on 3T systems using 32 diffusion-weighted (DW) directions and 4 non-DW volumes (b-value = 1,300 s/mm^2 and isotropic resolution of $2.4 \times 2.4 \times 2.4$ mm). No significant differences in WM structure were found in diffusion indices between carriers and non-carriers of the APOE $\varepsilon 4$ and $\varepsilon 2$ alleles, and dose-dependent effects of these variants were not established, suggesting that differences in WM structure are not modulated by the APOE polymorphism. In conclusion, our results suggest that microstructural properties of WM structure are not associated with the APOE $\varepsilon 4$ and $\varepsilon 2$ alleles in young adolescence, suggesting that the neural effects of these variants are not evident in 14-year-olds and may only develop later in life.

Keywords: Apolipoprotein E, diffusion tensor imaging, magnetic resonance imaging, tract based spatial statistics, young healthy adolescents

INTRODUCTION

The apolipoprotein E (APOE) gene is a low density glycoprotein which has a key metabolic role in facilitating the transport and delivery of lipids such as cholesterol from one cell type to another [1, 2]. A key understanding in its function beyond normal lipoprotein metabolism has led to the emergence of its role in modulating neuronal repair, brain plasticity, and axonal myelination. In particular, an isoform of APOE, APOE $\varepsilon 4$, has been associated with an increased risk of developing sporadic Alzheimer's disease (AD) [3–5], whereas the APOE $\varepsilon 2$ isoform has been suggested to confer a protective effect against the disease [6].

Neuroimaging studies of different APOE gene polymorphisms, particularly the APOE $\varepsilon 4$ allele, have provided evidence of its association with changes in gray matter structure in AD patients, subjects with mild cognitive impairment, and non-demented elderly controls [7–10]. A majority of these findings have shown that APOE $\varepsilon 4$ carriers reflect greater rates of atrophy in the hippocampus and entorhinal cortex—key regions known to be affected in early AD. Further, similar neuroanatomic effects of the APOE $\varepsilon 4$ allele have been observed in young healthy adults (20–35 years), suggesting that possession of the $\varepsilon 4$ allele may also be associated with a neural endophenotype that is more susceptible to age-related neurodegeneration in later life [11–13]. The emergence of these findings has led to an increased interest in exploring even earlier brain differences associated with the $\varepsilon 4$ allele. As a result, some have postulated that the neuroanatomic effect of the allele on brain phenotypes associated with AD risk could even precede birth [14].

Functional MRI studies performed in healthy adults both at rest and during a memory-encoding paradigm also reveal altered patterns of brain activation in healthy APOE $\varepsilon 4$ carrier subjects [15, 16]. However, findings on the functional effects of the APOE $\varepsilon 4$ allele are mixed, and evidence for both increased and decreased brain activation have been previously reported [17].

Diffusion tensor imaging (DTI) tractography is a technique that is being increasingly used to assess white matter (WM) changes in the brain by quantifying the microstructural density and orientation of axonal bundles connecting different regions of the brain [18, 19]. Understanding the neural mechanism by which the APOE polymorphism influences WM structure is crucial, particularly because APOE plays a major role in distributing essential lipids that contribute to the development of myelin sheath [20, 21].

Previous DTI studies of older healthy APOE $\varepsilon 4$ carriers, have found reduced fractional anisotropy (FA) in the splenium of the corpus collosum [22], the cingulum bundle [23, 24], and parahippocampal gyrus [25]. A recent study into younger APOE $\varepsilon 4$ carriers reported non-significant differences in WM structure, but found subtle differences within the prefrontal cortex between carriers and non-carriers [26]. Carriers of the APOE $\varepsilon 2$ allele are believed to have a decreased risk of developing AD [6], though the basis for this decreased vulnerability to the disease remains equivocal.

Myelination of intra-cortical fibers progresses gradually from birth to adulthood [27], and it is likely that asynchronous brain maturation processes during adolescence, particularly synaptic pruning and changes in axon caliber, may lead to a WM network that is more susceptible to structural damage in later life [28]. Using a large sample of young healthy adolescents from the European IMAGEN study, we assessed the diffusion characteristics of APOE $\varepsilon 4$, $\varepsilon 3$, and $\varepsilon 2$ carriers to determine if WM microstructure properties are modulated by the APOE polymorphism.

MATERIALS AND METHOD

Participants

Data analyzed for this study were obtained from healthy 14-year-olds from the IMAGEN project, a European multi-center neuroimaging-genetics study in adolescence. A total of 575 healthy adolescents were selected from the study with available diffusion imaging and APOE genotype data. Written informed consent was obtained from all participants and their legal guardians, further information on recruitment procedures has been previously provided [29]. Participants completed an extensive battery of neuropsychological, clinical, personality, and drug use assessments.

For each subject, blood samples were collected for DNA analysis and extraction. Samples were subsequently genotyped using the Illumina Quad 610 and 660 arrays (Illumina, San Diego, CA, USA). Two APOE single nucleotide polymorphisms, rs429358 (T, C) and rs7412 (C, T) were used to identify three allelic variants of APOE ($\varepsilon 2$, $\varepsilon 3$, and $\varepsilon 4$) in order to define a subject's genotype. Eight subjects with an APOE $\varepsilon 4$ and $\varepsilon 2$ genotype were excluded from the main analysis as previous studies have proposed an opposing neuroanatomic effect of the APOE $\varepsilon 4$ and $\varepsilon 2$ alleles. The demographic characteristics of our sample are described in Table 1.

Image acquisition

575 subjects (mean age 14.43 ± 0.47 years) from five imaging centers with compatible DTI acquisition protocols and with APOE genotype information available were selected. A standardized imaging protocol was used to ensure homogeneity in data acquisition across different scanners [29]. MR Diffusion data was acquired on 3T systems with the following parameters: TE = 104 ms, TR = 15000 ms, matrix size 128×128, number of slices = 60 and isotropic resolution of $2.4 \times 2.4 \times 2.4$ mm. Diffusion data was acquired with a b-value of 1300 s/mm^2 along 32 non-collinear diffusion gradient directions and 4 non-diffusion weighted volumes. More details are available in Schumann et al. [29].

Image analysis

Diffusion data was processed using ExploreDTI [30]. Data was first preprocessed to correct for eddy current distortions and head motion. For each subject the b-matrix was reoriented to provide a more accurate estimate of tensor orientations. Diffusion tensor was estimated using RESTORE [31] an automatic and iterative approach for the automatic rejection of data outliers. Finally, FA, mean diffusivity (MD), and axial and radial diffusivity maps were generated. Diffusion imaging data quality was assessed by automatically identifying outliers using residual maps of the tensor fitting and by visually inspecting each subject for major anatomical abnormalities (21 subjects were excluded from the analysis).

Voxel-wise statistical analysis on FA, MD, axial and radial diffusivity maps was carried out on the remaining 554 subjects using Tract-Based Spatial Statistics (TBSS) [32]. All subject's FA data were registered to the standard MNI space using a study specific template generated from 50 randomly selected subjects. To exclude low anisotropic regions, an FA threshold equal to 0.3 was selected to generate the FA skeleton. A more commonly used FA threshold of 0.2 was also applied to generate the WM skeleton, yet no significant effects of APOE genotype from the TBSS analysis were found. Consequently, we applied a FA threshold equal to 0.3 in order to restrict the analysis to more anisotropic regions with less significant inter-subject variability and partial volume effects with grey matter. In other words, we excluded peripheral tracts that we believe did not assume good tract correspondence and WM alignment across our subject sample.

Cognitive assessment

The Block Design and Matrix Reasoning subtests of the Wechsler Intelligence Scale for Children-Fourth Edition [33] were computed to generate a Perceptual Reasoning Index and assess nonverbal intelligence (nonverbal intelligence quotient, IQ). The Similarities and Vocabulary subtests were computed to generate a Verbal Comprehension Index measuring verbal

Table 1
Demographic and cognitive characteristics of APOE ε3 carriers, ε4 carriers and ε2 carriers from the IMAGEN study cohort

	ε3 carriers	ε4 carriers ($n=119$)		ε2 carriers ($n=55$)		
	ε3/ε3 ($n=372$)	ε3/ε4 ($n=114$)	ε4/ε4 ($n=5$)	ε2/ε3 ($n=53$)	ε2/ε2 ($n=2$)	p-value
Age (Years)	14.4 ± 0.5	14.4 ± 0.5	14.6 ± 0.5	14.4 ± 0.5	14.3 ± 0.1	0.975
Gender (Male/Female)	204/168	68/46	2/3	27/26	0/2	0.662
Handedness (Right/Left/Both)	321/46/5	106/8/0	4/1/0	48/4/1	2/0/0	0.477
Verbal IQ	114.0 ± 14.8	114.0 ± 14.7	116.8 ± 20.1	111.5 ± 14.1	125.5 ± 20.5	0.638
Nonverbal IQ	109.4 ± 13.5	110.4 ± 13.9	103.8 ± 8.3	109.5 ± 12.5	96.0 ± 5.7	0.821
CANTAB SWM	30.8 ± 5.4	30.7 ± 5.7	29.0 ± 6.0	30.1 ± 5.0	33.0 ± 4.2	0.727
Body mass index	20.6 ± 3.4	20.2 ± 2.5	21.0 ± 2.3	20.3 ± 3.2	17.3 ± 2.4	0.446
WISC Block Design	52.1 ± 8.0	52.5 ± 8.5	49.8 ± 5.0	51.7 ± 7.4	35.0 ± 5.7	0.598
WISC Matrix Reasoning	27.1 ± 3.7	27.4 ± 3.7	26.0 ± 5.2	27.4 ± 3.8	26.0 ± 1.4	0.790
WISC Similarities	31.3 ± 4.8	31.6 ± 5.0	33.0 ± 7.5	30.8 ± 4.2	33.5 ± 7.8	0.672
WISC Vocabulary	51.1 ± 7.5	51.1 ± 7.6	51.2 ± 9.4	49.9 ± 7.6	60.5 ± 5.0	0.726

Values represent Mean ± Standard Deviation. A p-value of 0.05 was considered significant for all tests. Continuous variables were inspected using analysis of variance (ANOVA) with *post-hoc* Bonferroni tests and categorical variables (Gender and Handedness) were inspected using fisher exact tests. All APOE ε4/ε2 allele carriers were excluded from the study. Verbal IQ, verbal intelligence scale; Nonverbal IQ, nonverbal intelligence scale; CANTAB SWM, CANTAB Spatial Working Memory; WISC, Wechsler Intelligence Scale for Children.

concept formation, that is, the subjects' ability to verbally reason (referred to as verbal IQ).

Statistical analysis

After quality control, 546 subjects from the IMAGEN cohort were used to perform non-parametric two sample *t-tests* (5000 permutations) using a generalized linear model on each diffusion index. Comparisons between carriers and non-carriers of the APOE ε4 and ε2 alleles were performed on the diffusion measures and differences between APOE ε4 and ε2 carriers were also investigated. Variables of gender, scan center, verbal and nonverbal IQ were included as covariates in the analysis. The R statistical software environment, version 3.1.0, was used to compare basic demographic statistics by APOE genotype [34].

RESULTS

Demographic characteristics

Healthy adolescents possessing either the APOE ε4 or ε2 alleles did not significantly differ in terms of demographics verbal IQ and nonverbal IQ in relation to APOE ε3/ε3 homozygote carriers. Furthermore, measures of cognitive functioning also did not significantly differ between the groups (Table 1).

Diffusion imaging TBSS

In the TBSS analysis, we firstly compared healthy adolescents with at least one APOE ε4 allele to non-carriers of the ε4 allele (ε3/ε3 homozygotes and ε3/ε2 carriers). The analysis revealed no significant differences between carriers and non-carriers of APOE ε4 for any index of diffusion (FA, MD, axial and radial diffusivity) at a p-value threshold of $\alpha = 0.05$. Similarly, no significant effect of the APOE ε2 genotype was found in ε2 carriers and non-carriers of the allele (ε3/ε3 homozygotes and ε3/ε4 carriers). Furthermore, comparisons between ε4 and ε2 carriers also yielded no significant findings in the TBSS analysis. Although our cohort had a small number of ε4 homozygote (ε4/ε4) carriers ($n=5$) and ε2 homozygote (ε2/ε2) carriers ($n=2$), there was no evidence to suggest any APOE ε4 or APOE ε2 dose-dependent effects on WM structure.

DISCUSSION

To our knowledge, this is the first study to investigate the diffusion characteristics of WM microstructure in relation to APOE ε4 and ε2 genotype in young healthy adolescents. Firstly, we investigated the neural effect of the APOE ε4 genotype on WM structure and TBSS analysis revealed no significant differences in diffusion indices including FA, MD, axial and radial diffusivity between ε4 carriers and non-carriers. Previously, we were able to show that no significant differences in hippocampal volume were present between APOE ε4 carriers and non-carriers in a wider group of these young subjects [35]. This finding, along with those from previous structural imaging studies in older adults, led us to postulate that WM changes could precede alterations in grey matter—possibly affecting key allocortical fiber pathways that may reflect APOE-driven vulnerabilities in the WM network. For instance, Heise and colleagues [36] were able to demonstrate that the APOE ε4 allele modulated the WM structure of young adult carriers despite no evidence of

changes in grey matter structure. Yet, diffusion-based imaging studies measuring regional patterns of WM changes in AD and older healthy subjects have reported mixed findings, with some providing support to the hypothesis of WM degeneration of later-myelinating fibers [37, 38] and others proposing WM damage to the medial temporal lobe and to prefrontal regions responsible for sustaining memory function [39, 40]. In particular, a number of DTI studies in AD patients and mild cognitive impairment subjects have reported reduced FA values in multiple regions, however, areas with more consistent findings include the hippocampal formation [39], parahippocampal gyrus [41], and the cingulum bundle [23, 42].

In contrast, healthy young adult APOE ε4 carriers studies have also shown reduced FA values in similar regions known to be affected in patients with AD [43, 44], with some in the absence of brain fibrillar amyloid plaque deposition [45]. Amyloid-β dysregulation is believed to begin several decades before memory impairment in sporadic AD. Many studies have since proposed that amyloid biomarkers are the first to become abnormal in the pathophysiological cascade of the disease. However, recent structural and functional studies have suggested that tau-mediated neurodegeneration may precede amyloid pathology in individuals possessing the APOE ε4 genotype [46, 47]. These findings in young adults have since prompted an increased interest to address brain changes associated with the APOE ε4 allele in infant brain development. In particular, Knickmeyer and colleagues [48] examined the effect of psychiatric risk variants, including APOE ε4 genotype, in prenatal brain development and discovered reduced temporal cortex volumes in ε4 carriers. However, as the authors of this study had acknowledged, the study sample was enriched to contain infants with a parental history of psychiatric and neurological illness. Building on the findings from this study, Dean and colleagues [49] compared measurements of WM and gray matter volume in typically-developing infants with no family history or AD or psychiatric illness. Specifically amongst APOE ε4 carriers, WM myelin content and gray matter volumes were reduced in the precuneus, lateral temporal and middle cingulate—regions of the cortex affected in late-onset AD. Despite the intriguing result, multiple regions were compared and most results did not survive multiple comparisons testing, and the number of ε4 carriers was substantially higher than the general population.

In adolescence, brain development represents a major transition in neurobiological processes which influence specific maturational changes in brain structure and function. These changes usually optimize the brain for underlying cognitive and behavioral changes that manifest at the time of puberty onset, but could also confer a neural vulnerability to certain forms of psychiatric illness later in life. It is therefore likely that dynamic stages of individual brain development, such as differences in the myelination of intra-cortical fibers [50], change in axon caliber [28], and synaptic density [27] could contribute to a variability in WM networks of adolescents. As a result, a decrease in statistical sensitivity could be attributed to one or some of these potential factors. Nonetheless, our finding that the APOE ε4 polymorphism does not modulate WM structure suggests that its effect is not detectable in young adolescence. Instead, a neuroanatomic effect of APOE ε4 allele may only become apparent in later adulthood, particularly when age-related changes in WM structure begin to gradually decline [51]. On the other hand, no genotypic effect of the APOE ε2 allele was found on any diffusion indices to suggest a protective effect on WM structure. To date, only one study, by Chiang and colleagues [52] found higher FA values in the posterior cingulate and anterior corpus collosum, suggesting those harboring an APOE ε2 genotype had more robust WM integrity, and consequently, decreased vulnerability to AD pathogenesis. In the past, several studies have proposed to explain the effects of this allele, including cellular models advocating its role in blocking the aggregation of amyloid β peptides [6, 53], and studies reporting thicker cortices in carrier groups [11, 54]. Yet, the neural mechanism of its putative protective effect still remains unclear.

Our findings should be noted in light of some limitations. Firstly, although TBBS, a localized statistical method, aims to alleviate problems in residual misalignment, partial gray matter volume contamination cannot be excluded, especially when the width of the tract is smaller than the original voxel size [32]. However, thresholding mean FA values between 0.2 and 0.3 on the WM skeleton has been known to successfully exclude voxels that are primarily grey matter or cerebrospinal fluid [55]. Although the procedures used here may be superior to standard registration procedures, the potential exists to apply more advanced methods that can better quantify the complexity of WM changes in the brain using full tensor information [56] and tract-specific indices of diffusion [57]. Given our observation of no APOE genotypic effect on WM structure, it would be interesting for future longitudinal studies to address when APOE modulated changes in the WM network begin to manifest and if they vary with age. Furthermore, since adolescence is a particularly

active neurodevelopmental period, we cannot exclude the possibility of a reduced APOE penetrance in this age. Nevertheless, previous studies in younger asymptomatic ε4 carriers have shown that APOE plays a fundamental role in modulating brain function in the absence of any differences in brain volume [16]. Future studies examining the pattern of brain activity both at rest and during a memory encoding paradigm in these individuals will help us understand if genotype-dependent changes in brain function manifest before structural differences.

Overall, this study demonstrated that individuals possessing the APOE ε4 and ε2 alleles do not have different WM microstructural properties at a young age (14 years). This suggests that WM structure in young adolescence is not modulated by the APOE polymorphism, but may reflect distinct genotype-dependent vulnerabilities in its structure later during adulthood.

ACKNOWLEDGMENTS

Support for this study was provided by the IMAGEN project, which receives research funding from the European Community's Sixth Framework Program (LSHM-CT-2007-037286) and coordinated project ADAMS (242257), as well as the NIHR Biomedical Research Centre for Mental Health and NIHR Biomedical Research Unit for Dementia at South London and Maudsley NHS Foundation Trust and Institute of Psychiatry, King's College London, Alzheimer Research UK and the IMI funded European Medical Information Framework. GJB received honoraria for teaching during the course of this study, and receives consultancy payments from IXICO.

Authors' disclosures available online (http://j-alz.com/manuscript-disclosures/14-0519r2).

REFERENCES

[1] Mahley RW, Rall SC (2000) Apolipoprotein E: Far more than a lipid transport protein. *Annu Rev Genomics Hum Genet* **1**, 507-537.

[2] Bales KR, Dodart JC, DeMattos RB, Holtzman DM, Paul SM (2002) Apolipoprotein E, amyloid, and Alzheimer disease. *Mol Interv* **2**, 339, 363-375.

[3] Poirier J, Davignon J, Bouthillier D, Kogan S, Bertrand P, Gauthier S (1993) Apolipoprotein E polymorphism and Alzheimer's disease. *Lancet* **342**, 697-699.

[4] Ghebremedhin E, Schultz C, Braak E, Braak H (1998) High frequency of apolipoprotein E epsilon4 allele in young individuals with very mild Alzheimer's disease-related neurofibrillary changes. *Exp Neurol* **153**, 152-155.

[5] Lehtovirta M, Laakso MP, Soininen H, Helisalmi S, Mannermaa A, Helkala EL, Partanen K, Ryynänen M, Vainio P, Hartikainen P (1995) Volumes of hippocampus, amygdala and frontal lobe in Alzheimer patients with different apolipoprotein E genotypes. *Neuroscience* **67**, 65-72.

[6] Qiu C, Kivipelto M, Aguero-Torres H, Winblad B, Fratiglioni L (2004) Risk and protective effects of the APOE gene towards Alzheimer's disease in the Kungsholmen project: Variation by age and sex. *J Neurol Neurosurg Psychiatry* **75**, 828-833.

[7] Jack CR, Petersen RC, Xu YC, O'Brien PC, Waring SC, Tangalos EG, Smith GE, Ivnik RJ, Thibodeau SN, Kokmen E (1998) Hippocampal atrophy and apolipoprotein E genotype are independently associated with Alzheimer's disease. *Ann Neurol* **43**, 303-310.

[8] Scarmeas N, Stern Y (2006) Imaging studies and APOE genotype in persons at risk for Alzheimer's disease. *Curr Psychiatry Rep* **8**, 11-17.

[9] Fleisher A, Grundman M, Jack CR, Petersen RC, Taylor C, Kim HT, Schiller DHB, Bagwell V, Sencakova D, Weiner MF, DeCarli C, DeKosky ST, van Dyck CH, Thal LJ (2005) Sex, apolipoprotein E epsilon 4 status, and hippocampal volume in mild cognitive impairment. *Arch Neurol* **62**, 953-957.

[10] Liu Y, Paajanen T, Westman E, Wahlund L-O, Simmons A, Tunnard C, Sobow T, Proitsi P, Powell J, Mecocci P, Tsolaki M, Vellas B, Muehlboeck S, Evans A, Spenger C, Lovestone S, Soininen H (2010) Effect of APOE ε4 allele on cortical thicknesses and volumes: The AddNeuroMed study. *J Alzheimers Dis* **21**, 947-966.

[11] Shaw P, Lerch JP, Pruessner JC, Taylor KN, Rose AB, Greenstein D, Clasen L, Evans A, Rapoport JL, Giedd JN (2007) Cortical morphology in children and adolescents with different apolipoprotein E gene polymorphisms: An observational study. *Lancet Neurol* **6**, 494-500.

[12] Alexopoulos P, Richter-Schmidinger T, Horn M, Maus S, Reichel M, Sidiropoulos C, Rhein C, Lewczuk P, Doerfler A, Kornhuber J (2011) Hippocampal volume differences between healthy young apolipoprotein E ε2 and ε4 carriers. *J Alzheimers Dis* **26**, 207-210.

[13] O'Dwyer L, Lamberton F, Matura S, Tanner C, Scheibe M, Miller J, Rujescu D, Prvulovic D, Hampel H (2012) Reduced hippocampal volume in healthy young ApoE4 carriers: An MRI study. *PLoS One* **7**, e48895.

[14] Knickmeyer RC, Gouttard S, Kang C, Evans D, Wilber K, Smith JK, Hamer RM, Lin W, Gerig G, Gilmore JH (2008) A structural MRI study of human brain development from birth to 2 years. *J Neurosci* **28**, 12176-12182.

[15] Bondi MW, Houston WS, Eyler LT, Brown GG (2005) fMRI evidence of compensatory mechanisms in older adults at genetic risk for Alzheimer disease. *Neurology* **64**, 501-508.

[16] Filippini N, MacIntosh BJ, Hough MG, Goodwin GM, Frisoni GB, Smith SM, Matthews PM, Beckmann CF, Mackay CE (2009) Distinct patterns of brain activity in young carriers of the APOE E4 allele. *Proc Natl Acad Sci U S A* **106**, 7209-7214.

[17] Mondadori CRA, De Quervain DJ-F, Buchmann A, Mustovic H, Wollmer MA, Schmidt CF, Boesiger P, Hock C, Nitsch RM, Papassotiropoulos A, Henke K (2007) Better memory and neural efficiency in young apolipoprotein E epsilon4 carriers. *Cereb Cortex* **17**, 1934-1947.

[18] Rose SE, Chen F, Chalk JB, Zelaya FO, Strugnell WE, Benson M, Semple J, Doddrell DM, Hospital A, Park D (2000) Loss of connectivity in Alzheimer's disease: An evaluation of white matter tract integrity with colour coded MR diffusion tensor imaging. *J Neurol Neurosurg Psychiatry* **69**, 528-530.

[19] Naggara O, Oppenheim C, Rieu D, Raoux N, Rodrigo S, Dalla Barba G, Meder J-F (2006) Diffusion tensor imaging in early Alzheimer's disease. *Psychiatry Res* **146**, 243-249.

[20] Mahley R (1988) Apolipoprotein E: Cholesterol transport protein with expanding role in cell biology. *Science* **240**, 622-630.
[21] Han X (2007) Potential mechanisms contributing to sulfatide depletion at the earliest clinically recognizable stage of Alzheimer's disease: A tale of shotgun lipidomics. *J Neurochem* **103**, 171-179.
[22] Bozzali M, Falini A, Franceschi M, Cercignani M, Zuffi M, Scotti G, Comi G, Filippi M (2002) White matter damage in Alzheimer's disease assessed *in vivo* using diffusion tensor magnetic resonance imaging. *J Neurol Neurosurg Psychiatry* **72**, 742-746.
[23] Choo IH, Lee DY, Oh JS, Lee JS, Lee DS, Song IC, Youn JC, Kim SG, Kim KW, Jhoo JH, Woo JI (2010) Posterior cingulate cortex atrophy and regional cingulum disruption in mild cognitive impairment and Alzheimer's disease. *Neurobiol Aging* **31**, 772-779.
[24] Felsky D, Voineskos A (2013) APOE ε4, aging, and effects on white matter across the adult life span. *JAMA Psychiatry* **70**, 646-647.
[25] Zhang Y, Schuff N, Jahng G-H, Bayne W, Mori S, Schad L, Mueller S, Du A-T, Kramer JH, Yaffe K, Chui H, Jagust WJ, Miller BL, Weiner MW (2007) Diffusion tensor imaging of cingulum fibers in mild cognitive impairment and Alzheimer disease. *Neurology* **68**, 13-19.
[26] O'Dwyer L, Lamberton F, Matura S, Scheibe M, Miller J, Rujescu D, Prvulovic D, Hampel H (2012) White matter differences between healthy young ApoE4 carriers and non-carriers identified with tractography and support vector machines. *PLoS One* **7**, e36024.
[27] Giedd JN, Blumenthal J, Jeffries NO, Castellanos FX, Liu H, Zijdenbos A, Paus T, Evans a C, Rapoport JL (1999) Brain development during childhood and adolescence: A longitudinal MRI study. *Nat Neurosci* **2**, 861-863.
[28] Paus T, Keshavan M, Giedd JN (2008) Why do many psychiatric disorders emerge during adolescence? *Nat Rev Neurosci* **9**, 947-957.
[29] Schumann G, Loth E, Banaschewski T, Barbot A, Barker G, Büchel C, Conrod PJ, Dalley JW, Flor H, Gallinat J, Garavan H, Heinz A, Itterman B, Lathrop M, Mallik C, Mann K, Martinot J-L, Paus T, Poline J-B, Robbins TW, Rietschel M, Reed L, Smolka M, Spanagel R, Speiser C, Stephens DN, Ströhle A, Struve M (2010) The IMAGEN study: Reinforcement-related behaviour in normal brain function and psychopathology. *Mol Psychiatry* **15**, 1128-1139.
[30] Leemans A, Jones DK (2009) The B-matrix must be rotated when correcting for subject motion in DTI data. *Magn Reson Med* **61**, 1336-1349.
[31] Chang L-C, Jones DK, Pierpaoli C (2005) RESTORE: Robust estimation of tensors by outlier rejection. *Magn Reson Med* **53**, 1088-1095.
[32] Smith SM, Jenkinson M, Johansen-Berg H, Rueckert D, Nichols TE, Mackay CE, Watkins KE, Ciccarelli O, Cader MZ, Matthews PM, Behrens TEJ (2006) Tract-based spatial statistics: Voxelwise analysis of multi-subject diffusion data. *Neuroimage* **31**, 1487-1505.
[33] Wechsler D (2003) The Wechsler Intelligence Scale for Children - Fourth Edition. Technical and Interpretive Manual, Psychological Association, San Antonio, TX, USA.
[34] R Development Core Team: A language and environment for statistical computing, R Foundation for Statistical Computing, 2009, Vienna, Austria.
[35] Khan W, Giampietro V, Ginestet C, Dell'acqua F, Bouls D, Newhouse S, Dobson R, Banaschewski T, Barker GJ, Bokde ALW, Büchel C, Conrod P, Flor H, Frouin V, Garavan H, Gowland P, Heinz A, Ittermann B, Lemaítre H, Nees F, Paus T, Pausova Z, Rietschel M, Smolka MN, Ströhle A, Gallinat J, Westman E, Schumann G, Lovestone S, Simmons A (2013) No differences in hippocampal volume between carriers and non-carriers of the ApoE ε4 and ε2 alleles in young healthy adolescents. *J Alzheimers Dis* **40**, 37-43.
[36] Heise V, Filippini N, Ebmeier KP, Mackay CE (2011) The APOE E4 allele modulates brain white matter integrity in healthy adults. *Mol Psychiatry* **16**, 1-9.
[37] Bartzokis G (2004) Age-related myelin breakdown: A developmental model of cognitive decline and Alzheimer's disease. *Neurobiol Aging* **25**, 5-18.
[38] Stricker NH, Schweinsburg BC, Delano-Wood L, Wierenga CE, Bangen KJ, Haaland KY, Frank LR, Salmon DP, Bondi MW (2009) Decreased white matter integrity in late-myelinating fiber pathways in Alzheimer's disease supports retrogenesis. *Neuroimage* **45**, 10-16.
[39] Salat DH, Tuch DS, van der Kouwe a JW, Greve DN, Pappu V, Lee SY, Hevelone ND, Zaleta a K, Growdon JH, Corkin S, Fischl B, Rosas HD (2010) White matter pathology isolates the hippocampal formation in Alzheimer's disease. *Neurobiol Aging* **31**, 244-256.
[40] Wee C-Y, Yap P-T, Li W, Denny K, Browndyke JN, Potter GG, Welsh-Bohmer KA, Wang L, Shen D (2011) Enriched white matter connectivity networks for accurate identification of MCI patients. *Neuroimage* **54**, 1812-1822.
[41] Buckner RL, Sepulcre J, Talukdar T, Krienen FM, Liu H, Hedden T, Andrews-Hanna JR, Sperling RA, Johnson KA (2009) Cortical hubs revealed by intrinsic functional connectivity: Mapping, assessment of stability, and relation to Alzheimer's disease. *J Neurosci* **29**, 1860-1873.
[42] Bozzali M, Giulietti G, Basile B, Serra L, Spanò B, Perri R, Giubilei F, Marra C, Caltagirone C, Cercignani M (2012) Damage to the cingulum contributes to Alzheimer's disease pathophysiology by deafferentation mechanism. *Hum Brain Mapp* **33**, 1295-1308.
[43] Nierenberg J, Pomara N, Hoptman MJ, Sidtis JJ, Ardekani BA, Lim KO (2005) Abnormal white matter integrity in healthy apolipoprotein E epsilon4 carriers. *Neuroreport* **16**, 1369-1372.
[44] Persson J, Lind J, Larsson A, Ingvar M, Cruts M, Van Broeckhoven C, Adolfsson R, Nilsson L-G, Nyberg L (2006) Altered brain white matter integrity in healthy carriers of the APOE e4 allele: A risk for AD? *Neurology* **66**, 1029-1033.
[45] Racine AM, Adluru N, Alexander AL, Christian BT, Okonkwo OC, Oh J, Cleary C, Birdsill A, Hillmer A, Murali AT, Barnhart D, Gallagher TE, Carlsson CL, Rowley CMH, Dowling A, Asthana NM, Sager SM, Bendlin A, Johnson BBSC (2014) Associations between white matter microstructure and amyloid burden in preclinical Alzheimer's disease: A multimodal imaging investigation. *Neuroimage Clin* **4**, 604-614.
[46] Sheline YI, Morris JC, Snyder AZ, Price JL, Yan Z, D'Angelo G, Liu C, Dixit S, Benzinger T, Fagan A, Goate A, Mintun MA (2010) APOE4 allele disrupts resting state fMRI connectivity in the absence of amyloid plaques or decreased CSF Aβ42. *J Neurosci* **30**, 17035-17040.
[47] Crivello F, Lemaítre H, Dufouil C, Grassiot B, Delcroix N, Tzourio-Mazoyer N, Tzourio C, Mazoyer B (2010) Effects of ApoE-epsilon4 allele load and age on the rates of grey matter and hippocampal volumes loss in a longitudinal cohort of 1186 healthy elderly persons. *Neuroimage* **53**, 1064-1069.
[48] Knickmeyer RC, Wang J, Zhu H, Geng X, Woolson S, Hamer RM, Konneker T, Lin W, Styner M, Gilmore JH (2014) Common variants in psychiatric risk genes predict brain structure at birth. *Cereb Cortex* **24**, 1230-1246.

[49] Dean DC, Jerskey B, Chen K, Protas H, Thiyyagura P, Roontiva A, O'Muircheartaigh J, Dirks H, Waskiewicz N, Lehman K, Siniard AL, Turk MN, Hua X, Madsen SK, Thompson PM, Fleisher AS, Huentelman MJ, Deoni SCL, Reiman EM (2014) Brain differences in infants at differential genetic risk for late-onset Alzheimer disease: A cross-sectional imaging study. *JAMA Neurol* **71**, 11-22.

[50] Perrin JS, Hervé P-Y, Leonard G, Perron M, Pike GB, Pitiot A, Richer L, Veillette S, Pausova Z, Paus T (2008) Growth of white matter in the adolescent brain: Role of testosterone and androgen receptor. *J Neurosci* **28**, 9519-9524.

[51] Gogtay N, Giedd JN, Lusk L, Hayashi KM, Greenstein D, Vaituzis a C, Nugent TF, Herman DH, Clasen LS, Toga AW, Rapoport JL, Thompson PM (2004) Dynamic mapping of human cortical development during childhood through early adulthood. *Proc Natl Acad Sci U S A* **101**, 8174-8179.

[52] Chiang GC, Zhan W, Schuff N, Weiner MW (2012) White matter alterations in cognitively normal apoE ε2 carriers: Insight into Alzheimer resistance? *AJNR Am J Neuroradiol* **33**, 1392-1397.

[53] Jiang Q, Lee CYD, Mandrekar S, Wilkinson B, Cramer P, Zelcer N, Mann K, Lamb B, Willson TM, Collins JL, Richardson JC, Smith JD, Comery TA, Riddell D, Holtzman DM, Tontonoz P, Landreth GE (2008) ApoE promotes the proteolytic degradation of Abeta. *Neuron* **58**, 681-693.

[54] Liu Y, Paajanen T, Westman E, Zhang Y, Wahlund L-O, Simmons A, Tunnard C, Sobow T, Proitsi P, Powell J, Mecocci P, Tsolaki M, Vellas B, Muehlboeck S, Evans A, Spenger C, Lovestone S, Soininen H (2010) APOE ε2 allele is associated with larger regional cortical thicknesses and volumes. *Dement Geriatr Cogn Disord* **30**, 229-237.

[55] Smith SM, Johansen-Berg H, Jenkinson M, Rueckert D, Nichols TE, Miller KL, Robson MD, Jones DK, Klein JC, Bartsch AJ, Behrens TEJ (2007) Acquisition and voxelwise analysis of multi-subject diffusion data with tract-based spatial statistics. *Nat Protoc* **2**, 499-503.

[56] Park H, Kubicki m, Shenton M, Guimond A, McCarley R, Maier S, Kikinis R (2003) Spatial normalization of diffusion tensor MRI using multiple channels. *Neuroimage* **20**, 1995-2009.

[57] Dell'Acqua F, Simmons A, Williams SCR, Catani M (2013) Can spherical deconvolution provide more information than fiber orientations? Hindrance modulated orientational anisotropy, a true-tract specific index to characterize white matter diffusion. *Hum Brain Mapp* **34**, 2464-2483.

CHAPTER 7: DISTINCT FUNCTIONAL PROPERTIES OF THE POSTEROMEDIAL CORTEX REVEAL ABERRANT FUNCTIONAL CONNECTIVITY PATTERNS IN ALZHEIMER'S DISEASE: MORE THAN JUST THE DEFAULT-MODE

This chapter has been written as a traditional thesis chapter

ABSTRACT

The posteromedial cortex (PMC), a highly metabolically active region anchored in the default-mode network (DMN), is understood to share a complex functional architecture with the rest of the brain. Recent functional imaging studies have shown that the region is not functionally homogeneous, but shares a complex and dynamic pattern of activity with multiple intrinsically stable networks. However, to date, there have been no attempts to characterise its functional neuroanatomy and selective vulnerability to Alzheimer's disease (AD) pathophysiology. Using clinical phenotyping and metadata, I report a resting-state functional magnetic resonance imaging study in the Alzheimer's Disease Neuroimaging Initiative (ADNI) dataset, to characterise a pattern of PMC functional heterogeneity with the rest of the brain. The PMC subdivisions were found to be consistent with previous anatomical studies in the monkey brain and functional imaging studies of the human PMC. The main findings were (i) AD patients demonstrated hyperconnectivity of the dorsal posterior cingulate region with the DMN compared to cognitively normal (CN) individuals, (ii) there was a connectivity failure of the retrosplenial cortex supporting memory and cognition, and a frontal hyperconnectivity burden in AD patients, and (iii) MCI subjects that converted to AD at a two year follow-up displayed similar PMC functional connectivity cascades to AD patients. Aberrant patterns of hypoconnectivity and hyperconnectivity in PMC cortical systems support the view that AD is a disconnected syndrome. These results provide evidence of a systems-level pathophysiology of PMC functional circuits and highlight its selective vulnerability to AD pathogenesis.

INTRODUCTION

Blood-oxygen level dependent (BOLD) functional MRI (fMRI) is an indirect measure of neuronal activity, believed to reflect the integrated synaptic activity of neuronal firing via MR signal changes due to changes in blood flow, blood volume, and the blood oxyhaemoglobin/deoxyhaemoglobin ratio [1–3]. Recently, considerable interest has been focused on the intrinsic functional connectivity of large-scale brain networks at rest, often referred to as resting-state fMRI (rsfMRI). These techniques evaluate the correlation between intrinsic oscillations or timecourse of the BOLD signal between brain regions, and have revealed several large-scale brain networks demonstrating functional coherence in the spontaneous activity of distributed nodes [4,5].

Both anatomical lesion studies and functional imaging evidence has demonstrated that higher-level memory and cognitive processes are subserved by a heteromodal network of brain regions collectively known as the Default-Mode Network (DMN) [6,7]. Anatomically, the DMN consists of prominent nodes in the posterior cingulate cortex (PCC), ventromedial prefrontal cortex (VMPFC), retrosplenial cortex (RSC), angular gyrus, and medial temporal lobe (MTL) structures [6,8]. Initially, fMRI studies using explicit task paradigms demonstrated high DMN activity during episodic and autobiographical memory retrieval but decreased activity during the performance of cognitive tasks that demand attention to external stimuli [9,10].

Earlier rsfMRI studies in the AD literature that have evaluated connectivity changes in the DMN have shown evidence of aberrant disruptions in AD patients and MCI subjects with prodromal stages of the disease [7,11–14]. Since that time, a consistent failure to modulate the activity of the DMN has been reported in AD patients and those at-risk of developing the disease [15,16]. Furthermore, converging evidence on the DMN points towards a pathological predilection to AD pathophysiology. For instance, the structures that are particularly vulnerable to Aβ pathology and tau neurodegeneration also appear to spatially overlap with the heteromodal cortices of the DMN [8]. This suggests that the functional integrity of this system may be is particularly important for characterising the cascading disruptions during different stages of AD that impart cognitive and clinical symptomology. However, the DMN is not only associated

with memory, but has also been linked to several other non-memory systems (language, visuospatial, attentional, and executive systems) [17].

A seminal study by Andrews-Hanna and colleagues [18] showed that the DMN could be topographically divided into subsystems each serving discrete functional roles. The DMN was segregated into three core subsystems: comprised of: (1) a midline core system, containing the PCC, and anterior medial prefrontal cortex (aMPFC), (2) a MTL system and (3) a dorsal medial prefrontal cortex (dMPFC) system. Previous work has shown that the pattern of connectivity changes differs between these subsystem regions, with decreased connectivity in the PCC and MTL, and increases in the medial frontal regions in AD [15]. Further functional brain parcellation methods identified several subsystems within one module that encompassed all the subsystems identified by Andrews-Hanna et al, termed the task-negative network. This included the ventral DMN (vDMN), posterior DMN (pDMN), anterior-ventral DMN (avDMN), and the anterior-dorsal DMN (adDMN) [16,19]. Recent investigations of these subsystems have observed a posterior-anterior DMN dissociation, characterised by a global decline in pDMN connectivity and the hyperconnectivity of the anterior portions of the DMN (adDMN and avDMN) in AD patients compared to controls [20].

However, recent evidence has suggested that AD is characterised by a functionally complex and dynamic failure of several large intrinsic networks other than the functional circuitry of the DMN. For example, other cognitive and attentional networks such as the salience and central executive networks have been found to play crucial roles in feeding information processing to the DMN, as well as in modulating its activity [21,22]. Interestingly, the PMC, which is anchored in the DMN, represents a critical hub of the brain and shares a complex functional organisation with the rest of the cortex. This current work addresses this open question regarding the functional architecture of the PMC and how it may provide new insights into the aberrant organisation of brain systems in AD pathogenesis.

Posteromedial Cortex Anatomy

The PMC is an architectonically discrete region which lies dorsal to the corpus callosum and largely consists of Brodmann areas 23, 29, 30, 31 and 7m. Specifically, this includes the PCC areas 23a, 23b, and 23c, the retrosplenial areas 29 and 30, the mesial parietal area 7m in the precuneal region, and area 31, which is situated between the PCC area 23c, and the medial parietal area 7m (Figure 1). Originally, Brodmann [23] proposed the anterior and posterior boundaries in both the PCC and precuneus regions. More recently, Vogt [24,25] has proposed further subdivisions to illustrate the cytoarchitectural differences between the PCC, precuneus and RSC regions. Here, we primarily employ the cytoarchitectonic map proposed by Vogt and subdivisions identified by previous resting-state studies [26,27] to characterise the major subdivisions of the PMC.

Recent work has highlighted that the PMC shares a differential functional properties with the rest of brain, with discrete regions that participate in distinct functional networks (Figure 2) [26]. Within the PMC, the PCC also displays considerable functional heterogeneity where activity 'echoes' of multiple other brain networks are observed in separate, yet spatially overlapping regions [27] (Figure 3).

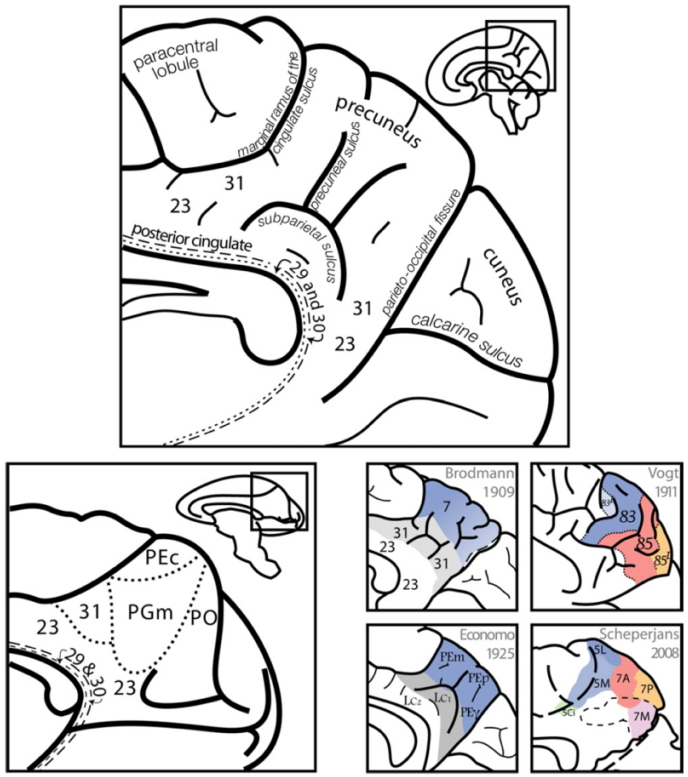

Figure 13 Illustration of the basic anatomy of the posteromedial cortex and connectivity based on the work of Margulies and colleagues.

(Top) Schematic diagram illustrating the human PMC, including the precuneus, PCC (area 23), RSC (areas 29 and 30) in the posterior callosal sulcus, and the transitional zone (area 31) that separates the precuneus from the cingulate cortex. Bottom left illustrates the cytoarchitectonic divisions of the PMC along the parieto-occipital fissure in the macaque monkey. Bottom right shows PMC derived from anatomical connectivity studies. Architectonic anatomical maps and their proposed subdivisions in the human PMC. Adapted from Margulies et al [26].

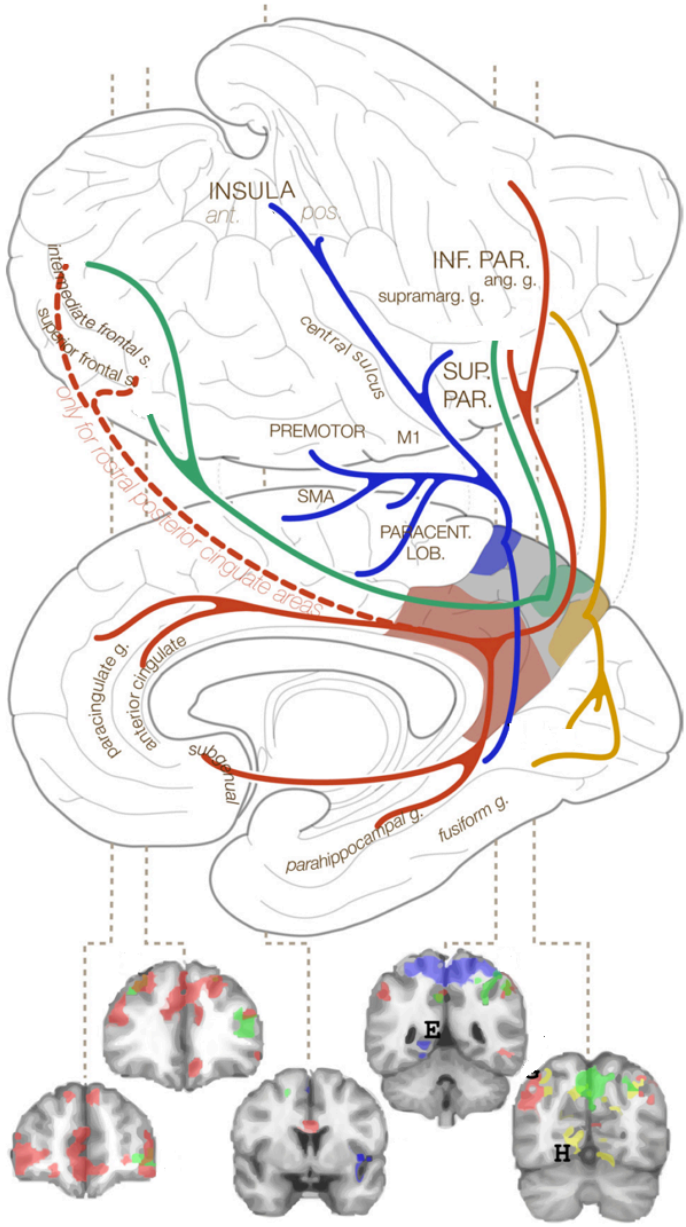

Figure 14: Functional specialisation of the Precuneus

This illustration provides a clear summary of the functional connectivity patterns emerging from the three subdivisions of the precuneus identified by Margulies et al [26]. In blue, the anterior zone along the marginal ramus of the cingulate sulcus displays connectivity with sensorimotor regions. In green, the central precuneal region displays connectivity with the posterior part of the inferior parietal lobule and adjacent superior temporal sulcus. In yellow, the posterior zone, along the parieto-occipital fissure exhibits connectivity with visual prestriate areas. Reproduced from Margulies et al [26].

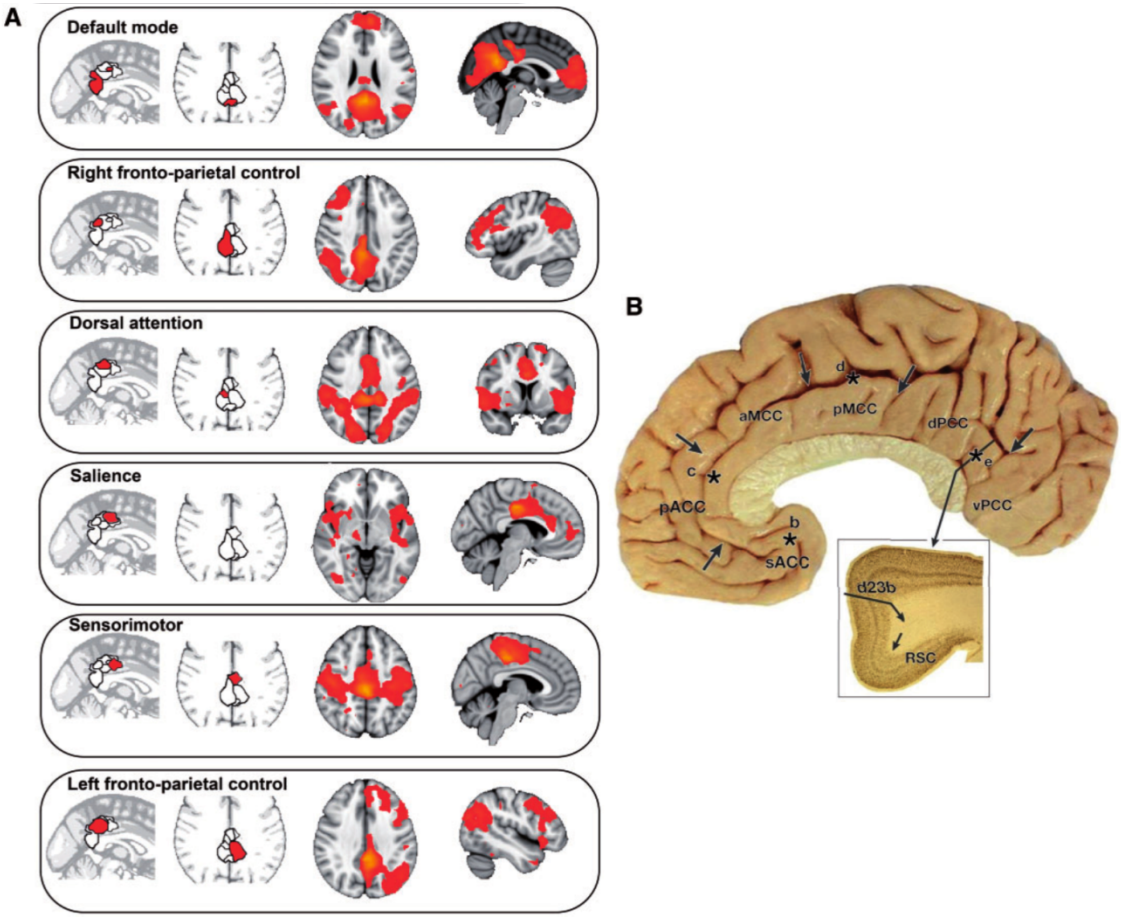

Figure 15: Functional connectivity of the PCC region

The dorsal PCC (dPCC shown in B) is anchored across multiple intrinsic connectivity networks (shown in A). Activity 'echoes' intrinsic connectivity networks in the rest of the brain. Sagittal and axial slices showing distinct but spatially overlapping regions in the PCC, defined in a data-driven way by their distinct activity pattern. These regions show functional connectivity with the networks illustrated in the sagittal and axial slices on the right of the panel. The networks are labelled in relation to their resemblance to well-defined intrinsic connectivity networks. Adapted from Leech et al. [27].

Although the PMC region covers a large area of the cortex, it is often analysed and discussed as having a unitary function. However, recent work has corroborated evidence to support its heterogeneous functional neuroanatomy [28,29]. Furthermore, the PMC also shows abnormal function in a range of psychiatric and neurological conditions, some of which are potential downstream risk factors for later neurodegeneration and AD. In contrast to its relative infrequent focal damage, it is commonly affected in neurodegenerative disease [30], traumatic brain injury [29], and major depression [31].

Previous work on the functional anatomy and physiology of the PCC, which lies within the PMC, has distinguished prominent dorsal and ventral subcomponents that can be used to explain its complex function [28,32]. Cytoarchitectonically, the PCC is characterised as having an anterior and dorsal (dorsal PCC) subregion situated superior to the splenium of the corpus callosum (areas d23a, d23b, 23d, anterior 31) and a ventral part (ventral PCC) posterior to the splenium (v23a and v23b, posterior 31). The dorsal PCC reveals a selective pattern of functional connectivity with connections to the DMN and other intrinsic networks such as the frontoparietal networks that encompass the attentional network, as well as with other networks involved in executive control [33,26]. By contrast, the ventral PCC shows strong connectivity with the DMN during internally focused states (such as resting-sate) [28,34]. This suggests that the dorsal PCC influences attentional focus by modulating whole-brain metastability and maintains stable brain activity over time. Alternatively, as the ventral PCC appears to be highly integrated within the DMN, it may serve a potential role in supporting internally directed cognition.

Since the PCC has been shown to be functionally anchored across numerous important intrinsic networks, several critical questions regarding the integrity of the PMC in AD remain unaddressed. For one, only a small number of studies have addressed the question of PMC function in AD pathophysiology [35,36]. Additionally, little is known about the functional heterogeneity of the PMC and how it interacts with the rest of the brain, as well as with prominent nodes of the DMN. Consequently, inadequate attention to the functional neuroanatomy of the PMC is a potential limitation of previous DMN studies in the AD literature.

Using rsfMRI neuroimaging data, clinical phenotyping and metadata from the publicly available Alzheimer's Disease Neuroimaging Initiative (ADNI) database, we aimed to characterise the functional architecture of the PMC in AD pathophysiology. We proposed that brain activity of the PMC region should reveal a complex and dynamic pattern of intrinsic connectivity with the rest of the brain. Moreover, key regions of the PMC with discrete roles in supporting cognition, memory and attentional control would be affected in AD and prodromal MCI patients. A disruption in the functional equilibrium of the PMC at rest would also have cascading effects on key nodes of the DMN, particularly the MTL and VMPFC that are preferentially disrupted in AD.

MATERIALS AND METHODS

Data used for this study was obtained from the Alzheimer's Disease Neuroimaging Initiative (ADNI) database (http://adni.loni.usc.edu/). The ADNI study was launched in 2003 by the National Institute on Aging, the National Institute of Biomedical Imaging and Bioengineering, the Food and Drug Administration, private pharmaceutical companies, and non-profit organizations as a $60 million, 5- year public–private partnership. The primary goal of ADNI has been to test whether serial MRI, PET, other biological markers, and clinical and neuropsychological assessment can be combined to measure the progression of mild cognitive impairment and early Alzheimer's disease. Determination of sensitive and specific markers of very early Alzheimer's disease progression is intended to aid researchers and clinicians to develop new treatments and monitor their effectiveness, as well as lessen the time and cost of clinical trials.

Participants

We identified all available task-free functional MRI scans in the ADNI database after baseline enrolment in ADNI-2 had been completed. We defined the first available scan for each subject as the baseline scan to be included in our analysis. The first scan of a subject was chosen if two task-free functional MRI sequences were performed on the same day, unless it did not fulfil ADNI quality control measures. In total, 213 subjects from ADNI-GO and ADNI-2 had available task-free functional MRI scans at baseline. If amyloid (Aβ) imaging or APOE genotyping was unavailable during baseline visit (n=22), these subjects were not included for further preprocessing and analysis. Subjects were classified as Aβ-positive (Aβ+) using a previously defined cut-off (1.11 SUVR) using the whole cerebellum region for Florbetapir Aβ imaging. These methods have been described in detail elsewhere [37,38] and have been recently validated in a large meta-analysis of Aβ-positivity [39,40]. All subjects that were classified as Aβ negative (n=35) were not included for further analysis as they were assumed to be on a non- Aβ pathophysiological trajectory of memory impairment.

Subjects with head motion found to exceed 1.5mm translation or 1.5° rotation were excluded from the study sample (*n*=1). Of the remaining 155 subjects that passed quality control criteria, all AD, MCI and CN individuals were selected (n=133) for rsfMRI analysis. For this study, we excluded participants with subjective memory complaints (n=22) as only 7 participants were found to be on the Aβ+ trajectory. Among our groups, there was no difference in framewise displacement *(p* = 0.54)[41] or the root mean square of translational parameters *(p* = 0.92) [42,43]. This information and further demographic characteristics are displayed in **Table 1**.

Image Acquisition

All subjects were scanned using a 3T Philips system. Task-free functional MRI scans were obtained using a single shot gradient echo-planar imaging sequence (EPI) with full brain coverage including the whole cerebellum. The following parameters were used: 140 functional volumes, repetition/echo time of 3000/30ms, flip angle of 80°, 48 axial slices, and a 64 x 64 in-plane acquisition matrix reconstructed to produce slice thickness of 3.3mm and a isotropic 3.3mm voxel size. Further information regarding slice ordering, quality control criteria, and other ADNI protocols is provided on the www.adni.loni.usc.edu/ website.

Structural image preprocessing

T1-weighted MRI images were acquired using the ADNI Philips 3D Magnetization Prepared Rapid Gradient Echo (MPRAGE) sequence, with 1x1mm in-plane resolution and 1.2mm slice thickness. A repetition time of ~7/3 ms was used. Detailed information on the ADNI imaging protocol is provided on the main website (www.adni.loni.usc.edu). Subjects in our study were elderly, had a generally larger ventricular size, and varying levels of cortical atrophy compared to younger subjects. Therefore, we decided to include all available baseline scans to create a study-specific custom template using the Diffeomorphic Anatomical Registration Through Exponentiated Lie Algebra (DARTEL) toolbox in the SPM12 toolbox (http://www.fil.ion.ucl.ac.uk/spm/). This toolbox performs a high dimensional warping process resulting in improved localisation and increased sensitivity in analyses. The entire baseline set of scans were initially segmented using the available SPM12 priors for six tissue classes (i.e.

grey matter, white matter, CSF, bone, lipid, and air). Grey matter images for each subject were used to calculate whole-brain volume (WBV) and the total sum of grey, white, and CSF matter volume for each subject was used to calculate intracranial volume (ICV).

Functional image preprocessing

The initial preprocessing steps involved discarding the first 10 functional volumes of the available 140 to allow for steady-state magnetization and to avoid including volumes contaminated with scanner artefact. AFNI's 3dDespike command (http://afni.nimh.nih.gov/) was used to despike the timeseries in each voxel. This step was performed prior to realignment, since realignment and motion correction of images may be improved with this procedure. On the remaining 130 volumes in each dataset we performed slice-timing correction followed by a two-pass realignment to the mean functional image. The gradwarp and bias corrected structural images were then co-registered to the mean EPI image. Unified segmentation and normalization to the ADNI DARTEL template was then performed.

Functional connectivity analysis

We performed all our functional connectivity analyses in accordance with the work of Leech et al [27] on the fractionation of the PCC.

Finding distinct patterns of functional connectivity within the PMC

We performed a constrained ICA analysis on the PMC region using a sample of AD patients and healthy controls matched for age, gender and years of education (Table 2). The group matching procedure was performed using the MatchIt package [44] for balancing experimental data in the R statistical software environment (version 3.2.1) The PMC region was defined by selecting the PCC and Precuneus regions using the Harvard-Oxford probabilistic atlas in fslview [45]. These regions were defined by only selecting voxels with a probability greater than 20% signal intensity and concatenating both anatomical masks to form the PMC. For the PCC region, the anatomical mask also included the RSC. A temporal concatenation group independent component analysis (ICA) was then run on the resting fMRI data within the mask of the PMC region using FSL's MELODIC (5.0.8)[46]. This approach identified subregions within the PMC with spatially and temporally distinct patterns of neural activity.

The analysis was constrained to extract 10 independent components. The dimensionality of the ICA reflects a trade-off between granularity and noise. To confirm that our results hold for other ICA dimensionalities, the analysis was also run with seven and 15 components, with qualitatively similar results.

Analysing PMC functional connectivity patterns with the whole-brain

For the next step, a GLM was used with the fMRI data simultaneously including the 10 spatial maps from the ICA as a design matrix; this approach resulted in a subject-specific time course for each spatial map controlling for the variance explained by the other spatial maps. It can be thought of as finding 10 independent signals (corresponding primarily to different but overlapping regions of interest) from within the PMC for each subject. We then investigated

whether these independent signals correlated with activity in the rest of the brain. A second GLM was used, this time entering whole-brain fMRI data. The time courses of the PMC subregions calculated in the previous step were simultaneously included in the design matrix to generate a set of voxelwise whole-brain statistical maps [this is a variant of the dual-regression procedure which has been implemented widely by others [28,29]].

Analysing PMC functional connectivity with the MTL and VMPFC

For this analysis, a GLM from the previous step was used in which the fMRI data is used as the design matrix simultaneously with the spatial maps from the 10 component ICA step. We defined the MTL node using the Harvard-Oxford subcortical probabilistic atlas in fslview (voxels > 20% probability) by creating an anatomical mask of the hippocampal, entorhinal, and parahippocampal structures. On the other hand, the VMPFC was created from Neurosynth (http://www.neurosynth.org/) using the reverse inference map and thresholded using $p = < 0.0001$ uncorrected, after smoothing the Z-map with a 6mm FWHM kernel and averaging the z-scores from the right and left hemispheres to create a symmetrical mask. We then investigated whether these 10 independent signals from each PMC subregion correlated with the activity in the MTL and VMPFC nodes. Therefore, in the second GLM fMRI activity from within the MTL and VMPFC nodes was entered along with the time courses from the PMC subregions in the design matrix. This subsequently generated a set of voxelwise statistical maps constrained to measure activity within the MTL and VMPFC nodes. This entire step was computed for the MTL and VMPFC nodes separately.

Statistical analysis

Finally, the resulting voxelwise spatial maps from each analysis step above were combined separately for the PMC whole-brain analysis and the PMC-MTL and PMC-VMPFC analyses respectively. A higher level GLM was computed and statistically evaluated using the FSL randomise tool which uses a nonparametric permutation testing method on the assumption that the null hypothesis implies complete exchangeability of the observations [47]. Using this procedure, voxelwise differences were evaluated by generating 5000 random permutations at

a family-wise error (FWE) corrected significance level of $p < 0.05$. The resulting statistical maps were corrected for multiple comparisons using the Threshold-Free Cluster Enhancement (TFCE) method which avoids using an arbitrary threshold for the initial cluster formation [48].

RESULTS

Demographic Characteristics

Our groups were found to significantly differ on cognitive measures of MMSE, CDR-SB, ADAS-Cog scores, Aβ deposition, and the number of APOE ε4 carriers (Table 2). There was no significant difference of age, gender, years of education, and motion parameters.

PMC shares intrinsic connections with distributed RSN networks

Consistent with the proposed functional heterogeneity of the PMC, we found that the 3 structural components, the PCC, precuneus and RSC, all exhibited extensive functional connectivity with other brain networks at rest. We define these intrinsic functional connections with the PMC below. For a more elementary interpretation, we also defined the sub-regions as belonging to the distinct cytoarchitectonics of the precuneus, PCC and RSC.

Precuneus

From the 10 independent PMC signals, 3 subregions were found to be a part of the precuneus. We found that this networks were remarkably consistent with the functional subdivisions proposed by Margulies et al [26]. The functional subdivisions of the precuneus along with their functional connectivity with whole-brain networks are displayed in Figure 4.

(1) *Anterior Precuneal Region (Sensorimotor Network)*: This region was found to exhibit extensive functional connectivity with sensorimotor related areas of the medial surface of the brain. Strong connections were observed with the paracentral lobule and premotor area on the precentral gyrus. Furthermore, strong connections with the ventral-most region of the precuneus was also observed with activity near the parieto-occipital sulcus.
(2) *Central Precuneal Region (Cognitive DMN)*: This subregion was functionally connected to nodal regions typically involved in the DMN, including the dorsolateral and VMPFC

cortices. Strong functional connectivity with parahippocampal structures of the MTL was also observed.

(3) *Posterior Precuneal Region (Visual Network):* This region, which reflects activity on the parieto-occipital sulcus, displays strong functional connectivity with the visually related cuneal and supracalcarine cortices, as well as the occipital fusiform cortex. Strong connectivity with the PCC and RSC were also found.

Posterior Cingulate Cortex (PCC)

Prominent signals within the PMC were also associated with the PCC. These were found to be consistent with what has been reported in the literature, with distinct cytoarchitectonics within the PCC, suggesting separation into dorsal and ventral areas [32]. Here, we identified 3 subregions that revealed the functional subdivisions of the PCC at rest. The dorsal PCC was found to be anchored across two intrinsic networks, consistent with previous evidence suggesting involvement in several networks for maintaining whole-brain metastability [50]. Moreover, the dorsal PCC was found to be divided into two regions: the predominately dorsal zone and anterior dorsal region. By contrast, the ventral PCC was only associated with the DMN. Two dorsal PCC subregions were identified with connections in both the DMN and central executive network. This suggests that the dorsal PCC may act as interface between these two networks primarily involved in cognitive and attentional control [28]. The subdivisions of the PCC and their functional connectivity with whole-brain networks are displayed in Figure 5.

(1) *Dorsal PCC (DMN):* The second PCC signal in the dorsal region showed functional connectivity with the DMN, particularly the entire PCC region, the VMPFC node, and the parahippocampal gyrus.
(2) *Anterior Dorsal PCC (Anterior Salience):* This subregion showed strong functional connectivity with the dorsal anterior cingulate gyrus (dACC), the supplementary motor cortex, the premotor cortex (BA6), the paracingulate gyrus, and the frontal pole. Key subcortical structures such as the putamen and the substantia nigra/ventral tegmental area were a part of the network. The network was spatially very similar to the anterior salience network identified by Shirer et al [51].
(3) *Ventral PCC (Cognitive):* Strong functional connectivity was observed for typical nodes of the DMN, including the MTL and VMPFC regions.

Retrosplenial Cortex (RSC)

Two RSC subregions exhibiting different patterns of whole-brain functional connectivity were identified. These RSC subdivisions are displayed along with their functional connectivity with whole-brain networks in Figure 6.

(1) *RSC region (BA29) (Cognitive):* This subregion in BA29 of the RSC region showed strong functional connectivity with the precuneus, VMPFC and hippocampal regions. We therefore ascribed this region a cognitive functional role as the DMN network.
(2) *RSC region (BA30) (Visual):* This subregion, immediately adjacent to the splenium of the corpus callosum, exhibited functional connectivity with the visually related cortex of the cuneus along the parieto-occipital fissure. More specifically, this subregion demonstrated strong functional connectivity with the visual cortex (BA17 and BA18).

Overall, separate rsfMRI signals from the PMC were found to be correlated with activity in several other brain networks. Spatially overlapping whole-brain functional connectivity maps of our independent PMC signals also demonstrated the greatest spatial overlap in the dorsal PCC region (Figure 7). This is consistent with previous work suggesting a strong functional connectivity pattern of the dorsal PCC with a wide range of other intrinsic brain networks [26,27]. Although the exact composition and spatial topology of the regions of interest extracted from the PMC region is sensitive to the number of independent components extracted, qualitatively similar results were obtained when fractionating the PMC region signals into 7, 10, and 15 components respectively (Figure 8).

Aberrant hyperconnectivity of Dorsal PCC subregion in Alzheimer's disease

Relative to the CN group, AD patients showed greater functional connectivity of the dorsal PCC region (Figure 9A). This dorsal PCC subregion showed functional connectivity with regions typically involved in the DMN at the whole-brain level. Dorsal PCC hyperconnectivity in AD patients was detected in the ventral PCC region (p = 0.03; *FWE* corrected). There were no regions that showed a significant decrease in functional connectivity in AD patients relative to the CN group.

Functional decline of MTL in RSC and Precuneal subregions supporting Cognition

Relative to the CN group, the RSC (BA29) and posterior precuneal subregions showed reduced functional connectivity with MTL in AD patients (Figure 9B). For the RSC subregion (BA29), hypoconnectivity in the MTL region was observed in the left entorhinal cortex (p = 0.01; *FWE* corrected). For the posterior precuneal region, hypoconnectivity was observed in the right entorhinal cortex and right subiculum (p = 0.01; *FWE* corrected). There were no PMC subregions that exhibited increased functional connectivity with the MTL in AD patients compared to the CN group.

Frontal hyperconnectivity of VMPFC in AD

Relative to the CN group, the ventral PCC subregion showed increased functional connectivity with the VMPFC in AD patients (Figure 9C). Frontal hyperconnectivity in AD patients was detected in the right frontal pole and right frontal medial cortex (p = 0.03; *FWE* corrected). There were no brain regions in AD patients that showed reduced functional connectivity in the VMPFC compared to the CN group.

Prodromal MCI patients with incipient AD show similar connectivity cascades in PMC-derived networks

MCI patients (MCI-converters) that progressed to an AD diagnosis at future follow-up and were Aβ+ were included in the overall sample, and compared to the CN group. We have provided a descriptive table to highlight the differences between subjects that converted to AD and those that remained clinically stable at follow-up (Table 3). At the whole-brain level we did not observe any significant functional connectivity differences. A trend level result for the ventral PCC subregion (p = 0.07) showed a similar pattern of increased functional connectivity with the DMN compared to the CN group.

Relative to the CN group, MCI-converters showed a reduced functional connectivity with the MTL in the central and anterior precuneal regions. For the central precuneal region in MCI-converters, hypoconnectivity with the MTL was detected in the right cornu ammonis (CA1), and right dentate gyrus (p = 0.01; *FWE* corrected) (Figure 10A). For the anterior precuneal region in MCI-converters (Figure 10B), hypoconnectivity was observed in the right entorhinal cortex and right subiculum (p = 0.03; *FWE* corrected). There were no PMC subregions that exhibited increased functional connectivity with the MTL in MCI-converters compared to the CN group.

Relative to the CN group, MCI-converters also showed a similar pattern of frontal hyperconnectivity with the VMPFC for the RSC (BA29) subregion (Figure 10C). This pattern of hyperconnectivity in MCI-converters was detected in the left subcallosal cortex and paracingulate gyrus (p = 0.03; *FWE* corrected). MCI-converters also exhibited reduced functional connectivity with VMPFC for the dorsal PCC subregion compared to the CN group (Figure 10D). Reduced functional connectivity in MCI-converters was detected in the paracingulate gyrus, and frontal medial cortex (p = 0.01; *FWE* corrected).

DISCUSSION

An emerging feature in the subspecialisation of the PMC is its role as a cortical hub integrating different networks that function to reciprocally support cognition and behaviour. Our findings extend recent neuroimaging evidence from studies of the DMN to show the functionally heterogeneous profile of the PMC and its vulnerability to AD pathogenesis.

In this study, we demonstrate that: (1) the PMC shares a complex functional connectivity architecture with rest of the brain, (2) highly integrated subdivisions of the PMC, such as the dorsal PCC, are preferentially affected in AD, and show complex patterns of hypoconnectivity and hyperconnectivity, and (3) MCI patients converting to AD at follow-up show similar PMC connectivity cascades to AD patients. In previous studies, clear dissociations are not often made between the complex functional assembly of the PCC and the precuneus. In this study, we observe clear distinctions between these two neighbouring regions of high metabolic activity.

In the precuneus, three clear subdivisions were discerned which were in accordance with the anatomical anterior-to-posterior functional differentiation proposed by Margulies et al [26]. Specifically, this includes (1) an anterior zone along the marginal ramus of the cingulate sulcus that displays functional connectivity with sensorimotor regions, (2) a central zone which plays a multimodal integrative cognitive role and displays functional connectivity with the DMN, and (3) a posterior zone along the parieto-occipital fissure that exhibits functional connectivity with the visual prestriate areas in the cuneus and the dorsal lateral occipital region. This demonstrates the substantial functional heterogeneity of the region and distinguishes its functional properties from those of the PCC and RSC regions. Functional connectivity between the precuneus and the primary motor cortex, which was specific to the anterior region, has been reported previously [4,52]. Functional connectivity in the central precuneal region, which we ascribed as reflecting the DMN has also been associated with earlier reports of a frontoparietal control system [53,54]. The inclusion of the precuneus in the DMN is a less consistent observation in previous fMRI studies. Some studies propose that the precuneus reflects a core hub of the DMN alongside the PCC [55]. Others argue that the precuneus does

not explicitly reflect a core of the DMN, and is more characteristically associated with ventral parts of the PCC [26]. The divergent findings across several studies with respect to the dorsal-ventral boundaries of the DMN would suggest that our precuneal findings regarding the DMN should be considered preliminary. Despite this, we would argue that consistency in the literature linked with the central precuneus sub-serving a cognitive/associate role is more widely reported [26,56].

Within the PCC, neural activity could be separated into functionally distinct dorsal and ventral subcomponents that have been previously observed to have an active role in regulating cognition [27,28]. Consistent with the anatomy and physiology of the PCC, we observed that the dorsal PCC showed strong functional connectivity with the DMN, but also with the salience network – which has been showed to modulate DMN activity. In particular, the dorsal PCC appeared to show more extensive connectivity. This is reflected in its densest structural connections to areas of the heteromodal association cortex. On the other hand, the ventral PCC is prominently linked with the DMN, as was observed in this study. Previous work has highlighted that different parts of the PCC show a complex pattern of interaction with intrinsic networks in the brain [27,49,57]. In accordance, our work shows that the dorsal PCC reflects an 'intermediate' pattern of connectivity coupling networks that are functionally distinct, but work reciprocally to coordinate cognitive function.

In contrast, the RSC is formally considered to be a part of the PCC and has been thought to underpin a core network of brain regions involved in a range of cognitive functions [58]. The importance of distinguishing the RSC from the PCC is underlined by its many morphological and connectivity differences arising from Brodmann areas 29 and 30 [59,60]. We also observed that the RSC subdivided into these two prominent subregions. The RSC BA29 region exhibited functional connectivity with the DMN, particularly since the densities of hippocampal connections are much higher than in adjacent PCC BA23 [61]. Consistent with previous anatomical studies, the RSC BA30 region showed distinct functional connectivity with more interconnected visual areas of the extrastriate cortex and primary visual cortex (BA17) [62]. This ubiquitous involvement of the RSC across an array of cognitive abilities is supported by several fMRI studies highlighting its role in spatial navigation and episodic memory [63,64]. These distinct patterns of functional connectivity in the RSC have also been linked to processes

associated with mentally generating a complex and coherent scene – which is believed to support autobiographical memory, navigation and thinking about the future [65]. Although previous neuroimaging and clinical studies have highlighted RSC dysfunction in the early stages of AD [66,67], there is a continued need for greater anatomical precision.

Thus, understanding the distinct functional contributions of the RSC to different parts of the brain independent of the PCC is important for characterising memory impairments following RSC dysfunction.

Dorsal PCC is hyperconnected in AD

We found that the dorsal PCC region demonstrated increased functional connectivity with the DMN in AD patients at the whole-brain level compared to CN individuals. Brain regions where such differences were noted included the ventral PCC region of the DMN. This region demonstrates the densest reciprocal connections within the PCC [25] and exhibits strong structural connections with the MTL via the cingulum bundle [7]. This is contrary to some previous findings that have observed significant decreases in functional connectivity in the PMC when characterising DMN failure in AD patients. Although commonly observed hyperconnectivity is typically interpreted as a compensatory mechanism, the metabolic demands associated with high connectivity may be a detrimental phenomenon. For instance, high connectivity is often a sign of high processing burden and/or maladaptive information processing efficiency at the synaptic level. This noisy inefficient communication may then be propagated to areas that are considered highly-connected hubs with the greatest metabolic demands. Such areas of high metabolism are relatively well-known to be the most susceptible to AD pathogenesis [8], and therefore hyperconnectivity in these critical circuits is unlikely to be an adaptive response to widespread network disruption [68]. This is particularly salient in the case of the PCC. We speculate that the dorsal PCC hyperconnectivity detected in the ventral PCC region may be related to its dense connections with the MTL. In AD, it can be understood that MTL networks (including the hippocampus that support memory) begin to succumb to degeneration, increased noise and processing burden in these cortical systems which then gets propagated back to hub regions such as the PCC. This is further supported by

a similar finding that was observed in our sample of MCI patients that converted to AD. Although the result did not achieve significance, the trend-level finding ($p = 0.07$) showed a similar hyperconnectivity pattern of the ventral PCC with the DMN at the whole-brain level.

To the best of our knowledge, this is the first study in AD to investigate the distinct functional properties of the PMC and to describe its functional heterogeneity with different brain networks. We therefore argue that a systems conceptualisation of solely decreases in functional connectivity is a simplistic one and propose that hyperconnectivity is indeed analogous to network failure in AD.

Functional decline of RSC with the MTL node of DMN supporting Memory

In the BA29 subregion of the RSC we found a decrease in functional connectivity in the MTL network. Interestingly, the RSC BA29 subregion also exhibited functional connectivity with regions collectively forming the DMN. The decrease in functional connectivity observed in the MTL network was detected in the entorhinal cortex in AD patients compared to CN individuals. This is consistent with previous studies that have demonstrated a widespread decline of networks supporting memory and cognition in AD [18,69]. Since the RSC and MTL regions are both anatomically and functionally connected, it is conceivable that Aβ pathology contributes to synaptic dysfunction and neuronal loss in the hippocampus and surrounding MTL regions, eventually leading to cognitive impairment. Furthermore, histological studies by Braak and Braak [70] show that tau pathology in later stages of AD is diffuse, affecting the MTL regions first followed by posterolateral cortical regions and the frontal cortex. In line with this research, it is plausible to observe functional RSC dysfunction because of pathological insults to its primary MTL circuits.

Frontal hyperconnectivity in the VMPFC node of DMN in AD

To evaluate previous reports of frontal hyperconnectivity in AD patients, we tested the functional connectivity of PMC subregions with the VMPFC node of the DMN. Consistent with previous findings, we found that the ventral PCC subregion displayed increased functional connectivity with the VMPFC node in AD patients compared CN individuals [14,16,20]. These differences were detected in the frontal pole and frontal medial cortex regions of the VMPFC. Previously, frontal hyperconnectivity patterns in the later stages of AD have been typically interpreted as reflecting a compensatory phenomenon as hippocampal regions increase processing via a 'degenerative feedback loop' [20]. Specifically, pre-existing tau pathology and neuronal loss in the MTL regions has been suggested to lower the noise-handling capacity of the cortical system. Since the VMPFC node harbours strong hippocampal efferent projections [71], it is conceivable that frontal regions begin to bear an aberrant high connectivity burden as the disease progresses. However, given the reliance of frontal circuits to hippocampal and posterior networks in memory functioning, it is unclear that frontal hyperconnectivity successfully facilitates an adaptive compensatory response to continued memory processing. It is more plausible to envisage such hyperconnectivity patterns as a common response to pathological insults in the brain.

Prodromal MCI patients converting to AD reveal similar patterns of connectivity

To assess whether we would observe similar functional connectivity cascades associated with the PMC in MCI patients, we retrospectively selected individuals that progressed to an AD diagnosis at future follow-up. Although we did not detect significant differences in PMC-derived networks at the whole-brain level, similar functional connectivity patterns to AD patients in the MTL and VMPFC nodes of the DMN were observed. Firstly, precuneal subregions of the PMC functionally coupled with the MTL node of the DMN were widely disrupted in MCI-converters. In particular, the central precuneal subregion showed decreased functional connectivity with the MTL network in the CA1 and dentate gyrus of the hippocampus in MCI-converters compared to CN individuals. Previous studies have shown that damaged connectivity between the MTL and PMC as a result of MTL lesions is thought to be

associated with PMC abnormalities [14,72]. Since the precuneus has strong reciprocal cortico-cortical connections to the PCC and RSC, studies have proposed that it may also have a key role in DMN activity and memory breakdown in AD pathogenesis [49]. Interestingly, the anterior precuneal region also showed decreased functional connectivity with the MTL network. Target brain regions of the MTL affected included the entorhinal cortex and subiculum region of the hippocampus. Although the anterior precuneal region typically exhibits functional connectivity with sensorimotor regions, its functional coupling with the MTL has been linked to cognitive processes such as the internal representation of self and episodic memory retrieval associated with theory of mind [73,74]. Despite observing a widespread disruption of precuneal networks supporting memory and cognition, the subregions of the PCC were relatively preserved in MCI-converters. Although tentative, we could speculate that MTL networks derived from PCC subregions may only begin to bear aberrant system failures in later stages of AD. Nonetheless, our results highlight the importance of precuneal subregions in a wide spectrum of highly integrated cognitive processes, and reveal their predilection to AD pathogenesis in prodromal disease.

As for the VMPFC region, MCI-converters displayed a similar frontal hyperconnectivity pattern that has been a matter of considerable debate in the AD literature. For instance, Bai et al [75] argued that evidence of increased functional connectivity within frontal regions in their sample of amnestic MCI patients was primarily associated with a disconnection between the PMC and prominent MTL regions. Consequently, they concluded that additional neural information-processing resources in prefrontal regions are used to compensate for cognitive dysfunction. Damoiseaux [76] further proposed that, within the DMN, hyperconnectivity manifests upstream to hypoconnectivity in aberrant functional cascades during different stages of AD pathophysiology. This hypothetical conceptualisation of a compensatory mechanism is seemingly triggered by a functional decline in posterior brain regions, collectively termed the posterior DMN – a prominent DMN subsystem disrupted in early AD [15,16]. Although claiming these mechanisms as compensatory is initially tentative, the noisy signals propagating from declining MTL cortical systems could explain the hyperconnectivity in well-connected prefrontal regions. What is clear is that these functional characteristics of frontal hyperconnectivity tend to occur when memory impairment and ensuing MTL lesions have already taken hold.

Taken together, our findings suggest that the PMC comprises a series of reciprocally connected discrete regions that participate in distinct functional networks. Our evidence suggests a selective vulnerability of the dorsal PCC in AD and MCI patients with prodromal stages of disease. Furthermore, complex functional connectivity cascades characterised by both hypoconnectivity and hyperconnectivity patterns with DMN-related circuits are prominently evident in the PMC in AD pathophysiology.

A number of limitations to our work must be taken into consideration and addressed by future studies. First, an important limitation in the rsfMRI dataset of the ADNI study should be made clear. While it is common to observe fMRI signal loss related to susceptibility artefacts in brain regions near the skull base, in the ADNI data, Jones et al [20] outlined a key 'penciling artefact' that decreases activity in the left lateral frontal lobe. Since we were uncertain how this may affect our analysis, we ensured that signal from this region was avoided in our analysis of DMN-related circuits, particularly in the ROI definition of the VMPFC region. This was done by creating an averaged mask of temporal signal-to-noise ratio across our sample to ensure that ROIs predominately avoided regions of high signal-to-noise. It would also be important to extend this work to patients with preclinical stages of AD that display little or no overt signs of memory decline. Several key findings in PMC connectivity disruption were associated with cortical connections with MTL circuits responsible for supporting memory and cognition. Future work should consider testing the relation of PMC vulnerability in AD pathophysiology with cognitive/clinical measures to assess whether they are predictive of severity. At present, there are no comparable studies evaluating PMC heterogeneity using the methodological approach outlined in this study. Consequently, we sought to understand PMC vulnerability in AD patients and MCI subjects that are known to convert to AD at future follow-up. To fully characterise the functional connectivity cascades of the PMC, it would also be valuable to assess the connectivity patterns of preclinical subjects with little or no memory decline.

Despite these limitations, our findings of a selective PMC disruption in AD pathophysiology further corroborates evidence that AD is a disconnected syndrome. Here we show that PMC heterogeneity can be used to understand the selective disruptions of this highly metabolically active region with other prominent cortical circuits beyond the DMN. We propose that PMC heterogeneity is important for understanding the complex connectivity patterns in AD

pathogenesis that may drive, or in part, accelerate tau-associated neurodegenerative processes.

REFERENCES

[1] Kwong KK, Belliveau JW, Chesler DA, Goldberg IE, Weisskoff RM, Poncelet BP, Kennedy DN, Hoppel BE, Cohen MS, Turner R (1992) Dynamic magnetic resonance imaging of human brain activity during primary sensory stimulation. Proc Natl Acad Sci U S A 89, 5675–5679.

[2] Ogawa S, Lee TM, Nayak a S, Glynn P (1990) Oxygenation-sensitive contrast in magnetic resonance image of rodent brain at high magnetic fields. Magn Reson Med 14, 68–78.

[3] Logothetis NK, Pauls J, Augath M, Trinath T, Oeltermann A (2001) Neurophysiological I nvestigation of the basis of the fMRI signal. Nature 412, 150–157.

[4] Biswal B, Yetkin FZ, Haughton VM, Hyde JS, Zerrin Yetkin F, Haughton VM, Hyde JS (1995) Functional connectivity in the motor cortex of resting human brain using echo-planar MRI. Magn Reson Med 34, 537–541.

[5] Cordes D, Haughton VM, Arfanakis K, Carew JD, Turski PA, Moritz CH, Quigley MA, Meyerand ME (2001) Frequencies contributing to functional connectivity in the cerebral cortex in “resting-state” data. AJNR Am J Neuroradiol 22, 1326–1333.

[6] Raichle ME, MacLeod AM, Snyder AZ, Powers WJ, Gusnard DA, Shulman GL (2001) A default mode of brain function. Proc Natl Acad Sci U S A 98, 676–82.

[7] Greicius MD, Srivastava G, Reiss AL, Menon V (2004) Default-mode network activity distinguishes Alzheimer’s disease from healthy aging: evidence from functional MRI. Proc. Natl. Acad. Sci. U. S. A. 101, 4637–4642.

[8] Buckner RL (2005) Molecular, structural, and functional characterization of Alzheimer’s disease: evidence for a relationship between default activity, amyloid, and memory. J. Neurosci 25, 7709–7717.

[9] Shulman GL, Fiez JA, Corbetta M, Buckner RL, Miezin FM, Raichle M, Petersen SE (1997) Common Blood Flow Changes across Visual Tasks: 11. Decreases in Cerebral Cortex. J Cogn Neurosci 9, 648–663.

[10] Gusnard D a, Raichle ME (2001) Searching for a baseline: functional imaging and the resting human brain. Nat Rev Neurosci 2, 685–694.

[11] He Y, Wang L, Zang Y, Tian L, Zhang X, Li K, Jiang T (2007) Regional coherence changes in the early stages of Alzheimer's disease: A combined structural and resting-state functional MRI study. Neuroimage 35, 488–500.

[12] Liu Y, Wang K, Yu C, He Y, Zhou Y, Liang M, Wang L, Jiang T (2008) Regional homogeneity, functional connectivity and imaging markers of Alzheimer's disease: A review of resting-state fMRI studies. Neuropsychologia 46, 1648–1656.

[13] Zhang HY, Wang SJ, Xing J, Liu B, Ma ZL, Yang M, Zhang ZJ, Teng GJ (2009) Detection of PCC functional connectivity characteristics in resting-state fMRI in mild Alzheimer's disease. Behav Brain Res 197, 103–108.

[14] Qi Z, Wu X, Wang Z, Zhang N, Dong H, Yao L, Li K (2010) Impairment and compensation coexist in amnestic MCI default mode network. Neuroimage 50, 48–55.

[15] Jones D, Machulda M, Vemuri P, McDade E, Zeng G, Senjem M, Gunter J, Przybelski S, Avula R, Knopman D, Boeve B, Petersen R, Jack C (2011) Age related changes in the default mode network are more advanced in Alzheimer's disease. Neurology 77, 1524–1531.

[16] Damoiseaux JS, Prater KE, Miller BL, Greicius MD (2012) Functional connectivity tracks clinical deterioration in Alzheimer's disease. Neurobiol Aging 33,.

[17] Agosta F, Pievani M, Geroldi C, Copetti M, Frisoni GB, Filippi M (2012) Resting state fMRI in Alzheimer's disease: Beyond the default mode network. Neurobiol Aging 33, 1564–1578.

[18] Andrews-Hanna JR, Reidler JS, Sepulcre J, Poulin R, Buckner RL (2010) Functional-Anatomic Fractionation of the Brain's Default Network. Neuron 65, 550–562.

[19] Uddin LQ, Kelly AMC, Biswal BB, Castellanos FX, Milham MP (2009) Functional Connectivity of Default Mode Network Components: Correlation, Anticorrelation, and Causality. Hum Brain Mapp 30, 625–637.

[20] Jones DT, Knopman DS, Gunter JL, Graff-radford J, Vemuri P, Boeve BF, Petersen RC, Weiner MW, Jack CR (2015) Cascading network failure across the Alzheimer's disease spectrum. Brain 1–16.

[21] Lim HK, Nebes R, Snitz B, Cohen A, Mathis C, Price J, Weissfeld L, Klunk W, Aizenstein HJ (2014) Regional amyloid burden and intrinsic connectivity networks in cognitively normal elderly subjects. Brain 137, 3327–38.

[22] Dipasquale O, Griffanti L, Clerici M, Nemni R, Baselli G, Baglio F (2015) High-Dimensional ICA Analysis Detects Within-Network Functional Connectivity Damage of Default-Mode and Sensory-Motor Networks in Alzheimer's Disease. Front Hum Neurosci 9, 43.

[23] Brodmann K (1909) Vergleichende Lokalisationslehre der Grosshirnrinde in ihren Prinzipien dargestellt auf Grund des Zellenbaues, Leipzig: J.A. Barth.

[24] Vogt BA, M G (1993) Structural organization of the cingulate cortex: areas, neurons, and somatodendritic transmitter receptors. In Neurobiology of cingulate cortex and limbic thalamus Boston: Birkhauser, pp. 19–70.

[25] Vogt BA (2009) Cingulate neurobiology and disease, Oxford: Oxford University Press.

[26] Margulies DS, Vincent JL, Kelly C, Lohmann G, Uddin LQ, Biswal BB, Villringer A, Castellanos FX, Milham MP, Petrides M (2009) Precuneus shares intrinsic functional architecture in humans and monkeys. Proc Natl Acad Sci U S A 106, 20069–20074.

[27] Leech R, Braga R, Sharp DJ (2012) Echoes of the brain within the posterior cingulate cortex. J Neurosci 32, 215–222.

[28] Leech R, Kamourieh S, Beckmann CF, Sharp DJ (2011) Fractionating the default mode network: distinct contributions of the ventral and dorsal posterior cingulate cortex to cognitive control. J Neurosci 31, 3217–24.

[29] Sharp DJ, Beckmann CF, Greenwood R, Kinnunen KM, Bonnelle V, De Boissezon X, Powell JH, Counsell SJ, Patel MC, Leech R (2011) Default mode network functional and structural connectivity after traumatic brain injury. Brain 134, 2233–2247.

[30] Minoshima S, Giordani B, Berent S, Frey KA, Foster NL, Kuhl DE (1997) Metabolic reduction in the posterior cingulate cortex in very early Alzheimer's disease. Ann Neurol 42, 85–94.

[31] Zhu X, Wang X, Xiao J, Liao J, Zhong M, Wang W, Yao S (2012) Evidence of a dissociation pattern in resting-state default mode network connectivity in first-episode, treatment-naive major depression patients. Biol Psychiatry 71, 611–617.

[32] Vogt BA, Vogt L, Laureys S (2006) Cytology and functionally correlated circuits of human posterior cingulate areas. Neuroimage 29, 452–466.

[33] Vincent JL, Snyder AZ, Fox MD, Shannon BJ, Andrews JR, Raichle ME, Buckner RL, Justin L, Shannon J (2006) Coherent Spontaneous Activity Identifies a Hippocampal-Parietal Memory Network. J Neurophysiol 96, 3517–3531.

[34] Dastjerdi M, Foster BL, Nasrullah S, Rauschecker AM, Dougherty RF, Townsend JD, Chang C, Greicius MD, Menon V, Kennedy DP, Parvizi J (2011) Differential electrophysiological response during rest, self-referential, and non-self-referential tasks in human posteromedial cortex. Proc Natl Acad Sci U S A 108, 3023–3028.

[35] Petrella JR, Prince SE, Wang L, Hellegers C, Doraiswamy PM (2007) Prognostic value of posteromedial cortex deactivation in mild cognitive impairment. PLoS One 2, 1–7.

[36] Cauda F, Geminiani G, D'Agata F, Sacco K, Duca S, Bagshaw AP, Cavanna AE (2010) Functional connectivity of the posteromedial cortex. PLoS One 5, 1–11.

[37] Clark CM, Schneider JA, Bedell BJ, Beach TG, Bilker WB, Mintun M a, Pontecorvo MJ, Hefti F, Carpenter AP, Flitter ML, Krautkramer MJ, Kung HF, Coleman RE, Doraiswamy PM, Fleisher AS, Sabbagh MN, Sadowsky CH, Reiman EP, Reiman PEM, Zehntner SP, Skovronsky DM (2011) Use of florbetapir-PET for imaging beta-amyloid pathology. JAMA 305, 275–83.

[38] Joshi AD, Pontecorvo MJ, Clark CM, Carpenter AP, Jennings DL, Sadowsky CH, Adler LP, Kovnat KD, Seibyl JP, Arora A, Saha K, Burns JD, Lowrey MJ, Mintun MA, Skovronsky DM (2012) Performance Characteristics of Amyloid PET with Florbetapir F 18 in Patients with Alzheimer's Disease and Cognitively Normal Subjects. J Nucl Med 53, 378–384.

[39] Ossenkoppele R, Jansen WJ, Rabinovici GD, Knol DL, van der Flier WM, van Berckel BNM, Scheltens P, Visser PJ, Verfaillie SCJ, Zwan MD, Adriaanse SM, Lammertsma AA, Barkhof F, Jagust WJ, Miller BL, Rosen HJ, Landau SM, Villemagne VL, Rowe CC, Lee DY, Na DL, Seo SW, Sarazin M, Roe CM, Sabri O, Barthel H, Koglin N, Hodges J, Leyton CE, Vandenberghe R, van Laere K, Drzezga A, Forster S, Grimmer T, Sánchez-Juan P, Carril JM, Mok V, Camus V, Klunk WE, Cohen AD, Meyer PT, Hellwig S, Newberg A, Frederiksen KS, Fleisher AS, Mintun MA, Wolk DA, Nordberg A, Rinne JO, Chételat G, Lleo A, Blesa R, Fortea J, Madsen K, Rodrigue KM, Brooks DJ (2015) Prevalence of Amyloid PET Positivity in Dementia Syndromes. JAMA 313, 1939.

[40] Jansen WJ, Ossenkoppele R, Knol DL, Tijms BM, Scheltens P, Verhey FRJ, Visser PJ, Aalten P, Aarsland D, Alcolea D, Alexander M, Almdahl IS, Arnold SE, Baldeiras I, Barthel H, van Berckel BNM, Bibeau K, Blennow K, Brooks DJ, van Buchem M a., Camus V, Cavedo E, Chen K, Chetelat G, Cohen AD, Drzezga A, Engelborghs S, Fagan AM, Fladby T, Fleisher AS, van der Flier WM, Ford L, Förster S, Fortea J, Foskett N, Frederiksen KS, Freund-Levi Y, Frisoni GB, Froelich L, Gabryelewicz T, Gill KD, Gkatzima O, Gómez-

Tortosa E, Gordon MF, Grimmer T, Hampel H, Hausner L, Hellwig S, Herukka S-K, Hildebrandt H, Ishihara L, Ivanoiu A, Jagust WJ, Johannsen P, Kandimalla R, Kapaki E, Klimkowicz-Mrowiec A, Klunk WE, Köhler S, Koglin N, Kornhuber J, Kramberger MG, Van Laere K, Landau SM, Lee DY, de Leon M, Lisetti V, Lleó A, Madsen K, Maier W, Marcusson J, Mattsson N, de Mendonça A, Meulenbroek O, Meyer PT, Mintun M a., Mok V, Molinuevo JL, Møllergård HM, Morris JC, Mroczko B, Van der Mussele S, Na DL, Newberg A, Nordberg A, Nordlund A, Novak GP, Paraskevas GP, Parnetti L, Perera G, Peters O, Popp J, Prabhakar S, Rabinovici GD, Ramakers IHGB, Rami L, Resende de Oliveira C, Rinne JO, Rodrigue KM, Rodríguez-Rodríguez E, Roe CM, Rot U, Rowe CC, Rüther E, Sabri O, Sanchez-Juan P, Santana I, Sarazin M, Schröder J, Schütte C, Seo SW, Soetewey F, Soininen H, Spiru L, Struyfs H, Teunissen CE, Tsolaki M, Vandenberghe R, Verbeek MM, Villemagne VL, Vos SJB, van Waalwijk van Doorn LJC, Waldemar G, Wallin A, Wallin ÅK, Wiltfang J, Wolk DA, Zboch M, Zetterberg H (2015) Prevalence of Cerebral Amyloid Pathology in Persons Without Dementia. JAMA 313, 1924.

[41] Power JD, Barnes KA, Snyder AZ, Schlaggar BL, Petersen SE (2012) Spurious but systematic correlations in functional connectivity MRI networks arise from subject motion. Neuroimage 59, 2142–2154.

[42] Jenkinson M, Bannister P, Brady M, Smith S (2002) Improved optimization for the robust and accurate linear registration and motion correction of brain images. Neuroimage 17, 825–841.

[43] van Dijk KRA, Sabuncu MR, Buckner RL (2012) The influence of head motion on intrinsic functional connectivity MRI. Neuroimage 59, 431–438.

[44] Ho DE, Imai K, King G, Stuart EA (2011) MatchIt : Nonparametric Preprocessing for Parametric Causal Inference. J. Stat. Softw. 42, 1–28.

[45] Smith SM, Jenkinson M, Woolrich MW, Beckmann CF, Behrens TEJ, Johansen-Berg H, Bannister PR, De Luca M, Drobnjak I, Flitney DE, Niazy RK, Saunders J, Vickers J, Zhang Y, De Stefano N, Brady JM, Matthews PM (2004) Advances in functional and structural MR image analysis and implementation as FSL. Neuroimage 23, Supple, S208–S219.

[46] Beckmann CF, DeLuca M, Devlin JT, Smith SM (2005) Investigations into resting-state connectivity using independent component analysis. Philos. Trans. R. Soc. B Biol. Sci. 360, 1001–1013.

[47] Nichols TE, Holmes AP (2002) Nonparametric permutation tests for functional neuroimaging: A primer with examples. Hum. Brain Mapp. 15, 1–25.

[48] Smith SM, Nichols TE (2009) Threshold-free cluster enhancement: Addressing problems of smoothing, threshold dependence and localisation in cluster inference. Neuroimage 44, 83–98.

[49] Fransson P, Marrelec G (2008) The precuneus/posterior cingulate cortex plays a pivotal role in the default mode network: Evidence from a partial correlation network analysis. Neuroimage 42, 1178–1184.

[50] Leech R, Sharp DJ (2014) The role of the posterior cingulate cortex in cognition and disease. Brain 137, 12–32.

[51] Shirer WR, Ryali S, Rykhlevskaia E, Menon V, Greicius MD (2011) Decoding Subject-Driven Cognitive States with Whole-Brain Connectivity Patterns. Cereb Cortex 22, 158–165.

[52] Fox MD, Snyder AZ, Vincent JL, Raichle ME (2007) Intrinsic Fluctuations within Cortical Systems Account for Intertrial Variability in Human Behavior. Neuron 56, 171–184.

[53] Damoiseaux JS, Rombouts SARB, Barkhof F, Scheltens P, Stam CJ, Smith SM, Beckmann CF (2006) Consistent resting-state networks across healthy subjects. Proc Natl Acad Sci U S A 103, 13848–53.

[54] Vincent JL, Kahn I, Snyder AZ, Raichle ME, Buckner RL (2008) Evidence for a frontoparietal control system revealed by intrinsic functional connectivity. J Neurophysiol 100, 3328–42.

[55] Utevsky A V., Smith D V., Huettel SA (2014) Precuneus Is a Functional Core of the Default-Mode Network. J Neurosci 34, 932–940.

[56] Cavanna AE, Trimble MR (2006) The precuneus : a review of its functional anatomy and behavioural correlates. Brain 129, 564–583.

[57] Bzdok D, Heeger A, Langner R, Laird AR, Fox PT, Palomero-Gallagher N, Vogt BA, Zilles K, Eickhoff SB (2015) Subspecialization in the human posterior medial cortex. Neuroimage 106, 55–71.

[58] Vann SD, Aggleton JP, Maguire EA (2009) What does the retrosplenial cortex do? Nat Rev Neurosci 10, 792–802.

[59] Kobayashi Y, Amaral DG (2000) Macaque monkey retrosplenial cortex: I. Three-dimensional and cytoarchitectonic organization. J Comp Neurol 426, 339–365.

[60] Kobayashi Y, Amaral DG (2003) Macaque monkey retrosplenial cortex: II. Cortical afferents. J Comp Neurol 466, 48–79.

[61] Kobayashi Y, Amaral DG (2007) Macaque monkey retrosplenial cortex: III. Cortical efferents. J Comp Neurol 502, 810–833.

[62] Vogt B a, Miller MW (1983) Cortical connections between rat cingulate cortex and visual, motor, and postsubicular cortices. J Comp Neurol 216, 192–210.

[63] Epstein RA (2008) Parahippocampal and retrosplenial contributions to human spatial navigation. Trends Cogn Sci 12, 388–396.

[64] Svoboda E, McKinnon MC, Levine B (2006) The functional neuroanatomy of autobiographical memory: A meta-analysis. Neuropsychologia 44, 2189–2208.

[65] Hassabis D, Maguire EA (2007) Deconstructing episodic memory with construction. Trends Cogn Sci 11, 299–306.

[66] Nestor PJ, Fryer TD, Ikeda M, Hodges JR (2003) Retrosplenial cortex (BA 29/30) hypometabolism in mild cognitive impairment (prodromal Alzheimer's disease). Eur J Neurosci 18, 2663–2667.

[67] Dillen KNH, Jacobs HIL, Kukolja J, von Reutern B, Richter N, Onur ÖA, Dronse J, Langen K-J, Fink GR (2016) Aberrant functional connectivity differentiates retrosplenial cortex from posterior cingulate cortex in prodromal Alzheimer's disease. Neurobiol Aging 44, 114–126.

[68] Hillary FG, Roman CA, Venkatesan U, Rajtmajer SM, Bajo R, Castellanos ND (2015) Hyperconnectivity is a Fundamental Response to Neurological Disruption Introduction : Disconnecting the Brain. Neuropsychology 29, 59–75.

[69] Buckner RL (2004) Memory and executive function in aging and ad: Multiple factors that cause decline and reserve factors that compensate. Neuron 44, 195–208.

[70] Braak H, Braak E (1991) Acta H ' pathologica Neuropathological stageing of Alzheimer-related changes. Acta Neuropathol. 239–259.

[71] Roy M, Shohamy D, Wager TD (2012) Ventromedial prefrontal-subcortical systems and the generation of affective meaning. Trends Cogn Sci 16, 147–156.

[72] Wang L, Zang Y, He Y, Liang M, Zhang X, Tian L, Wu T, Jiang T, Li K (2006) Changes in hippocampal connectivity in the early stages of Alzheimer's disease: Evidence from resting state fMRI. Neuroimage 31, 496–504.

[73] Damasio A (1999) The Feeling of What Happens: Body and Emotion in the Making of Consciousness, Harcourt Brace and Co, New York.

[74] Ochsner KN, Knierim K, Ludlow DH, Hanelin J, Ramachandran T, Glover G, Mackey SC (2004) Reflecting upon feelings: an fMRI study of neural systems supporting the attribution of emotion to self and other. J Cogn Neurosci 16, 1746–1772.

[75] Bai F, Watson DR, Yu H, Shi Y, Yuan Y, Zhang Z (2009) Abnormal resting-state functional connectivity of posterior cingulate cortex in amnestic type mild cognitive impairment. Brain Res 1302, 167–174.

[76] Damoiseaux JS (2012) Resting-state fMRI as a biomarker for Alzheimer's disease? Alzheimer's Res Ther 4, 8.

Table 25: Subject demographics and metadata

	AD (n = 30)	CN (n = 42)	EMCI (n = 34)	LMCI (n = 27)	*P*-value
Age	72.6 ± 7.6	75.5 ± 7.2	71.0 ± 6.1	72.6 ± 8.0	0.11
Male (%)	14 (22.2)	18 (28.6)	14 (22.2)	17 (27.0)	0.32
Years of Education	15.5 ± 2.6	16.3 ± 2.2	15.6 ± 2.9	16.9 ± 2.5	0.10
MMSE	22.5 ± 2.5	28.8 ± 1.3	27.9 ± 1.8	27.5 ± 1.6	<0.001
CDR-SB	6.5 ± 3.4	0.4 ± 1.1	2.7 ± 2.1	4.4 ± 3.4	<0.001
ADAS-Cog	34.4 ± 9.3	9.7 ± 4.1	13.3 ± 5.6	18.9 ± 7.3	<0.001
Amyloid AV45	1.45 ± 0.20	1.13 ± 0.19	1.34 ± 0.18	1.36 ± 0.20	<0.001
APOE ε4 carrier (%)	22 (27.8)	14 (17.7)	26 (32.9)	17 (21.5)	<0.001
MCI to AD conversion (%)	--	--	9 (26.5)	14 (51.9)	--
WBV (mL)	1495 ± 204	1494 ± 133	1435 ± 181	1547 ± 163	0.10
Motion $_{FD}$	0.22 ± 0.27	0.24 ± 0.46	0.21 ± 0.20	0.24 ± 0.46	0.54
Motion $_{RMS}$	0.20 ± 0.33	0.14 ± 0.08	0.15 ± 0.08	0.13 ± 0.06	0.92

AD = Alzheimer's disease; CN = Cognitively normal; EMCI = Early Mild Cognitive Impairment (Amyloid-Positive); LMCI = Late Mild Cognitive Impairment (Amyloid-Positive); MMSE = Mini Mental State Examination; CDR-SB = Clinical Dementia Rating Scale Sub of Boxes; ADAS-Cog = 13-item Alzheimer's Disease Assessment Scale – cognitive subscale; Amyloid AV45 = Amyloid Florbetapir PET positivity; APOE = Apolipoprotein E ε4 genotype; MCI to AD conversion = MCI subjects that converted to AD at a 2 year follow-up period; WBV = Whole-Brain Volume; Motion $_{FD}$ = Motion parameter for maximum framewise-displacement; Motion RMS = motion parameter for root-mean square of translational parameters.
* Bold highlights a significant difference
Kruskall-Wallis One-Way ANOVA was used for continuous variables with post-hoc comparisons performed using Mann-Whitney U-Tests.
Chi-squared was used for categorical variables.

Table 26: Matched sample of AD patients and CN individuals for temporal concatenation ICA.

	AD (n = 20)	CN (n =18)	P-value
Age	74.2 ± 5.1	74.2 ± 5.3	0.91
Male (%)	9 (45.0)	8 (44.4)	0.97
Years of Education	15.5 ± 2.9	15.9 ± 2.0	0.49
MMSE	22.6 ± 2.6	28.6 ± 1.5	<0.001
CDR-SB	6.3 ± 3.9	0.4 ± 0.7	<0.001
ADAS-Cog	32.7 ± 9.0	10.4 ± 4.2	<0.001
Amyloid AV45	1.45 ± 0.19	1.12 ± 0.23	<0.001
APOE ε4 carrier (%)	16 (80.0)	6 (33.3)	0.004
WBV (mL)	1518 ± 205	1514 ± 138	0.90
Motion $_{FD}$	0.25 ± 0.32	0.31 ± 0.71	0.41
Motion $_{RMS}$	0.24 ± 0.40	0.13 ± 0.08	0.23

AD = Alzheimer's disease; CN = Cognitively normal; MMSE = Mini Mental State Examination; CDR-SB = Clinical Dementia Rating Scale Sub of Boxes; ADAS-Cog = 13-item Alzheimer's Disease Assessment Scale – cognitive subscale; Amyloid AV45 = Amyloid Florbetapir PET positivity; APOE = Apolipoprotein E ε4 genotype; WBV = Whole-Brain Volume; Motion $_{FD}$ = Motion parameter for maximum framewise-displacement; Motion RMS = motion parameter for root-mean square of translational parameters.

* Bold highlights a significant difference

Kruskall-Wallis One-Way ANOVA was used for continuous variables with post-hoc comparisons performed using Mann-Whitney U-Tests.

Chi-squared was used for categorical variables.

Table 27: Descriptive statistics for MCI subjects that converted to AD (MCI-c) and those that remained stable (MCI-nc)

	MCI-c (*n* = 23)	MCI-nc (*n* =38)	*P*-value
Age	74.0 ± 6.7	70.2 ± 6.9	0.04
Male (%)	13 (56.5)	18 (47.4)	0.49
Years of Education	16.5 ± 2.3	16.0 ± 3.1	0.58
MMSE	27.5 ± 1.7	27.9 ± 1.7	0.32
CDR-SB	5.8 ± 3.3	2.0 ± 1.2	<0.001
ADAS-Cog	19.1 ± 6.8	13.8 ± 6.3	0.004
Amyloid AV45	1.45 ± 0.15	1.28 ± 0.18	<0.001
APOE ε4 carrier (%)	15 (65.2)	28 (73.7)	0.48
WBV (mL)	1528 ± 198	1458 ± 167	0.10
Motion $_{FD}$	0.25 ± 0.50	0.20 ± 0.19	0.60
Motion $_{RMS}$	0.13 ± 0.05	0.15 ± 0.08	0.74

MCI-c = MCI-converter; MCI-nc = MCI non-converter; MMSE = Mini Mental State Examination; CDR-SB = Clinical Dementia Rating Scale Sub of Boxes; ADAS-Cog = 13-item Alzheimer's Disease Assessment Scale – cognitive subscale; Amyloid AV45 = Amyloid Florbetapir PET positivity; APOE = Apolipoprotein E ε4 genotype; WBV = Whole-Brain Volume; Motion $_{FD}$ = Motion parameter for maximum framewise-displacement; Motion RMS = motion parameter for root-mean square of translational parameters.

* Bold highlights a significant difference

Kruskall-Wallis One-Way ANOVA was used for continuous variables with post-hoc comparisons performed using Mann-Whitney U-Tests.

Chi-squared was used for categorical variables.

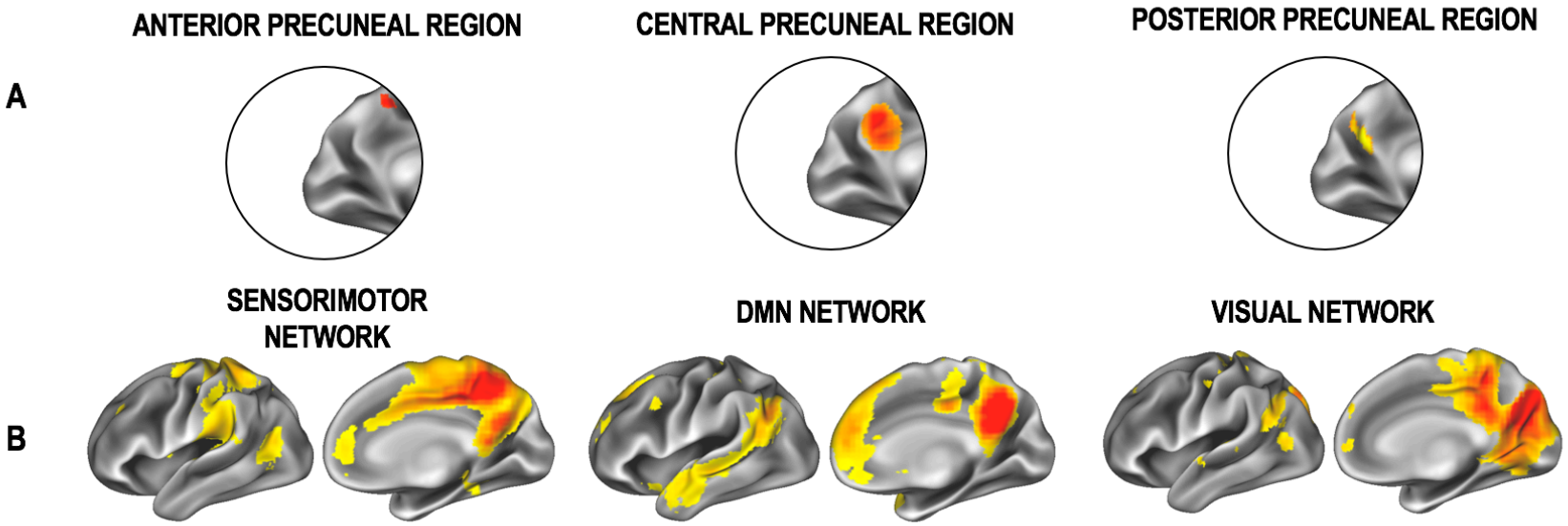

Figure 16: Functional connectivity patterns emerging from the precuneus region of the posteromedial cortex
The locations (A) and the resulting whole-brain maps of functional connectivity (B) of the 3 precuneal subdivisions. The results of the functional connectivity analysis are thresholded at $p < 0.05$, corrected for multiple comparisons.

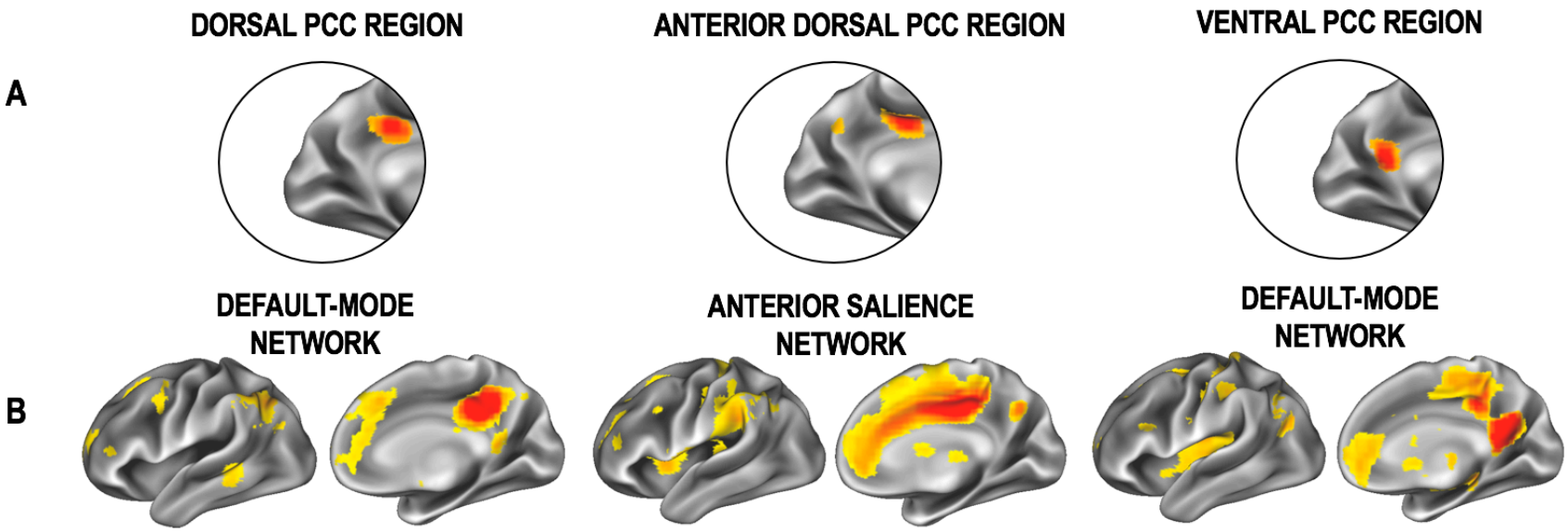

Figure 17:Functional connectivity patterns emerging from the PCC region of the posteromedial cortex
The locations (A) and the resulting whole-brain maps of functional connectivity (B) of the 3 PCC subdivisions. The results of the functional connectivity analysis are thresholded at $p < 0.05$, corrected for multiple comparisons.

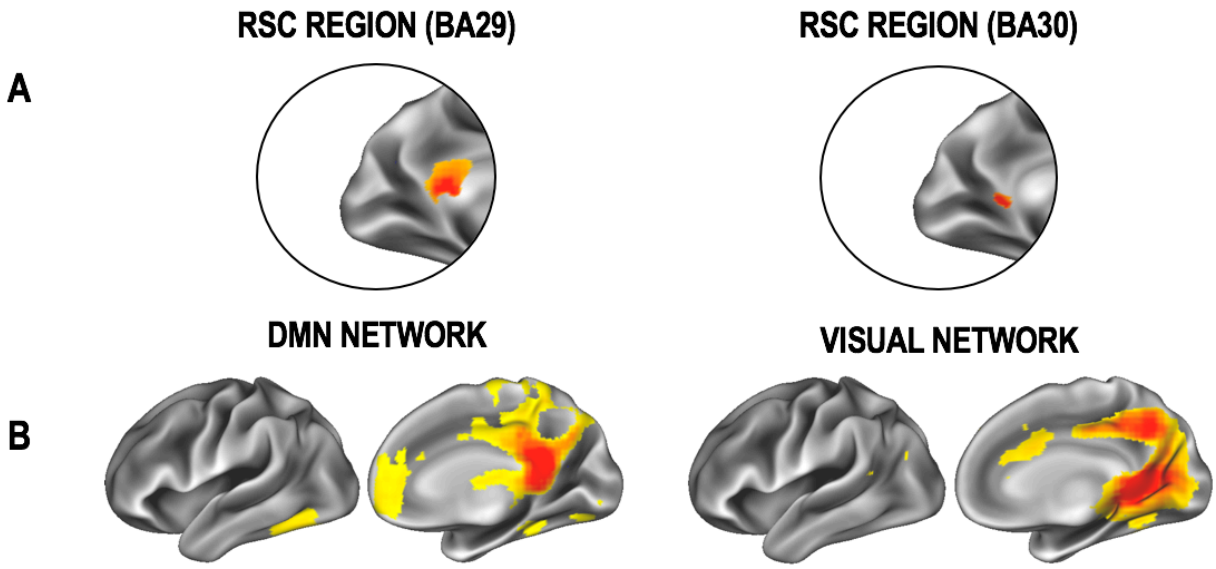

Figure 18: Functional connectivity patterns emerging from the RSC region of the posteromedial cortex

The locations (A) and the resulting whole-brain maps of functional connectivity (B) of the 2 RSC subdivisions. The results of the functional connectivity analysis are thresholded at $p < 0.05$, corrected for multiple comparisons.

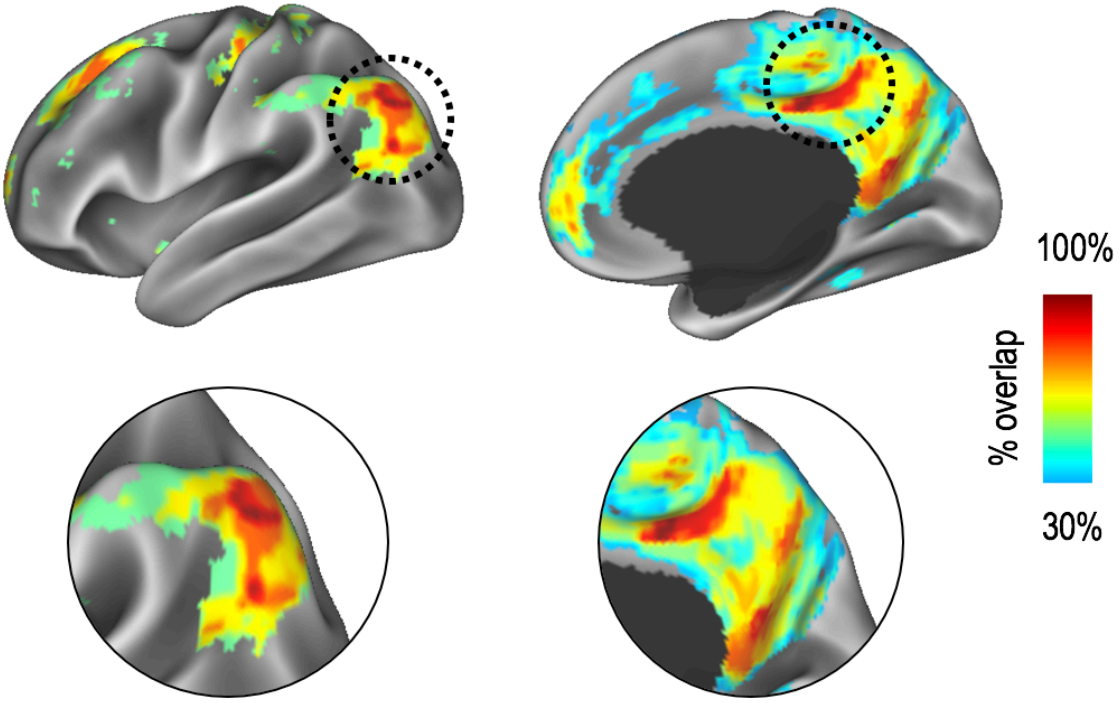

Figure 19: Functional overlap of 8 out of 10 resulting whole-brain networks from posteromedial cortex signals

Here, we illustrate the spatial overlap from the resulting whole-brain networks of 8 out of 10 independent posteromedial cortex signals. Warmer colours indicate the highest overlap across the 8 PMC spatial maps. The dorsal PCC region (circled), which is considered to be anchored across several RSN networks showed the greatest spatial overlap across our PMC-derived whole-brain networks.

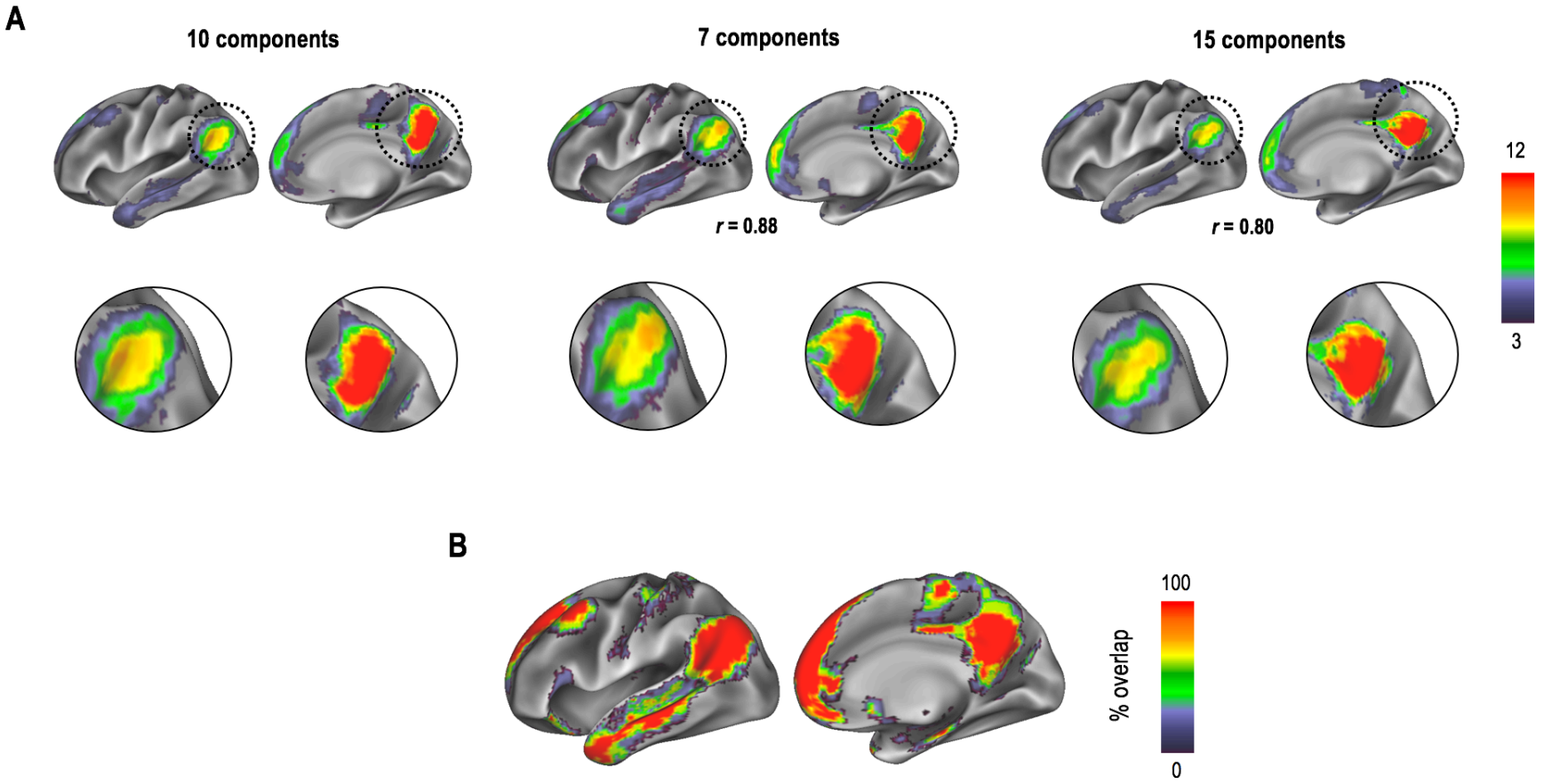

Figure 20: Consistency in topology of resulting networks across different ICA constraints

Illustrating the consistency of resulting networks by fractionation of the posteromedial cortex. (A) Resulting whole-brain networks from the precuneus network with 10 (left), 7 (middle), and 15 (right) components. *r* values correspond to the coefficient of the spatial correlation between spatial maps from the 10 component analysis with the spatial maps from the 7 and 15 component analysis respectively. (B) The functional overlap of voxels in the whole-brain network from the central precuneus network across 7, 10 and 15 ICA component analyses.

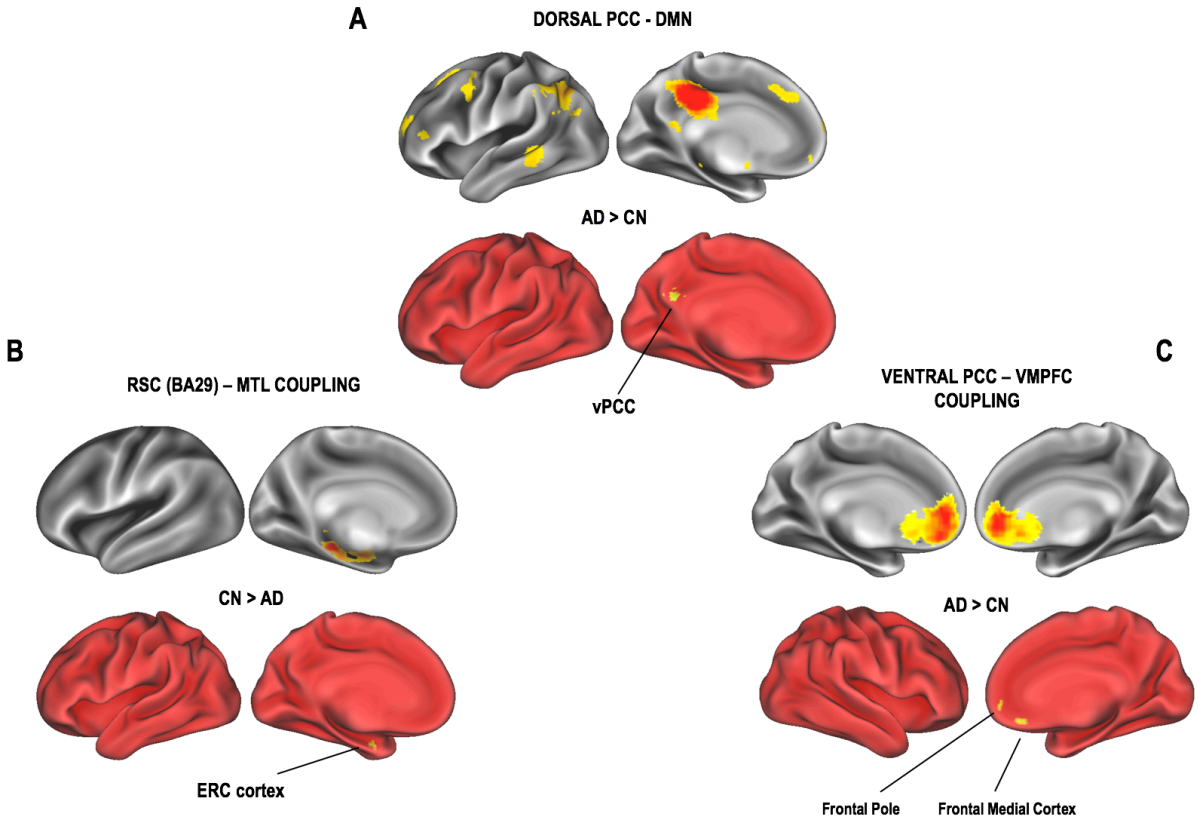

Figure 21: AD patients demonstrate both hyperconnectivity and hypoconnectivity patterns in posteromedial cortex subdivisions.

The first spatial map illustrates the whole-brain network derived from the significantly different PMC subregions and the second spatial map shows the significant cluster using the TFCE method. (A) The dorsal PCC region displayed hyperconnectivity with the DMN in AD patients compared to CN individuals (AD > CN). (B) The RSC subregion (BA29) displayed a functional decline with the MTL in AD patients compared to CN individuals (CN > AD). (C) A frontal hyperconnectivity burden was observed in the ventral PCC subregion with the VMPFC in AD patients compared to CN individuals (AD > CN).

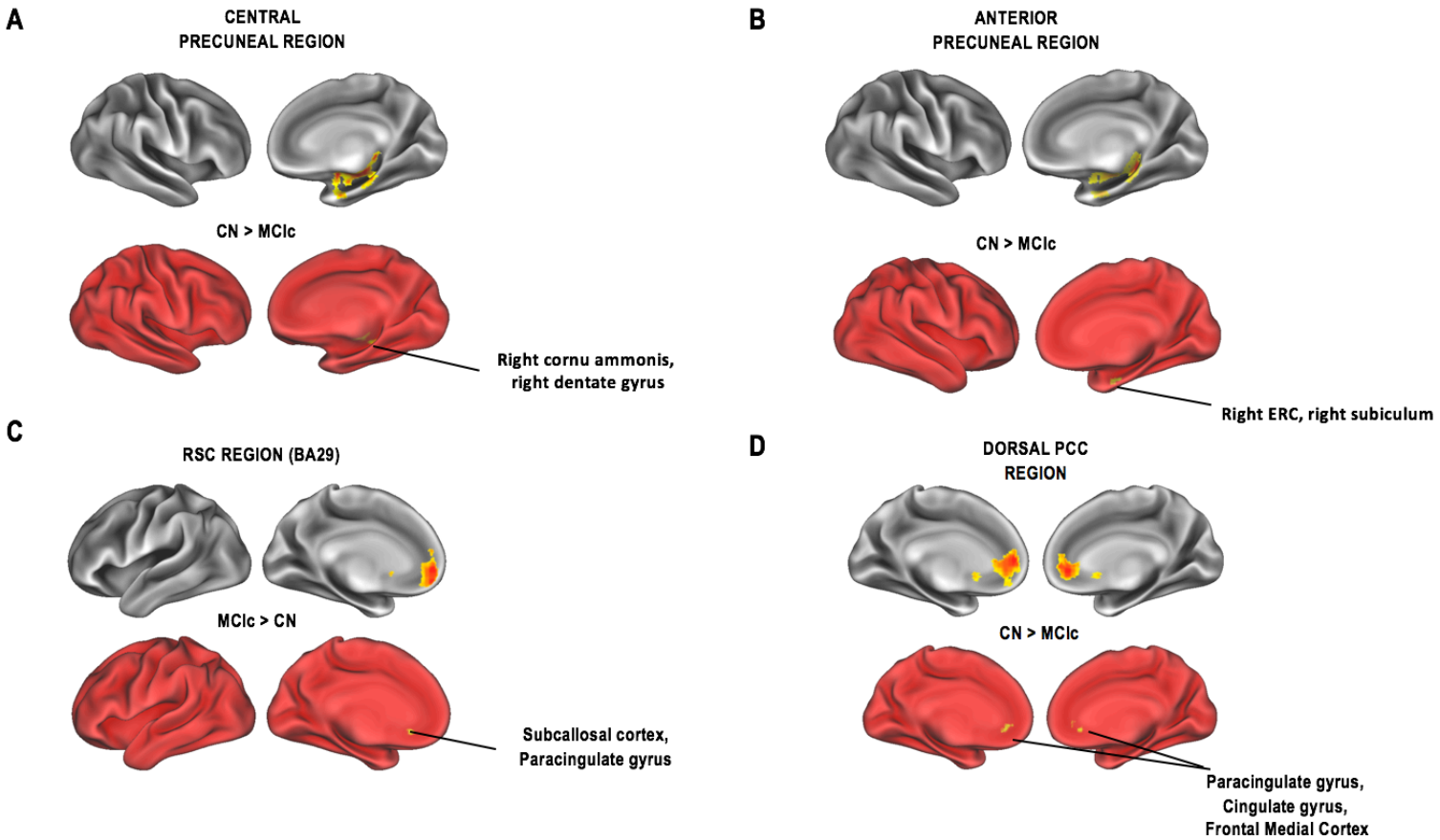

Figure 22: MCI patients converting to AD show similar functional connectivity cascades in posteromedial cortex subdivisions. The first spatial map illustrates the whole-brain network derived from the significantly different PMC subregions and the second spatial map shows the significant cluster using the TFCE method. (A) MCI-converters show reduced connectivity with MTL in central precuneal region compared to CN individuals (CN > MCIc). (B) MCI-converters show reduced connectivity with MTL in anterior precuneal region compared to CN individuals (CN > MCIc). (C) MCI-converters demonstrate frontal hyperconnectivity burden in RSC subregion (BA29) with VMPFC compared to CN individuals. All comparisons are FWE-corrected.

CHAPTER 8: DISCUSSION

The key aims of this thesis were: (1) To compare a new automated hippocampal subfield analysis technique over standard hippocampal volume measurements for disease classification and prediction (*Chapter 2*), (2) Testing the diagnostic and predictive ability of combining alternative CSF candidates with structural MRI markers for AD classification and MCI to AD conversion prediction (*Chapter 3*), (3) To assess the effect of different APOE gene polymorphisms on hippocampal volume and Aβ deposition in a large multi-cohort study (*Chapter 4*), (4) To explore the neurodevelopmental relationship between the APOE gene and brain structure in a large sample of healthy 14-yr old adolescents (*Chapters 5 and 6*), and (5) Testing the application of rsfMRI techniques in AD by exploring the complex functional architecture of the posteromedial cortex (*Chapter 7).*

SUMMARY OF FINDINGS

In *Chapter 2*, I investigated the effectiveness of a relatively new automated hippocampal subfield analysis technique against global hippocampal volume measurements for disease classification and prediction. I found that subfield volume measurements performed only as accurately as global hippocampal measurements for distinguishing AD patients from healthy controls. This suggests that hippocampal subfields offer no particular advantage over global hippocampal volume measurements for detecting AD. However, I showed that the combination of hippocampal subfield measures, and the presubiculum were the most robust at accurately detecting prodromal MCI patients that converted to AD at future follow-up. The results of these analyses suggest that hippocampal subfield vulnerability may be more selective at the MCI stage of AD pathophysiology, and later becomes more widespread as the disease progresses. These findings potentially highlight the prognostic efficacy of hippocampal subfield measures for detecting incipient stages of AD in prodromal MCI patients. Since cross-sectional data was used, models characterising longitudinal changes in subfield volumetry would be better served to further corroborate this evidence.

One outstanding question is whether fully automated hippocampal subfield measurements are yet as accurate as manual delineation of the same regions. In particular, some inconsistencies in the literature have arisen involving the demarcation of the CA4/Dentate gyrus boundaries and the presence of hippocampal cysts which can further exacerbate this problem. New initiatives, such as the EADC-ADNI Harmonized Hippocampal Protocol (HarP) [1] have been established for defining a harmonized protocol for the manual segmentation of the hippocampus. Similar initiatives and quality-control studies comparing the effectiveness of automated and manual hippocampal subfield measurements would further help in addressing this methodological issue. Recent quantitative comparisons of manual segmentation protocols for labelling hippocampal substructures provide possible strategies towards developing a harmonized protocol [2]. Furthermore, a new longitudinal method for automated hippocampal segmentation will provide more localised and accurate method for quantification [3], particularly for atrophy rates that are useful for tracking AD progression. Another issue highlighted in the chapter was the specificity of our predictive models for MCI classification. Although the sensitivity of classifiers in predicting MCI patients that converted to AD was generally good, specificity was limited in predicting those that did not convert to AD at the time of follow-up. Since AD symptomatology sufficient for diagnosis may take several years to manifest, limited specificity could be attributed to a short-follow up. Future studies with longer follow-up times would determine whether many of the MCI subjects misclassified as converting to AD will indeed convert at some point in the future.

To address limitations in specificity, recent evidence has suggested that the effective combination of different biomarkers may provide mutually complimentary information for disease diagnosis and prediction compared to using single biomarkers alone [4,5]. Two core biomarkers, structural MRI biomarkers and core CSF biomarkers (Aβ ($_{1-42}$), t-tau, and p-tau$_{181}$), reflect different aspects of AD pathology and have been shown to provide reciprocal diagnostic and predictive information [6]. Although combining different biomarkers is more effective [7], the level of model specificity for accurate MCI prediction is not adequate [8]. Previous studies have indicated that this may be associated with the need for better prognostic ability in current CSF biomarkers of AD [9].

To address this issue, in *Chapter 3*, I tested alternative CSF proteins associated with inflammation, microglial activity and synaptic function in combination with regional MRI measures for disease classification and prediction. Although existing CSF biomarkers have been extensively validated, there still remains a substantial overlap in biomarker values between AD patients, prodromal MCI patients and CN individuals. Therefore, using a 159-multiplex panel of proteins, I aimed to determine whether a novel subset of proteins could improve the diagnostic accuracy and predictive ability of MRI and CSF biomarkers.

The results from this neuroimaging-proteomics investigation suggested that a subset of proteins (*n*=24) can complement existing CSF biomarkers (Aβ ($_{1-42}$), *t*-tau, and *p*-tau$_{181}$) for the detection of AD. Although the addition of this subset panel of CSF proteins did improve model specificity for detecting AD, it did not improve the overall accuracy of the combined regional MRI and CSF biomarker model. Given the multifactorial nature of AD pathophysiology, it is likely that these CSF proteins, though not complimentary for AD detection, might possess significant prognostic potential for predicting MCI individuals likely to convert to AD. As a result, I then tested whether this same subset panel could complement regional MRI measures and CSF biomarkers for predicting MCI to AD conversion at a one year follow-up. The MCI prediction results showed that the combination of the CSF protein subset, MRI and CSF biomarkers gave the best result (94.1%) and outperformed the MRI and CSF biomarkers model (76.5%).

These MCI results were consistent with previous proteomic studies showing that alternative CSF candidates can complement other biomarkers for improved disease prediction [10,11]. This was the first neuroimaging study to show that candidate CSF proteins of inflammation, microglial activity, and synaptic function could be used to improve the predictive ability of prodromal AD in MCI individuals. However, issues with model specificity in disease prediction still existed, despite significant improvements in model sensitivity. This may be linked to the heterogeneity of the MCI population, and is supported by the bimodal distribution of predictive scores in our MCI-nc sample indicating an AD-like phenotype. A study by Davatzikos and colleagues [12], found that estimates of model specificity increase with longer follow-up times and further illustrates the complex heterogeneity of the MCI-nc population. Although longer follow-up may refine our estimates of specificity, accurately predicting short-term conversion

is also important as individuals classified as positive would be good targets for future disease-modifying therapies.

In contrast, the development and progression of AD pathology can also be modified by APOE ε4 genotype. Several previous studies have attempted to understand the neuroanatomic relationship between APOE and brain structure [13–15] and how APOE ε4 may increase the susceptibility of hippocampal atrophy in AD [16]. However, there are a number of studies that demonstrate a neuroanatomic influence of the APOE gene in modulating AD and equally others that do not [17]. Limitations in either sample size or the use of either manual or semi-automated methods of volume estimation in the hippocampus could be attributed to these diverse findings.

To further elucidate these APOE mechanisms in AD, and capture the heterogeneity of varying AD risk, in *Chapter 4* I used an extensive multi-cohort dataset of AD, MCI, and normal ageing (n=1781) subjects. Consistent with a number of previous studies, I found that APOE ε4 was associated with hippocampal differences in AD and MCI patients in a dose-dependent fashion. Interestingly, APOE ε4 did not appear to modify hippocampal volume differences in non-demented individuals and the cognitively normal (CN) elderly. Since recent work has shown that approximately one-third of CN individuals harbouring Aβ accumulation have a heightened AD risk [18], I tested whether a synergistic relationship between Aβ and APOE ε4 could better explain hippocampal volumes of CN individuals. Although Aβ+ ε4+ participants showed greater hippocampal differences than Aβ- ε4+ participants in general, there were no hippocampal differences in these two groups within the CN sample. This is interesting because it suggests that there is no observable synergistic effect of APOE ε4 and Aβ on hippocampal volume in CN individuals. However, a study by Fortea and colleagues found that there was a significant interaction between CSF $A\beta_{(1-42)}$ levels and CSF levels of *p*-tau_{181} affecting brain structure [19]. They concluded that interactions between biomarkers in AD results in a 2-phase phenomenon of pathological cortical thickening associated with $A\beta_{(1-42)}$, followed by atrophy once levels of p-tau become abnormal. Since Aβ accumulation was measured using Aβ PET methods in this investigation, I was unable to directly investigate this relationship. Furthermore, no CSF data was publicly available for the AIBL study, and the number of CN individuals in the ADNI study

with available Aβ PET and CSF data was very limited. One explanation for the negative finding may be that the synergistic interaction between Aβ and APOE ε4 in preclinical stages of AD is dependent on p-tau becoming abnormal. Together, these results suggest that the APOE ε4 driven hippocampal changes become most prominent in the later stages of AD pathophysiology, with MCI and AD patients becoming most affected. CN individuals and non-demented individuals demonstrate no independent APOE ε4 risk on hippocampal volume. The work in chapter 4 of this thesis highlights the importance of these complex biomarker interactions during the different stages of AD and should be considered in future clinical trials and therapeutic interventions of AD.

Recent evidence has suggested that although Aβ deposition begins many decades prior to cognitive impairment, structural alterations may precede Aβ accumulation in APOE ε4 carriers [20]. To investigate this proposed neurodevelopmental foothold of the APOE gene, I tested its neuroanatomic effect on hippocampal volumes in healthy 14-yr old adolescents from the large IMAGEN study in *Chapter 5*. Results suggested that there was no effect of the APOE gene on the hippocampal volumes of 14-yr old healthy adolescents.

One explanation for this finding may be related to the dynamic and asynchronous neurobiological processes occurring during brain maturation in adolescence. For instance, neurobiological changes such as intracortical myelination, synaptic pruning, and dendritic arborisation usually optimize the brain for challenges ahead in adulthood. In cases of antagonistic pleiotropy, these optimized changes may actually confer beneficial effects during adolescent development and early adulthood, at the expense of more rapid decline in older age [21]. To investigate this phenomenon, I tested the effect of different APOE groups on cognitive performance, but did not find any significant differences. Primarily, the negative finding in hippocampal APOE comparisons is consistent the pattern of hippocampal changes observed in the APOE multi-cohort investigation in *Chapter 4*. In particular, APOE ε4 did not appear to be associated with hippocampal loss in normal healthy ageing, suggesting that its detrimental effect on the brain may be linked to the pathological cascade of events in AD pathogenesis. In contrast, it is also possible that white-matter (WM) changes could precede grey matter alterations associated with APOE in adolescence. Deviations in optimised

neurobiological changes during adolescence could render key allocortical fibre pathways susceptible to vulnerabilities in the WM network.

To investigate this potential phenomenon, in *Chapter 6*, I compared the diffusion characteristics of WM microstructure in relation to the APOE gene in the diffusion imaging subset of 14-yr old healthy adolescents. The results of the unbiased whole-brain analysis revealed no significant differences, across all diffusion indices, in healthy adolescents in APOE ε4 and ε2 comparisons. This negative finding, which consistently follows on from our hippocampal comparisons in the same cohort, firmly establishes that the APOE gene showed no effect on brain structure. Together, these results are consistent with previous work in young APOE ε4 carriers that found the gene to be more commonly associated with changes in brain function, both at rest and during a memory-encoding paradigm, in the absence of differences in brain volume [22]. Moreover, studies in young adult APOE ε4 carriers show that brain structure becomes particularly vulnerable in middle and old age. This early pretangle phase of tau lesions, though protracted, is believed to begin in young adulthood [23,24]. However, what is less consistent is whether these neuropathological changes associated with APOE in later age are congruous with AD pathogenesis or simply constitute a non-pathological ageing process.

In *Chapter 7*, I extended the biomarker comparisons in AD and MCI patients by testing the application of rsfMRI to measure functional brain changes associated with AD pathogenesis. The rationale for applying this technique originated from recent work indicating the potential of rsfMRI as an emerging biomarker for AD, particularly since functional changes are believed to precede structural changes [25]. The majority of rsfMRI studies in the AD literature have focused on aberrant functional connectivity patterns of the DMN, as it is widely considered a heteromodal network of regions underlying significant hypometabolism and Aβ deposition [26]. The posteromedial cortex (PMC), a region consisting of the precuneus, posterior cingulate cortex (PCC) and retrosplenial cortex (RSC), is a cortical hub anchored in the DMN that has dense structural connectivity to widespread brain regions [27]. To explain the complex functional connectivity cascades described in AD, I conducted the first investigation to explore the discrete functional roles subserved by the PMC across multiple intrinsic brain networks.

It has been reported previously that the PCC region of the PMC consists of prominent dorsal and ventral subdivisions that show a complex pattern of brain activity partially reflecting activity in other networks. Distinct patterns of activity modulation in these areas have subsequently been used to explain the functional disconnection of the PCC in traumatic brain injury [28]. My results showed that AD patients demonstrated aberrant functional connectivity cascades in the PMC, with (i) hyperconnectivity of the dorsal PCC with the DMN, (ii) a functional decline of the RSC with MTL networks supporting memory and cognition, and (iii) a frontal hyperconnectivity burden of the ventral PCC with the VMPFC region, compared to CN individuals.

To investigate whether a similar pattern of PMC systems-level pathophysiology could be observed in MCI patients, I performed additional rsfMRI analyses in MCI patients that converted to AD at a 2 year follow-up period. Although no whole-brain differences in PMC-derived networks were observed, MCI converters showed (i) a similar functional decline of MTL networks to AD patients, but from PMC-subregions derived from the precuneus instead of the RSC, and (ii) a frontal hyperconnectivity burden of the VMPFC, similar to AD patients, compared to CN individuals. A key difference noted in this investigation was the relative sparing of the PCC subdivisions in MCI-converters. One explanation for this, although tentative, may be that aberrant noisy signals propagating from MTL networks only begin to disrupt PCC functional homeostasis in the later stages of AD. Comparing this investigation to previous work [29], this rsfMRI study shows that a selective vulnerability of PMC-related functional circuits leads to a cascading failure of intrinsic networks beyond the DMN. This work provides further evidence of the complex cytoarchitecture of the PMC. Future neuroimaging studies would benefit from treating this region as functionally heterogeneous to sensitively elucidate its vulnerability to AD pathogenesis.

LIMITATIONS

Many limitations of the studies in this thesis have been discussed extensively in the respective chapters. However, there are several that apply to this work in general. One notable limitation is that several of our investigations were cross-sectional in nature. Quantifying neuroimaging changes longitudinally are important as they are advantageous for monitoring annual brain changes over time. However, the availability of sufficiently powered longitudinal datasets and the range of available of longitudinal image analysis pipelines was limited at the time this work was carried out. In particular, limitations in adequately accounting for within-patient variability across scans was one of the reasons why cross-sectional data was used at the time.

Furthermore, baseline MRI changes were a key focus of several parts of this thesis because they provide the potential to estimate antecedent changes in prodromal MCI patients that might imminently convert to AD. Perhaps the best ways to track brain changes across structures over time may be to devise a combination of longitudinal and cross-sectional designs. For instance, life-span studies will advance our knowledge in the effect of age and other AD biomarker interactions on regional cortical decline. A recent study of developmental and lifespan changes in cortical thickness [30] will hopefully influence future studies to address how these brain changes are driven by genetic make-up and APOE risk.

The use of the Alzheimer's Disease Neuroimaging Initiative (ADNI) study cohort and European AddNeuroMed cohort in this thesis may not be entirely representative of the general population, and could be deemed a limitation in this regard. Both studies are quite selective in that participants were highly educated, had few existing or untreated medical, neurological or psychiatric illnesses, and had been enriched for high risk groups. Although there are potential benefits for discovering sensitive biomarkers of AD in this way, the results would need to be replicated in more representative and ethnically diverse prospective cohorts for robust validation.

In *Chapter 2*, I investigated the utility of an automated hippocampal subfield segmentation technique for detecting AD and predicting future MCI to AD conversion. Although this method is fully automated and based on a generative model of MRI data, it is based on a probabilistic

atlas which was originally built from an in-vivo dataset with a with lower signal-to-noise ratio [31]. Consequently, this atlas was only sufficient to produce a coarse segmentation of the subfields in standard-resolution (1mm). Although the investigation in this chapter was conducted on 1.5T MRI data, new higher resolution scans with better visualised delineations of the subfields would require a more accurate model of the anatomical boundaries.

Another issue is that the delineation protocol of the in-vivo atlas data had been designed for the hippocampal body but did not translate well to the hippocampal head. This could explain the contradictory findings in our investigation compared to earlier reports of more pronounced volumetric differences in the CA1 region [32]. Furthermore, it has been shown that the volumes generated from this atlas also do not agree well with those from histological studies. To overcome these methodological issues, a new segmentation algorithm was developed and ex-vivo MRI data from autopsy brains was acquired for the latest version of FreeSurfer (v6.0) [33]. The advantage of using post-mortem samples allows for an extremely high resolution and signal-to-noise ratio through longer acquisitions which can identify subfields more accurately in the delineation protocol. Recently, a novel Bayesian approach has further developed an automated method allowing for the segmentation of hippocampal subfields across multiple timepoints [3]. This method can be applied to longitudinal studies and allows for the quantification of within-subject neuroanatomical changes in the hippocampal subfields.

In *Chapters 2* and *3*, I was able to show that measures derived from structural MRI can be used in multivariate computational algorithms for predicting the progression to AD in MCI individuals. Despite the models showing good prognostic ability in detecting AD in MCI patients that eventually converted to AD at follow-up, model performance for MCI subjects that remained clinically stable was poor. According to previous studies this is a well -recognised problem [8,12,34]. MCI subjects represent a heterogeneous population of individuals that will convert to some form of neurodegenerative disease, whereas others will remain clinically stable for long periods of time. Often clinically stable MCI patients that do not progress to AD are misclassified as being AD-like at their baseline scan. One interpretation may be that these individuals do show an AD phenotype as they will likely progress to AD in the future but die before showing symptoms for clinical diagnosis.

Addressing the challenge of detecting the earliest stages of AD has been further complicated by evidence suggesting that the normal healthy ageing brain is also characterised by the presence of cortical atrophy, albeit of a non-AD, non-pathological origin [35]. Contrary to this view, others have suggested that the presence of cortical decline is not a feature concomitant of normal healthy ageing but rather a cause of preclinical cognitive pathology [36]. Thus, conceptualising the temporal gap between latent pathology in a yet undetected neurodegenerative disease such as AD, and that of a presumable normal ageing process has been problematic. In order to better define the different biomarker phenotypes of AD pathology, the NIA-AA preclinical criteria has been proposed using a two feature biomarker classification system of Aβ pathology and tau neurodegeneration. In general, two key points of view convey the conceptualisation of biomarker changes across the AD spectrum. One is an Aβ-centric standpoint that biomarker evidence of Aβ pathology is alone sufficient to define AD, and thus Aβ-negative evidence of atrophy should be classified as a 'non-AD' condition. The other perspective is that biomarker evidence of Aβ pathology is not solely sufficient to define AD pathophysiology, and therefore atypical trajectories of development are also important. Both views demonstrate an abstruse distinction between brain changes corresponding to AD pathophysiology and those relating to a normal ageing process. This has led to studies now conceptualising dynamic biomarker changes that should also be expected in normal ageing to demonstrate an overlap with pathophysiological changes in AD [37,38]. This approach has since been applied in MCI populations [39] and should prompt future studies to characterise biomarker trajectories in atypical MCI cases.

In *Chapters 4 and 5*, I explore the proposed neurodevelopmental effect of the APOE gene on brain structure in a large well-characterised study of healthy 14-yr old adolescents. Although the entire sample was ethnically homogeneous (Caucasian), I could not rule out the low genetic penetrance of APOE ε4 in the sample and other phenomena affecting brain maturation in adolescence. For instance, the maturation of the adolescent brain is influenced by heredity, environment, and sex hormones (oestrogen, progesterone, and testosterone), which play a crucial role in myelination. Unfortunately, since information regarding sex hormones was not available for the IMAGEN study, I was unable to ascertain their effects on brain structure.

Finally, in *Chapter 6,* I characterised the functional architecture of the PMC in AD and found that the RSC region subdivided into two prominent Brodmann regions (BA29 and BA30). Both subregions exhibited different patterns of functional connectivity with the rest of the brain. In particular, BA29 showed functional connectivity with the DMN, whereas BA30 showed connectivity with visual extrastriate areas of the brain. Although this finding is supported by previous RSC work [40], we cannot exclude the possibility that the rsfMRI derived time-courses from these subregions does not reflect the anatomical precision of the RSC. Future work could address this issue by exploring RSC function using high-field 7T systems or investigating selective patient samples with localised RSC lesions. In addition, I did not investigate the functional vulnerability of PMC functional circuits across the entire AD spectrum. In particular, it would have been interesting to further explore this in a sample of CN individuals with a pre-clinical risk of AD. However, the number of CN individuals with both Aβ PET imaging and rsfMRI data was limited. This number was further reduced upon also considering the number of APOE ε4 carriers. As will be discussed in the next section, it may be best to pursue this avenue of work in an independent rsfMRI dataset to acquire a better conceptualisation of network failures in AD.

As prevailing evidence accumulates to suggest that different neuroimaging modalities can detect pathological changes years before AD manifests clinically there has also been an increased interest to measure clinical usefulness. Currently, FDG-PET is a well-established method for the prognosis of dementia in MCI patients and structural MRI provides a quantitative approach for staging of neuronal loss [41]. Studies show that measurements from hippocampal volumetry can achieve accuracy rates of up to 80% in predicting the progression of dementia in MCI patients with over 3 years of follow-up [42]. However, to predict clinical progression at an individual level, neuroimaging biomarkers as diagnostic tools must have a sensitivity well over 90% and a specificity near 100%, be reliable, easily accessible and inexpensive, and be able to detect one or more fundamental features of the neuropathology.

The clinical usefulness of imaging biomarkers can be determined by its diagnostic efficacy in specialised care settings, such as memory clinics or primary care settings which is often the first point of contact for patients with a suspected dementia. This has recently been tested

using fully automated atlas-based hippocampal volumetry in a secondary care memory clinical outpatient sample demonstrating a promising 84% accuracy in detecting AD [43]. Despite this, several non-medical factors influence the use of imaging techniques for routine clinical application. For instance, economic factors relating to the high cost of new technology in neuroimaging, such as combined MRI/PET systems and high-field innovations currently limit broad application. Moreover, regulatory requirements for standardisation and certification of imaging techniques means accurate harmonized reference standards and cut-offs of normality must be established before introduction to clinical practice. New frameworks for standardised hippocampal volumetry and Aβ PET quantification have already been proposed [1,44], but further studies are required to comprehensively test for validation and reproducibility.

New conceptual strategies are beginning to challenge the limitations that imaging biomarkers pose for routine clinical implementation and use as enrichment tools for clinical trials. A multidisciplinary working group has proposed a framework to translate robust imaging techniques in AD research to clinical practice [45]. Consisting of five conceptual phases, the framework describes the steps required to advance diagnostic imaging from research settings to clinical practice. Following this, the international working group criteria and the US National Institutes of Aging – Alzheimer's Association have contributed to the diagnostic criteria of AD by better defining clinical phenotypes of AD and the integration of biomarkers in the diagnostic process [46,47]. The aim of these initiatives is to balance costs of care, and non-medical factors for selection of diagnostic imaging (such as standardised and qualified methods and scanner availability) and allow adjustments on the basis of empirical evidence and expert consensus.

Standardisation of methods still remains a significant challenge, although international consortia have made substantial progress in this area and provide lessons for future standardisation efforts. In addition to this, primary care research initiatives, such as the DelpHi study [48] will hopefully provide more heterogeneous at-risk dementia cases for determining the efficacy and cost-effectiveness of imaging biomarkers in the clinic.

IMPLICATIONS AND FUTURE DIRECTIONS

In this thesis, I have endeavoured to make a novel contribution to neuroimaging research in AD. At large, I have explored the utility of different neuroimaging techniques for characterising the in-vivo assessment of cortical atrophy using structural MRI techniques, studying the complex relationship between brain atrophy and Aβ deposition, using Aβ PET imaging methods, and finally, investigating the efficacy of rsfMRI techniques for characterising brain functional connectivity. From a disease classification and prediction perspective, I have shown that (1) hippocampal subfield measures provide a more sensitive measure for predicting future MCI to AD conversion than global hippocampal volume measurements, and (2) that combining novel CSF candidates of inflammation, microglial activity, and synaptic function can complement regional MRI measures of brain atrophy for AD classification and MCI prediction.

Building on previous neuroimaging APOE studies, I have explored the relationship between APOE and brain structure across the AD clinical spectrum, and healthy young adolescents with differential APOE risk. These comparisons provide strong support to suggest hippocampal atrophy is moderated by APOE ε4 in AD patients and MCI patients. However, I was unable to show that (1) neuroanatomic mechanisms of APOE ε4 on the hippocampus were present in healthy older non-demented individual and (2) APOE ε4 shares a neurodevelopmental foothold on brain structure in adolescence. Lastly, I was able to demonstrate that rsfMRI techniques can successfully be used to evaluate the disruption of PMC-functional circuits in the pathophysiology of AD.

Despite the different neuroimaging techniques adopted in this thesis, I was unable to show the temporal patterns of these biomarkers and the different endophenotypes they share in AD pathogenesis. Given the complexity and sometimes overlapping characteristics of AD pathophysiology, it is unlikely that a single biomarker would be able to provide the diagnostic certainty required for the earlier detection of AD. To gain a better insight into dynamic neuroimaging biomarker trajectories, we will require a wider use in the arsenal of AD biomarkers to study of the cognitively intact elderly. It has become clear that almost 20-30% of cognitively normal persons show abnormal patterns of Aβ deposition on PET scans [44]. Since, longitudinal studies of reliable biomarkers of Aβ pathology have shown promise in

tracking disease progression in Aβ-positive CN individuals over time[49]. However, a key outstanding question remains: What can be expected in normal ageing, when does normal ageing stop, and pathological AD-related changes begin?

The use of biomarkers in AD represents a paradigm shift in diagnosing the disease years ahead of full-blown symptomatic dementia, yet rather limited and stagnating therapeutic strategies and preventive options are available for patients worldwide. This raises several ethical questions with the potential benefits of biomarker-driven early diagnosis weighted against possible disadvantages. Currently, there are very few arguments favouring early diagnosis for prevention, due to the lack of effective disease-modifying therapy. However, a possible benefit of early diagnosis is that it may enable early decision making and could facilitate the introduction of disease management tools to help assist patients to cope with progressive decline. The ethical implications of a false positive diagnosis resulting in treatment and leading to a harmful side effect should also be considered. In such a case, it would represent a serious infringe on the basic medical ethics principle of nonmaleficence. Therefore, the positive effects of treatment must be considered against side effects, as well as treatment cost, when determining decision limits for diagnostic tests. At present, several ethical implications of biomarker assisted early diagnosis remain unanswered, and knowledge is particularly scarce on how patients react to early diagnosis. As we progress in our quest for effective surrogate markers of earlier detection and effective treatment strategies; any treatment will have to be evaluated from a cost-benefit perspective, and will remain a question for clinicians, politicians, and society as a whole.

Furthermore, recent studies have suggested that abnormal tau proteins are present in the pretangle stages of NFT pathology, sometimes without the presence of Aβ pathology [23]. This has prompted a reconceptualization of the temporal cascade of Aβ and tau proteinopathies in AD. The advent of tau PET imaging promises to help address fundamental questions regarding the longitudinal relationship between Aβ and tau in the pathogenesis of AD, and how each drive clinical progression. Understanding which protein serves its role as a ‘trigger’ driving neurodegeneration and the ‘bullet’ for eventual cognitive decline is highly relevant for developing and testing effective future therapies. Several avenues of future biomarker

research are underway to broaden our current arsenal of AD biomarkers to cover the full spectrum of molecular events in AD [37].

PET imaging of tau deposition in AD

The use of selective in-vivo tau imaging of hyperphosphorylated tau lesions will provide a better understanding of tau aggregation in the brain, addressing the mechanisms that drive clinical, anatomical, and functional heterogeneity in AD. Tau imaging represents a promising step towards disentangling the complex relationship between Aβ and tau, and understanding whether tau aggregation is part of normal healthy ageing or represents a pathological process. Combined Aβ and tau PET imaging has the potential to test the entire Aβ cascade hypothesis in-vivo and elucidate whether Aβ synergistically triggers the spread of tau pathology outside the temporal mesial cortex.

Substantial progress has been achieved in tau imaging in the past few years, with more selective tau PET tracers better equipped to tackle issues pertinent to tracer kinetics, binding affinity, and partial volume effects caused by brain atrophy. To my knowledge, at least seven different tau PET tracers have been developed and tested in clinical studies: ^{11}C-PBB3, ^{18}F- THK-523, ^{18}F-THK-5105, ^{18}F-THK-5117, ^{18}F-T808, ^{18}F-FDDNP, and ^{18}F-T807 [50,51]. However, not all exhibit the desired binding affinity to tau aggregates, high permeability of the blood-brain barrier, and other tracer kinetics to accurately reflect the spatial pattern of tau deposition in the brain. However, ^{18}F-AV-1451, a benzimidazole pyrimidine derivative, is in Phase 2 development as a diagnostic tau PET tracer, and currently represents the common tau PET tracer for quantifying tau pathology in AD [52,53]. The PET tracer characteristics for ^{18}F-AV-1451 suggest that it selectively binds to paired-helical filaments of abnormal tau pathology, and has very weak to no binding affinity with Aβ fibrils [54]. Recently, this ligand was able to show an increased uptake in inferior temporo-parietal regions in patients with AD [55].

These are very early days for tau PET imaging. The development and assessment of new compounds might yield improved ligands that will enable a more precise characterisation of tau deposits and be useful as a diagnostic and prognostic marker.

Blood-based biomarkers of AD – Silver lining on the horizon?

Since blood is more accessible than routine CSF collection, for which a lumbar puncture is needed, blood-based biomarkers are desirable as a potential high-throughput frontline screening tool. In theory, a simple blood test for AD would have a tremendous effect on geriatric healthcare worldwide, as it would be minimally invasive, easy, economical and rapid to perform. In CSF, Aβ ($_{1\text{-}42}$), *p*-tau$_{181}$ and *t*-tau have shown good sensitivity and specificity for distinguishing AD patients from healthy controls. However, proteomic studies have failed to replicate the success of these proteins in blood plasma [56]. Despite this, studies using both untargeted and candidate-based approaches have identified a substantial number of proteins related to the detection of AD and MCI [57] and has been validated in relation to neuroimaging markers of AD pathology [58]. Given the complexity of AD pathogenesis, it seems that an optimised panel of proteins are superior to single candidates [59]. Recent studies have provided some evidence to suggest their diagnostic and prognostic efficacy in AD classification [60], and relation to brain atrophy and Aβ endophenotypes [61]. However, there appears to be only a partial overlap of biomarkers across studies, suggesting that the optimal panel of blood biomarkers are yet to be determined. Future efforts to address the standardisation and harmonization of blood collection and analysis, as well as further independent replication of blood markers would enable more consistent findings.

The importance of big data initiatives in future AD research

Massive investment and technological advances in the collection of extensive and longitudinal data can potentially advance neurodegenerative research and drug development. Recent initiatives proposing the use of integrative predictive platforms to create a systems-based understanding of AD could help build new treatment paradigms where potential new drug targets can be identified [62]. A similar framework in AD, known as the European Medical Information Framework for Alzheimer's Disease (EMIF-AD), provides an extensive catalogue and database structure that can be utilised to pool different biomarker information for the earlier detection of AD [63]. To extend the work in this thesis, it would be interesting to explore the relationship of APOE on brain structure using MRI data from EMIF-AD. More specifically, it

would be of interest to explore how APOE mechanisms on brain structure change in different biomarker interactions of CSF Aβ and p-tau in the pre-dementia phase.

The UK biobank (ww.ukbiobank.ac.uk) represents a major national and international health resource with the aim of improving the diagnosis and prevention of several illnesses, including various forms of dementia. It is also a rich resource for extensive neuroimaging data which could be used to characterise the structural vulnerabilities of the brain in normal ageing. Elucidating the mechanisms of non-pathological brain changes may help inform on why the ageing brain is so much more susceptible to AD than is the younger brain. For instance, the role of the PMC from a structural connectivity perspective in normal ageing would be an interesting extension of the rsfMRI work in this thesis.

Exploring the human connectome – The Human Connectome Project (HCP)

The Human Connectome Project consortium led by Washington University, University of Minnesota, and Oxford University is undertaking a systematic effort to map macroscopic human brain circuits and their relationship to behaviour in a large population of healthy adults [64]. Refining methods for data acquisition and preprocessing will enable the analysis and visualisation of brain structure, function, and connectivity with exceptional high quality. Advances in diffusion MRI acquisition techniques, fibre orientation estimation and tractography will enable a higher quality quantification of structural brain connectivity [65].

Another key objective for HCP is to generate a detailed in-vivo mapping of functional connectivity using an advanced acquisition protocol for multiband-accelerated rsfMRI data with better temporal resolution and lower signal-to-noise ratio [66]. Hopefully, refinements in data quality, resolution and quantity will provide the impetus for future neuroimaging studies of AD to adopt advanced high-quality data-generating protocols. Doing so will enable a more detailed understanding into the systems-level pathophysiology of AD from a structural and functional connectivity perspective.

CONCLUSION

In conclusion, the studies in this thesis suggest that neuroimaging biomarkers of brain structure and function demonstrate sensitivity in detecting AD pathology, even in the prodromal MCI stages of development. The first study of this thesis demonstrates that automated hippocampal subfield measurements provide increased sensitivity for detecting incipient stages of AD in prodromal MCI patients. This is followed by a second study which shows that novel CSF candidates can mutually complement structural neuroimaging measures for disease classification and prediction. The direct comparison between hippocampal volume and APOE genotype confirms that atrophy in the hippocampus is modulated by APOE ε4 in AD and MCI patients, but did not influence the hippocampus in older non-demented individuals and did not appear to possess a neurodevelopmental foothold on brain structure in adolescence. I demonstrate that rsfMRI applications, particularly the functional heterogeneity of the posteromedial cortex, is an emerging biomarker for quantifying the breakdown in the functional architecture of AD. Through these empirically well-characterised studies, I conclude that neuroimaging biomarkers are a valuable tool for elucidating the pathological cascade of events underlying the complex aetiology of AD pathogenesis. More detailed and refined neuroimaging methods alongside an extensive pool of multimodal biomarker data will hopefully facilitate a better understanding into the temporal overlap between AD pathogenesis and non-pathological age-related events in the future.

REFERENCES

[1] Frisoni GB, Jack CR, Bocchetta M, Bauer C, Frederiksen KS, Liu Y, Preboske G, Swihart T, Blair M, Cavedo E, Grothe MJ, Lanfredi M, Martinez O, Nishikawa M, Portegies M, Stoub T, Ward C, Apostolova LG, Ganzola R, Wolf D, Barkhof F, Bartzokis G, DeCarli C, Csernansky JG, DeToledo-Morrell L, Geerlings MI, Kaye J, Killiany RJ, Lehéricy S, Matsuda H, O'Brien J, Silbert LC, Scheltens P, Soininen H, Teipel S, Waldemar G, Fellgiebel A, Barnes J, Firbank M, Gerritsen L, Henneman W, Malykhin N, Pruessner JC, Wang L, Watson C, Wolf H, DeLeon M, Pantel J, Ferrari C, Bosco P, Pasqualetti P, Duchesne S, Duvernoy H, Boccardi M (2015) The EADC-ADNI Harmonized Protocol for manual hippocampal segmentation on magnetic resonance: Evidence of validity. Alzheimer's Dement 11, 111–125.

[2] Yushkevich PA, Amaral RSC, Augustinack JC, Bender AR, Bernstein JD, Boccardi M, Bocchetta M, Burggren AC, Carr VA, Chakravarty MM, Chételat G, Daugherty AM, Davachi L, Ding SL, Ekstrom A, Geerlings MI, Hassan A, Huang Y, Iglesias JE, La Joie R, Kerchner GA, LaRocque KF, Libby LA, Malykhin N, Mueller SG, Olsen RK, Palombo DJ, Parekh MB, Pluta JB, Preston AR, Pruessner JC, Ranganath C, Raz N, Schlichting ML, Schoemaker D, Singh S, Stark CEL, Suthana N, Tompary A, Turowski MM, Van Leemput K, Wagner AD, Wang L, Winterburn JL, Wisse LEM, Yassa MA, Zeineh MM (2015) Quantitative comparison of 21 protocols for labeling hippocampal subfields and parahippocampal subregions in in vivo MRI: Towards a harmonized segmentation protocol. Neuroimage 111, 526–541.

[3] Iglesias JE, Van Leemput K, Augustinack J, Insausti R, Fischl B, Reuter M (2016) Bayesian longitudinal segmentation of hippocampal substructures in brain MRI using subject-specific atlases. Neuroimage 141, 542–555.

[4] Vemuri P, Wiste HJ, Weigand SD, Shaw LM, Trojanowski JQ, Weiner MW, Knopman DS, Petersen RC, Jack CR (2009) MRI and CSF biomarkers in normal, MCI, and AD subjects: predicting future clinical change. Neurology 73, 294–301.

[5] Westman E, Muehlboeck JS, Simmons A (2012) Combining MRI and CSF measures for classification of Alzheimer's disease and prediction of mild cognitive impairment conversion. Neuroimage 62, 229–238.

[6] Jack CR, Knopman DS, Jagust WJ, Shaw LM, Aisen PS, Weiner MW, Petersen RC, Trojanowski JQ (2010) Hypothetical model of dynamic biomarkers of the Alzheimer's pathological cascade. Lancet Neurol. 9, 119–28.

[7] Albert MS, DeKosky ST, Dickson D, Dubois B, Feldman HH, Fox NC, Gamst A, Holtzman DM, Jagust WJ, Petersen RC, Snyder PJ, Carrillo MC, Thies B, Phelps CH (2011) The diagnosis of mild cognitive impairment due to Alzheimer's disease: Recommendations from the National Institute on Aging-Alzheimer's Association workgroups on diagnostic guidelines for Alzheimer's disease. Alzheimers Dement 7, 270–279.

[8] Misra C, Fan Y, Davatzikos C (2009) Baseline and longitudinal patterns of brain atrophy in MCI patients, and their use in prediction of short-term conversion to AD: results from ADNI. Neuroimage 44, 1415–22.

[9] Hu WT, Chen-Plotkin A, Arnold SE, Grossman M, Clark CM, Shaw LM, Pickering E, Kuhn M, Chen Y, McCluskey L, Elman L, Karlawish J, Hurtig HI, Siderowf A, Lee VM-Y, Soares H, Trojanowski JQ (2010) Novel CSF biomarkers for Alzheimer's disease and mild cognitive impairment. Acta Neuropathol 119, 669–78.

[10] Craig-Schapiro R, Kuhn M, Xiong C, Pickering EH, Liu J, Misko TP, Perrin RJ, Bales KR, Soares H, Fagan AM, Holtzman DM (2011) Multiplexed immunoassay panel identifies novel CSF biomarkers for Alzheimer's disease diagnosis and prognosis. PLoS One 6, e18850.

[11] Paterson RW, Bartlett JW, Blennow K, Fox NC, Shaw LM, Trojanowski JQ, Zetterberg H, Schott JM (2014) Cerebrospinal fluid markers including trefoil factor 3 are associated with neurodegeneration in amyloid-positive individuals. Transl Psychiatry 4, 419.

[12] Davatzikos C, Bhatt P, Shaw LM, Batmanghelich KN, Trojanowski JQ (2010) Prediction of MCI to AD conversion, via MRI, CSF biomarkers, and pattern classification. Neurobiol Aging.

[13] Jack CR, Petersen RC, Xu YC, O'Brien PC, Waring SC, Tangalos EG, Smith GE, Ivnik RJ, Thibodeau SN, Kokmen E (1998) Hippocampal atrophy and apolipoprotein E genotype are independently associated with Alzheimer's disease. Ann Neurol 43, 303–310.

[14] Wishart H a, Saykin a J, McAllister TW, Rabin L a, McDonald BC, Flashman L a, Roth RM, Mamourian a C, Tsongalis GJ, Rhodes CH (2006) Regional brain atrophy in cognitively intact adults with a single APOE epsilon4 allele. Neurology 67, 1221–4.

[15] Liu Y, Paajanen T, Westman E, Wahlund L-O, Simmons A, Tunnard C, Sobow T, Proitsi P, Powell J, Mecocci P, Tsolaki M, Vellas B, Muehlboeck S, Evans A, Spenger C, Lovestone S, Soininen H (2010) Effect of APOE ε4 allele on cortical thicknesses and volumes: the AddNeuroMed study. J Alzheimers Dis 21, 947–66.

[16] Schuff N, Woerner N, Boreta L, Kornfield T, Shaw LM, Trojanowski JQ, Thompson PM, Jack CR, Weiner MW (2009) MRI of hippocampal volume loss in early Alzheimer's disease in relation to ApoE genotype and biomarkers. Brain 132, 1067–77.

[17] Cherbuin N, Leach LS, Christensen H, Anstey KJ (2007) Neuroimaging and APOE genotype: a systematic qualitative review. Dement Geriatr Cogn Disord 24, 348–62.

[18] Jansen WJ, Ossenkoppele R, Knol DL, Tijms BM, Scheltens P, Verhey FRJ, Visser PJ, Aalten P, Aarsland D, Alcolea D, Alexander M, Almdahl IS, Arnold SE, Baldeiras I, Barthel H, van Berckel BNM, Bibeau K, Blennow K, Brooks DJ, van Buchem M a., Camus V, Cavedo E, Chen K, Chetelat G, Cohen AD, Drzezga A, Engelborghs S, Fagan AM, Fladby T, Fleisher AS, van der Flier WM, Ford L, Förster S, Fortea J, Foskett N, Frederiksen KS, Freund-Levi Y, Frisoni GB, Froelich L, Gabryelewicz T, Gill KD, Gkatzima O, Gómez-Tortosa E, Gordon MF, Grimmer T, Hampel H, Hausner L, Hellwig S, Herukka S-K, Hildebrandt H, Ishihara L, Ivanoiu A, Jagust WJ, Johannsen P, Kandimalla R, Kapaki E, Klimkowicz-Mrowiec A, Klunk WE, Köhler S, Koglin N, Kornhuber J, Kramberger MG, Van Laere K, Landau SM, Lee DY, de Leon M, Lisetti V, Lleó A, Madsen K, Maier W, Marcusson J, Mattsson N, de Mendonça A, Meulenbroek O, Meyer PT, Mintun M a., Mok V, Molinuevo JL, Møllergård HM, Morris JC, Mroczko B, Van der Mussele S, Na DL, Newberg A, Nordberg A, Nordlund A, Novak GP, Paraskevas GP, Parnetti L, Perera G, Peters O, Popp J, Prabhakar S, Rabinovici GD, Ramakers IHGB, Rami L, Resende de Oliveira C, Rinne JO, Rodrigue KM, Rodríguez-Rodríguez E, Roe CM, Rot U, Rowe CC, Rüther E, Sabri O, Sanchez-Juan P, Santana I, Sarazin M, Schröder J, Schütte C, Seo SW, Soetewey F, Soininen H, Spiru L, Struyfs H, Teunissen CE, Tsolaki M, Vandenberghe R, Verbeek MM, Villemagne VL, Vos SJB, van Waalwijk van Doorn LJC, Waldemar G, Wallin A, Wallin ÅK, Wiltfang J, Wolk DA, Zboch M, Zetterberg H (2015) Prevalence of Cerebral Amyloid Pathology in Persons Without Dementia. JAMA 313, 1924.

[19] Fortea J, Vilaplana E, Alcolea D, Carmona-Iragui M, Sánchez-Saudinos M-B, Sala I, Antón-Aguirre S, González S, Medrano S, Pegueroles J, Morenas E, Clarimón J, Blesa R,

Lleó A (2014) Cerebrospinal fluid β-amyloid and phospho-tau biomarker interactions affecting brain structure in preclinical Alzheimer disease. Ann Neurol 76, 223–30.

[20] Dean DC, Jerskey B, Chen K, Protas H, Thiyyagura P, Roontiva A, O'Muircheartaigh J, Dirks H, Waskiewicz N, Lehman K, Siniard AL, Turk MN, Hua X, Madsen SK, Thompson PM, Fleisher AS, Huentelman MJ, Deoni SCL, Reiman EM (2014) Brain Differences in Infants at Differential Genetic Risk for Late-Onset Alzheimer Disease: A Cross-sectional Imaging Study. JAMA Neurol 71, 11–22.

[21] Jochemsen HM, Muller M, van der Graaf Y, Geerlings MI (2012) APOE ε4 differentially influences change in memory performance depending on age. The SMART-MR study. Neurobiol Aging 33, 832.e15-832.e22.

[22] Filippini N, MacIntosh BJ, Hough MG, Goodwin GM, Frisoni GB, Smith SM, Matthews PM, Beckmann CF, Mackay CE (2009) Distinct patterns of brain activity in young carriers of the APOE E4 allele. Proc Natl Acad Sci U S A 106, 7209–14.

[23] Braak H, Thal DR, Ghebremedhin E, Del Tredici K (2011) Stages of the Pathologic Process in Alzheimer Disease: Age Categories From 1 to 100 Years. J Neuropathol Exp Neurol 70, 960–969.

[24] Duyckaerts C (2011) Tau pathology in children and young adults: Can you still be unconditionally baptist? Acta Neuropathol 121, 145–147.

[25] Damoiseaux JS (2012) Resting-state fMRI as a biomarker for Alzheimer's disease? Alzheimer's Res Ther 4, 8.

[26] Buckner RL, Sepulcre J, Talukdar T, Krienen FM, Liu H, Hedden T, Andrews-Hanna JR, Sperling R a, Johnson K a (2009) Cortical hubs revealed by intrinsic functional connectivity: mapping, assessment of stability, and relation to Alzheimer's disease. J Neurosci 29, 1860–73.

[27] Leech R, Kamourieh S, Beckmann CF, Sharp DJ (2011) Fractionating the default mode network: distinct contributions of the ventral and dorsal posterior cingulate cortex to cognitive control. J Neurosci 31, 3217–24.

[28] Sharp DJ, Beckmann CF, Greenwood R, Kinnunen KM, Bonnelle V, De Boissezon X, Powell JH, Counsell SJ, Patel MC, Leech R (2011) Default mode network functional and structural connectivity after traumatic brain injury. Brain 134, 2233–2247.

[29] Damoiseaux JS, Prater KE, Miller BL, Greicius MD (2012) Functional connectivity tracks clinical deterioration in Alzheimer's disease. Neurobiol Aging 33,.

[30] Fjell AM, Grydeland H, Krogsrud SK, Amlien I, Rohani D a, Ferschmann L, Storsve AB, Tamnes CK, Sala-Llonch R, Due-Tønnessen P, Bjørnerud A, Sølsnes AE, Håberg AK, Skranes J, Bartsch H, Chen C-H, Thompson WK, Panizzon MS, Kremen WS, Dale AM, Walhovd KB (2015) Development and aging of cortical thickness correspond to genetic organization patterns. Proc Natl Acad Sci U S A 112, 15462–15467.

[31] Van Leemput K, Bakkour A, Benner T, Wiggins G, Wald LL, Augustinack J, Dickerson BC, Golland P, Fischl B (2009) Automated segmentation of hippocampal subfields from ultra-high resolution in vivo MRI. Hippocampus 19, 549–57.

[32] Mueller SG, Stables L, Du a T, Schuff N, Truran D, Cashdollar N, Weiner MW (2007) Measurement of hippocampal subfields and age-related changes with high resolution MRI at 4T. Neurobiol. Aging 28, 719–26.

[33] Iglesias JE, Augustinack JC, Nguyen K, Player CM, Player A, Wright M, Roy N, Frosch MP, McKee AC, Wald LL, Fischl B, Van Leemput K (2015) A computational atlas of the hippocampal formation using ex vivo, ultra-high resolution MRI: Application to adaptive segmentation of in vivo MRI. Neuroimage 115, 117–137.

[34] Westman E, Simmons A, Muehlboeck J-S, Mecocci P, Vellas B, Tsolaki M, Kłoszewska I, Soininen H, Weiner MW, Lovestone S, Spenger C, Wahlund L-O (2011) AddNeuroMed and ADNI: similar patterns of Alzheimer's atrophy and automated MRI classification accuracy in Europe and North America. Neuroimage 58, 818–28.

[35] Nyberg L, Lovden M, Riklund K, Lindenberger U, Backman L (2012) Memory aging and brain maintenance. Trends Cogn Sci 16, 292–305.

[36] Becker JA, Hedden T, Carmasin J, Maye J, Rentz DM, Putcha D, Fischl B, Greve DN, Marshall GA, Salloway S, Marks D, Buckner RL, Sperling RA, Johnson KA (2011) Amyloid-β associated cortical thinning in clinically normal elderly. Ann Neurol 69, 1032–42.

[37] Jack CR, Wiste HJ, Weigand SD, Rocca WA, Knopman DS, Mielke MM, Lowe VJ, Senjem ML, Gunter JL, Preboske GM, Pankratz VS, Vemuri P, Petersen RC (2014) Age-specific population frequencies of cerebral β-amyloidosis and neurodegeneration among people with normal cognitive function aged 50–89 years: a cross-sectional study. Lancet Neurol 13, 997–1005.

[38] Burnham SC, Bourgeat P, Doré V, Savage G, Brown B, Laws S, Maruff P, Salvado O, Ames D, Martins RN, Masters CL, Rowe CC, Villemagne VL (2016) Clinical and cognitive trajectories in cognitively healthy elderly individuals with suspected non-Alzheimer's

disease pathophysiology (SNAP) or Alzheimer's disease pathology: a longitudinal study. Lancet Neurol 15, 1044–1053.

[39] Caroli A, Prestia A, Galluzzi S, Ferrari C, Berckel B Van, Teunissen C, Wall AE, Carter SF, Schöll M, Redolfi A, Nordberg A, Drzezga A, Frisoni GB (2015) Mild cognitive impairment with suspected nonamyloid pathology (SNAP) Prediction of progression. Neurology 5, 508–15.

[40] Vann SD, Aggleton JP, Maguire EA (2009) What does the retrosplenial cortex do? Nat Rev Neurosci 10, 792–802.

[41] Panegyres PK, Rogers JM, McCarthy M, Campbell A, Wu JS (2009) Fluorodeoxyglucose-positron emission tomography in the differential diagnosis of early-onset dementia: a prospective, community-based study. BMC Neurol. 9, 41.

[42] Clerx L, van Rossum IA, Burns L, Knol DL, Scheltens P, Verhey F, Aalten P, Lapuerta P, Van de Pol L, Van Schijndel R, De Jong R, Barkhof F, Wolz R, Rueckert D, Bocchetta M, Tsolaki M, Nobili F, Wahlund LO, Minthon L, Frölich L, Hampel H, Soininen H, Visser PJ (2013) Measurements of medial temporal lobe atrophy for prediction of Alzheimer's disease in subjects with mild cognitive impairment. Neurobiol Aging 34, 2003–2013.

[43] Suppa P, Anker U, Spies L, Bopp I, Rüegger-Frey B, Klaghofer R, Gocke C, Hampel H, Beck S, Buchert R (2015) Fully automated atlas-based hippocampal volumetry for detection of Alzheimer's disease in a memory clinic setting. J Alzheimers Dis 44, 183–193.

[44] Klunk WE, Koeppe RA, Price JC, Benzinger TL, Devous MD, Jagust WJ, Johnson KA, Mathis CA, Minhas D, Pontecorvo MJ, Rowe CC, Skovronsky DM, Mintun MA (2015) The Centiloid Project: Standardizing quantitative amyloid plaque estimation by PET. Alzheimer's Dement 11, 1–15.e4.

[45] Möller I, Gharbi M, Serrano HM, Barbero MH, Milano JV, Henrotin Y, Goldring S, Goldring M, Kraus V, Burnett B, Coindreau J, Cottrell S, Eyre D, Gendreau M, Gardiner J, Garnero P, Hardin J, Henrotin Y, Lotz M, Martel-Pelletier J, Christiansen C, Brandi M, Bruyere O, Chapurlat R, Collette J, Cooper C, Giacovelli G, Kanis J, Henrotin Y, Addison S, Kraus V, Deberg M, Birmingham J, Vilim V, Kraus V, Henrotin Y, Deberg M, Dubuc J, Quettier E, Christgau S, Reginster J, Deberg M, Labasse A, Christgau S, Cloos P, Henriksen DB, Chapelle J, Zegels B, Reginster J, Henrotin Y, Deberg M, Labasse A, Collette J, Seidel L, Reginster J, Henrotin Y, Dougados M, Clegg D, Reda D, Harris C, Klein

M, O'Dell J, Hooper M, Bradley J, Bingham C, Weisman M, Jackson C, Uebelhart D, Malaise M, Marcolongo R, DeVathaire F, Piperno M, Mailleux E, Fioravanti A, Matoso L, Vignon E, Uebelhart D, Thonar E, Delmas P, Chantraine A, Vignon E, Kahan A, Uebelhart D, Vathaire F, Delmas P, Reginster J, Verbruggen G, Goemaere S, Veys E, Verbruggen G, Goemaere S, Veys E, Wildi L, Raynauld J, Martel-Pelletier J, Beaulieu A, Bessette L, Morin F, Abram F, Dorais M, Pelletier J, Altman R, Asch E, Bloch D, Bole G, Borenstein D, Brandt K, Christy W, Cooke T, Greenwald R, Hochberg M, Kellgren J, Lawrence J, Wolfe F, Smythe H, Yunus M, Bennett R, Bombardier C, Goldenberg D, Tugwell P, Campbell S, Abeles M, Clark P, Wolfe F, Clauw D, Fitzcharles M, Goldenberg D, Hauser W, Katz R, Mease P, Russell A, Russell I, Winfield J, Pham T, Heijde D, Lassere M, Altman R, Anderson J, Bellamy N, Hochberg M, Simon L, Strand V, Woodworth T, Huskisson E, Lequesne M, Kraus V, Gabay C, Medinger-Sadowski C, Gascon D, Kolo F, Finckh A, Lequesne M, Wagner J, Williams S, Webster C, Conrozier T, Balblanc J, Richette P, Mulleman D, Maillet B, Henrotin Y, Rannou F, Piroth C, Hilliquin P, Mathieu P, Henrotin Y, Chevalier X, Deberg M, Balblanc J, Richette P, Mulleman D, Maillet B, Rannou F, Piroth C, Mathieu P (2001) Biomarkers and surrogate endpoints: Preferred definitions and conceptual framework. Clin. Pharmacol. Ther.

[46] Dubois B, Feldman HH, Jacova C, Dekosky ST, Barberger-Gateau P, Cummings J, Delacourte A, Galasko D, Gauthier S, Jicha G, Meguro K, O'brien J, Pasquier F, Robert P, Rossor M, Salloway S, Stern Y, Visser PJ, Scheltens P (2007) Research criteria for the diagnosis of Alzheimer's disease: revising the NINCDS-ADRDA criteria. Lancet Neurol 6, 734–46.

[47] Dubois B, Feldman HH, Jacova C, Hampel H, Molinuevo JL, Blennow K, Dekosky ST, Gauthier S, Selkoe D, Bateman R, Cappa S, Crutch S, Engelborghs S, Frisoni GB, Fox NC, Galasko D, Habert MO, Jicha GA, Nordberg A, Pasquier F, Rabinovici G, Robert P, Rowe C, Salloway S, Sarazin M, Epelbaum S, de Souza LC, Vellas B, Visser PJ, Schneider L, Stern Y, Scheltens P, Cummings JL (2014) Advancing research diagnostic criteria for Alzheimer's disease: The IWG-2 criteria. Lancet Neurol 13, 614–629.

[48] Thyrian JR, Fiß T, Dreier A, Böwing G, Angelow A, Lueke S, Teipel S, Fleßa S, Grabe HJ, Freyberger HJ, Hoffmann W (2012) Life- and person-centred help in Mecklenburg-Western Pomerania, Germany (DelpHi): study protocol for a randomised controlled trial. Trials 13, 56.

[49] Villemagne VL, Burnham S, Bourgeat P, Brown B, Ellis K a, Salvado O, Szoeke C, Macaulay SL, Martins R, Maruff P, Ames D, Rowe CC, Masters CL (2013) Amyloid β deposition, neurodegeneration, and cognitive decline in sporadic Alzheimer's disease: a prospective cohort study. Lancet Neurol 12, 357–67.

[50] Villemagne VL, Fodero-tavoletti MT, Masters CL, Rowe CC (2015) Tau imaging : early progress and future directions. Lancet Neurol 14, 114–124.

[51] James OG, Doraiswamy PM, Borges-Neto S (2015) PET imaging of tau pathology in Alzheimer's disease and tauopathies. Front Neurol 6, 1–4.

[52] Ossenkoppele R, Schonhaut ÃDR, Scholl ÃM, Lockhart SN, Ayakta N, Baker SL, Neil JPO, Janabi M, Lazaris A, Cantwell A, Vogel J, Santos M, Miller ZA, Bettcher BM, Vossel KA, Kramer JH, Gorno-tempini ML, Miller BL, Jagust WJ, Rabinovici GD (2016) Tau PET patterns mirror clinical and neuroanatomical variability in Alzheimer's disease. Brain 139, 1551–1567.

[53] Lockhart SN, Schonhaut DR, Schwimmer HD, Rabinovici GD, Jagust WJ, Lockhart SN, Schonhaut DR, Neil JPO, Janabi M, Ossenkoppele R, Baker SL, Vogel JW, Faria J, Schwimmer HD, Rabinovici GD (2016) PET Imaging of Tau Deposition in the Aging Human Brain. Neuron 89, 971–982.

[54] Chien DT, Bahri S, Szardenings AK, Walsh JC, Mu F, Su MY, Shankle WR, Elizarov A, Kolb HC (2013) Early Clinical PET Imaging Results with the Novel PHF-Tau Radioligand [F-18]-T807. J Alzheimers Dis 34, 457–468.

[55] Johnson KA, Schultz A, Betensky RA, Becker JA, Sepulcre J, Rentz D, Mormino E, Chhatwal J, Amariglio R, Papp K, Marshall G, Albers M, Mauro S, Pepin L, Alverio J, Judge K, Philiossaint M, Shoup T, Yokell D, Dickerson B, Gomez-Isla T, Hyman B, Vasdev N, Sperling R (2016) Tau positron emission tomographic imaging in aging and early Alzheimer disease. Ann Neurol 79, 110–119.

[56] Baird AL, Westwood S, Lovestone S (2015) Blood-based proteomic biomarkers of Alzheimer's disease pathology. Front Neurol 6,.

[57] Olsson B, Lautner R, Andreasson U, Öhrfelt A, Portelius E, Bjerke M, Hölttä M, Rosén C, Olsson C, Strobel G, Wu E, Dakin K, Petzold M, Blennow K, Zetterberg H (2016) CSF and blood biomarkers for the diagnosis of Alzheimer's disease: A systematic review and meta-analysis. Lancet Neurol 15, 673–684.

[58] Thambisetty M, Simmons A, Velayudhan L, Hye A, Campbell J, Zhang Y, Wahlund L-O, Westman E, Kinsey A, Güntert A, Proitsi P, Powell J, Causevic M, Killick R, Lunnon K, Lynham S, Broadstock M, Choudhry F, Howlett DR, Williams RJ, Sharp SI, Mitchelmore C, Tunnard C, Leung R, Foy C, O'Brien D, Breen G, Furney SJ, Ward M, Kloszewska I, Mecocci P, Soininen H, Tsolaki M, Vellas B, Hodges A, Murphy DGM, Parkins S, Richardson JC, Resnick SM, Ferrucci L, Wong DF, Zhou Y, Muehlboeck S, Evans A, Francis PT, Spenger C, Lovestone S (2010) Association of plasma clusterin concentration with severity, pathology, and progression in Alzheimer disease. Arch Gen Psychiatry 67, 739–748.

[59] Laske C (2012) Alzheimer disease: blood-based biomarkers in AD--a silver lining on the horizon. Nat. Rev. Neurol. 8, 541–2.

[60] Doecke JD, Laws SM, Faux NG, Wilson W, Burnham SC, Lam C-P, Mondal A, Bedo J, Bush AI, Brown B, De Ruyck K, Ellis K a, Fowler C, Gupta VB, Head R, Macaulay SL, Pertile K, Rowe CC, Rembach A, Rodrigues M, Rumble R, Szoeke C, Taddei K, Taddei T, Trounson B, Ames D, Masters CL, Martins RN (2012) Blood-Based Protein Biomarkers for Diagnosis of Alzheimer Disease. Arch Neurol 1–8.

[61] Burnham SC, Faux NG, Wilson W, Laws SM, Ames D, Bedo J, Bush a I, Doecke JD, Ellis K a, Head R, Jones G, Kiiveri H, Martins RN, Rembach A, Rowe CC, Salvado O, Macaulay SL, Masters CL, Villemagne VL (2013) A blood-based predictor for neocortical Aβ burden in Alzheimer's disease: results from the AIBL study. Mol Psychiatry 1–8.

[62] Geerts H, Dacks PA, Devanarayan V, Haas M, Khachaturian ZS, Gordon MF, Maudsley S, Romero K, Stephenson D (2016) Big data to smart data in Alzheimer's disease: The brain health modeling initiative to foster actionable knowledge. Alzheimer's Dement 12, 1014–1021.

[63] Visser PJ, Streffer JR, Lovestone S (2014) A European Medical Information Framework for Alzheimer'S Disease (EMIF-AD). In Alzheimer's Dement Elsevier Ltd, p. P799.

[64] Van Essen DC, Smith SM, Barch DM, Behrens TEJ, Yacoub E, Ugurbil K (2013) The WU-Minn Human Connectome Project: An overview. Neuroimage 80, 62–79.

[65] Sotiropoulos SN, Jbabdi S, Xu J, Andersson JL, Moeller S, Auerbach EJ, Glasser MF, Hernandez M, Sapiro G, Jenkinson M, Feinberg DA, Yacoub E, Lenglet C, Van Essen DC, Ugurbil K, Behrens TEJ (2013) Advances in diffusion MRI acquisition and processing in the Human Connectome Project. Neuroimage 80, 125–143.

[66] Smith SM, Beckmann CF, Andersson J, Auerbach EJ, Bijsterbosch J, Douaud G, Duff E, Feinberg DA, Griffanti L, Harms MP, Kelly M, Laumann T, Miller KL, Moeller S, Petersen S, Power J, Salimi-Khorshidi G, Snyder AZ, Vu AT, Woolrich MW, Xu J, Yacoub E, Uğurbil K, Van Essen DC, Glasser MF (2013) Resting-state fMRI in the Human Connectome Project. Neuroimage 80, 144–168.

APPENDICES

APPENDIX 1: SUPPLEMENTARY ONLINE MATERIALS FROM CHAPTER 3

Table S1: List of RBM analytes from the multiplex panel available for analysis

Table S1. List of RBM analytes from the multiplex panel that were available for analysis (*n*=89).

Tr indicates that the analyte was transformed to approximate a normal distribution following inspection by Box-Cox methods. Accession numbers for each of these analytes and details of the assays are listed on www.rulesbasedmedicine.com.

RBM analyte	RBM analyte
Alpha-1-Antitrypsin (AAT)	Tr Alpha-2-Macroglobulin (A2Macro)
Alpha-1-Microglobulin (A1Micro)	Tr Apolipoprotein A-I (Apo A-I)
Angiopoietin-2 (ANG-2)	Tr Apolipoprotein C-III (Apo C-III)
Angiotensin-Converting Enzyme (ACE)	Tr Apolipoprotein E (Apo E)
Apolipoprotein D (Apo D)	Tr Apolipoprotein(a) (Lp(a))
Apolipoprotein H (Apo H)	Tr AXL Receptor Tyrosine Kinase (AXL)
CD 40 antigen (CD40)	Tr Beta-2-Microglobulin (B2M)
Chromogranin-A (CgA)	Tr Calcitonin
Clusterin (CLU)	Tr Cancer Antigen 19-9 (CA-19-9)
Cystatin-C	Tr Chemokine CC-4 (HCC-4)
Ferritin (FRTN)	Tr Complement C3 (C3)
Immunoglobulin A (IgA)	Tr Cortisol
Interleukin-6 receptor (IL-6r)	Tr C-Reactive Protein (CRP)
Macrophage Colony-Stimulating Factor 1 (M-CSF)	Tr Endothelin-1 (ET-1)
Matrix Metalloproteinase-3 (MMP-3)	Tr Fas Ligand (FasL)
Monocyte Chemotactic Protein 1 (MCP-1)	Tr Fatty Acid-Binding Protein, heart (FABP, heart)
Neutrophil Gelatinase-Associated Lipocalin (NGAL)	Tr Fibrinogen
N-terminal prohormone of brain natriuretic peptide (NT proBNP)	Tr Fibroblast Growth Factor 4 (FGF-4)
Osteopontin	Tr Follicle-Stimulating Hormone (FSH)
Pancreatic Polypeptide (PPP)	Tr Heparin-Binding EGF-Like Growth Factor (HB-EGF)
Serum Glutamic Oxaloacetic Transaminase (SGOT)	Tr Hepatocyte Growth Factor (HGF)
Sortilin	Tr Insulin-like Growth Factor-Binding Protein 2 (IGFBP-2)
Tissue Factor (TF)	Tr Intercellular Adhesion Molecule 1 (ICAM-1)
TNF-Related Apoptosis-Inducing Ligand Receptor 3 (TRAIL-R3)	Tr Interferon gamma Induced Protein 10 (IP-10)
Tr Adiponectin	Tr Interleukin-16 (IL-16)
Tr Agouti-Related Protein (AGRP)	Tr Interleukin-25 (IL-25)
Tr Interleukin-3 (IL-3)	Tr T Lymphocyte-Secreted Protein I-309 (I-309)
Tr Interleukin-8 (IL-8)	Tr T-Cell-Specific Protein RANTES (RANTES)
Tr Lectin-Like Oxidized LDL Receptor 1 (LOX-1)	Tr Thrombomodulin (TM)
Tr Leptin	Tr Thyroxine-Binding Globulin (TBG)
Tr Macrophage Inflammatory Protein-1 beta (MIP-1 beta)	Tr Tissue Inhibitor of Metalloproteinases 1 (TIMP-1)
Tr Macrophage Migration Inhibitory Factor (MIF)	Tr Transforming Growth Factor alpha (TGF-alpha)
Tr Matrix Metalloproteinase-2 (MMP-2)	Tr Trefoil Factor 3 (TFF3)
Tr Monocyte Chemotactic Protein 2 (MCP-2)	Tr Tumor Necrosis Factor Receptor 2 (TNFR2)
Tr Monokine Induced by Gamma Interferon (MIG)	Tr Vascular Cell Adhesion Molecule-1 (VCAM-1)
Tr Myoglobin	Tr von Willebrand Factor (vWF)
Tr Placenta Growth Factor (PLGF)	Vascular Endothelial Growth Factor (VEGF)
Tr Plasminogen Activator Inhibitor 1 (PAI-1)	
Tr Pregnancy-Associated Plasma Protein A (PAPP-A)	
Tr Prolactin	
Tr Prostatic Acid Phosphatase (PAP)	
Tr Resistin	
Tr S100 calcium-binding protein B (S100-B)	
Tr Serum Amyloid P-Component (SAP)	
Tr Sex Hormone-Binding Globulin (SHBG)	
Tr Stem Cell Factor (SCF)	

Table S2: List of Regional MRI Measures used in Support Vector Machine Algorithm

Table S2: List of Regional MRI measures used in the support vector machine algorithm. Note: Both left and right hemisphere regions were used in the analysis.

Cortical Thickness measures (n=34)	Volumetric measures (n=23)
Banks of superior temporal sulcus	Third ventricle
Caudal anterior cingulate	Fourth ventricle
Caudal middle frontal gyrus	Brainstem
Cuneus cortex	Corpus callosum anterior
Entorhinal cortex	Corpus callosum central
Fusiform gyrus	Corpus callosum midanterior
Inferior parietal cortex	Corpus callosum midposterior
Inferior temporal gyrus	Corpus callosum posterior
Isthmus of cingulate cortex	CSF
Lateral occipital cortex	Accumbens
Lateral orbitofrontal cortex	Amygdala
Lingual gyrus	Caudate
Medial orbitofrontal cortex	Cerebellum cortex
Middle temporal gyrus	Cerebellum white matter
Parahippocampal gyrus	Hippocampus
Paracentral sulcus	Inferior lateral ventricle
Frontal operculum	Putamen
Orbital operculum	Cerebral cortex
Triangular part of inferior frontal gyrus	Cerebral white matter
Pericalcarine cortex	Lateral ventricle
Postcentral gyrus	Pallidum
Posterior cingulate cortex	Thalamus proper
Precentral gyrus	Ventral DC
Precuneus cortex	
Rostral anterior cingulate cortex	
Rostral middle frontal gyrus	
Superior frontal gyrus	
Superior parietal gyrus	
Superior temporal gyrus	
Supramarginal gyrus	
Frontal pole	
Temporal pole	
Transverse temporal cortex	
Insular Banks of superior temporal sulcus	

Table S3: CSF Proteins from the multiplex panel associated with neuroimaging markers of atrophy, SPARE-AD score, and CSF biomarkers of AD

RBM analyte	Spearman's Rank Correlation	Uncorrected *P*-value	False-Discovery Rate Corrected *P*-value
Hippocampal Volume			
Chromogranin A (CgA) [ng/mL][a]	**0.293**	**<0.0001**	**<0.001**
Tissue Factor (TF) [ng/mL][a]	0.212	0.002	0.176
Angiotensin-Converting Enzyme (ACE) [ng/mL][a]	0.204	0.003	0.272
CD 40 antigen (CD40) [ng/mL]	0.198	0.004	0.363
Stem Cell Factor (SCF) [pg/mL]	0.197	0.005	0.378
Vascular Endothelial Growth Factor (VEGF) [ng/mL][a]	0.193	0.006	0.457
Cystatin – C [ng/mL][a]	-0.171	0.014	1.000
Monokine Induced by Gamma Interferon (MI) [pg/mL]	0.144	0.040	1.000
AXL Receptor Tyrosine Kinase (AXL) [ng/mL]	-0.143	0.040	1.000
Placenta Growth Factor (PLGF) [pg/mL]	0.143	0.041	1.000
Entorhinal Volume			
Chromogranin A (CgA) [ng/mL]	**0.265**	**0.000**	**0.008**
Vascular Endothelial Growth Factor (VEGF) [ng/mL]	0.207	0.003	0.232
Heparin-Binding EGF-Like Growth Factor (HB-EGF) [pg/mL]	0.192	0.006	0.470
Plasminogen Activator Inhibitor 1 (PAI-1) [ng/mL]	0.168	0.016	1.000
Lectin-Like Oxidized LDL Receptor 1 (LOX-1) [ng/mL]	-0.166	0.017	1.000
Cystatin – C [ng/mL]	-0.166	0.018	1.000
Macrophage Colony-Stimulating Factor 1 (M-CSF) [ng/mL]	0.158	0.023	1.000
Tissue Factor (TF) [ng/mL]	0.149	0.033	1.000
Angiotensin-Converting Enzyme (ACE) [ng/mL]	0.146	0.037	1.000
SPARE-AD Score			
Fatty Acid-Binding Protein, heart (FABP, heart)	**0.236**	**0.000**	**0.003**
Chromogranin A (CgA) [ng/mL]	-0.163	0.005	0.416
CD 40 antigen (CD40) [ng/mL]	-0.162	0.005	0.447
N-terminal prohormone of brain natriuretic peptide (NT proBNP) [pg/mL]	0.154	0.008	0.662
Macrophage Migration Inhibitory Factor (MIF) [ng/mL]	-0.127	0.029	1.000
Pancreatic Polypeptide (PPP) [pg/mL]	0.120	0.041	1.000
Osteopontin [ng/mL]	0.118	0.043	1.000
Interleukin-6 receptor (IL-6r) [ng/mL]	-0.113	0.052	1.000
Aβ 1-42			
Hepatocyte Growth Factor (HGF) [ng/mL]	-0.196	0.005	0.391
Osteopontin [ng/mL]	-0.193	0.005	0.444
Immunoglobulin A (IgA) [mg/mL]	0.160	0.022	1.000
Sex Hormone-Binding Globulin (SHBG) [nmol/L]	-0.139	0.047	1.000
C-Reactive Protein (CRP) [ug/mL]	0.138	0.049	1.000
Chromogranin A (CgA) [ng/mL]	-0.136	0.052	1.000

Table continues on next page

P-Tau181			
Fatty Acid-Binding Protein, heart (FABP, heart)	**0.556**	**<0.001**	**<0.001**
Tissue Factor (TF) [ng/mL]	**0.479**	**<0.001**	**<0.001**
Cystatin – C [ng/mL]	**-0.479**	**<0.001**	**<0.001**
Chromogranin A (CgA) [ng/mL]	**0.431**	**<0.001**	**<0.001**
Hepatocyte Growth Factor (HGF) [ng/mL]	**0.410**	**<0.001**	**<0.001**
Angiopoietin-2 (ANG-2) [ng/mL]	**0.403**	**<0.001**	**<0.001**
Lectin-Like Oxidized LDL Receptor 1 (LOX-1) [ng/mL]	**-0.386**	**<0.001**	**<0.001**
Tumor Necrosis Factor Receptor 2 (TNFR2) [ng/mL]	**-0.380**	**<0.001**	**<0.001**
Apolipoprotein E (Apo E) [ug/mL]	**0.373**	**<0.001**	**<0.001**
Matrix Metalloproteinase-3 (MMP-3) [ng/mL]	**0.351**	**<0.001**	**<0.001**
Angiotensin-Converting Enzyme (ACE) [ng/mL]	**0.349**	**<0.001**	**<0.001**
Heparin-Binding EGF-Like Growth Factor (HB-EGF) [pg/mL]	**0.338**	**<0.001**	**<0.001**
Transforming Growth Factor alpha (TGF-alpha) [pg/mL]	**0.321**	**<0.001**	**<0.001**
Vascular Endothelial Growth Factor (VEGF) [ng/mL]	**0.315**	**<0.001**	**<0.001**
Macrophage Colony-Stimulating Factor 1 (M-CSF) [ng/mL]	**0.314**	**<0.001**	**<0.001**
Beta-2-Microglobulin (B2M) [ug/mL]	**-0.311**	**<0.001**	**<0.001**
CD 40 antigen (CD40) [ng/mL]	**0.310**	**<0.001**	**<0.001**
Stem Cell Factor (SCF) [pg/mL]	**0.301**	**<0.001**	**<0.001**
Osteopontin [ng/mL]	**0.294**	**<0.001**	**0.001**
AXL Receptor Tyrosine Kinase (AXL) [ng/mL]	**-0.290**	**<0.001**	**0.002**
Clusterin (CLU) [ug/mL]	**0.288**	**<0.001**	**0.002**
Insulin-like Growth Factor-Binding Protein 2 (IGFBP-2) [ng/mL]	**-0.281**	**<0.001**	**0.003**
Ferritin (FRTN) [ng/mL]	**0.277**	**<0.001**	**0.004**
Trefoil Factor 3 (TFF3) [ug/mL]	**-0.271**	**<0.001**	**0.006**
Fibroblast Growth Factor 4 (FGF-4) [pg/mL]	**-0.268**	**<0.001**	**0.007**
von Willebrand Factor (vWF) [ug/mL]	**-0.251**	**<0.001**	**0.020**
Interleukin-6 receptor (IL-6r) [ng/mL]	**0.249**	**<0.001**	**0.024**
S100 calcium-binding protein B (S100-B) [ng/mL]	**0.247**	**<0.001**	**0.026**
Vascular Cell Adhesion Molecule-1 (VCAM-1) [ng/mL]	**-0.234**	**<0.001**	**0.056**
TNF-Related Apoptosis-Inducing Ligand Receptor 3 (TRAIL-R3) [ng/mL]	**0.227**	**<0.001**	**0.080**
Alpha-2-Macroglobulin (A2Macro) [mg/mL]	-0.215	0.002	0.152
Sortilin [ng/mL]	0.210	0.002	0.202
T-Cell-Specific Protein RANTES (RANTES) [ng/mL]	-0.184	0.008	0.662
Interleukin-3 (IL-3) [ng/mL]	0.179	0.010	0.850
Resistin [ng/mL]	0.163	0.020	1.000
Fas Ligand (FasL) [pg/mL]	-0.161	0.021	1.000
Leptin [ng/mL]	-0.160	0.022	1.000
Cancer Antigen 19-9 (CA-19-9) [U/mL]	-0.158	0.024	1.000
N-terminal prohormone of brain natriuretic peptide (NT proBNP) [pg/mL]	0.148	0.034	1.000
Follicle-Stimulating Hormone (FSH) [pg/mL]	0.141	0.044	1.000

Table continues on next page

T-Tau			
Fatty Acid-Binding Protein, heart (FABP, heart)	**0.634**	**<0.001**	**<0.001**
Tissue Factor (TF) [ng/mL]	**0.590**	**<0.001**	**<0.001**
Cystatin – C [ng/mL]	**-0.582**	**<0.001**	**<0.001**
Chromogranin A (CgA) [ng/mL]	**0.535**	**<0.001**	**<0.001**
Lectin-Like Oxidized LDL Receptor 1 (LOX-1) [ng/mL]	**-0.512**	**<0.001**	**<0.001**
Osteopontin [ng/mL]	**0.478**	**<0.001**	**<0.001**
Apolipoprotein E (Apo E) [ug/mL]	**0.476**	**<0.001**	**<0.001**
Hepatocyte Growth Factor (HGF) [ng/mL]	**0.463**	**<0.001**	**<0.001**
Tumor Necrosis Factor Receptor 2 (TNFR2) [ng/mL]	**-0.461**	**<0.001**	**<0.001**
Vascular Endothelial Growth Factor (VEGF) [ng/mL][a]	**0.452**	**<0.001**	**<0.001**
Angiotensin-Converting Enzyme (ACE) [ng/mL]	**0.447**	**<0.001**	**<0.001**
Matrix Metalloproteinase-3 (MMP-3) [ng/mL]	**0.436**	**<0.001**	**<0.001**
AXL Receptor Tyrosine Kinase (AXL) [ng/mL]	**-0.435**	**<0.001**	**<0.001**
Beta-2-Microglobulin (B2M) [ug/mL]	**-0.421**	**<0.001**	**<0.001**
Heparin-Binding EGF-Like Growth Factor (HB-EGF) [pg/mL]	**0.417**	**<0.001**	**<0.001**
Angiopoietin-2 (ANG-2) [ng/mL]	**0.400**	**<0.001**	**<0.001**
CD 40 antigen (CD40) [ng/mL]	**0.387**	**<0.001**	**<0.001**
Clusterin (CLU) [ug/mL]	**0.387**	**<0.001**	**<0.001**
Macrophage Colony-Stimulating Factor 1 (M-CSF) [ng/mL]	**0.386**	**<0.001**	**<0.001**
Transforming Growth Factor alpha (TGF-alpha) [pg/mL]	**0.377**	**<0.001**	**<0.001**
Stem Cell Factor (SCF) [pg/mL]	**0.363**	**<0.001**	**<0.001**
Ferritin (FRTN) [ng/mL]	**0.343**	**<0.001**	**<0.001**
S100 calcium-binding protein B (S100-B) [ng/mL]	**0.339**	**<0.001**	**<0.001**
Sortilin [ng/mL]	**0.337**	**<0.001**	**<0.001**
von Willebrand Factor (vWF) [ug/mL]	**-0.314**	**<0.001**	**<0.001**
Vascular Cell Adhesion Molecule-1 (VCAM-1) [ng/mL]	**-0.307**	**<0.001**	**<0.001**
Interleukin-6 receptor (IL-6r) [ng/mL]	0.290	<0.001	0.002
Trefoil Factor 3 (TFF3) [ug/mL]	-0.269	<0.001	0.006
Insulin-like Growth Factor-Binding Protein 2 (IGFBP-2) [ng/mL]	-0.263	<0.001	0.010
TNF-Related Apoptosis-Inducing Ligand Receptor 3 (TRAIL-R3) [ng/mL]	0.251	<0.001	0.020
Alpha-2-Macroglobulin (A2Macro) [mg/mL]	-0.248	<0.001	0.024
Fibroblast Growth Factor 4 (FGF-4) [pg/mL]	-0.248	<0.001	0.024
Interleukin-3 (IL-3) [ng/mL]	0.201	0.004	0.309
N-terminal prohormone of brain natriuretic peptide (NT proBNP) [pg/mL]	0.193	0.005	0.440
Leptin [ng/mL]	-0.184	0.008	0.684
Monocyte Chemotactic Protein 1 (MCP-1) [pg/mL]	0.175	0.012	0.987
Matrix Metalloproteinase-2 (MMP-2) [ng/mL]	0.170	0.015	1.000
Cancer Antigen 19-9 (CA-19-9) [U/mL]	-0.168	0.016	1.000
Intercellular Adhesion Molecule 1 (ICAM-1) [ng/mL]	-0.159	0.023	1.000
Fibrinogen [mg/mL]	-0.159	0.023	1.000
Follicle-Stimulating Hormone (FSH) [pg/mL]	0.136	0.051	1.000

*Bold indicates statistically significant effect

APPENDIX 1: SUPPLEMENTARY ONLINE MATERIALS FROM CHAPTER 4

Each cohort that was included in the AD and normal ageing dataset (n=1781) is shown below with demographic characteristics and APOE hippocampal comparisons.

Table S1: Demographic Characteristics and Hippocampal volumes of the ADNI cohort (n=779)

	ε2 carriers (*n*=52)	**ε3 carriers (*n*=351)**	**ε4 carriers (*n*=376)**	
	ε2/ε3 (n=50) ε2/ε2 (*n*=2)	ε3 Homozygotes	ε4/ε3 (*n*=290) ε4/ε4 (n=86)	*p*-value
Alzheimer's disease (*n*=177)				
Number of subjects (*n* (%)) †	5 (9.6)	54 (15.4)	118 (31.4)	--
Age (years)	76.5 ± 9.8	77.0 ± 8.4	74.5 ± 7.0	0.121
Male sex (*n* (%)) **	1 (1.1)	25 (26.3)	69 (72.6)	0.102
Education	14.0 ± 3.2	15.1 ± 3.4	14.5 ± 3.1	0.532
MMSE	21.8 ± 1.6	23.5 ± 2.0	23.2 ± 2.0	0.187
ICV (mL)	1453 ± 127	1554 ± 185	1550 ± 192	0.514
Left Hippocampal volume (mL)	1.60 ± 0.4	1.84 ± 0.4[C]	1.76 ± 0.3	0.028
Right Hippocampal volume (mL)	1.62 ± 0.5[B]	1.91 ± 0.5[C]	1.79 ± 0.3	0.004
Mild Cognitive Impairment (*n*=383)				
Number of subjects (*n* (%)) †	16 (30.8)	165 (47.0)	202 (53.7)	--
Age (years)	76.7 ± 7.3	75.7 ± 8.1	74.0 ± 7.0	0.049
Male sex (*n* (%)) **	8 (3.3)	112 (45.7)	125 (51.0)	0.243
Education	15.6 ± 2.7	15.7 ± 3.1	15.6 ± 3.0	0.980
MMSE	27.5 ± 1.5	27.1 ±1.8	26.8 ± 1.8	0.189
ICV (mL)	1511 ± 194	1581 ± 172	1571 ± 172	0.292
Left Hippocampal volume (mL)	2.14 ± 0.3[C]	2.03 ± 0.4[C]	1.95 ± 0.4[B]	0.001
Right Hippocampal volume (mL)	2.19 ± 0.3[C]	2.06 ± 0.4[C]	1.98 ± 0.4[A,B]	0.001
Healthy Controls (*n*=219)				
Number of subjects (*n* (%)) †	31 (59.6)	132 (37.6)	56 (14.9)	--
Age (years)	75.7 ± 5.6	76.1 ± 5.0	75.7 ± 5.0	0.859
Male sex (*n* (%)) **	13 (11.4)	72 (63.2)	29 (25.4)	0.449
Education	15.8 ± 3.5	16.2 ± 2.8	16.1 ± 2.8	0.784
MMSE	28.8 ± 1.2	29.2 ± 0.9	29.3 ± 0.8	0.134
ICV (mL)	1493 ± 173	1549 ± 157	1534 ± 154	0.214
Left Hippocampal volume (mL)	2.43 ± 0.4	2.32 ± 0.3	2.30 ± 0.3	0.187
Right Hippocampal volume (mL)	2.44 ± 0.3	2.32 ± 0.3	2.30 ± 0.3	0.182

Abbreviations: MMSE, Mini Mental State Examination; ICV, Intracranial Volume; CANTAB SWM, Cambridge Neuropsychological Test Automated Battery [CANTAB] Spatial Working Memory; IQ, Intelligence Quotient.
Data are Mean ± SD. Percentages are displayed in parentheses.
** percentage calculated as number of males by each ApoE group
[A] significant compared to ε2 carriers
[B] significant compared to ε3 carriers
[C] significant compared to ε4 carriers

Table S2: Demographic Characteristics and Hippocampal volumes of the AIBL cohort (n=228)

	ε2 carriers (*n*=24)		**ε3 carriers (*n*=91)**		**ε4 carriers (*n*=113)**		
	ε2/ε3 (n=24) ε2/ε2 (*n*=0)		ε3 Homozygotes		ε4/ε3 (*n*=93) ε4/ε4 (n=20)		*p*-value
Alzheimer's disease (*n*=46)							
Number of subjects (*n* (%)) †	5 (20.8)		15 (16.5)		26 (23.0)		--
Age (years)	78.6 ± 6.0		76.7 ± 6.7		76.8 ± 7.7		0.864
Male sex (*n* (%)) **	2 (4.3)		8 (17.4)		13 (28.3)		0.875
Education	--		--		--		--
MMSE	18.6 ± 8.2		22.3 ± 2.9		19.6 ± 4.9		0.155
ICV (mL)	1411 ± 158		1555 ± 115		1593 ± 195		0.101
Left Hippocampal volume (mL)	2.36 ± 0.4		2.36 ± 0.3		2.14 ± 0.4		0.096
Right Hippocampal volume (mL)	2.44 ± 0.3[C]		2.39 ± 0.3[C]		2.13 ± 0.4[A,B]		0.034
Mild Cognitive Impairment (*n*=42)							
Number of subjects (*n* (%)) †	4 (16.6)		16 (17.6)		22 (19.5)		--
Age (years)	79.5 ± 6.6		74.3 ± 7.6		75.6 ± 9.4		0.556
Male sex (*n* (%)) **	2 (4.8)		5 (11.9)		11 (26.2)		0.491
Education	--		--		--		--
MMSE	28.5 ± 1.7		26.6 ±2.7		27.1 ± 2.2		0.380
ICV (mL)	1467 ± 104		1491 ± 176		1533 ± 116		0.542
Left Hippocampal volume (mL)	2.45 ± 0.2		2.47 ± 0.5		2.14 ± 0.4		0.068
Right Hippocampal volume (mL)	2.46 ± 0.2		2.50 ± 0.5		2.22 ± 0.4		0.175
Healthy Controls (*n*=140)							
Number of subjects (*n* (%)) †	15 (62.5)		132 (65.9)		65 (57.5)		--
Age (years)	78.3 ± 7.4		77.5 ± 7.9		76.4 ± 6.6		0.561
Male sex (*n* (%)) **	8 (5.7)		28 (20.0)		33 (23.6)		0.852
Education	--		--		--		--
MMSE	28.7 ± 1.0		28.7 ± 1.1		28.9 ± 1.2		0.509
ICV (mL)	1588 ± 189		1516 ± 169		1524 ± 150		0.298
Left Hippocampal volume (mL)	2.33 ± 0.2		2.41 ± 0.4[C]		2.23 ± 0.4		0.008
Right Hippocampal volume (mL)	2.42 ± 0.3		2.49 ± 0.4[C]		2.28 ± 0.4		0.003

Abbreviations: MMSE, Mini Mental State Examination; ICV, Intracranial Volume
Data are Mean ± SD. Percentages are displayed in parentheses.
** percentage calculated as number of males by each ApoE group
[A] significant compared to ε2 carriers
[B] significant compared to ε3 carriers
[C] significant compared to ε4 carriers

Table S3: Demographic Characteristics and Hippocampal volumes of the AddNeuroMed cohort (n=303)

	ε2 carriers (*n*=25)		**ε3 carriers (*n*=148)**		**ε4 carriers (*n*=130)**		
	ε2/ε3 (n=25) ε2/ε2 (*n*=0)		ε3 Homozygotes		ε4/ε3 (*n*=103) ε4/ε4 (n=27)		*p*-value
Alzheimer's disease (*n*=109)							
Number of subjects (*n* (%)) †	4 (16.0)		42 (28.4)		63 (48.5)		--
Age (years)	76.3 ± 2.9		76.8 ± 6.3		74.5 ± 5.7		0.155
Male sex (*n* (%))	0 (0)		17 (15.6)		20 (18.3)		0.224
Education	8.0 ± 1.2		7.8 ± 4.2		7.8 ± 3.4		0.995
MMSE	21.5 ± 6.5		20.5 ± 4.8		21.0 ± 4.7		0.866
ICV (mL)	1339 ± 172		1465 ± 161		1477 ± 175		0.293
Left Hippocampal volume (mL)	2.26 ± 0.2[C]		1.87 ± 0.3[C]		1.74 ± 0.3[A,B]		0.001
Right Hippocampal volume (mL)	2.19 ± 0.4[C]		1.95 ± 0.4[C]		1.73 ± 0.4[A,B]		0.001
Mild Cognitive Impairment (*n*=97)							
Number of subjects (*n* (%)) †	9 (36.0)		52 (35.1)		36 (27.7)		--
Age (years)	72.5 ± 6.3		74.3 ± 5.2		74.7 ± 6.6		0.606
Male sex (*n* (%))	5 (5.2)		27 (27.8)		16 (16.5)		0.733
Education	10.8 ± 4.2		8.7 ± 4.0		9.1 ± 4.6		0.395
MMSE	27.4 ± 1.2		27.4 ±1.7		26.3 ± 1.7		0.007
ICV (mL)	1467 ± 166		1506 ± 164		1509 ± 177		0.793
Left Hippocampal volume (mL)	2.26 ± 0.4		2.15 ± 0.4		2.03 ± 0.4		0.157
Right Hippocampal volume (mL)	2.31 ± 0.5		2.21 ± 0.4		2.06 ± 0.5		0.115
Healthy Controls (*n*=97)							
Number of subjects (*n* (%)) †	12 (48.0)		54 (36.5)		31 (23.9)		--
Age (years)	73.2 ± 8.4		72.8 ± 6.5		72.2 ± 5.9		0.873
Male sex (*n* (%))	3 (3.1)		27 (27.8)		15 (15.5)		0.281
Education	11.1 ± 1.2		10.5 ± 5.1		11.7 ± 4.3		0.573
MMSE	29.1 ± 1.0		29.1 ± 1.2		29.0 ± 1.4		0.993
ICV (mL)	1436 ± 145		1487 ± 139		1486 ± 166		0.545
Left Hippocampal volume (mL)	2.42 ± 0.3		2.41 ± 0.3		2.42 ± 0.3		0.917
Right Hippocampal volume (mL)	2.43 ± 0.4		2.43 ± 0.3		2.48 ± 0.3		0.691

Abbreviations: MMSE, Mini Mental State Examination; ICV, Intracranial Volume
Data are Mean ± SD. Percentages are displayed in parentheses.
** percentage calculated as number of males by each ApoE group
[A] significant compared to ε2 carriers
[B] significant compared to ε3 carriers
[C] significant compared to ε4 carriers

Table S4: Demographic Characteristics and Hippocampal volumes of the BRC-AD Cohort (n=89)

	ε2 carriers (*n*=11)		**ε3 carriers (*n*=43)**		**ε4 carriers (*n*=35)**	
	ε2/ε3 (n=11) ε2/ε2 (*n*=0)		ε3 Homozygotes		ε4/ε3 (*n*=27) ε4/ε4 (n=8)	*p*-value
Alzheimer's disease (*n*=33)						
Number of subjects (*n* (%)) †	3 (27.3)		14 (32.6)		16 (45.7)	--
Age (years)	82.4 ± 5.6		77.2 ± 8.1		77.0 ± 5.7	0.444
Male sex (*n* (%))	1 (3.0)		6 (18.2)		10 (30.3)	0.452
Education	14.0 ± 1.7		11.4 ± 4.6		11.7 ± 3.5	0.589
MMSE	24.7 ± 5.9		21.1 ± 7.0		21.9 ± 3.9	0.599
ICV (mL)	1584 ± 190		1519 ± 108		1518 ± 162	0.753
Left Hippocampal volume (mL)	1.72 ± 0.06		1.75 ± 0.3		1.74 ± 0.4	0.913
Right Hippocampal volume (mL)	1.89 ± 0.07		1.93 ± 0.3		1.81 ± 0.4	0.718
Healthy Controls (*n*=56)						
Number of subjects (*n* (%)) †	8 (72.7)		29 (67.4)		19 (54.3)	--
Age (years)	75.9 ± 4.1		77.3 ± 6.3		78.6 ± 6.7	0.572
Male sex (*n* (%))	4 (7.1)		12 (21.4)		7 (12.5)	0.817
Education	13.8 ± 2.9		13.0 ± 3.7		12.9 ± 3.5	0.833
MMSE	29.0 ± 1.1		29.1 ± 1.3		29.0 ± 0.9	0.974
ICV (mL)	1510 ± 153		1473 ± 187		1507 ± 204	0.792
Left Hippocampal volume (mL)	2.34 ± 0.3		2.37 ± 0.4		2.35 ± 0.4	0.987
Right Hippocampal volume (mL)	2.39 ± 0.3		2.40 ± 0.4		2.35 ± 0.4	0.935

Abbreviations: MMSE, Mini Mental State Examination; ICV, Intracranial Volume
Data are Mean ± SD. Percentages are displayed in parentheses.
** percentage calculated as number of males by each ApoE group
[A] significant compared to ε2 carriers
[B] significant compared to ε3 carriers
[C] significant compared to ε4 carriers